NASA Contractor Report 187210

Hierarchic Extensions in the Static and Dynamic Analysis of Elastic Beams

Robert A. Watson
Washington University
Sever Institute of Technology
Saint Louis, Missouri

September 1991

Prepared for
Lewis Research Center
Under Training Grant NGT-50138

National Aeronautics and
Space Administration

HIERARCHIC EXTENSIONS IN THE STATIC AND DYNAMIC ANALYSIS OF ELASTIC BEAMS

Robert A. Watson
WASHINGTON UNIVERSITY
SEVER INSTITUTE OF TECHNOLOGY

ABSTRACT

Approximate solutions of static and dynamic beam problems by the p-version of the finite element method are investigated. Within a hierarchy of engineering beam idealizations, rigorous formulations of the strain and kinetic energies for straight and circular beam elements are presented. These formulations include rotating coordinate system effects and geometric nonlinearities to allow for the evaluation of vertical-axis wind turbines, the motivating problem for this research. Hierarchic finite element spaces, based on extensions of the polynomial orders used to approximate the displacement variables, are constructed. The developed models are implemented into a general-purpose computer program for evaluation.

Quality control procedures are examined for a diverse set of sample problems. These procedures include:
1) estimating discretization errors in energy norm and natural frequencies,
2) performing static and dynamic equilibrium checks,
3) observing convergence for quantities of interest, and
4) comparing with more exacting theories and experimental data.
It will be demonstrated that p-extensions produce exponential rates of convergence in the approximation of strain energy *and* natural frequencies for the class of problems investigated.

Sequential eigensolutions of problems utilizing hierarchic extensions allow for algorithmic enhancements of some iterative eigensolver techniques. This study will detail the theoretical basis for these improvements and document the resulting computational benefits.

TABLE OF CONTENTS

LIST OF TABLES

LIST OF FIGURES

HIERARCHIC EXTENSIONS IN THE STATIC AND DYNAMIC ANALYSIS OF ELASTIC BEAMS

1. INTRODUCTION

Finite element modeling of complex structures has become standard practice in today's engineering environment. Analytical capabilities within the field continue to expand to the limits of current and future computer resources. Further efforts are being expended to integrate analysis with other branches of computer-aided design and manufacturing.

Though different in content and methodology, the engineering design process remains literally unchanged. A problem statement is defined with respect to goals and restrictions of the product. Design variables are identified to provide flexibility as well as constraints for the design optimization. Models are developed and analyzed to quantify the effects of the design parameters. Feedback from nonengineering functions such as manufacturing and marketing may be required during the iterative design optimization. Eventually, the design is finalized and documented in a manner suitable for production.

From an analytical perspective, the modeling process involves interaction between the engineer and an analysis tool. The tool provides the system response

to any given set of design parameters specified by the engineer. The engineer is not only responsible for specifying the iterations leading to the optimal solution but also for ensuring that the analytical results are appropriate and correct.

Efficiency and accuracy are the two key requirements for the analysis tool. Efficiency is necessary to allow for enough iterations to define the optimal design within the specified time frame. Accuracy and reliability are important in ensuring that the design constraints have been satisfied within some allowable margin of error. These two requirements oppose one another. Typically, accuracy is sacrificed in the early stages of analysis for efficient evaluation of the design options. As the final design is approached, the need for accuracy dominates that of efficiency.

Efforts in finite element development focus on reducing the conflict between these two requirements. Efficiency has been greatly improved with the introduction of pre- and post-processing capabilities. Graphics has reduced the once burdensome collection of printed output to a manageable level. Interactive computing allows the engineer better quality control and faster access to the significant analytical results.

Though more abstract, the reliability requirement is also being addressed. A relatively recent analytical improvement involves the formulation of p-version finite elements [1].* Simply stated, p-version finite elements employ a sequence of polynomials, or other functions, in generating the basis functions for a sequence of hierarchic finite element spaces. Hierarchic spaces have the property that the approximation of polynomial order, p, is a subset of the approximation of order, $p+1$. The polynomials are typically "higher-order," implying an order exceeding the minimum required for finite strain energy.

* The numbers in brackets in the text indicate references in the Bibliography. The numbers in parentheses in the text indicate equations.

The p-version and (conventional) h-version are special classes of the finite element method. Errors of discretization may be reduced through systematic refinements of the mesh (h-extensions), increases in the polynomial order (p-extensions), or a combination of both (hp-extensions). In practice, the hp-version of the finite element method involves the application of p-extensions in conjunction with properly designed finite element meshes. By all measures of performance with respect to discretization error, the p- and hp-versions provide improved analytical accuracy over their h-version counterpart for the class of problems considered in this research.

The p-version of the finite element method also addresses the requirement of analyzer efficiency. The procedure for p-extension is quite automated and can even be made to be adaptive. For problems devoid of singularities [2], the engineer needs only to discretize the model with the minimum number of elements necessary to capture the model geometry. Extension of polynomial order then controls the accuracy of the solution and may continue until the desired convergence is reached. Furthermore, the generation of a hierarchic sequence of solutions based on extensions allows for the estimation of discretization error [3].

Implementation of p-version finite elements is substantially different from that of conventional elements. A major difference exists in the interrelationship between the shape functions used to approximate displacements (or other dependent variables) and the mapping functions used to transform any finite element into a standard element. Conventional methods typically employ isoparametric mapping, where the mapping functions are identical to the shape functions [4]. Thus, the true geometry of the problem may not be modeled exactly. Refinement of the mesh concurrently improves the mapping and solution accuracy.

Mapping for p-version finite elements is essentially independent of the shape functions. Ideally, the model must be described in geometric terms such that the true geometry is represented even at the lowest p-levels. Mapping into standard elements may then be achieved using techniques such as blending functions [5]. In this context, implementation of the p-version finite element method involves:

1) refinement of established pre- and post-processors to explicitly provide the geometric representation of a problem,
2) reeducation of the engineer away from the connect-the-dots mentality of h-version mesh generation, and
3) increase of computational costs associated with exact mapping.

In beam problems, the transition to p-version finite elements takes on a slightly different emphasis. The engineer still desires a minimum number of elements to capture the model geometry. Features such as taper and curvature must be explicitly incorporated into the elements rather than be approximated by a large number of straight, untapered elements. Thus, the formulation of new element *types* is critical for p-version analyses of beam problems.

Errors of idealization must also factor into the engineer's assessment of accuracy. Sources of idealization errors include assumptions in formulation [6], geometry [7], and loading [8]. This concept is fundamentally different from errors in discretization, is much more difficult to quantify, and is far too often overlooked by the unsuspecting engineer. Yet, errors in idealization may indeed be the major source of inaccuracy in even the simplest of analyses. Therefore, the concept of "finite element modeling" must be replaced by an understanding of the estimation and control of discretization errors *and* of the errors of idealization.

1.1 FORMULATION OVERVIEW

Application of numerical methods to the dynamic analysis of continuous systems was borne out of mathematical necessity. Exact eigensolutions to boundary value problems exist for a large class of relatively simple systems. Often these solutions involve *a priori* simplifications of a more general formulation. Complexities in geometry, loading, and/or constraints typically preclude an exact solution, however. One is left with the realization that an approximate solution is the only recourse for most practical engineering problems.

Various techniques have been developed throughout the history of structural analysis for the approximate solution of dynamic problems. Two major categories may be used to distinguish these techniques. Lumped modeling involves concentrating the system mass at discrete points (stations) and connecting them with massless springs. Holzer's method for torsional vibration [9] and Myklestad's method for beam bending vibration [10] fall within this general category. The second category assumes a solution in the form of a finite series of known functions with unknown coefficients. The latter category is by far the most common and encompasses a wide variety of analytical perspectives. Hybrid formulations between the two major categories also exist. The common trait among all approximate techniques is that continuous eigenproblems are transformed into discrete eigenproblems characterized by a finite number of degrees-of-freedom (dof's).

Functions used in the second category of approximate solution techniques must satisfy certain conditions which depend on the analytical approach. For example, comparison functions are those which are differentiable to the order of the governing differential equation, r, over the entire domain, Υ, and its boundary. Also, they must satisfy all of the prescribed geometric (kinematic) and natural boundary conditions. The order, r, has been defined from a one-dimensional

perspective but may be generalized easily to higher dimensions. The Galerkin, or weighting function, method as described by Meirovitch [11] requires the use of comparison functions.

Functions which possess a square integrable derivative of order $\frac{r}{2}$ over the entire closed domain constitute the infinite $E(\Upsilon)$ space. The subset of this space, $\tilde{E}(\Upsilon)$, which satisfies *only* the specified geometric boundary conditions is comprised of all admissible functions. Comparison functions form a more restrictive subset of the $\tilde{E}(\Upsilon)$ space and, thus, are used less frequently. Energy-based techniques only require the use of admissible functions; the restriction on the $E(\Upsilon)$ space ensures finite strain energy. An energy-based formulation is used in this research and merits further discussion.

Rayleigh's principle [12] provides the basis for many energy-based approximate solutions to dynamic problems. Simply stated:

> *The estimated frequency of vibration of a conservative system oscillating about the equilibrium position has a stationary value in the neighborhood of a natural mode. Furthermore, this stationary value is a minimum in the neighborhood of the fundamental mode.*

The simplest application of this principle, Rayleigh's energy method, results in an estimate of the fundamental natural frequency by:

1) estimating the fundamental mode shape, $u_1(x)$, from the set of admissible functions *and* assuming harmonic response,
2) computing the potential energy, V, and the kinetic energy, T, for the assumed shape, and
3) forming the Rayleigh quotient from the maximum potential and kinetic energies, with the maxima being taken independently and with respect to time.

Generalizing to more than one dimension poses no serious problem. In a generic sense, the resulting computation takes the form:

$$\omega_1^2 = \mathrm{R}(u_1) \equiv \frac{V_{\max}}{T^*} \geq (\omega_1^2)_{EX}, \tag{1.1}$$

where $\mathrm{R}(u_1)$ is the Rayleigh quotient for u_1, ω_1 and $(\omega_1)_{EX}$ are the approximate and exact fundamental natural frequencies, respectively, and:

$$T_{\max} \equiv \omega_1^2 T^*, \tag{1.2}$$

based on the assumption of harmonic response. The equal condition in (1.1), $\omega_1^2 = (\omega_1^2)_{EX}$, is true if and only if $u_1 = (u_1)_{EX}$.

The Rayleigh-Ritz method [13] is a natural extension to Rayleigh's energy method used to improve the estimate of the fundamental frequency as well as provide estimates for higher frequencies. Rather than using a single function, a set of linearly independent admissible basis functions, $\theta_j(x) \in \tilde{E}$, is constructed. The subspace, $\tilde{S}^{(n)}$, is defined as the set of all functions which can be written in the form:

$$u_k(x) = \sum_{j=1}^{n} U_{k,j}\theta_j(x) = \{U_k\}^T \{\theta\}, \tag{1.3}$$

where $U_{k,1}, U_{k,2}, \ldots, U_{k,n}$ are arbitrary finite numbers. The k subscript merely denotes the approximation of *any* individual mode shape with natural frequency, ω_k. Therefore, for any $u_k \in \tilde{S}^{(n)}$:

$$V_{\max} = \tfrac{1}{2} \{U_k\}^T [K] \{U_k\}, \text{ and} \tag{1.4a}$$

$$T^* = \tfrac{1}{2} \{U_k\}^T [M] \{U_k\}, \tag{1.4b}$$

where $[K]$ and $[M]$ are referred to as the stiffness and mass matrices, respectively, and depend on both the problem and the θ_j's. Both matrices will be symmetric

for the formulations developed in this research. Efficient storage and solution techniques exploit this property.

The Rayleigh quotient is formed as before:

$$\omega_k^2 = \mathrm{R}(u_k) = \frac{V_{\max}}{T^*} = \frac{\{U_k\}^T[K]\{U_k\}}{\{U_k\}^T[M]\{U_k\}}, \text{ where} \tag{1.5a}$$

$$\omega_1^2 = \min_{u_k \in \bar{S}^{(n)}} \Big(\mathrm{R}(u_k)\Big) \geq (\omega_1^2)_{EX}. \tag{1.5b}$$

Approximations for the higher frequencies are obtained by imposing the (necessary and sufficient) stationary conditions on the quotient:

$$\frac{\partial \mathrm{R}(u_k)}{\partial U_{k,j}} \equiv 0, \quad j = 1, 2, \ldots, n, \tag{1.6}$$

resulting in:

$$\left[[K] - \omega^2[M]\right]\{U\} = \{0\}, \tag{1.7}$$

where the k subscript has been dropped for simplicity. This defines the n-dof discretized approximation for the continuous eigenproblem. There are n eigenvalues which satisfy (1.7), each with a unique corresponding eigenvector. Thus:

$$\omega_k^2 = \lambda_k \equiv \text{eigenvalues}, \tag{1.8a}$$

$$\omega_k \equiv \text{natural frequencies}, \tag{1.8b}$$

$$\{U_k\} \equiv \text{eigenvectors, and} \tag{1.8c}$$

$$u_k = \{U_k\}^T\{\theta\} \equiv \text{eigenfunctions or mode shapes, for} \tag{1.8d}$$

$$k = 1, 2, \ldots, n. \tag{1.8e}$$

Note that the eigenvectors resulting from the homogeneous eigenproblem may only be determined to within an arbitrary multiplicative constant.

The natural frequencies computed from the discretized linear eigenproblem provide an upper bound for the first n exact natural frequencies [11], namely:

$$\omega_k \geq (\omega_k)_{EX}, \quad k = 1, 2, \ldots, n, \tag{1.9}$$

provided that the natural frequencies are arranged in ascending order. If the basis functions form a *complete* set such that any admissible function can be represented by an infinite linear combination of the θ_j's, then:

$$\tilde{S}^{(n)}(\Upsilon) \to \tilde{E}(\Upsilon), \text{ as} \tag{1.10a}$$

$$n \to \infty; \text{ thus} \tag{1.10b}$$

$$\omega_k \to (\omega_k)_{EX}, \text{ and} \tag{1.10c}$$

$$u_k \to (u_k)_{EX}. \tag{1.10d}$$

In other words, the θ_j's form the basis for the space of admissible functions. The complete infinite-dimensional space contains the exact solution while the finite-dimensional space results in an approximate solution. Again, the equal condition in (1.9) signifies $(u_k)_{EX} \in \tilde{S}^{(n)}$.

A more important result occurs during hierarchic extensions of linear systems, when additional θ_j terms are included in the approximation of u_k such that $\tilde{S}^{(n)} \subset \tilde{S}^{(n+1)} \subset \tilde{S}^{(n+2)} \ldots$. If $\omega_k^{(n)}$ and $\omega_k^{(n+1)}$ represent the natural frequencies from (n)- and $(n+1)$-dof linear approximations, respectively, and are arranged in ascending order, then the natural frequencies form a Sturm sequence [14]:

$$\omega_1^{(n+1)} \leq \omega_1^{(n)} \leq \omega_2^{(n+1)} \leq \cdots \leq \omega_n^{(n)} \leq \omega_{n+1}^{(n+1)}. \tag{1.11}$$

Therefore, as n increases, the computed natural frequencies approach the exact natural frequencies monotonically from above. The strain energy for hierarchic linear static problems also exhibits monotonic convergence.

Basis functions for Rayleigh-Ritz formulations are defined over the entire domain. For complex structures, the definition of suitable basis functions by this method is impractical. One is led to the idea of defining such functions over a small region within the domain and enforcing suitable displacement compatibilities across the boundaries of the subdomains. This is the fundamental principle behind the finite element approach. Basis functions for the space of admissible functions are constructed such that they are nonzero over a small number of subdomains. Such functions are said to have local support. The finite element method is nothing more than a systematic procedure for constructing basis functions with local support. When viewed in this fashion, the finite element method can be formulated within the framework of the Rayleigh-Ritz method.

The assumed-modes method as described by Meirovitch [11] is equivalent to the Rayleigh-Ritz method in that the resulting approximate eigenproblems are identical. However, use of the assumed-modes method provides an intelligible process for including rotating coordinate system effects. The fundamental displacement assumption initially includes time as an independent variable, namely:

$$u(x,t) = \sum_{j=1}^{n} q_j(t)\theta_j(x), \tag{1.12}$$

where the k subscript as defined in (1.3) has been omitted for simplicity. The potential and kinetic energies thus assume a time-dependent form:

$$V(t) = \tfrac{1}{2}\{q\}^T[K]\{q\}, \text{ and} \tag{1.13a}$$

$$T(t) = \tfrac{1}{2}\{\dot{q}\}^T[M]\{\dot{q}\}, \tag{1.13b}$$

where $\dot{} \equiv d/dt$. In this form, the approximate differential equations may be obtained via application of Lagrange's equation [11]:

$$\frac{d}{dt}\left(\frac{\partial T}{\partial \dot{q}_j}\right) - \frac{\partial T}{\partial q_j} + \frac{\partial V}{\partial q_j} = R_j, \quad j = 1,2,\ldots,n, \tag{1.14}$$

where the generalized forces, R_j, are derived from the principle of virtual work but are assumed zero for the free-response solution. The resulting free-response system of differential equations obtained by substituting (1.13) into (1.14) is:

$$[M]\{\ddot{q}\} + [K]\{q\} = \{0\}. \tag{1.15}$$

Finally, a complex harmonic response is assumed such that:

$$q_j(t) = U_j e^{i\omega t}, \quad j = 1, 2, \ldots, n, \tag{1.16}$$

where $i \equiv \sqrt{-1}$. It is implicitly understood that $q_j(t)$ must be a real quantity (i.e., $q_j(t) = \Re\{U_j e^{i\omega t}\}$), but the substitution as specified in (1.16) will be used throughout this text for simplicity. The resulting matrix equation is:

$$[[K] - \omega^2[M]]\{U\} = \{0\}, \tag{1.17}$$

which, for the same θ_j's, is identical to the formal Rayleigh-Ritz result (1.7). Note that the approximate static ($\dot{q}_j \equiv 0$) problem:

$$[K]\{U_S\} = \{R\}, \tag{1.18}$$

where:

$$\{U_S\} \equiv \text{static solution vector, and} \tag{1.19a}$$

$$u_S(x) = \{U_S\}^T\{\theta\} \equiv \text{approximate static solution,} \tag{1.19b}$$

may be obtained from the same formulation.

Using assumed-modes, a simple system subject to rotation may have energies of the form:

$$V(t) = \tfrac{1}{2}\{q\}^T[K]\{q\}, \text{ and} \tag{1.20a}$$

$$\begin{aligned} T(t) = {} & \tfrac{1}{2}\{\dot{q}\}^T[M]\{\dot{q}\} \\ & + \Omega\{q\}^T[C_1]\{\dot{q}\} \\ & + \tfrac{1}{2}\Omega^2\{q\}^T[K_1]\{q\} \\ & + \Omega^2\{q\}^T\{R_1\}, \end{aligned} \tag{1.20b}$$

where Ω is the magnitude of the rotation vector and $[C_1]$, $[K_1]$, and $\{R_1\}$ merely represent generic forms. Applying Lagrange's equation (1.14) and substituting the general harmonic response (1.16) result in the free-response, complex eigenproblem:

$$[[K + K_S] + i\omega[C] - \omega^2[M]]\{U\} = \{0\}, \tag{1.21}$$

where:

$$[K_S] = -\Omega^2[K_1], \text{ and} \tag{1.22a}$$

$$[C] = \Omega\left[[C_1]^T - [C_1]\right]. \tag{1.22b}$$

Thus, rotation introduces a symmetric (as formulated) centrifugal softening matrix to the system stiffness as well as a skew-symmetric Coriolis, or gyroscopic, matrix. The Coriolis terms involve velocities, but it is inappropriate to refer to them as "damping" terms since there is no energy dissipation. The resulting eigenvalues are real, but the eigenvectors will be complex due to the Coriolis coupling [15]. The corresponding static problem is:

$$[K + K_S]\{U_S\} = \{R + R_\Omega\}, \tag{1.23}$$

where:

$$\{R_\Omega\} = \Omega^2\{R_1\}. \tag{1.24}$$

Therefore, rotation also introduces centrifugal terms to the load vector.

Geometric nonlinearities form the basis for a large number of fundamental stability analyses. In a generic sense, many first-order bifurcation analyses using assumed-modes result in the eigenproblem [16]:

$$[[K] - \lambda[K_G]]\{U_B\} = \{0\}, \tag{1.25}$$

where λ is some load-dependent scale factor that *must* be applicable to all loads in a multiple-load problem, $[K_G]$ is the symmetric (as formulated in this research)

geometric nonlinearity matrix, and $\{U_B\}$ is the bifurcation vector. Assuming the basis functions are complete and $n \rightarrow \infty$, the smallest λ from the above eigenproblem defines the critical load for the structure. That is:

$$\lambda_1 \rightarrow (\lambda_1)_{EX} \equiv \lambda_{crit}. \tag{1.26}$$

From a dynamic perspective, stability may be inferred from an eigenproblem of the form:

$$[[K] - \Lambda[K_G] - \omega^2[M]]\,\{U\} = \{0\}, \tag{1.27}$$

where Λ is a specified value of the scale factor, λ. Thus, for:

$$\Lambda < \lambda_{crit}: \quad (\omega_1)_{EX} > 0, \text{ and} \tag{1.28a}$$

$$\Lambda = \lambda_{crit}: \quad (\omega_1)_{EX} \equiv 0. \tag{1.28b}$$

Geometric nonlinearities which can be characterized by a λ-factor result from (or lead to) linear, load-related terms in the governing differential equations. However, this often is not the case; deformations within the structure frequently change the internal loads used to compute the nonlinear terms. Solving for the critical load then involves a combination of incremental loading coupled with updates to the geometric nonlinearity matrix [17].

For a large class of dynamic problems, static preloads on the structure produce significant softening *or* stiffening effects on the natural frequencies ([18] for example). These effects may be approximated by the inclusion of static geometric nonlinearities in the dynamic eigenproblem. Starting with the linear static solution:

$$\left\{U_S^{(1)}\right\} = [K]^{-1}\,\{R\}, \tag{1.29}$$

the initial estimate of the geometric nonlinearity matrix may be computed as a function of the linear static solution vector:

$$\left[K_G^{(1)}\right] = \left[K_G^{(1)}\left(\left\{U_S^{(1)}\right\}\right)\right]. \tag{1.30}$$

The initial nonlinear static solution may then be computed as:

$$\left\{U_S^{(2)}\right\} = \left[K + K_G^{(1)}\right]^{-1}\{R\}. \tag{1.31}$$

Note that the system is unstable if the inverse in (1.31) does not exist. Further iterations may be performed:

$$\left[K_G^{(\ell)}\right] = \left[K_G^{(\ell)}\left(\left\{U_S^{(\ell)}\right\}\right)\right], \text{ and} \tag{1.32a}$$

$$\left\{U_S^{(\ell+1)}\right\} = \left[K + K_G^{(\ell)}\right]^{-1}\{R\}, \text{ for} \tag{1.32b}$$

$$\ell \geq 1, \tag{1.32c}$$

until convergence is reached to some acceptable tolerance. A useful check for convergence is defined using the strain energy:

$$V^{(\ell)} = \frac{1}{2}\left\{U_S^{(\ell)}\right\}^T\left[K + K_G^{(\ell-1)}\right]\left\{U_S^{(\ell)}\right\}, \tag{1.33}$$

such that:

$$e = \frac{\left|V^{(\ell+1)} - V^{(\ell)}\right|}{V^{(\ell+1)}}, \tag{1.34}$$

defines the error condition. Noting $[K_G^{(0)}] \equiv [0] \equiv$ null matrix, a zero error for $\ell = 1$ implies the system is capable of an eigensolution of the form in (1.25). Finally, the resulting free-response for a system subject to static preload is represented by:

$$\left[[K + K_G] - \omega^2[M]\right]\{U\} = \{0\}. \tag{1.35}$$

The geometric nonlinearity matrix no longer carries an iteration superscript. This signifies that it is assumed constant for small vibrations about the nonlinear, statically deformed position.

For problems involving rotation, the destabilizing effects of centrifugal softening *may* be canceled exactly by tensile geometric nonlinearities [19]. To allow for this possibility, the centrifugal softening and initial geometric nonlinearity matrices must be introduced concurrently into the nonlinear static iteration. Therefore:

$$\left\{U_S^{(1)}\right\} = [K]^{-1}\{R + R_\Omega\}, \text{ then} \tag{1.36a}$$

$$\left[K_G^{(\ell)}\right] = \left[K_G^{(\ell)}\left(\left\{U_S^{(\ell)}\right\}\right)\right], \text{ and} \tag{1.36b}$$

$$\left\{U_S^{(\ell+1)}\right\} = \left[K + K_S + K_G^{(\ell)}\right]^{-1}\{R + R_\Omega\}, \text{ for} \tag{1.36c}$$

$$\ell \geq 1, \text{ where} \tag{1.36d}$$

$$V^{(\ell)} = \frac{1}{2}\left\{U_S^{(\ell)}\right\}^T\left[K + K_S + K_G^{(\ell-1)}\right]\left\{U_S^{(\ell)}\right\}. \tag{1.36e}$$

The resulting dynamic eigenproblem with combined geometric nonlinearities and rotating coordinate system effects is:

$$[[K + K_S + K_G] + i\omega[C] - \omega^2[M]]\{U\} = \{0\}. \tag{1.37}$$

Observe that $[K_G]$ is not necessarily hierarchic in the sense that the matrix associated with the n-dof system may change when additional θ_j's are included. Thus, the Sturm sequence property for the natural frequencies (1.11) does not apply. As n increases, the approximate natural frequencies (and strain energy) will still approach the exact values asymptotically, but not necessarily monotonically or from above. This condition is detrimental to the estimation of the discretization error for nonlinear systems.

1.2 SCOPE OF RESEARCH

Within the context of the previous discussion, the goal of this research is:

Establish a general-purpose, p-version, finite element capability for the static and dynamic analysis of a large class of elastic beam problems.

The major focus of the research is to explore the ramifications of the p-version on eigenproblems. Particular objectives pertaining to the fundamental goal are discussed in the following paragraphs. The brief list of references included in this introduction will be expanded as the topics are developed.

Objective 1: *Develop elemental formulations for untapered, straight and circular beams in three-dimensional space with provisions for hierarchic extensions of the polynomial shape functions.* Chapters 3 and 4 detail the elemental formulations. Chapter 7 addresses the construction of the hierarchic finite element spaces for the developed formulations. Hierarchic extensions have been applied previously to straight Bernoulli-Euler beam elements which are both untapered [20,21] and tapered [22]. Some aspects of the hierarchic approach have also been incorporated in straight, untapered Timoshenko beam elements [23]. Tapered beam elements are excluded from this research but may be developed based on the formulations presented.

Circular p-version beam elements are a new development and reflect the desire to minimize the number of elements necessary to capture the problem geometry. Higher-order functions have been used previously for shape functions in static [24,25] and dynamic [26] arch problems, but not in the context of p-extensions. An "arch" is defined for the purposes of this text as a circular beam with displacements confined to the plane of the arc.

Objective 2: *Formulate beam elements using Bernoulli-Euler, Rayleigh, and Timoshenko idealizations.* This objective addresses the need to quantify the

errors in idealization by providing the complete hierarchy of theories for "engineering" beam elements. Chapter 2 expands on the characterization of beams and fully discusses the assumptions and limitations. The rigorous set of assumptions leading to the various idealizations are presented in Chapters 3 and 4.

Objective 3: *Incorporate first-order geometric nonlinearities and rotating coordinate system effects.* The primary motivation for including static analyses was to be able to incorporate geometric nonlinearities into the dynamic eigenproblem. However, the static capability soon proved invaluable in verifying the strain energy formulations and extracted engineering quantities. Complete formulation of the geometric nonlinearities for three-dimensional circular beams is a new development. Chapter 6 provides details of these formulations.

The vibrational behavior of rotating beams plays an important role in the design of shafts, turbine blades, propellers, satellite booms, and so on. Again, previous developments of rotating coordinate effects have been limited to straight h-version elements [27,28] and often have restrictions on the spin axis. The rotating coordinate system effects are incorporated directly into the kinetic energy formulations of Chapter 4.

Objective 4: *Develop a rational hierarchy of curvature approximations for the definition of circular beam properties.* This objective results from the desire to compare and correlate the developed formulations with those found in the literature. This research presents the effect of these approximations for the first time and helps to explain some previously confusing results. Chapter 5 is devoted exclusively to this objective.

Objective 5: *Apply error estimation and quality control techniques for p-version finite elements to eigenproblems.* Error estimation based on energy norm is well established for displacement formulations. The error in energy norm is

closely related to the root-mean-square measure of error in stresses [29], and eigenvalues are quite easily related to strain energy. This forms the basis for evaluating the errors of discretization for eigenproblems. Refer to Chapter 8 for the theoretical discussion.

Objective 6: *Explore algorithmic enhancements for sequential eigensolutions of problems utilizing hierarchic extensions.* Eigensolvers require iteration to extract the desired information to some prescribed level of accuracy. For methods such as subspace iteration [30], the number of iterations depends significantly on the initial estimate of the solution. This research documents the benefits of utilizing the previous eigensolution to reduce the number of iterations required to solve the next eigenproblem in a hierarchic sequence. Chapter 8 provides the necessary information for implementation.

The theoretical formulations developed in this research are implemented into the "**p**-Version Analysis of Elastic Beams" (PVAEB) computer program. PVAEB is a fully self-contained code written in VAX-11 FORTRAN (V5.1-10). The NASTRAN-like model input is described in Appendix 14.1. Chapters 8-10 document sample problems which illustrate and verify the program performance.

The primary motivation for this research is the evaluation of vertical-axis wind turbines. Chapter 11 provides a complete analysis for this type of structure.

2. CHARACTERIZATION OF BEAMS

The study of beams encompasses a formidable assortment of perspectives and approaches. Perusal of the nearly boundless collection of literature only serves to cloud the simple perception enjoyed by most engineers. By necessity, any research related to beams must be focused on a small portion of this ever-expanding field.

A fundamental step in pursuing beam research is the explicit definition of the beam characteristics to be used in the analysis. More accurately, it is the choosing of a collection of assumptions and limitations which serve as a framework for the formulations. For this research, the chosen limitations are identified and discussed below. They have been collectively designated as the assumptions leading to an "engineering" beam formulation due to their reliance on the classical strength of materials approach. A large number of formulations are based, at least implicitly, on these assumptions.

Application of *a priori* simplifications to a more general formulation presents a serious dilemma. Historically, this approach has been adopted to render a problem analytically manageable while maintaining sufficient accuracy of the desired results. Classical beam, plate, and shell theories may all be derived (with difficulty) by imposing simplifying assumptions on the equations of three-dimensional elasticity, which is itself formulated with implicit assumptions on the strain/displacement and stress/strain relationships. The shortcoming of this approach is that the errors of idealization associated with these simplifications are impractical, if not impossible, to quantify.

The computer era has spawned a reevaluation of the classical theories. In particular, the concept of hierarchic *formulations* is beginning to emerge [6,29].

Simply stated, this concept proposes to delay the application of simplifying assumptions until *after* the problem has been posed in a more general formulation. The classical theories may be viewed as lower-order approximations of the general formulation. Extensions within the hierarchy of formulations then allow the errors of idealization to be addressed and the applicability of the classical theories to be ascertained.

A more restrictive hierarchy already exists within the formulations for engineering beams. Some assumptions are imposed immediately to produce the Timoshenko beam idealization from the three-dimensional theory of elasticity. Further simplifications are then introduced for the Rayleigh and Bernoulli-Euler idealizations. The initial assumptions allow conventional beam cross-sectional properties to be used in the definition of ensuing models; this was a precondition imposed on the formulations in this study. However, these same simplifications preclude the extension of formulations to the underlying three-dimensional theory. This compromise was deemed acceptable for the class of problems and analytical objectives addressed in this research.

The engineering beam is characterized by a line which defines the beam axis. This axis may be straight or circular for the formulations presented. The cross-sectional properties are defined in the plane normal to the beam axis and with respect to the beam axis. All material points within such a plane are rigidly linked to the point of the beam axis that intersects the plane. Thus, the cross sections remain plane though not necessarily normal to the beam axis. This assumption was first postulated by Jacob Bernoulli (1654-1705) even prior to a thorough understanding of the neutral axis and moments of inertia [31].

The rigid planes imply that all cross-sectional movements can be related to the displacements and rotations of the intersecting point on the beam axis. For

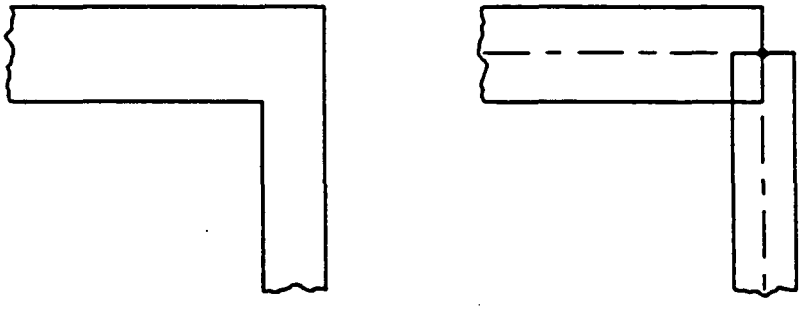

Physical Model *Beam Idealization*

Figure 2.1 Idealization of a reentrant corner using engineering beams.

two-dimensional problems, two displacements and one rotation may exist. Three displacements and three rotations are possible for problems in three-dimensional space. Furthermore, it is assumed that the rotations are "small." The ramifications of this limitation will be expanded on in Section 2.2.

The cross-sectional dimensions are assumed small in comparison to the length of the beam axis. Thus, engineering beams utilize a linear, one-dimensional stress/strain law in the direction of the beam axis, based on the assumption that Poisson ratio effects are negligible (see Chapter 3). This is the significant limitation, when coupled with the previously defined displacement assumptions, that prohibits the hierarchic extension of beam formulations to the general three-dimensional theory.

The assumptions for engineering beams may be better visualized by the sample problem in Figure 2.1. Engineering beams allow nontangential intersections of the beam axes for adjoining elements. Discontinuous changes in the cross-sectional properties between elements (and possibly within elements) is also allowed. The beam axis displacements and rotations and the system strain energy

and natural frequencies are assumed to be minimally affected by the beam idealization. Force and moment transfer between such elements poses no problem but details, such as the stress concentration within the reentrant corner in Figure 2.1, cannot be quantified. Thus, the benefits of modeling ease and flexibility are offset by limitations on the types of information which can be accurately extracted from the solution. The engineer must recognize whether the desired objectives of the analysis are affected by these limitations.

Obviously, there is a variety of idealizations which do not prescribe to all or some of the assumptions for engineering beams. Characteristics of "extended" engineering beams may include, for example:

1) adoption of nonlinear material laws,
2) generalization to moderate or large rotations,
3) inclusion of additional "warping" degrees-of-freedom defined over the cross section, and
4) utilization of two- or three-dimensional linear stress/strain laws.

As will be seen in Section 2.2, large deformation analyses are fundamentally nonlinear and, thus, not able to be formulated as a linear eigenproblem. Yet, large deformations are necessary in accurately evaluating such problems as modern helicopter rotors. References 32 and 33 provide an excellent introduction into this class of problem.

Warping terms have been used extensively to improve the accuracy of beam analyses. Correction factors which are incorporated into the engineering beam formulations may be quantified with the aid of warping-type analyses. These correction factors will be identified and discussed as they appear in the beam formulations. Both Krishna Murty [34] and Levinson [35] have included warping terms in evaluating straight, rectangular beam vibrations. Gardner and Bert [36]

applied the same principle to the in-plane, dynamic analysis of rings with rectangular cross sections. Lincoln and Volterra [37] coupled hierarchic displacement assumptions (including warping) with three-dimensional stress/strain relationships in an eigenanalysis of toroids.

Warping degrees-of-freedom cannot be included without an associated sacrifice in generality. Analyses are practically, if not theoretically, restricted to the most elementary of cross-sectional shapes. Interelement tangency is typically required, as are continuous changes in cross-sectional properties. Such limitations were deemed too restrictive for inclusion in this research, the focus being on the class of problems and types of information for which warping effects are insignificant.

2.1 DEFINITION OF BEAM PROPERTIES

The cross-sectional properties of beams have been briefly mentioned in the previous discussion. This section is devoted to their definition. Explicit assumptions and limitations of the beams considered in this research are identified.

Figures 2.2 and 2.3 illustrate generic straight and circular beam elements and the conventions used throughout these formulations. The x-axis serves as the beam axis as previously defined and coincides with the center of area (centroid) of each cross-sectional slice for both the straight and circular beams. The y- and z-axes represent the in-plane and out-of-plane directions, respectively. The arc of a circular element, defined by the constant radius, R, is contained within the xy-plane. Note that the orientation of the local x- and y-axes varies along the length of the circular beam such that:

$$y = r - R, \tag{2.1}$$

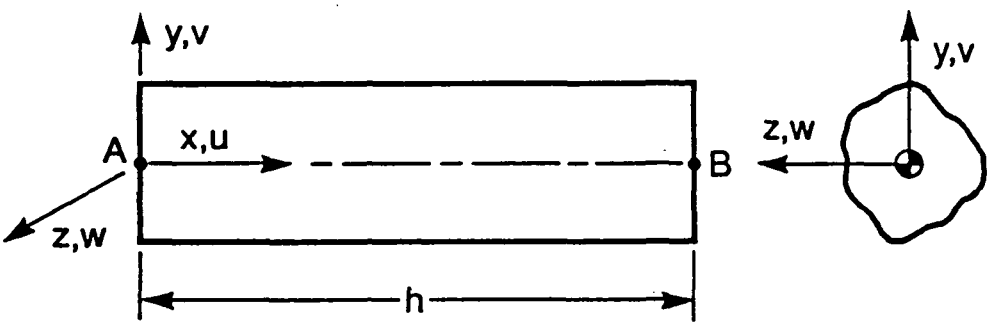

Figure 2.2 Generic straight beam element.

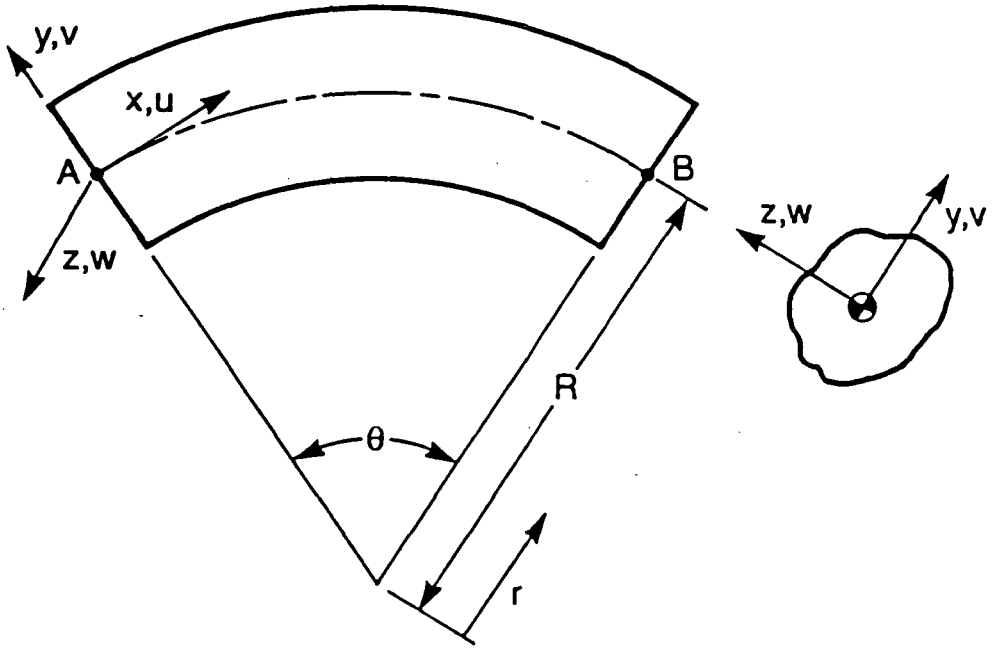

Figure 2.3 Generic circular beam element.

as depicted in Figure 2.3. The length of the beam element is defined by:

$$h = \int_{x_A}^{x_B} dx, \tag{2.2}$$

where A and B refer to the ends of the beam element. For circular beams, this equates to:

$$h = R\theta. \tag{2.3}$$

The cross-sectional area of the elements is defined as:

$$A = \iint dydz. \tag{2.4}$$

The material density, ρ, is assumed constant such that the mass per unit length may be represented by:

$$m = \rho A. \tag{2.5}$$

A constant material density implies that the center of mass coincides with the centroid for straight, but *not* circular, beams. The curvature-induced shift in the center of mass for circular beams will be addressed shortly. For now, the centroidal position of the beam axis implies:

$$\bar{y} = \iint ydydz \equiv 0, \text{ and} \tag{2.6a}$$

$$\bar{z} = \iint zdydz \equiv 0. \tag{2.6b}$$

Area moments of inertia are defined by:

$$I_{yy} = \iint y^2 dydz, \tag{2.7a}$$

$$I_{zz} = \iint z^2 dydz, \text{ and} \tag{2.7b}$$

$$I_{yz} = \iint yzdydz \equiv 0. \tag{2.7c}$$

Therefore, the y- and z-axes are assumed to coincide with the principal axes of the cross section. The torsional stiffness is specified separately:

$$I_0 \neq I_{yy} + I_{zz}, \tag{2.8}$$

in keeping with the Saint-Venant theory of torsion for noncircular cross sections [38]. Mass moments of inertia per unit length are defined by:

$$J_{yy} = \rho I_{yy}, \tag{2.9a}$$

$$J_{zz} = \rho I_{zz}, \text{ and} \tag{2.9b}$$

$$J_0 = J_{yy} + J_{zz}. \tag{2.9c}$$

For circular beams, additional terms arise in the energy formulations as a result of curvature. The center of mass in terms of radius may be computed from:

$$\bar{r}_m \equiv \frac{\rho \iiint r(rd\theta)(dr)(dz)}{\rho \iiint (rd\theta)(dr)(dz)}. \tag{2.10}$$

Substituting in the local beam coordinates and eliminating common factors from the numerator and denominator result in:

$$\bar{r}_m = \frac{\iiint (R+y)^2 \, dxdydz}{\iiint (R+y) dxdydz}. \tag{2.11}$$

Substituting in the previously defined cross-sectional properties produces:

$$\bar{r}_m = \frac{\int \left(AR^2 + I_{yy}\right) dx}{\int (AR) dx}, \tag{2.12}$$

such that:

$$\bar{r}_m = R + \frac{I_{yy}}{AR}, \text{ or} \tag{2.13a}$$

$$\bar{y}_m = \frac{I_{yy}}{AR}. \tag{2.13b}$$

There is no corresponding shift of the center of mass in the z-direction since the cross-sectional axes and principal axes coincide.

Additional pseudo-moments of area result from the circular-beam curvature. Using the convention of Bickford and Maganty [39], they are defined by:

$$I_{ij} \equiv \iint \left(\frac{R}{R+y}\right) y^i z^j dydz, \quad i,j = 0,1,2. \tag{2.14}$$

These terms will be discussed in detail in Chapter 5. Also, the mass moments:

$$J_{yyy} = \rho \iint y^3 dydz \equiv \rho I_{yyy}, \tag{2.15a}$$

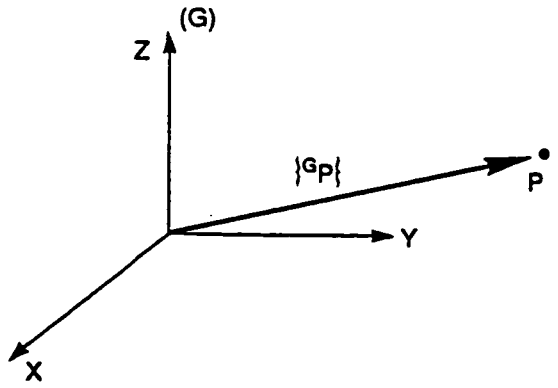

Figure 2.4 Vector relative to a frame.

$$J_{yyz} = \rho \iint y^2 z dy dz \equiv \rho I_{yyz}, \text{ and} \tag{2.15b}$$

$$J_{yzz} = \rho \iint y z^2 dy dz \equiv \rho I_{yzz}, \tag{2.15c}$$

will enter into the kinetic energy formulation for circular beams.

2.2 SMALL ROTATION APPROXIMATION

The kinematics of engineering beams is rarely discussed in the literature. The assumption of small rotations, especially in three-dimensional space, receives little more than a token mention. However, the inclusion of circular beams and rotating coordinate system effects in this research mandates a more rigorous understanding of beam kinematics. This section focuses on the application and significance of the small rotation approximation. Also, it provides the necessary framework for incorporating rotating coordinate system effects.

Displacements are nothing more than changes in position, and velocities are the time derivatives of displacements. Assuming that a global coordinate system has been established, any spatial point can be located by a three-coordinate position vector. Figure 2.4 illustrates the position of a point, P, in an orthogonal,

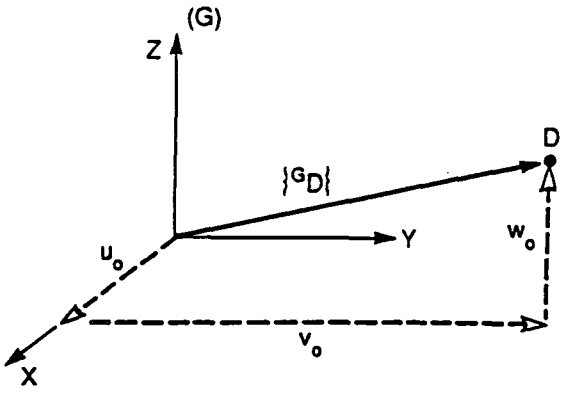

Figure 2.5 Orthogonal displacement sequence.

right-handed frame, (G). Its position is defined as:

$$\{\hat{e}_G\}^T \{{}^G P\} = \lfloor \hat{e}_X, \hat{e}_Y, \hat{e}_Z \rfloor \begin{Bmatrix} p_X \\ p_Y \\ p_Z \end{Bmatrix}, \tag{2.16}$$

where p_X, p_Y, and p_Z are the position coordinates and $\hat{e}_X$, $\hat{e}_Y$, $\hat{e}_Z$ are unit vectors in the direction of their respective global axes. The leading superscript denotes the frame in which the position is defined.

Now, consider the following displacement sequence illustrated in Figure 2.5:

Start with a point, D, located at the origin of a known frame, (G). First, displace D along X by a distance, u_0, then displace D along Y by a distance, v_0, and finally displace D along Z by a distance, w_0.

The final position is defined by:

$$\{{}^G D\} = \begin{Bmatrix} u_0 \\ 0 \\ 0 \end{Bmatrix} + \begin{Bmatrix} 0 \\ v_0 \\ 0 \end{Bmatrix} + \begin{Bmatrix} 0 \\ 0 \\ w_0 \end{Bmatrix} = \begin{Bmatrix} u_0 \\ v_0 \\ w_0 \end{Bmatrix}. \tag{2.17}$$

The important feature to note is that displacements are governed by the commutative law of vector addition; the displacements may be performed in any order

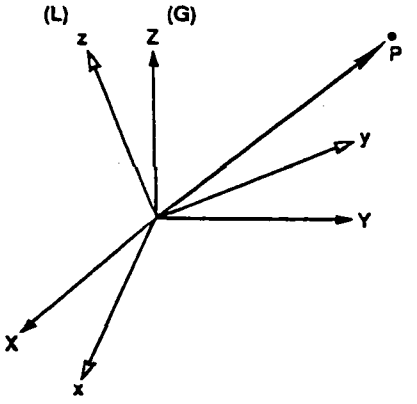

Figure 2.6 Frames with different orientations.

and the final position will be the same. The velocity of the point relative to the global frame and defined in the global frame is:

$$\left\{ {}^{G}v^{D/G} \right\} = \begin{Bmatrix} \dot{u}_0 \\ \dot{v}_0 \\ \dot{w}_0 \end{Bmatrix}. \tag{2.18}$$

This is the absolute velocity of the point only if the global frame is stationary. Absolute velocities are represented without a relative superscript, such as $\{{}^{G}v^{D}\}$ for the case of (2.18) when the global frame is stationary.

In a similar fashion, rotations are nothing more than changes in orientation, and angular velocities are the time derivatives of rotations. Orientation describes the relationship between two frames as seen in Figure 2.6:

$$\begin{Bmatrix} \hat{e}_x \\ \hat{e}_y \\ \hat{e}_z \end{Bmatrix} = \begin{bmatrix} t_{xX} & t_{xY} & t_{xZ} \\ t_{yX} & t_{yY} & t_{yZ} \\ t_{zX} & t_{zY} & t_{yZ} \end{bmatrix} \begin{Bmatrix} \hat{e}_X \\ \hat{e}_Y \\ \hat{e}_Z \end{Bmatrix}, \text{ or} \tag{2.19a}$$

$$\{\hat{e}_L\} = [{}^{L}_{G}T]\,\{\hat{e}_G\}, \tag{2.19b}$$

where $\hat{e}_x$, $\hat{e}_y$, and $\hat{e}_z$ are unit vectors in the direction of their respective local axes and $[{}^{L}_{G}T]$ is referred to as the rotation matrix or transformation matrix from the global frame, (G), to the local frame, (L). The leading subscript and superscript define the direction of the transformation.

The transformation matrix as defined in (2.19) is made up of the cosines of the angles between the local and global unit vectors, namely:

$$[{}^L_G T] = [{}^L_G t_{iJ}] = \hat{e}_i \cdot \hat{e}_J, \quad i = x, y, z, \; J = X, Y, Z. \tag{2.20}$$

Thus, the individual columns (or rows) within the rotation matrix are orthonormal and the transpose of the matrix is also its inverse [40]:

$$[{}^G_L T] = [{}^L_G T]^{-1} \equiv [{}^L_G T]^T, \text{ or} \tag{2.21a}$$

$$[{}^L_G T]\,[{}^L_G T]^T \equiv [I], \tag{2.21b}$$

where $[I]$ is the identity matrix. Adding the restriction that all frames are right-handed [41]:

$$\det [{}^G_L T] \equiv 1, \tag{2.22}$$

the necessary and sufficient conditions for $[{}^G_L T]$ to be a rotation matrix are given by (2.21) and (2.22). Therefore, only three of the nine equations in (2.20) are independent.

Transformation matrices allow the position of a point, P, specified in one frame, (L), to be related to the position with respect to a second frame, (G), with the same origin. Transposing (2.19) with the help of (2.21):

$$\{\hat{e}_L\}^T = \{\hat{e}_G\}^T [{}^G_L T], \tag{2.23}$$

then:

$$\{\hat{e}_L\}^T \{{}^L P\} = \{\hat{e}_G\}^T [{}^G_L T] \{{}^L P\} = \{\hat{e}_G\}^T \{{}^G P\}, \tag{2.24}$$

or (see Figure 2.6):

$$\{{}^G P\} = [{}^G_L T] \{{}^L P\}. \tag{2.25}$$

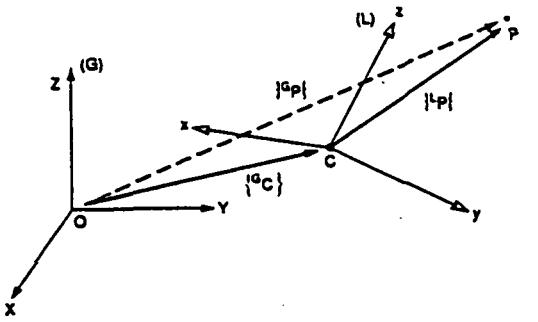

Figure 2.7 General transform of a vector.

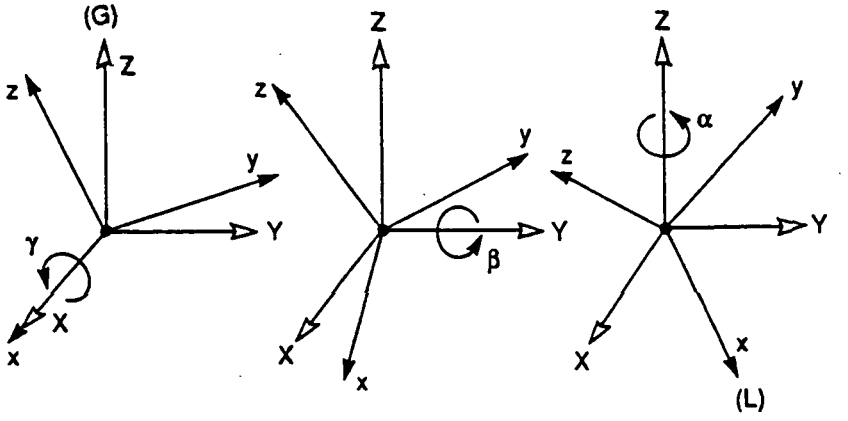

Figure 2.8 Roll, pitch, yaw rotation sequence.

When the origins of the two frames are not coincident, the position transformation may be represented as:

$$\{^G P\} = \{^G C\} + [{}^G_L T]\,\{^L P\}\,, \text{ or} \tag{2.26a}$$

$$\left\{^{L/G} P\right\} = [{}^L_G T]\,\{^G P\} = [{}^L_G T]\,\{^G C\} + \{^L P\}\,. \tag{2.26b}$$

The latter equation defines the position of the point in the global frame but in terms of local coordinates. This situation is depicted in Figure 2.7.

Now, consider the following rotation sequence illustrated in Figure 2.8:

Start with a frame, (L), coincident with a known frame, (G). First, rotate (L) about X by an angle, γ, then rotate (L) about Y by an angle, β, and then rotate (L) about Z by an angle, α.

Craig [42] has shown that these three rotation operators may be combined such that the overall transformation matrix is:

$$[{}^{G}_{L}T] = \begin{bmatrix} c\alpha & -s\alpha & 0 \\ s\alpha & c\alpha & 0 \\ 0 & 0 & 1 \end{bmatrix} \begin{bmatrix} c\beta & 0 & s\beta \\ 0 & 1 & 0 \\ -s\beta & 0 & c\beta \end{bmatrix} \begin{bmatrix} 1 & 0 & 0 \\ 0 & c\gamma & -s\gamma \\ 0 & s\gamma & c\gamma \end{bmatrix}, \text{ or} \tag{2.27a}$$

$$[{}^{G}_{L}T] = \begin{bmatrix} c\alpha c\beta & c\alpha s\beta s\gamma - s\alpha c\gamma & c\alpha s\beta c\gamma + s\alpha s\gamma \\ s\alpha c\beta & s\alpha s\beta s\gamma + c\alpha c\gamma & s\alpha s\beta c\gamma - c\alpha s\gamma \\ -s\beta & c\beta s\gamma & c\beta c\gamma \end{bmatrix}, \tag{2.27b}$$

where the shorthand notation:

$$c\alpha = \cos\alpha, \tag{2.28a}$$

$$s\alpha = \sin\alpha, \text{ etc.}, \tag{2.28b}$$

is used. This rotation sequence is known as the "roll, pitch, yaw convention," where γ, β, and α are the roll, pitch and yaw angles, respectively, with respect to a fixed coordinate system. Other conventions [32,42] have been formulated to meet specific analytical needs.

Comparison of (2.17) with (2.27) illustrates the fundamental differences between displacements and rotations. Matrix multiplication is not commutative; thus, the rotations for (2.27) must be performed in the specified order. Furthermore, the presence of trigonometric functions indicates the fundamentally nonlinear nature of nominal rotations.

The assumption of small rotations may now be applied with a better understanding of its implications. If the roll, pitch, and yaw angles are small, they may be represented by the first terms of their series expansions, namely:

$$\cos\alpha = 1 + O\left(\alpha^2\right), \tag{2.29a}$$

$$\sin\alpha = \alpha + O\left(\alpha^3\right), \text{ etc.}, \tag{2.29b}$$

where $O(\alpha^n)$ is the order notation used to represent an expression which approaches zero at least as fast as a fixed multiple of α^n as $\alpha \to 0$. Inserting the small angle approximation into (2.27) produces:

$$[{}^G_L T] \cong \begin{bmatrix} 1 & -\alpha & 0 \\ \alpha & 1 & 0 \\ 0 & 0 & 1 \end{bmatrix} \begin{bmatrix} 1 & 0 & \beta \\ 0 & 1 & 0 \\ -\beta & 0 & 1 \end{bmatrix} \begin{bmatrix} 1 & 0 & 0 \\ 0 & 1 & -\gamma \\ 0 & \gamma & 1 \end{bmatrix}, \text{ or} \tag{2.30a}$$

$$[{}^G_L T] \cong \begin{bmatrix} 1 & -\alpha & \beta \\ \alpha & 1 & -\gamma \\ -\beta & \gamma & 1 \end{bmatrix}. \tag{2.30b}$$

Thus, small rotations allow for linearization of the transformation matrix *and* make the order in which the rotations are applied insignificant.

It is interesting to note that, for the roll, pitch, yaw rotation sequence, the angular velocity of the local frame relative to the global frame and expressed in global variables is:

$$\left\{ {}^G\Omega^{L/G} \right\} = \begin{Bmatrix} \dot{\gamma} \\ \dot{\beta} \\ \dot{\alpha} \end{Bmatrix}. \tag{2.31}$$

$\{{}^G\Omega^L\}$ would represent the absolute velocity of the local frame defined in global coordinates, and $\{{}^G\Omega^{L/G}\} = \{{}^G\Omega^L\}$ only if the global frame is stationary. Note that no small rotation assumptions are necessary for the relation in (2.31); angular velocities are much easier to characterize than orientations.

2.3 DEFINITION OF BEAM DISPLACEMENTS AND ROTATIONS

For engineering beams, all cross-sectional movements are related to the displacements and small rotations of the corresponding point on the beam axis. These movements may be defined relative to the beam coordinate system and will be related to the global system at a later time. The beam axes as defined allow for the same displacements and rotations to be used for both straight and circular beams. These may now be defined with reference to Figures 2.2 and 2.3.

For planar problems, the displacements of all material points may be defined to be parallel to the global XY-plane *and* the local xy-plane. The beam axis is limited to axial and transverse displacements, u_0 and v_0, respectively, and a rotation coincident with the local z-axis, u_y. A positive u_y rotation is assumed to provide a positive u displacement for all material points above the z-axis such that the complete, planar, material point displacement may be defined as:

$$u(x,y,t) = u_0(x,t) + yu_y(x,t), \text{ and} \tag{2.32a}$$

$$v(x,t) = v_0(x,t). \tag{2.32b}$$

Note that time is defined as an independent variable, consistent with an assumed-modes formulation. A simple example of warping terms in a planar problem would be:

$$u(x,y,t) = \sum_{j=0}^{n} y^j u_j(x,t), \quad n > 1, \text{ and} \tag{2.33a}$$

$$v(x,t) = v_0(x,t). \tag{2.33b}$$

For general problems in three dimensions, out-of-plane displacement, w_0, axial rotation, ϕ_1, and a rotation coincident with the local y-axis, u_z, are added to the planar terms. No distinction will be made between the planar variables and their identical three-dimensional counterparts. Thus:

$$u(x,y,z,t) = u_0(x,t) + yu_y(x,t) + zu_z(x,t), \tag{2.34a}$$

$$v(x,z,t) = v_0(x,t) - z\phi_1(x,t), \text{ and} \tag{2.34b}$$

$$w(x,y,t) = w_0(x,t) + y\phi_1(x,t). \tag{2.34c}$$

Note that the axial rotation is assumed to occur about the beam axis. This implies that the center of twist (or shear via reciprocity) coincides with the

centroid, which is strictly true only for straight beams with doubly-symmetric cross sections. However, no such restrictions were enforced in this research.

It is worthy to note the three-dimensional displacements (2.34) with the planar variables (u_0, v_0, and u_y) omitted:

$$u(x,z,t) = zu_z(x,t), \tag{2.35a}$$

$$v(x,z,t) = -z\phi_1(x,t), \text{ and} \tag{2.35b}$$

$$w(x,y,t) = w_0(x,t) + y\phi_1(x,t). \tag{2.35c}$$

Note that rotation-induced planar displacements still exist. However, for a large class of three-dimensional problems, the planar response characterized by (2.32) and the "out-of-plane" response characterized by (2.35) uncouple. This can be very beneficial from the computational point of view. Problems with Coriolis coupling *cannot* be treated in this manner.

3. STRAIN ENERGY FORMULATION FOR BEAMS

This chapter develops the strain energy formulations for straight and circular engineering beam elements. These formulations are rigorously presented in order of increasing complexity, from planar straight beams to three-dimensional circular beams. This allows for a convenient discussion and consistent application of the underlying assumptions for engineering beams.

3.1 PLANAR FORMULATION FOR STRAIGHT BEAMS

Given that the assumed beam displacements and rotations have been defined in Chapter 2, the steps leading to the definition of strain energy are:

1) definition of strain/displacement relationships,
2) definition of the stress/strain relationships, and
3) integration of the strain energy in terms of known cross-sectional properties (2.4, 2.6-8, and 2.14) and additional corrective constants.

The linear strain/displacement relations assume infinitesimal deformations [43]. In a Cartesian coordinate system, they are defined by:

$$\epsilon_x = \frac{\partial u}{\partial x}, \tag{3.1a}$$

$$\epsilon_y = \frac{\partial v}{\partial y}, \tag{3.1b}$$

$$\epsilon_z = \frac{\partial w}{\partial z}, \tag{3.1c}$$

$$\gamma_{xy} = \frac{\partial u}{\partial y} + \frac{\partial v}{\partial x}, \tag{3.1d}$$

$$\gamma_{yz} = \frac{\partial v}{\partial z} + \frac{\partial w}{\partial y}, \text{ and} \tag{3.1e}$$

$$\gamma_{zx} = \frac{\partial w}{\partial x} + \frac{\partial u}{\partial z}. \tag{3.1f}$$

Applying the planar displacement assumptions (2.32) results in:

$$\epsilon_x = u_0' + y u_y', \tag{3.2a}$$

$$\gamma_{xy} = u_y + v_0' = (\gamma_{xy})_{F_y}, \text{ and} \tag{3.2b}$$

$$\epsilon_y = \epsilon_z = \gamma_{yz} = \gamma_{zx} = 0, \tag{3.2c}$$

where $' \equiv \partial/\partial x$ and the F_y subscript denotes those terms associated with the shear force in the y-direction. The stress/strain relationships assume a linearly elastic, isotropic material. The three-dimensional strains in terms of the stresses are:

$$\epsilon_x = \frac{1}{E}\Big[\sigma_x - \nu(\sigma_y + \sigma_z)\Big], \tag{3.3a}$$

$$\epsilon_y = \frac{1}{E}\Big[\sigma_y - \nu(\sigma_z + \sigma_x)\Big], \tag{3.3b}$$

$$\epsilon_z = \frac{1}{E}\Big[\sigma_z - \nu(\sigma_x + \sigma_y)\Big], \tag{3.3c}$$

$$\gamma_{xy} = \frac{\tau_{xy}}{G}, \tag{3.3d}$$

$$\gamma_{yz} = \frac{\tau_{yz}}{G}, \text{ and} \tag{3.3e}$$

$$\gamma_{zx} = \frac{\tau_{zx}}{G}, \tag{3.3f}$$

where E is the elastic modulus, ν is Poisson's ratio, and $G \equiv E/[2(1+\nu)]$ is the shear modulus. These material properties are assumed constant within each beam element.

The assumption of the rigid cross-sectional planes suggests the existence of normal stresses within the local yz-plane, σ_y and σ_z, which are assumed to be zero in the engineering beam theories. Alternatively, defining $\sigma_y = \sigma_z = 0$ implies cross-sectional strains which cannot be characterized by differentiation of the assumed displacements. To allow for this contradiction, a one-dimensional

stress/strain law must be adopted in conjunction with the assumed beam displacements, namely:

$$\sigma_x = E\epsilon_x, \tag{3.4}$$

which in effect is the axial stress/strain law if Poisson's ratio is zero. Note, however, that $\nu \not\equiv 0$ is still used in the interrelationship between the elastic and shear moduli.

The idealized shear stress for the planar beam presents a similar conflict. Equations 3.2*b* and 3.3*d* imply a constant shear stress over the entire cross section. However, this violates the requirement that the exact shear stress normal to the perimeter of the cross section be identically zero (in the absence of shear tractions). The net result of this idealization is an overestimation of the shear *stiffness*, which may be reduced by the introduction of a shear correction coefficient, $k_y < 1$. This (assumed) constant does not correct the erroneous shear stress distribution but, for the sake of introducing the factor into the formulation, merely reduces the stiffness relating the integrated shear force to the (constant) idealized shear deformation for any given cross section. Therefore:

$$k_y \equiv \frac{\iint (\tau_{xy})_{F_y} dydz}{\left(G \iint (\gamma_{xy})_{F_y} dydz\right)_{TI}} = \frac{F_y}{GA(u_y + v_0')}, \text{ or} \tag{3.5a}$$

$$Gk_yA \equiv \frac{F_y}{u_y + v_0'}, \tag{3.5b}$$

where the *TI* subscript denotes the Timoshenko beam idealization and Gk_yA is the effective shear stiffness.

Stephen P. Timoshenko is generally credited with identifying the effect of shear deformations on beam vibrations and introducing the shear correction constant [44]. The shear coefficient is primarily a function of the cross section, and Timoshenko's original paper spawned much research into its proper definition

and quantification. Equation 3.5 is the most common means of introducing the factor, but it is neither unique nor particularly useful in quantifying the constant. Two typical approaches for estimating the coefficient involve matching shear wave velocities of beams [45] and applying simplifying assumptions within the linear theory of elasticity [46,47]. Cowper's approach is often cited due to its ability to handle complex cross sections, but its formulation is based on slightly different definitions of the displacements and correction factor [47]. Hutchinson's comparison between exact and approximate solutions for beams of circular cross section clearly confirms earlier findings that the shear coefficient is also a function of Poisson's ratio and diminishes with increasing frequency [48].

The general definition of strain energy is [49]:

$$V = \frac{1}{2}\iiint (\sigma_x\epsilon_x + \sigma_y\epsilon_y + \sigma_z\epsilon_z + \tau_{xy}\gamma_{xy} + \tau_{yz}\gamma_{yz} + \tau_{xz}\gamma_{xz})\,dxdydz. \tag{3.6}$$

Applying (3.2), (3.4), and (3.5) reduces this to:

$$V_{TI} = \frac{E}{2}\iiint \epsilon_x^2\,dxdydz + \frac{Gk_y}{2}\iiint (\gamma_{xy})^2_{F_y}\,dxdydz, \text{ or} \tag{3.7a}$$

$$V_{TI} = \frac{E}{2}\iiint (u_0' + yu_y')^2\,dxdydz + \frac{Gk_y}{2}\iiint (u_y + v_0')^2\,dxdydz, \tag{3.7b}$$

where the *TI* subscript again refers to Timoshenko beams. Substituting the previously defined cross-sectional properties results in the strain energy for straight, planar, Timoshenko beams:

$$V_{TI} = \frac{EA}{2}\int_0^h (u_0')^2\,dx + \frac{EI_{yy}}{2}\int_0^h (u_y')^2\,dx + \frac{Gk_yA}{2}\int_0^h (u_y + v_0')^2\,dx. \tag{3.8}$$

The individual terms in (3.8) represent extension, bending, and shear energies, respectively. Again, all cross-sectional and material properties are assumed constant over the length of any beam element.

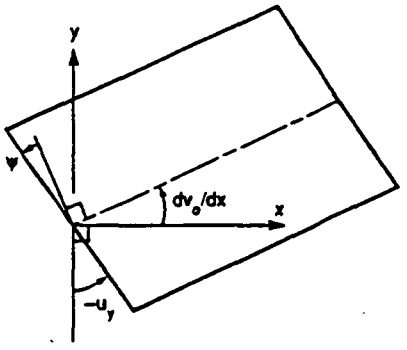

Figure 3.1 Relationship between v_0, u_y, and ψ.

Accounting for variations in nomenclature and sign conventions, this formulation represents the major category of Timoshenko beams with respect to the displacement variables [50]. An alternate representation replaces the cross-sectional rotation, u_y, with the shear deformation angle, ψ. The relationship:

$$\psi = -u_y - v_0', \tag{3.9}$$

is depicted in Figure 3.1. The strain energy in terms of ψ is:

$$V_{TI} = \frac{EA}{2}\int_0^h (u_0')^2 dx + \frac{EI_{yy}}{2}\int_0^h (\psi' + v_0'')^2 dx + \frac{Gk_yA}{2}\int_0^h (\psi)^2 dx. \tag{3.10}$$

However, use of ψ requires care in the specification of boundary conditions for transverse deflections. The pinned condition is enforced in both representations by constraining v_0. The clamped condition involves constraining both v_0 and u_y. Specifying $\psi = 0$ invokes the natural boundary condition of zero shear, which is an improper constraint for the space of admissible functions. Also, generalized moments entering Lagrange's equation (1.14) must be defined with respect to virtual rotations of u_y, not ψ. Reference 50 provides an excellent summary of the various Timoshenko beam representations.

Rayleigh and Bernoulli-Euler beams assume that the strain energy of shear is insignificant in the quantification of transverse vibrations. Ignoring the shear

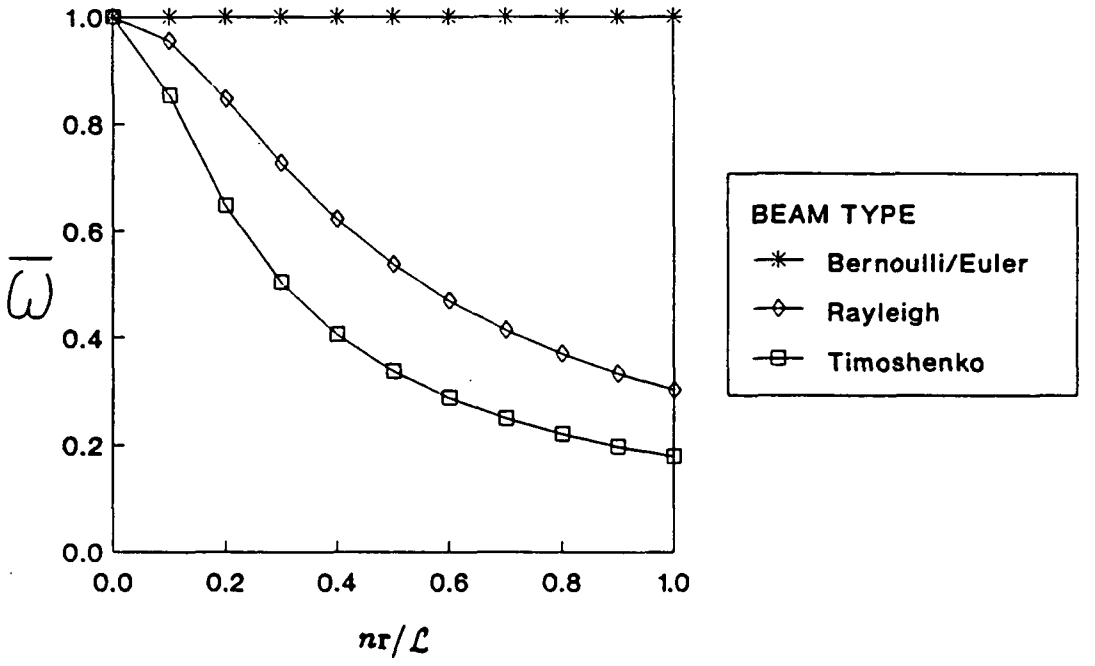

Figure 3.2 Natural frequency comparison for a pinned-pinned beam. The Timoshenko beam results are for $E/k_yG = 3$.

strain energy term in (3.8) implies an infinite shear wave velocity. Additionally, Bernoulli-Euler beams ignore kinetic energy terms involving rotatory inertia (see Chapter 4). For all three beam types, the exact eigensolution for the transverse vibration of a straight beam with pinned ends takes the form:

$$\left(v_0(x,t)\right)_n = C_n \sin\frac{n\pi x}{\mathcal{L}} \cos\omega_n t, \quad n = 1, 2, \ldots, \infty, \tag{3.11}$$

where n is the mode number, C_n are arbitrary constants, and $\mathcal{L}$ is the beam length. Figure 3.2 compares the natural frequencies of the three formulations where [51]:

$$\overline{\omega} = \frac{\omega_n \mathcal{L}^2}{n^2\pi^2 \mathrm{r}}\sqrt{\frac{\rho}{E}}, \text{ and} \tag{3.12a}$$

$$\mathrm{r} = \sqrt{\frac{I_{yy}}{A}} \equiv \text{radius of gyration.} \tag{3.12b}$$

Thus, the Timoshenko beam theory is required for the accurate evaluation of short beams and higher natural frequencies. Note that the natural frequencies

for Timoshenko beams is a function of both $nr/\mathcal{L}$ and E/k_yG. It is more important to note that all three theories converge to the identical limiting frequency as $nr/\mathcal{L} \to 0$. This is the unifying aspect for *all* valid beam formulations.

The "no-shear assumption" (commonly termed the Kirchhoff assumption in the theory of plates and shells) for Rayleigh and Bernoulli-Euler beams involves more than just exclusion of the shear energy term in (3.8). Zero shear energy implies:

$$u_y + v_0' = 0, \text{ or} \tag{3.13a}$$

$$u_y = -v_0'. \tag{3.13b}$$

Thus, the planar rotation can be equated to the slope of the transverse displacement; cross sections remain plane *and* normal to the beam axis. Inserting (3.13) into (3.8) results in:

$$V_{BE/RA} = \frac{EA}{2}\int_0^h (u_0')^2 dx + \frac{EI_{yy}}{2}\int_0^h (v_0'')^2 dx, \tag{3.14}$$

where the *BE* and *RA* subscripts refer to Bernoulli-Euler and Rayleigh beams, respectively. Note that the Timoshenko shear factor no longer enters into this equation.

3.2 THREE-DIMENSIONAL FORMULATION FOR STRAIGHT BEAMS

The strain energy derivation for a straight beam in three dimensions follows the same procedure outlined in Section 3.1. Inserting the displacement assumptions (2.34) into the strain/displacement relations (3.1) results in:

$$\epsilon_x = u_0' + y(u_y') + z(u_z'), \tag{3.15a}$$

$$\gamma_{xy} = (u_y + v_0') - z(\phi_1') = (\gamma_{xy})_{F_y} + (\gamma_{xy})_T, \tag{3.15b}$$

$$\gamma_{xz} = (u_z + w_0') + y(\phi_1') = (\gamma_{xz})_{F_z} + (\gamma_{xz})_T, \text{ and} \tag{3.15c}$$

$$\epsilon_y = \epsilon_z = \gamma_{yz} = 0, \tag{3.15d}$$

where the F_y, F_z, and T subscripts refer to the shear forces in the y- and z-direction and the torque, respectively. Two additional corrective constants must be specified. The Timoshenko shear factor for the out-of-plane direction is defined by the relation:

$$k_z \equiv \frac{\iint (\tau_{xz})_{F_z} dydz}{\left(G \iint (\gamma_{xz})_{F_z} dydz\right)_{TI}} = \frac{F_z}{GA(u_z + w_0')}, \tag{3.16}$$

where k_z may be different from k_y in (3.5) depending on the cross section. The torsional stiffness for straight beams is defined as:

$$I_0 \equiv k_T \iint (y^2 + z^2) dydz = k_T (I_{yy} + I_{zz}). \tag{3.17}$$

The resulting strain energy for a straight Timoshenko beam in three dimensions is:

$$\begin{aligned} V_{TI} = &\frac{E}{2} \int_0^h \left[A(u_0')^2 + I_{yy}(u_y')^2 + I_{zz}(u_z')^2\right] dx \\ &+ \frac{G}{2} \int_0^h \left[k_y A(u_y + v_0')^2 + k_z A(u_z + w_0')^2 + I_0(\phi_1')^2\right] dx. \end{aligned} \tag{3.18}$$

Adding the no-shear assumption in the out-of-plane direction:

$$u_z + w_0' = 0, \text{ or} \tag{3.19a}$$

$$u_z = -w_0', \tag{3.19b}$$

with its in-plane counterpart in (3.13) results in the three-dimensional strain energy for straight Bernoulli-Euler and Rayleigh beams, namely:

$$\begin{aligned} V_{BE/RA} = &\frac{E}{2} \int_0^h \left[A(u_0')^2 + I_{yy}(v_0'')^2 + I_{zz}(w_0'')^2\right] dx \\ &+ \frac{G}{2} \int_0^h I_0(\phi_1')^2 dx. \end{aligned} \tag{3.20}$$

The constant cross-sectional properties are included within the integrals of (3.18) and (3.20) for simplicity. Again, no distinction is made between the comparable variables in the planar and three-dimensional formulations. Note that the assumption of zero shear energy has reduced the number of dependent, three-dimensional displacement variables from six in TI beams to the four found in BE/RA beams.

3.3 PLANAR FORMULATION FOR CIRCULAR BEAMS

With the exception of the strain/displacement and strain energy relationships and constants of integration, the planar formulations for straight and circular beams are identical. Curvature may be taken into account by specifying the strain/displacement relationships in cylindrical coordinates, namely [52]:

$$\epsilon_\theta = \frac{1}{r}\left(\frac{\partial u}{\partial \theta} + v\right) = \frac{R}{R+y}\left(\frac{\partial u}{\partial x} + \frac{v}{R}\right), \tag{3.21a}$$

$$\epsilon_r = \frac{\partial v}{\partial r} = \frac{\partial v}{\partial y}, \tag{3.21b}$$

$$\epsilon_z = \frac{\partial w}{\partial z}, \tag{3.21c}$$

$$\gamma_{\theta r} = \frac{\partial u}{\partial r} - \frac{u}{r} + \frac{1}{r}\frac{\partial v}{\partial \theta} = \frac{\partial u}{\partial y} - \frac{u}{R+y} + \frac{R}{R+y}\frac{\partial v}{\partial x}, \tag{3.21d}$$

$$\gamma_{rz} = \frac{\partial v}{\partial z} + \frac{\partial w}{\partial r} = \frac{\partial v}{\partial z} + \frac{\partial w}{\partial y}, \text{ and} \tag{3.21e}$$

$$\gamma_{z\theta} = \frac{1}{r}\frac{\partial w}{\partial \theta} + \frac{\partial u}{\partial z} = \frac{R}{R+y}\frac{\partial w}{\partial x} + \frac{\partial u}{\partial z}. \tag{3.21f}$$

Substituting the planar displacement assumptions results in:

$$\epsilon_\theta = \left(\frac{R}{R+y}\right)\left[\left(u_0' + \frac{v_0}{R}\right) + y\left(u_y'\right)\right], \tag{3.22a}$$

$$\gamma_{\theta r} = \left(\frac{R}{R+y}\right)\left(u_y + v_0' - \frac{u_0}{R}\right) = (\gamma_{\theta r})_{F_y}, \text{ and} \tag{3.22b}$$

$$\epsilon_r = \epsilon_z = \gamma_{rz} = \gamma_{z\theta} = 0. \tag{3.22c}$$

The strain energy in cylindrical coordinates is defined by:

$$V = \frac{1}{2}\iiint (\sigma_\theta \epsilon_\theta + \sigma_r \epsilon_r + \sigma_z \epsilon_z + \tau_{\theta r}\gamma_{\theta r} + \tau_{rz}\gamma_{rz} + \tau_{z\theta}\gamma_{z\theta})(r\,d\theta)(dr)(dz), \text{ or} \tag{3.23a}$$

$$V = \frac{1}{2}\iiint (\sigma_\theta \epsilon_\theta + \sigma_r \epsilon_r + \sigma_z \epsilon_z + \tau_{\theta r}\gamma_{\theta r} + \tau_{rz}\gamma_{rz} + \tau_{z\theta}\gamma_{z\theta})\left(\frac{R+y}{R}\right) dx\,dy\,dz. \tag{3.23b}$$

Again, the one-dimensional axial stress/strain law ($\nu \equiv 0$) must be used in conjunction with the assumed beam displacements:

$$\sigma_\theta = E\epsilon_\theta, \tag{3.24}$$

along with the shear assumption:

$$k_y \equiv \frac{\iint (\tau_{\theta r})_{F_y} dy\,dz}{\left(G\iint (\gamma_{\theta r})_{F_y} dy\,dz\right)_{TI}} = \frac{F_y}{GI_{00}(u_y + v_0' - \frac{u_0}{R})}. \tag{3.25}$$

This definition of the shear correction coefficient implies a dependence upon the curvature, as well as the previously mentioned parameters, which has not been quantified in the literature. Thus, k_y is assumed to be independent of curvature for this study; the difference in the k_y's in (3.5) and (3.25) is inferred only from the element type, for simplicity as well as practicality. Further discussions of curvature approximations are found in Chapter 5.

Utilizing the Bickford/Maganty convention (2.14) and (3.22-25) results in the planar strain energy for circular Timoshenko beams, namely:

$$\begin{aligned} V_{TI} = {} & \frac{E}{2}\int_0^h \left[I_{00}\left(u_0' + \frac{v_0}{R}\right)^2 + I_{20}\left(u_y'\right)^2\right] dx \\ & + \frac{Gk_y}{2}\int_0^h I_{00}\left(u_y + v_0' - \frac{u_0}{R}\right)^2 dx. \end{aligned} \tag{3.26}$$

Note that the beam displacement variables are coupled in the extensional and shear energies due to the circular geometry. A benefit of this formulation is that the zero shear energy assumption may be readily identified, namely:

$$u_y + v_0' - \frac{u_0}{R} = 0, \text{ or} \tag{3.27a}$$

$$u_y = -v_0' + \frac{u_0}{R}. \tag{3.27b}$$

Thus, the planar strain energy for a circular Bernoulli-Euler or Rayleigh beam is:

$$V_{BE/RA} = \frac{E}{2}\int_0^h \left[I_{00}\left(u_0' + \frac{v_0}{R}\right)^2 + I_{20}\left(-v_0'' + \frac{u_0'}{R}\right)^2 \right] dx. \tag{3.28}$$

The following observations are useful to note with respect to similar formulations found in the literature:

1) The strain energies in (3.26) and (3.28) are derived without any assumptions of global (system) or local (element) shallowness which would allow certain $(1/R)$-terms to be ignored [53].
2) Inextensional assumptions used to simplify the analysis of thin arches and rings in bending will not be used. However, the ramifications of such assumptions will be discussed in Chapter 5.
3) Virtual rotations of u_y must be used to define the generalized moments entering Lagrange's equation (1.14). Equation 3.27 defines the proper rotation for circular Bernoulli-Euler and Rayleigh beams. The pinned boundary condition for radial deflections involves fixing v_0; the clamped boundary condition results from constraining v_0 and either u_y for TI beams or $(-v_0' + u_0/R)$ for BE/RA beams. The use of the shear deformation parameter, ψ, instead of u_y leads to even more confusion in circular beams.

4) The strain energies in (3.26) and (3.28) are derived assuming a constant arc radius, R, but are written in a form which allow generalization to variable curvature [54].

3.4 THREE-DIMENSIONAL FORMULATION FOR CIRCULAR BEAMS

Formulation of the strain energy for circular beams in three dimensions follows the now familiar procedure. However, an assumption which effectively isolates the shear strains which are force-induced from those that are torque-induced must be invoked. This became obvious only through static patch tests of the resulting formulations, and at least one dynamic formulation in the literature has mistakenly omitted this assumption [39].

Inserting the three-dimensional displacements (2.34) into the cylindrical strain/displacement relations (3.21) results in:

$$\epsilon_\theta = \left(\frac{R}{R+y}\right)\left[\left(u_0' + \frac{v_0}{R}\right) + y\left(u_y'\right) + z\left(u_z' - \frac{\phi_1}{R}\right)\right], \tag{3.29a}$$

$$\gamma_{\theta r} = \left(\frac{R}{R+y}\right)\left(u_y + v_0' - \frac{u_0}{R}\right) - z\left(\frac{R}{R+y}\right)\left(\phi_1' + \frac{u_z}{R}\right) = (\gamma_{\theta r})_{F_y} + (\gamma_{\theta r})_T, \tag{3.29b}$$

$$\gamma_{z\theta} = \left(\frac{R}{R+y}\right)\left(u_z + w_0'\right) + y\left(\frac{R}{R+y}\right)\left(\phi_1' + \frac{u_z}{R}\right) = (\gamma_{z\theta})_{F_z} + (\gamma_{z\theta})_T, \text{ and} \tag{3.29c}$$

$$\epsilon_r = \epsilon_z = \gamma_{rz} = 0. \tag{3.29d}$$

Coupling now includes that of the two additional rotations, ϕ_1 and u_z. The out-of-plane shear correction factor is defined such that:

$$k_z \equiv \frac{\iint (\tau_{z\theta})_{F_z} dydz}{\left(G \iint (\gamma_{z\theta})_{F_z} dydz\right)_{TI}} = \frac{F_z}{GI_{00}(u_z + w_0')}, \tag{3.30}$$

and the torsional stiffness may be defined by:

$$I_0 \equiv k_T \iint (y^2 + z^2)\left(\frac{R}{R+y}\right) dydz = k_T(I_{20} + I_{02}). \tag{3.31}$$

Again, no distinction is made between the k_z's and I_0's of the straight and circular elements.

The collected assumptions may now be incorporated as follows:

$$V_{TI} = \frac{1}{2}\iiint \left[\sigma_\theta \epsilon_\theta + k_y(\tau_{\theta r})_{F_y}(\gamma_{\theta r})_{F_y} + k_T(\tau_{\theta r})_T(\gamma_{\theta r})_T + k_z(\tau_{x\theta})_{F_z}(\gamma_{x\theta})_{F_z} + k_T(\tau_{x\theta})_T(\gamma_{x\theta})_T\right]\left(\frac{R+y}{R}\right)dxdydz \tag{3.32a}$$

$$= \frac{1}{2}\iiint \left[E(\epsilon_\theta)^2 + Gk_y(\gamma_{\theta r})^2_{F_y} + Gk_z(\gamma_{x\theta})^2_{F_z} + Gk_T\left((\gamma_{\theta r})^2_T + (\gamma_{x\theta})^2_T\right)\right]\left(\frac{R+y}{R}\right)dxdydz, \tag{3.32b}$$

or:

$$V_{TI} = \frac{E}{2}\int_0^h \left[I_{00}\left(u_0' + \frac{v_0}{R}\right)^2 + I_{20}\left(u_y'\right)^2 + I_{02}\left(u_z' - \frac{\phi_1}{R}\right)^2 + 2I_{10}\left(u_y'\right)\left(u_0' + \frac{v_0}{R}\right) + 2I_{11}\left(u_y'\right)\left(u_z' - \frac{\phi_1}{R}\right) + 2I_{01}\left(u_0' + \frac{v_0}{R}\right)\left(u_z' - \frac{\phi_1}{R}\right)\right]dx$$
$$+\frac{G}{2}\int_0^h \left[k_y I_{00}\left(u_y + v_0' - \frac{u_0}{R}\right)^2 + k_z I_{00}\left(u_z + w_0'\right)^2 + I_0\left(\phi_1' + \frac{u_z}{R}\right)^2\right]dx. \tag{3.33}$$

The no shear assumption equates to:

$$u_y = -v_0' + \frac{u_0}{R}, \text{ and} \tag{3.34a}$$

$$u_z = -w_0'. \tag{3.34b}$$

Therefore:

$$V_{BE/RA} = \frac{E}{2}\int_0^h \left[I_{00}\left(u_0' + \frac{v_0}{R}\right)^2 + I_{20}\left(-v_0'' + \frac{u_0'}{R}\right)^2 + I_{02}\left(-w_0'' - \frac{\phi_1}{R}\right)^2 + 2I_{10}\left(-v_0'' + \frac{u_0'}{R}\right)\left(u_0' + \frac{v_0}{R}\right) + 2I_{11}\left(-v_0'' + \frac{u_0'}{R}\right)\left(-w_0'' - \frac{\phi_1}{R}\right) + 2I_{01}\left(u_0' + \frac{v_0}{R}\right)\left(-w_0'' - \frac{\phi_1}{R}\right)\right]dx$$
$$+\frac{G}{2}\int_0^h \left[I_0\left(\phi_1' - \frac{w_0'}{R}\right)^2\right]dx. \tag{3.35}$$

3.5 EXTRACTION OF ENGINEERING QUANTITIES FROM BEAM FORMULATIONS

The definition of stresses in terms of the beam displacements is an important step in the formulations of strain energy. Thus:

$$(\sigma_x)_{TI} = E[u_0' + yu_y' + zu_z'], \text{ or} \tag{3.36a}$$

$$(\sigma_x)_{BE/RA} = E[u_0' - yv_0'' - zw_0''], \tag{3.36b}$$

for straight beams and:

$$(\sigma_\theta)_{TI} = E\left(\frac{R}{R+y}\right)\left[\left(u_0' + \frac{v_0}{R}\right) + y\left(u_y'\right) + z\left(u_z' - \frac{\phi_1}{R}\right)\right], \text{ or} \tag{3.37a}$$

$$(\sigma_\theta)_{BE/RA} = E\left(\frac{R}{R+y}\right)\left[\left(u_0' + \frac{v_0}{R}\right) + y\left(-v_0'' + \frac{u_0'}{R}\right) + z\left(-w_0'' - \frac{\phi_1}{R}\right)\right], \tag{3.37b}$$

for circular beams are useful results coming out of the beam analysis. Note that the curvature dependence in (3.37) produces a nonlinear variation of axial stress in the y-direction and a corresponding shift in the neutral axis of bending. The stresses from (3.36-7) allow the engineer to perform first-order analyses, mindful of the fact that stress concentrations cannot be quantified. Also recall that the shear stress distribution for engineering beams is totally erroneous. Thus, the integrated forces and moments on a cross section become the significant quantities coming out of an analysis using engineering beam elements. Figure 3.3 illustrates the desired quantities and the assumed sign conventions with respect to a cross-sectional face with a positive x outward normal. Their definitions are as follows.

The axial force is defined by:

$$F_x = \iint \sigma_x dydz, \text{ or } F_x = \iint \sigma_\theta dydz, \tag{3.38}$$

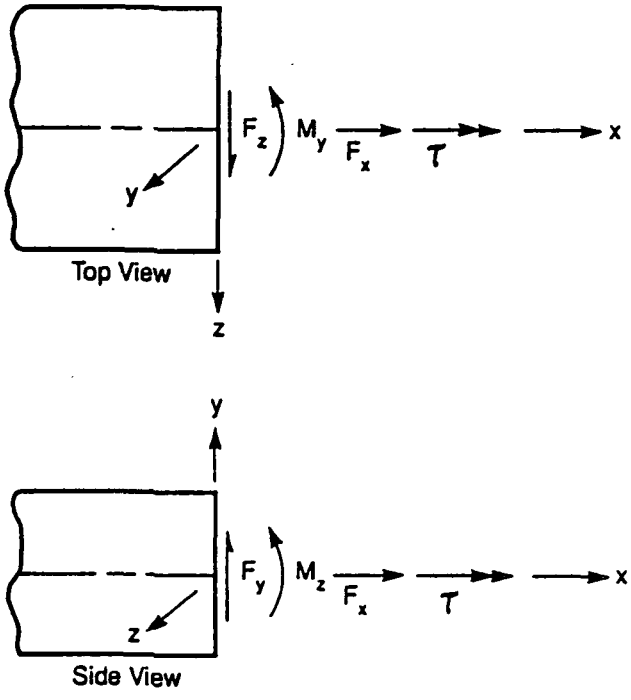

Figure 3.3 Sign conventions for resultant beam forces and moments.

depending on the type of element. Inserting the appropriate stress relation from (3.36) or (3.37) and utilizing the cross-sectional properties (2.4, 2.6-8, and 2.14) result in:

$$(F_x)_{BE/RA/TI} = EAu_0', \tag{3.39}$$

for straight beams and:

$$(F_x)_{TI} = E\left[I_{00}\left(u_0' + \frac{v_0}{R}\right) + I_{10}\left(u_y'\right) + I_{01}\left(u_z' - \frac{\phi_1}{R}\right)\right], \text{ or} \tag{3.40a}$$

$$(F_x)_{BE/RA} = E\left[I_{00}\left(u_0' + \frac{v_0}{R}\right) + I_{10}\left(-v_0'' + \frac{u_0'}{R}\right) + I_{01}\left(-w_0'' - \frac{\phi_1}{R}\right)\right], \tag{3.40b}$$

for circular beams. The torque is defined by:

$$T = \iint \left(y(\tau_{xz})_T - z(\tau_{xy})_T\right) dydz, \text{ or} \tag{3.41a}$$

$$\tau = \iint \left(y(\tau_{x\theta})_T - z(\tau_{\theta r})_T\right) dydz, \tag{3.41b}$$

such that:

$$\tau_{BE/RA/TI} = GI_0\phi_1', \tag{3.42}$$

for straight beams and:

$$\tau_{TI} = GI_0\left(\phi_1' + \frac{u_x}{R}\right), \text{ or} \tag{3.43a}$$

$$\tau_{BE/RA} = GI_0\left(\phi_1' - \frac{w_0'}{R}\right), \tag{3.43b}$$

for circular beams. In a similar fashion:

$$M_y = \iint z\sigma_x dydz, \text{ or } M_y = \iint z\sigma_\theta dydz, \tag{3.44}$$

such that:

$$(M_y)_{TI} = EI_{zz}u_x', \text{ or} \tag{3.45a}$$

$$(M_y)_{BE/RA} = -EI_{zz}w_0'', \tag{3.45b}$$

for straight beams and:

$$(M_y)_{TI} = E\left[I_{01}\left(u_0' + \frac{v_0}{R}\right) + I_{11}\left(u_y'\right) + I_{02}\left(u_x' - \frac{\phi_1}{R}\right)\right], \text{ or} \tag{3.46a}$$

$$(M_y)_{BE/RA} = E\left[I_{01}\left(u_0' + \frac{v_0}{R}\right) + I_{11}\left(-v_0'' + \frac{u_0'}{R}\right) + I_{02}\left(-w_0'' - \frac{\phi_1}{R}\right)\right], \tag{3.46b}$$

for circular beams. Also:

$$M_x = -\iint y\sigma_x dydz, \text{ or } M_x = -\iint y\sigma_\theta dydz, \tag{3.47}$$

such that:

$$(M_x)_{TI} = -EI_{yy}u_y', \text{ or} \tag{3.48a}$$

$$(M_x)_{BE/RA} = EI_{yy}v_0'', \tag{3.48b}$$

for straight beams and:

$$(M_z)_{TI} = -E\left[I_{10}\left(u_0' + \frac{v_0}{R}\right) + I_{20}\left(u_y'\right) + I_{11}\left(u_z' - \frac{\phi_1}{R}\right)\right], \text{ or} \tag{3.49a}$$

$$(M_z)_{BE/RA} = -E\left[I_{10}\left(u_0' + \frac{v_0}{R}\right) + I_{20}\left(-v_0'' + \frac{u_0'}{R}\right) + I_{11}\left(-w_0'' - \frac{\phi_1}{R}\right)\right], \tag{3.49b}$$

for circular beams.

The shear forces for Timoshenko beams fall directly out of the definitions of the shear correction factors, namely:

$$(F_y)_{TI} = \iint (\tau_{xy})_{F_y} dydz, \text{ or } (F_y)_{TI} = \iint (\tau_{\theta r})_{F_y} dydz, \tag{3.50}$$

such that:

$$(F_y)_{TI} = Gk_y A(u_y + v_0'), \tag{3.51}$$

for straight beams and:

$$(F_y)_{TI} = Gk_y I_{00}\left(u_y + v_0' - \frac{u_0}{R}\right), \tag{3.52}$$

for circular beams. Also:

$$(F_z)_{TI} = \iint (\tau_{xz})_{F_z} dydz, \text{ or } (F_z)_{TI} = \iint (\tau_{z\theta})_{F_z} dydz, \tag{3.53}$$

such that:

$$(F_z)_{TI} = Gk_z A(u_z + w_0'), \tag{3.54}$$

for straight beams and:

$$(F_z)_{TI} = Gk_z I_{00}(u_z + w_0'), \tag{3.55}$$

for circular beams. However, exclusion of the shear energies in BE/RA beams precludes a similar integration. The shear forces must be derived from elementary moment balances on an infinitesimal length of the beam [55]. Noting the sign

conventions in Figure 3.3, the resulting shear force equations for BE/RA beams are:

$$(F_y)_{BE/RA} = -\frac{d(M_z)_{BE/RA}}{dx}, \tag{3.56}$$

such that:

$$(F_y)_{BE/RA} = -EI_{yy}v_0''', \tag{3.57}$$

for straight beams and:

$$(F_y)_{BE/RA} = E\left[I_{10}\left(u_0'' + \frac{v_0'}{R}\right) + I_{20}\left(-v_0''' + \frac{u_0''}{R}\right) + I_{11}\left(-w_0''' - \frac{\phi_1'}{R}\right)\right], \tag{3.58}$$

for circular beams. For straight beams:

$$(F_z)_{BE/RA} = \frac{d(M_y)_{BE/RA}}{dx}, \tag{3.59}$$

such that:

$$(F_z)_{BE/RA} = -EI_{zz}w_0'''. \tag{3.60}$$

However, the shear force in the z-direction is coupled with the torque for circular beams, namely:

$$(F_z)_{BE/RA} = \frac{d(M_y)_{BE/RA}}{dx} - \frac{\tau}{R}, \tag{3.61}$$

such that:

$$(F_z)_{BE/RA} = E\left[I_{01}\left(u_0'' + \frac{v_0'}{R}\right) + I_{11}\left(-v_0''' + \frac{u_0''}{R}\right) + I_{02}\left(-w_0''' - \frac{\phi_1'}{R}\right)\right] - \frac{GI_0}{R}\left(\phi_1' - \frac{w_0'}{R}\right). \tag{3.62}$$

4. KINETIC ENERGY FORMULATIONS IN A ROTATING FRAME

The kinetic energy of a structure is a characterization of the system inertia. As discussed in Chapter 1, the kinetic energy formulation with respect to a rotating frame also introduces centrifugal softening, Coriolis coupling, and centrifugal loading terms to the static and dynamic equations. This chapter presents the formulation of the kinetic energy terms starting with a generic distributed mass (with inertia) and leading to circular beams in three-dimensional space. The effects of an arbitrarily oriented, rotating coordinate system are incorporated immediately within the context of the small rotation assumption. The distinction between Bernoulli-Euler and Rayleigh beams will be identified and the simplification to nonrotating problems will be apparent.

4.1 FORMULATION FOR A DISTRIBUTED MASS

The position of a distributed mass with inertia in a rotating frame is depicted in Figure 4.1. The various frames in the figure are defined as:

(I) ≡ inertial frame. The inertial frame is defined such that its absolute angular velocity and the absolute velocity of its origin are zero, namely:

$$\{\Omega^I\} = 0, \text{ and} \tag{4.1a}$$

$$\{v^F\} = 0. \tag{4.1b}$$

(G) ≡ global frame. The global frame is used as the reference for defining the model geometry. The angular velocity of the global frame relative to the inertial frame is assumed constant and defined by:

$$\left\{{}^G\Omega^{G/I}\right\} = \{{}^G\Omega^G\} \equiv \begin{Bmatrix} \Omega_X \\ \Omega_Y \\ \Omega_Z \end{Bmatrix}. \tag{4.2}$$

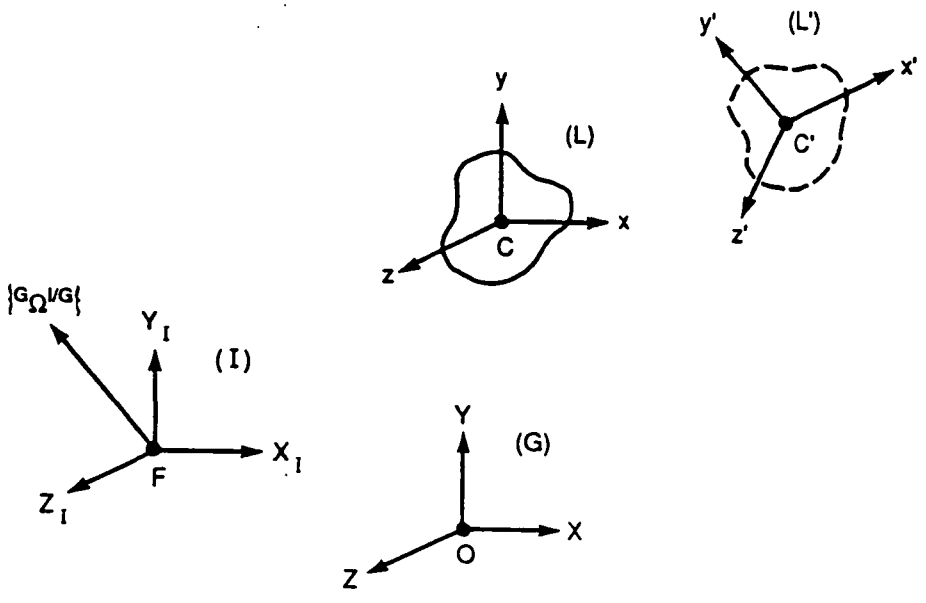

Figure 4.1 Distributed mass in a rotating frame.

This angular velocity is conveniently defined in the global frame and is absolute since the inertial frame is stationary. Note that (4.2) implies:

$$\left\{{}^{G}\Omega^{I/G}\right\} = \begin{Bmatrix} -\Omega_X \\ -\Omega_Y \\ -\Omega_Z \end{Bmatrix}. \tag{4.3}$$

In other words, the relative angular velocity of the inertial frame may be nonzero even though the frame is stationary. Figure 4.1 is depicted from a global perspective.

(L) ≡ undeformed local frame. This frame is used to define the properties of the distributed mass. Its orientation is assumed coincident with the global frame, and its origin, C, is assumed to be at the mass center. The properties associated with the distributed mass in its undeformed position are:

$$M = \iiint \rho dx dy dz, \tag{4.4}$$

and:

$$J_{IJ} = \iiint \rho ij dx dy dz, \quad i,j = x,y,z. \tag{4.5}$$

$\mathcal{M}$ is used to distinguish the integrated mass from the beam mass per unit length, m. The IJ subscripts ($I,J = X,Y,Z$) on the distributed inertias help to distinguish them from similar beam terms and serve as a reminder that the local and global frames are parallel, that is $[{}^{G}_{L}T] = [I]$.

(L') $\equiv$ deformed local frame. The deformed local frame represents the position and orientation of the distributed mass at any instant in time. The deformed frame is defined relative to the undeformed local frame by three displacements, U_1, U_2, and U_3, and three rotations, U_4, U_5, and U_6, with respect to the undeformed local axes, x, y, and z, respectively. Note that the distributed mass properties in the deformed position are identical to those in (4.4-5) relative to the undeformed position.

The kinetic energy of the distributed mass may be conveniently separated into translational and rotational components. The translational kinetic energy is [56]:

$$T_{TRANS} = \frac{1}{2}\mathcal{M}\left[(v_x^{C'})^2 + (v_y^{C'})^2 + (v_z^{C'})^2\right], \tag{4.6}$$

where:

$$\left\{v^{C'}\right\} \equiv \begin{Bmatrix} v_x^{C'} \\ v_y^{C'} \\ v_z^{C'} \end{Bmatrix}, \tag{4.7}$$

is the absolute velocity of the deformed center of mass. Given:

$$\{{}^{G}F\} \equiv \begin{Bmatrix} X_O \\ Y_O \\ Z_O \end{Bmatrix}, \quad \{{}^{G}C\} \equiv \begin{Bmatrix} X_C \\ Y_C \\ Z_C \end{Bmatrix}, \tag{4.8}$$

and:

$$\{{}^{L}C'\} = \begin{Bmatrix} U_1 \\ U_2 \\ U_3 \end{Bmatrix}, \tag{4.9}$$

then taking into account that (L) is parallel to (G) and utilizing the vector cross product to compute rotation-induced velocity terms result in:

$$\left\{{}^{G}v^{C'}\right\} = \left\{{}^{L}v^{C'}\right\} = \left\{\begin{array}{l} \Omega_Y(Z_C - Z_\Omega + U_3) - \Omega_Z(Y_C - Y_\Omega + U_2) + \dot{U}_1 \\ \Omega_Z(X_C - X_\Omega + U_1) - \Omega_X(Z_C - Z_\Omega + U_3) + \dot{U}_2 \\ \Omega_X(Y_C - Y_\Omega + U_2) - \Omega_Y(X_C - X_\Omega + U_1) + \dot{U}_3 \end{array}\right\}. \tag{4.10}$$

Therefore:

$$\begin{aligned} T_{TRANS} = \frac{1}{2}\mathcal{M}\Big\{ & \Big[\Omega_Y(Z_C - Z_\Omega + U_3) - \Omega_Z(Y_C - Y_\Omega + U_2) + \dot{U}_1\Big]^2 \\ & + \Big[\Omega_Z(X_C - X_\Omega + U_1) - \Omega_X(Z_C - Z_\Omega + U_3) + \dot{U}_2\Big]^2 \\ & + \Big[\Omega_X(Y_C - Y_\Omega + U_2) - \Omega_Y(X_C - X_\Omega + U_1) + \dot{U}_3\Big]^2\Big\}. \end{aligned} \tag{4.11}$$

Note that the rotations, U_4-U_6, do not enter into the translational kinetic energy. Even though the deformed distributed mass has changed orientation, it is not necessary to specify the absolute velocity of the mass center in the deformed local frame.

Two different approaches may be adopted in the formulation of the rotational kinetic energy. The first involves formulation with respect to the undeformed local frame taking into account the deformation-dependent changes in the inertias. Actually, the inertia changes are often ignored and the kinetic energy is computed (similar to the strain energy) by simple integrations in the local frame. However, this simplification produces erroneous rotating coordinate system effects. The second approach formulates the angular velocity and, thus, the rotational kinetic energy, in terms of the deformed local frame where the inertias remain constant. The latter approach is adopted for this research such that [56]:

$$\begin{aligned} T_{ROT} = \frac{1}{2}\Big[& (J_{YY} + J_{ZZ})\left(\Omega_{x'}^{L'}\right)^2 + (J_{ZZ} + J_{XX})\left(\Omega_{y'}^{L'}\right)^2 + (J_{XX} + J_{YY})\left(\Omega_{z'}^{L'}\right)^2\Big] \\ & - \Big[J_{XY}\left(\Omega_{x'}^{L'}\right)\left(\Omega_{y'}^{L'}\right) + J_{YZ}\left(\Omega_{y'}^{L'}\right)\left(\Omega_{z'}^{L'}\right) + J_{ZX}\left(\Omega_{z'}^{L'}\right)\left(\Omega_{x'}^{L'}\right)\Big], \end{aligned} \tag{4.12}$$

where:

$$\left\{{}^{L'}\Omega^{L'}\right\} \equiv \left\{ \begin{array}{c} \Omega_{x'}^{L'} \\ \Omega_{y'}^{L'} \\ \Omega_{z'}^{L'} \end{array} \right\}. \tag{4.13}$$

Using the roll, pitch, yaw convention, the absolute angular velocity of the distributed mass specified in undeformed local coordinates is:

$$\left\{{}^{L}\Omega^{L'}\right\} = \left\{ \begin{array}{c} \Omega_X + \dot{U}_4 \\ \Omega_Y + \dot{U}_5 \\ \Omega_Z + \dot{U}_6 \end{array} \right\}. \tag{4.14}$$

Invoking the small rotation assumption results in:

$$\left\{{}^{L'}\Omega^{L'}\right\} = \left[{}^{L'}_{L}T\right]\left\{{}^{L}\Omega^{L'}\right\} \cong \left[\begin{array}{ccc} 1 & U_6 & -U_5 \\ -U_6 & 1 & U_4 \\ U_5 & -U_4 & 1 \end{array} \right] \left\{ \begin{array}{c} \Omega_X + \dot{U}_4 \\ \Omega_Y + \dot{U}_5 \\ \Omega_Z + \dot{U}_6 \end{array} \right\}, \tag{4.15}$$

or:

$$\left\{{}^{L'}\Omega^{L'}\right\} \cong \left\{ \begin{array}{l} +(\Omega_X + \dot{U}_4) + U_6(\Omega_Y + \dot{U}_5) - U_5(\Omega_Z + \dot{U}_6) \\ -U_6(\Omega_X + \dot{U}_4) + (\Omega_Y + \dot{U}_5) + U_4(\Omega_Z + \dot{U}_6) \\ +U_5(\Omega_X + \dot{U}_4) - U_4(\Omega_Y + \dot{U}_5) + (\Omega_Z + \dot{U}_6) \end{array} \right\}. \tag{4.16}$$

Thus:

$$\begin{aligned} T_{ROT} \cong & \frac{1}{2}(J_{YY} + J_{ZZ})\left[+\left(\Omega_X + \dot{U}_4\right) + U_6\left(\Omega_Y + \dot{U}_5\right) - U_5\left(\Omega_Z + \dot{U}_6\right)\right]^2 \\ & + \frac{1}{2}(J_{ZZ} + J_{XX})\left[-U_6\left(\Omega_X + \dot{U}_4\right) + \left(\Omega_Y + \dot{U}_5\right) + U_4\left(\Omega_Z + \dot{U}_6\right)\right]^2 \\ & + \frac{1}{2}(J_{XX} + J_{YY})\left[-U_5\left(\Omega_X + \dot{U}_4\right) - U_4\left(\Omega_Y + \dot{U}_5\right) + \left(\Omega_Z + \dot{U}_6\right)\right]^2 \\ & - J_{XY}\left[+\left(\Omega_X + \dot{U}_4\right) + U_6\left(\Omega_Y + \dot{U}_5\right) - U_5\left(\Omega_Z + \dot{U}_6\right)\right] \\ & \quad \left[-U_6\left(\Omega_X + \dot{U}_4\right) + \left(\Omega_Y + \dot{U}_5\right) + U_4\left(\Omega_Z + \dot{U}_6\right)\right] \\ & - J_{YZ}\left[-U_6\left(\Omega_X + \dot{U}_4\right) + \left(\Omega_Y + \dot{U}_5\right) + U_4\left(\Omega_Z + \dot{U}_6\right)\right] \\ & \quad \left[+U_5\left(\Omega_X + \dot{U}_4\right) - U_4\left(\Omega_Y + \dot{U}_5\right) + \left(\Omega_Z + \dot{U}_6\right)\right] \\ & - J_{ZX}\left[+U_5\left(\Omega_X + \dot{U}_4\right) - U_4\left(\Omega_Y + \dot{U}_5\right) + \left(\Omega_Z + \dot{U}_6\right)\right] \\ & \quad \left[+\left(\Omega_X + \dot{U}_4\right) + U_6\left(\Omega_Y + \dot{U}_5\right) - U_5\left(\Omega_Z + \dot{U}_6\right)\right]. \end{aligned} \tag{4.17}$$

The total kinetic energy of a distributed mass subject to a rotating frame is provided by the sum of (4.11) and (4.17). The small rotation assumption has been invoked, but the rotational kinetic energy still contains cubic and quartic terms of the U_i's *and* their time derivatives. These terms are assumed to be small in relation to the linear and quadratic terms such that the resulting eigenproblem is linear. This additional restriction allows the kinetic energy to be placed in the general form of (1.20*b*).

Substituting the general harmonic response and applying Lagrange's equation produces the centrifugal softening $[K_S]$, Coriolis coupling $[C]$, mass $[M]$, and centrifugal loading $\{R_0\}$ terms associated with the distributed mass. These terms will be related to the six global degrees-of-freedom of a grid point located at the mass center and added to the global matrices of the finite element problem (see Chapter 7). Note that the rotational kinetic energy of the distributed mass (4.17) is ignored in problems involving Bernoulli-Euler beams.

4.2 FORMULATION FOR STRAIGHT BEAMS

The kinetic energy formulation for beams in a rotating frame follows a similar procedure to that for a distributed mass. An infinitesimal length of an element is considered and the resulting terms are integrated over the entire beam length. Figure 4.2 illustrates the differential length of a straight beam with respect to the various frames. The frames are identical to those for the distributed mass with the following exceptions:

1) The orientation of the undeformed local frame, (L), does not coincide with the global frame, (G). However, the transformation matrix relating the two frames, $[{}^G_L T]$, is defined *exactly* from the problem geometry; no small angle

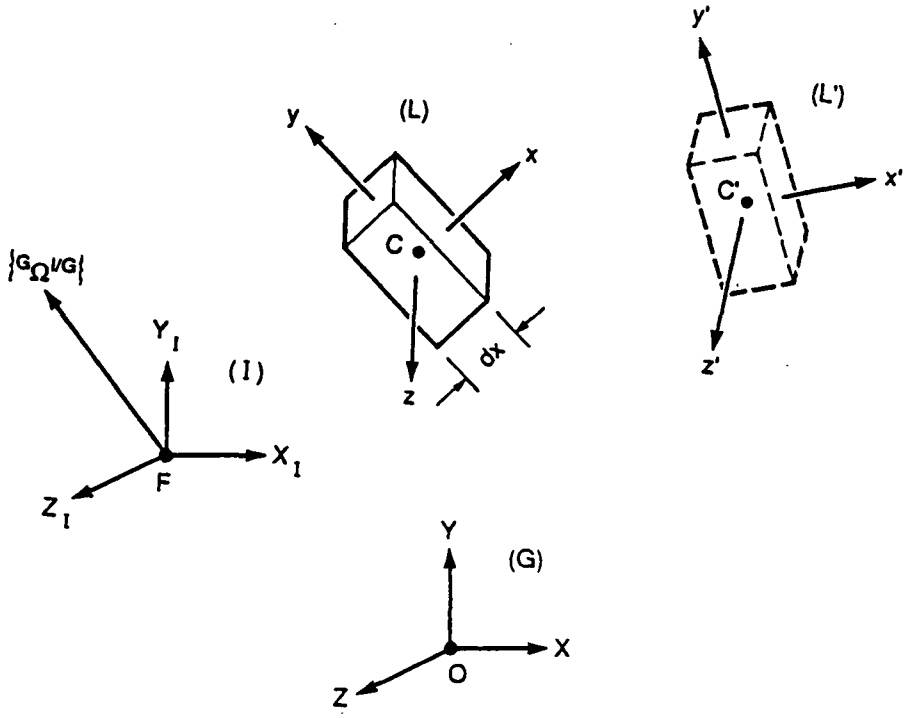

Figure 4.2 Infinitesimal straight beam element in a rotating frame.

approximations are used in relating the local and global frames. $[{}^{G}_{L}T]$ is constant over the entire length of a straight beam.

2) The origin of the local frame, C, lies on the beam axis of the straight element and coincides with the center of mass of the infinitesimal length.

3) The deformed local frame, (L'), is defined relative to the undeformed frame by three displacements, u_0, v_0, and w_0, and three (Timoshenko) rotations, ϕ_1, u_z, and $-u_y$, with respect to the undeformed local axes, x, y, and z, respectively. These terms are consistent with their use in defining the three-dimensional beam displacements in (2.34).

The translational kinetic energy for the straight beam element is represented by:

$$T_{TRANS} = \frac{1}{2}\int_0^h m\left[\left(v_x^{C'}\right)^2 + \left(v_y^{C'}\right)^2 + \left(v_z^{C'}\right)^2\right] dx, \tag{4.18}$$

similar to that of the distributed mass in (4.6). Since the local frame is no longer parallel to the global frame but still fixed relative to the global frame:

$$\{^L\Omega^L\} = \{^L\Omega^G\} = [^L_G T]\,\{^G\Omega^G\}$$
$$= [^L_G T] \begin{Bmatrix} \Omega_X \\ \Omega_Y \\ \Omega_Z \end{Bmatrix} \equiv \begin{Bmatrix} \Omega_x \\ \Omega_y \\ \Omega_z \end{Bmatrix}. \tag{4.19}$$

Furthermore:

$$\left\{^{L/I}C\right\} = [^L_G T]\left\{^{G/I}C\right\}$$
$$= [^L_G T] \begin{Bmatrix} X_C - X_\Omega \\ Y_C - Y_\Omega \\ Z_C - Z_\Omega \end{Bmatrix} \equiv \begin{Bmatrix} x_C \\ y_C \\ z_C \end{Bmatrix}, \tag{4.20}$$

defines the position of C with respect to the inertial frame in terms of local coordinates; this vector varies along the length of the beam axis. The position of the deformed center of mass with respect to the undeformed local frame is:

$$\{^L C'\} = \begin{Bmatrix} u_0 \\ v_0 \\ w_0 \end{Bmatrix}. \tag{4.21}$$

Thus:

$$\left\{^L v^{C'}\right\} = \begin{Bmatrix} v_x^{C'} \\ v_y^{C'} \\ v_z^{C'} \end{Bmatrix} = \begin{Bmatrix} \Omega_y (z_C + w_0) - \Omega_z (y_C + v_0) + \dot{u}_0 \\ \Omega_z (x_C + u_0) - \Omega_x (z_C + w_0) + \dot{v}_0 \\ \Omega_x (y_C + v_0) - \Omega_y (x_C + u_0) + \dot{w}_0 \end{Bmatrix}, \tag{4.22}$$

defines the absolute velocity of the deformed center of mass in terms of the undeformed local frame.

The rotational kinetic energy formulation is again similar to that of the distributed mass in (4.12):

$$T_{ROT} = \frac{1}{2}\int_0^h \left[(J_{yy} + J_{zz})\left(\Omega_{x'}^{L'}\right)^2 + J_{zz}\left(\Omega_{y'}^{L'}\right)^2 + J_{yy}\left(\Omega_{z'}^{L'}\right)^2\right] dx. \tag{4.23}$$

The mass moments of inertia per unit length are defined in (2.9) relative to the local axes. Note that J_{xx}, J_{xy}, and J_{xz} are higher-order terms relative to the

differential length, dx, and $J_{yz} = 0$ since the local y- and z-axes are principal axes of the cross section. Similar to (4.14) except with the beam variables:

$$\left\{{}^{L}\Omega^{L'}\right\} = \begin{Bmatrix} \Omega_x + \dot{\phi}_1 \\ \Omega_y + \dot{u}_z \\ \Omega_z - \dot{u}_y \end{Bmatrix}. \tag{4.24}$$

Then, invoking the small rotation assumption results in:

$$\left\{{}^{L'}\Omega^{L'}\right\} = \begin{Bmatrix} \Omega^{L'}_{x'} \\ \Omega^{L'}_{y'} \\ \Omega^{L'}_{z'} \end{Bmatrix} \cong \begin{Bmatrix} +(\Omega_x + \dot{\phi}_1) - u_y\,(\Omega_y + \dot{u}_z) - u_z\,(\Omega_z - \dot{u}_y) \\ +u_y(\Omega_x + \dot{\phi}_1) + (\Omega_y + \dot{u}_z) + \phi_1\,(\Omega_z - \dot{u}_y) \\ +u_z(\Omega_x + \dot{\phi}_1) - \phi_1\,(\Omega_y + \dot{u}_z) + (\Omega_z - \dot{u}_y) \end{Bmatrix}. \tag{4.25}$$

The entire kinetic energy for a straight Timoshenko beam is the sum of (4.18) and (4.23) with the necessary substitutions:

$$\begin{aligned} T_{TI} = \frac{1}{2}\int_0^h m\Big\{ & \left[\Omega_y\,(z_C + w_0) - \Omega_z\,(y_C + v_0) + \dot{u}_0\right]^2 + \\ & \left[\Omega_z\,(x_C + u_0) - \Omega_x\,(z_C + w_0) + \dot{v}_0\right]^2 + \\ & \left[\Omega_x\,(y_C + v_0) - \Omega_y\,(x_C + u_0) + \dot{w}_0\right]^2\Big\}dx \\ + \frac{1}{2}\int_0^h & J_0\left[(\Omega_x + \dot{\phi}_1) - u_y\,(\Omega_y + \dot{u}_z) - u_z\,(\Omega_z - \dot{u}_y)\right]^2 dx \\ + \frac{1}{2}\int_0^h & J_{zz}\left[u_y(\Omega_x + \dot{\phi}_1) + (\Omega_y + \dot{u}_z) + \phi_1\,(\Omega_z - \dot{u}_y)\right]^2 dx \\ + \frac{1}{2}\int_0^h & J_{yy}\left[u_z(\Omega_x + \dot{\phi}_1) - \phi_1\,(\Omega_y + \dot{u}_z) + (\Omega_z - \dot{u}_y)\right]^2 dx, \end{aligned} \tag{4.26}$$

where $J_0 = J_{yy} + J_{zz}$. The kinetic energy for a straight Rayleigh beam merely involves substituting the no-shear relations of (3.13) and (3.19), namely:

$$\begin{aligned} T_{RA} = \frac{1}{2}\int_0^h m\Big\{ & \left[\Omega_y\,(z_C + w_0) - \Omega_z\,(y_C + v_0) + \dot{u}_0\right]^2 + \\ & \left[\Omega_z\,(x_C + u_0) - \Omega_x\,(z_C + w_0) + \dot{v}_0\right]^2 + \\ & \left[\Omega_x\,(y_C + v_0) - \Omega_y\,(x_C + u_0) + \dot{w}_0\right]^2\Big\}dx \end{aligned}$$

$$+\frac{1}{2}\int_0^h J_0\left[(\Omega_x+\dot{\phi}_1)+v_0'(\Omega_y-\dot{w}_0')+w_0'(\Omega_z+\dot{v}_0')\right]^2 dx$$

$$+\frac{1}{2}\int_0^h J_{zz}\left[-v_0'(\Omega_x+\dot{\phi}_1)+(\Omega_y-\dot{w}_0')+\phi_1(\Omega_z+\dot{v}_0')\right]^2 dx$$

$$+\frac{1}{2}\int_0^h J_{yy}\left[-w_0'(\Omega_x+\dot{\phi}_1)-\phi_1(\Omega_y-\dot{w}_0')+(\Omega_z+\dot{v}_0')\right]^2 dx. \qquad (4.27)$$

Bernoulli-Euler beams further simplify the kinetic energy by ignoring the rotational kinetic energy terms involving the in-plane and out-of-plane displacement variables, v_0 and w_0, respectively. Recalling (3.11-12) and Figure 3.2, it is easy to see that given a characteristic *system* length, $\mathcal{L}$, and a characteristic cross-sectional dimension, r, the system inertia ($\sim(r/\mathcal{L})^4$) represents a higher-order term in comparison to the system mass ($\sim(r/\mathcal{L})^2$) for transverse vibrations in the limit as $(nr/\mathcal{L}) \to 0$. Note that the mode number, n, affects the validity of the Bernoulli-Euler simplification. As seen in (4.27), this limiting assumption involves ignoring all J_{yy}- and J_{zz}-terms *and* some J_0-terms such that:

$$T_{BE} = \frac{1}{2}\int_0^h m\Big\{[\Omega_y(z_C+w_0)-\Omega_z(y_C+v_0)+\dot{u}_0]^2+$$
$$[\Omega_z(x_C+u_0)-\Omega_x(z_C+w_0)+\dot{v}_0]^2+$$
$$[\Omega_x(y_C+v_0)-\Omega_y(x_C+u_0)+\dot{w}_0]^2\Big\}dx$$
$$+\frac{1}{2}\int_0^h J_0\left(\Omega_x+\dot{\phi}_1\right)^2 dx. \qquad (4.28)$$

Again, the beam displacements and rotations *and* their time derivatives must be assumed small enough to allow cubic and quadratic terms in those variables to be ignored in the beam kinetic energies (4.26-28).

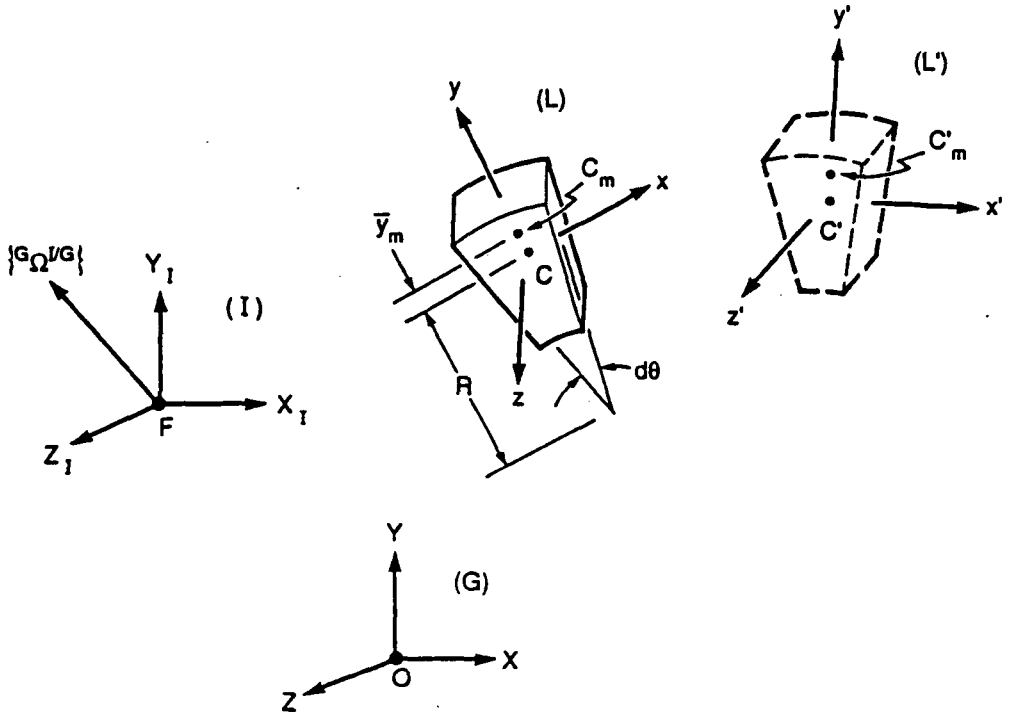

Figure 4.3 Infinitesimal circular beam element in a rotating frame.

4.3 FORMULATION FOR CIRCULAR BEAMS

The kinetic energy formulation for circular beams is complicated by the following two factors:

1) The center of mass C_m, and cross-sectional centroid, C, do not coincide (see (2.13)). Since the beam axis is chosen to be coincident with the cross-sectional centroids, the kinetic energy formulations must take the mass eccentricity into account. This condition is illustrated for the infinitesimal circular beam element in Figure 4.3.

2) Enforcement of the planar no-shear assumption (3.27) induces further coupling of the axial and transverse displacements, u_0 and v_0, respectively, in Rayleigh and Bernoulli-Euler beams.

The frames for the circular element are the same as those for the straight element. Recall that the orientation of the local x- and y-axes change along the length of

a circular beam. Therefore, $[{}^{G}_{L}T]$ is not constant for a circular element, but this transformation matrix may still be defined exactly from the problem geometry.

The translational kinetic energy:

$$T_{TRANS} = \frac{1}{2}\int_0^h m\left[\left(v_x^{C'_m}\right)^2 + \left(v_y^{C'_m}\right)^2 + \left(v_z^{C'_m}\right)^2\right] dx, \tag{4.29}$$

must be defined using the absolute velocity of the mass center. Given that:

$$\left\{{}^{L}C_m\right\} = \left\{{}^{L'}C'_m\right\} = \begin{Bmatrix} 0 \\ \bar{y}_m \\ 0 \end{Bmatrix}, \tag{4.30}$$

the absolute velocity of the deformed center of mass in terms of the undeformed local frame is:

$$\left\{{}^{L}v^{C'_m}\right\} \equiv \begin{Bmatrix} v_x^{C'_m} \\ v_y^{C'_m} \\ v_z^{C'_m} \end{Bmatrix} = \left\{{}^{L}v^{C'}\right\} + \left\{{}^{L}\Omega^{L'}\right\} \times [{}^{L}_{L'}T]\left\{{}^{L'}C'_m\right\}, \tag{4.31}$$

where $\left\{{}^{L}v^{C'}\right\}$ and $\left\{{}^{L}\Omega^{L'}\right\}$ are defined in (4.22) and (4.24), respectively. Using the small rotation assumption:

$$[{}^{L}_{L'}T] \cong \begin{bmatrix} 1 & u_y & u_z \\ -u_y & 1 & -\phi_1 \\ -u_z & \phi_1 & 1 \end{bmatrix}, \tag{4.32}$$

produces:

$$\left\{{}^{L}v^{C'_m}\right\} \cong \begin{Bmatrix} \Omega_y\left(z_C + w_0 + \bar{y}_m\phi_1\right) - \Omega_z\left(y_C + v_0 + \bar{y}_m\right) + \dot{u}_0 + \dot{u}_y\bar{y}_m + \dot{u}_z\phi_1\bar{y}_m \\ \Omega_z\left(x_C + u_0 + \bar{y}_m u_y\right) - \Omega_x\left(z_C + w_0 + \bar{y}_m\phi_1\right) + \dot{v}_0 - \dot{u}_y u_y\bar{y}_m - \dot{\phi}_1\phi_1\bar{y}_m \\ \Omega_x\left(y_C + v_0 + \bar{y}_m\right) - \Omega_y\left(x_C + u_0 + \bar{y}_m u_y\right) + \dot{w}_0 + \dot{\phi}_1\bar{y}_m - \dot{u}_z u_y\bar{y}_m \end{Bmatrix}. \tag{4.33}$$

The important fact to note is that the small rotation approximation must be utilized in the translational kinetic energy formulation due to the mass center shift. The effect of the approximation is minimized by defining the absolute

velocity in terms of the undeformed local frame such that the transformation of $\left\{{}^{L'}C'_m\right\}$ is all that is required.

The rotational kinetic energy is also affected by the shift in the mass center. The formulation of the rotational kinetic energy listed in (4.12) requires that the mass moments of inertia be defined about the mass center. Using the principal axis theorem in conjunction with the cross-sectional properties in Section 2.1:

$$J_{gg} = \iint \rho y^2 \left(\frac{R+y}{R}\right) dydz - m\bar{y}_m^2 = J_{yy}\left(1 - \frac{\bar{y}_m}{R}\right) + \frac{J_{yyy}}{R}, \tag{4.34a}$$

$$J_{zz} = \iint \rho z^2 \left(\frac{R+y}{R}\right) dydz - m\bar{z}_m^2 = J_{zz} + \frac{J_{yzz}}{R}, \tag{4.34b}$$

$$J_{gz} = \iint \rho yz \left(\frac{R+y}{R}\right) dydz - m\bar{y}_m\bar{z}_m = \frac{J_{yyz}}{R}, \text{ and} \tag{4.34c}$$

$$J_{\bar{0}} = J_{gg} + J_{zz}. \tag{4.34d}$$

The overbars over the subscripts denote the mass moments on inertia per unit length with respect to the mass center. Therefore, the rotational kinetic energy may be specified as:

$$T_{ROT} = \frac{1}{2}\int_0^h \left[J_{\bar{0}}\left(\Omega_{x'}^{L'}\right)^2 + J_{zz}\left(\Omega_{y'}^{L'}\right)^2 + J_{gg}\left(\Omega_{z'}^{L'}\right)^2 - 2J_{gz}\left(\Omega_{y'}^{L'}\right)\left(\Omega_{z'}^{L'}\right)\right] dx, \tag{4.35}$$

where the Ω-terms are defined in (4.25).

The entire kinetic energy of a circular Timoshenko beam is the sum of (4.29) and (4.35) with the necessary substitutions:

$$\begin{aligned} T_{TI} = \frac{1}{2}\int_0^h m\Big\{ &\Big[\Omega_y\left(z_C + w_0 + \bar{y}_m\phi_1\right) - \Omega_z\left(y_C + v_0 + \bar{y}_m\right) + \dot{u}_0 + \dot{u}_y\bar{y}_m + \dot{u}_z\phi_1\bar{y}_m\Big]^2 \\ &\Big[\Omega_z\left(x_C + u_0 + \bar{y}_m u_y\right) - \Omega_x\left(z_C + w_0 + \bar{y}_m\phi_1\right) + \dot{v}_0 - \dot{u}_y u_y\bar{y}_m - \dot{\phi}_1\phi_1\bar{y}_m\Big]^2 \\ &\Big[\Omega_x\left(y_C + v_0 + \bar{y}_m\right) - \Omega_y\left(x_C + u_0 + \bar{y}_m u_y\right) + \dot{w}_0 + \dot{\phi}_1\bar{y}_m - \dot{u}_z u_y\bar{y}_m\Big]^2\Big\} dx \end{aligned}$$

$$+\frac{1}{2}\int_0^h J_0\left[(\Omega_x+\dot{\phi}_1)-u_y\,(\Omega_y+\dot{u}_z)-u_z\,(\Omega_z-\dot{u}_y)\right]^2 dx$$

$$+\frac{1}{2}\int_0^h J_{zz}\left[u_y(\Omega_x+\dot{\phi}_1)+(\Omega_y+\dot{u}_z)+\phi_1\,(\Omega_z-\dot{u}_y)\right]^2 dx$$

$$+\frac{1}{2}\int_0^h J_{yy}\left[u_z(\Omega_x+\dot{\phi}_1)-\phi_1\,(\Omega_y+\dot{u}_z)+(\Omega_z-\dot{u}_y)\right]^2 dx$$

$$-\int_0^h J_{yz}\left[u_y(\Omega_x+\dot{\phi}_1)+(\Omega_y+\dot{u}_z)+\phi_1\,(\Omega_z-\dot{u}_y)\right]$$

$$\left[u_z(\Omega_x+\dot{\phi}_1)-\phi_1\,(\Omega_y+\dot{u}_z)+(\Omega_z-\dot{u}_y)\right]dx. \tag{4.36}$$

The separation of the translational and rotational kinetic energy terms is explicit in this equation. However, significant simplifications can be made by utilizing (4.34), realizing that $m\bar{g}_m = J_{yy}/R$, *and* delaying application of the small rotation approximation. Then:

$$T_{TI} = \frac{1}{2}\int_0^h m\Big\{\left[\Omega_y\,(z_C+w_0)-\Omega_z\,(y_C+v_0)+\dot{u}_0\right]^2+$$

$$\left[\Omega_z\,(x_C+u_0)-\Omega_x\,(z_C+w_0)+\dot{v}_0\right]^2+$$

$$\left[\Omega_x\,(y_C+v_0)-\Omega_y\,(x_C+u_0)+\dot{w}_0\right]^2\Big\}dx$$

$$+\int_0^h \frac{J_{yy}}{R}\Big\{\left[\Omega_y\,(z_C+w_0)-\Omega_z\,(y_C+v_0)+\dot{u}_0\right]\left[\phi_1\,(\Omega_y+\dot{u}_z)-(\Omega_z-\dot{u}_y)\right]+$$

$$\left[\Omega_z\,(x_C+u_0)-\Omega_x\,(z_C+w_0)+\dot{v}_0\right]\left[u_y\,(\Omega_z-\dot{u}_y)-\phi_1(\Omega_x+\dot{\phi}_1)\right]+$$

$$\left[\Omega_x\,(y_C+v_0)-\Omega_y\,(x_C+u_0)+\dot{w}_0\right]\left[(\Omega_x+\dot{\phi}_1)-u_y(\Omega_y+\dot{u}_z)\right]\Big\}dx$$

$$+\frac{1}{2}\int_0^h\left[J_0+\frac{J_{yyy}+J_{yzz}}{R}\right]\left[(\Omega_x+\dot{\phi}_1)-u_y\,(\Omega_y+\dot{u}_z)-u_z\,(\Omega_z-\dot{u}_y)\right]^2 dx$$

$$+\frac{1}{2}\int_0^h\left[J_{zz}+\frac{J_{yzz}}{R}\right]\left[u_y(\Omega_x+\dot{\phi}_1)+(\Omega_y+\dot{u}_z)+\phi_1\,(\Omega_z-\dot{u}_y)\right]^2 dx$$

$$+\frac{1}{2}\int_0^h\left[J_{yy}+\frac{J_{yyy}}{R}\right]\left[u_z(\Omega_x+\dot{\phi}_1)-\phi_1\,(\Omega_y+\dot{u}_z)+(\Omega_z-\dot{u}_y)\right]^2 dx$$

$$-\int_0^h\frac{J_{yyz}}{R}\left[u_y(\Omega_x+\dot{\phi}_1)+(\Omega_y+\dot{u}_z)+\phi_1\,(\Omega_z-\dot{u}_y)\right]$$

$$\left[u_z(\Omega_x+\dot{\phi}_1)-\phi_1\,(\Omega_y+\dot{u}_z)+(\Omega_z-\dot{u}_y)\right]dx. \tag{4.37}$$

The first two integrals in (4.37) relate to the translational kinetic energy even though J_{yy} enters the second integral. The last four integrals are the remaining rotational kinetic energy terms after cancellation. Invoking the no-shear assumption results in:

$$
\begin{aligned}
T_{RA} = \frac{1}{2}\int_0^h m\Big\{&[\Omega_y(z_C+w_0)-\Omega_z(y_C+v_0)+\dot{u}_0]^2+\\
&[\Omega_z(x_C+u_0)-\Omega_x(z_C+w_0)+\dot{v}_0]^2+\\
&[\Omega_x(y_C+v_0)-\Omega_y(x_C+u_0)+\dot{w}_0]^2\Big\}dx\\
+\int_0^h \frac{J_{yy}}{R}\Big\{&\Big[\Omega_y(z_C+w_0)-\Omega_z(y_C+v_0)+\dot{u}_0\Big]\\
&\Big[\phi_1\Big(\Omega_y-\dot{w}_0'\Big)-\Big(\Omega_z+\dot{v}_0'-\frac{\dot{u}_0}{R}\Big)\Big]+\\
&\Big[\Omega_z(x_C+u_0)-\Omega_x(z_C+w_0)+\dot{v}_0\Big]\\
&\Big[\Big(\frac{u_0}{R}-v_0'\Big)\Big(\Omega_z+\dot{v}_0'-\frac{\dot{u}_0}{R}\Big)-\phi_1\Big(\Omega_x+\dot{\phi}_1\Big)\Big]+\\
&\Big[\Omega_x(y_C+v_0)-\Omega_y(x_C+u_0)+\dot{w}_0\Big]\\
&\Big[\Big(\Omega_x+\dot{\phi}_1\Big)+\Big(v_0'-\frac{u_0}{R}\Big)\Big(\Omega_y-\dot{w}_0'\Big)\Big]\Big\}dx\\
+\frac{1}{2}\int_0^h &\Big[J_0+\frac{J_{yyy}+J_{yzz}}{R}\Big]\\
&\Big[\Big(\Omega_x+\dot{\phi}_1\Big)+\Big(v_0'-\frac{u_0}{R}\Big)\Big(\Omega_y-\dot{w}_0'\Big)+w_0'\Big(\Omega_z+\dot{v}_0'-\frac{\dot{u}_0}{R}\Big)\Big]^2dx\\
+\frac{1}{2}\int_0^h &\Big[J_{zz}+\frac{J_{yzz}}{R}\Big]\Big[\Big(\frac{u_0}{R}-v_0'\Big)\Big(\Omega_x+\dot{\phi}_1\Big)+\Big(\Omega_y-\dot{w}_0'\Big)+\phi_1\Big(\Omega_z+\dot{v}_0'-\frac{\dot{u}_0}{R}\Big)\Big]^2dx\\
+\frac{1}{2}\int_0^h &\Big[J_{yy}+\frac{J_{yyy}}{R}\Big]\Big[-w_0'\Big(\Omega_x+\dot{\phi}_1\Big)-\phi_1\Big(\Omega_y-\dot{w}_0'\Big)+\Big(\Omega_z+\dot{v}_0'-\frac{\dot{u}_0}{R}\Big)\Big]^2dx\\
-\int_0^h &\frac{J_{yyz}}{R}\Big[\Big(\frac{u_0}{R}-v_0'\Big)\Big(\Omega_x+\dot{\phi}_1\Big)+\Big(\Omega_y-\dot{w}_0'\Big)+\phi_1\Big(\Omega_z+\dot{v}_0'-\frac{\dot{u}_0}{R}\Big)\Big]\\
&\Big[-w_0'\Big(\Omega_x+\dot{\phi}_1\Big)-\phi_1\Big(\Omega_y-\dot{w}_0'\Big)+\Big(\Omega_z+\dot{v}_0'-\frac{\dot{u}_0}{R}\Big)\Big]dx. \qquad (4.38)
\end{aligned}
$$

The Bernoulli-Euler simplification for circular beams requires an explicit understanding of the underlying assumptions. A circular beam element introduces the *elemental* radius, R, into the kinetic energy formulation without any *a priori* assumption regarding its magnitude in relation to the characteristic *system* length, $\mathcal{L}$. Thus, when rotational kinetic energy terms are ignored via the Bernoulli-Euler assumption with respect to *system* scaling, certain translational kinetic energy terms associated with the *elemental* shift in the center of mass no longer cancel (as in the case of Timoshenko and Rayleigh formulations). Therefore, the no-shear assumption must be introduced into the circular Timoshenko beam equation which explicitly separates the translational and rotational kinetic energy terms (4.36). Then, the appropriate rotational kinetic energy terms are omitted based on the Bernoulli-Euler assumption. Finally, after simplification using (4.34), the resulting kinetic energy for a circular Bernoulli-Euler beam in a rotating frame is:

$$
\begin{aligned}
T_{BE} = \frac{1}{2}\int_0^h m\Big\{ & \left[\Omega_y\left(z_C + w_0\right) - \Omega_z\left(y_C + v_0\right) + \dot{u}_0\right]^2 + \\
& \left[\Omega_z\left(x_C + u_0\right) - \Omega_x\left(z_C + w_0\right) + \dot{v}_0\right]^2 + \\
& \left[\Omega_x\left(y_C + v_0\right) - \Omega_y\left(x_C + u_0\right) + \dot{w}_0\right]^2\Big\} dx \\
+ \int_0^h \frac{J_{yy}}{R}\Big\{ & \Big[\Omega_y\left(z_C + w_0\right) - \Omega_z\left(y_C + v_0\right) + \dot{u}_0\Big] \\
& \Big[\phi_1\left(\Omega_y - \dot{w}_0'\right) - \left(\Omega_z + \dot{v}_0' - \frac{\dot{u}_0}{R}\right)\Big] + \\
& \Big[\Omega_z\left(x_C + u_0\right) - \Omega_x\left(z_C + w_0\right) + \dot{v}_0\Big] \\
& \Big[\left(\frac{u_0}{R} - v_0'\right)\left(\Omega_z + \dot{v}_0' - \frac{\dot{u}_0}{R}\right) - \phi_1\left(\Omega_x + \dot{\phi}_1\right)\Big] + \\
& \Big[\Omega_x\left(y_C + v_0\right) - \Omega_y\left(x_C + u_0\right) + \dot{w}_0\Big] \\
& \Big[\left(\Omega_x + \dot{\phi}_1\right) + \left(v_0' - \frac{u_0}{R}\right)\left(\Omega_y - \dot{w}_0'\right)\Big]\Big\} dx
\end{aligned}
$$

$$+\frac{1}{2}\int_0^h J_{yy}\frac{I_{yy}}{AR^2}\left\{\left[\phi_1\left(\Omega_y-\dot{w}_0'\right)-\left(\Omega_z+\dot{v}_0'-\frac{\dot{u}_0}{R}\right)\right]^2+\right.$$

$$\left[\left(\frac{u_0}{R}-v_0'\right)\left(\Omega_z+\dot{v}_0'-\frac{\dot{u}_0}{R}\right)-\phi_1\left(\Omega_x+\dot{\phi}_1\right)\right]^2+$$

$$\left.\left[\left(\Omega_x+\dot{\phi}_1\right)+\left(v_0'-\frac{u_0}{R}\right)\left(\Omega_y-\dot{w}_0'\right)\right]^2\right\}dx$$

$$+\frac{1}{2}\int_0^h\left[J_0+\frac{J_{yyy}+J_{yzz}}{R}-J_{yy}\frac{I_{yy}}{AR^2}\right]\left(\Omega_x+\dot{\phi}_1\right)^2dx. \tag{4.39}$$

Comparing (4.38) with (4.39) reveals translational kinetic energy terms involving $J_{yy}\frac{I_{yy}}{AR^2}$ which are no longer cancelled by rotational kinetic energy terms as a result of the Bernoulli-Euler simplification. These terms may indeed be insignificant, but only if R is of the same order of magnitude or larger than $\mathcal{L}$. This possibility is addressed by defining curvature approximations for the circular beam properties, which are derived independently of the assumptions for beam type in the following chapter.

5. CURVATURE APPROXIMATIONS FOR CIRCULAR BEAMS

The circular-beam strain and kinetic energy formulations of the previous chapters are developed with an exact (EX) characterization of the curvature. The strain energy formulations of (3.33) and (3.35) contain curvature-dependent moments of area defined via the Bickford-Maganty convention [39], namely:

$$I_{ij} = \iint \left(\frac{R}{R+y}\right) y^i z^j \, dydz, \quad i,j = 0,1,2. \tag{5.1}$$

The kinetic energy formulations account for the curvature-induced shift in the center of mass defined by:

$$\bar{y}_m = \frac{I_{yy}}{AR}, \text{ and} \tag{5.2a}$$

$$\bar{z}_m = 0, \tag{5.2b}$$

with respect to the beam axis located at the centroids of the cross sections and mindful of the coincident orientation of the y- and z-axes with the principal axes of the cross sections. Additional mass moments of inertia per unit length, J_{yyy}, J_{yyz}, and J_{yzz}, are introduced as a direct result of the shifted mass center.

For planar problems, the I_{ij}'s may be defined using the conventional cross-sectional properties in conjunction with the Winkler-Bach constant, Z, namely [57]:

$$I_{00} = A(1+Z), \tag{5.3a}$$

$$I_{10} = -ARZ, \text{ and} \tag{5.3b}$$

$$I_{20} = AR^2 Z. \tag{5.3c}$$

There is no similar constant relating I_{01}, I_{11}, and I_{02}. Thus, the burden of computing the I_{ij}'s has been relieved somewhat but may still prove too difficult for complex cross sections in general use. This chapter is devoted to developing

suitable approximations for the I_{ij}'s. These approximations form a natural hierarchy, and their rigorous derivations provide the means for correlating the various theories in the literature and understanding some heretofore surprising results.

The straight-beam (St) formulations for this research are characterized entirely by the cross-sectional area, A, and the moments of inertia, I_{yy} and I_{zz}, in conjunction with the mass density, ρ. Thus, developing curvature approximations (CA's) in terms of these properties would be most convenient. This is accomplished by utilizing the binomial expansion:

$$\frac{R}{R+y} = 1 - \frac{y}{R} + \left(\frac{y}{R}\right)^2 - \cdots. \tag{5.4}$$

Substituting this into (5.1), ignoring the terms involving $y^k z^\ell$, $(k+\ell) \geq 3$, and utilizing the principal-axis simplifications produce:

$$I_{00} \cong A + \frac{I_{yy}}{R^2}, \tag{5.5a}$$

$$I_{10} \cong -\frac{I_{yy}}{R}, \tag{5.5b}$$

$$I_{01} \cong 0, \tag{5.5c}$$

$$I_{20} \cong I_{yy}, \tag{5.5d}$$

$$I_{11} \cong 0, \text{ and} \tag{5.5e}$$

$$I_{02} \cong I_{zz}. \tag{5.5f}$$

This forms the basis for the "truncated series" approximation, designated by TR. This approximation also assumes that $J_{yyy} = J_{yyz} = J_{yzz} = 0$. Note that the approximation of the Winkler-Bach constant is merely:

$$Z \cong \frac{I_{yy}}{AR^2}. \tag{5.6}$$

More important is the fact that the mass center shift in (5.2) is represented *exactly* using the TR approximation.

A further simplification may be employed when the arc radius, R, is significantly larger than the cross-sectional dimensions such that:

$$\frac{R}{R+y} \cong 1. \tag{5.7}$$

This implies no curvature dependence of the cross-sectional properties, namely:

$$I_{00} \cong A, \tag{5.8a}$$

$$I_{20} \cong I_{yy}, \tag{5.8b}$$

$$I_{02} \cong I_{zz}, \text{ and} \tag{5.8c}$$

$$I_{ij} \cong 0, \text{ otherwise;} \tag{5.8d}$$

also:

$$Z \cong 0. \tag{5.9}$$

In addition, this "straight" curvature approximation, designated by ST (to distinguish it from the St designation for straight beams), produces no shift in the center of mass. Recalling the definition of axial stress (3.37) shows that the ST approximation eliminates the nonlinear variation of axial stress in the y-direction and the corresponding shift in the neutral axis of bending. A comparison of the curvature approximations for rectangular and toroidal beams is provided in Appendix 14.2.

The implications of the curvature approximations will be discussed in the context of Bernoulli-Euler beams, noting that similar trends occur for Rayleigh

and Timoshenko beams. Recall the strain energy of the circular Bernoulli-Euler beam in terms of the EX variables:

$$V_{BE:EX} = \frac{E}{2}\int_0^h \Big[I_{00}\Big(u_0' + \frac{v_0}{R}\Big)^2 + I_{20}\Big(-v_0'' + \frac{u_0'}{R}\Big)^2 + I_{02}\Big(-w_0'' - \frac{\phi_1}{R}\Big)^2 + 2I_{10}\Big(-v_0'' + \frac{u_0'}{R}\Big)\Big(u_0' + \frac{v_0}{R}\Big) + 2I_{11}\Big(-v_0'' + \frac{u_0'}{R}\Big)\Big(-w_0'' - \frac{\phi_1}{R}\Big) + 2I_{01}\Big(u_0' + \frac{v_0}{R}\Big)\Big(-w_0'' - \frac{\phi_1}{R}\Big)\Big]dx + \frac{G}{2}\int_0^h \Big[I_0\Big(\phi_1' - \frac{w_0'}{R}\Big)^2\Big]dx, \text{ or} \tag{5.10a}$$

$$V_{BE:EX} = \frac{E}{2}\int_0^h \Big[A\Big(u_0' + \frac{v_0}{R}\Big)^2 + AR^2Z\Big(-v_0'' - \frac{v_0}{R^2}\Big)^2 + I_{02}\Big(-w_0'' - \frac{\phi_1}{R}\Big)^2 + 2I_{11}\Big(-v_0'' + \frac{u_0'}{R}\Big)\Big(-w_0'' - \frac{\phi_1}{R}\Big) + 2I_{01}\Big(u_0' + \frac{v_0}{R}\Big)\Big(-w_0'' - \frac{\phi_1}{R}\Big)\Big]dx + \frac{G}{2}\int_0^h \Big[I_0\Big(\phi_1' - \frac{w_0'}{R}\Big)^2\Big]dx. \tag{5.10b}$$

Inserting the TR approximations of the I_{ij}'s produces:

$$V_{BE:TR} = \frac{E}{2}\int_0^h \Big[\Big(A + \frac{I_{yy}}{R^2}\Big)\Big(u_0' + \frac{v_0}{R}\Big)^2 + I_{yy}\Big(-v_0'' + \frac{u_0'}{R}\Big)^2 + I_{zz}\Big(-w_0'' - \frac{\phi_1}{R}\Big)^2 - 2\frac{I_{yy}}{R}\Big(-v_0'' + \frac{u_0'}{R}\Big)\Big(u_0' + \frac{v_0}{R}\Big)\Big]dx + \frac{G}{2}\int_0^h \Big[I_0\Big(\phi_1' - \frac{w_0'}{R}\Big)^2\Big]dx, \text{ or} \tag{5.11a}$$

$$V_{BE:TR} = \frac{E}{2}\int_0^h \Big[A\Big(u_0' + \frac{v_0}{R}\Big)^2 + I_{yy}\Big(-v_0'' - \frac{v_0}{R^2}\Big)^2 + I_{zz}\Big(-w_0'' - \frac{\phi_1}{R}\Big)^2\Big]dx + \frac{G}{2}\int_0^h \Big[I_0\Big(\phi_1' - \frac{w_0'}{R}\Big)^2\Big]dx. \tag{5.11b}$$

The two different forms shown in (5.10-11) illustrate the coupling of the strain energies associated with extension and in-plane bending due to the shift in the

neutral axis. Applying the ST approximation eliminates this coupling and reduces the strain energy to:

$$V_{BE:ST} = \frac{E}{2}\int_0^h \left[A\left(u_0' + \frac{v_0}{R}\right)^2 + I_{yy}\left(-v_0'' + \frac{u_0'}{R}\right)^2 + I_{zz}\left(-w_0'' - \frac{\phi_1}{R}\right)^2\right] dx$$

$$+ \frac{G}{2}\int_0^h \left[I_0\left(\phi_1' - \frac{w_0'}{R}\right)^2\right] dx. \tag{5.12}$$

From (4.39), the kinetic energy for a circular BE beam in a nonrotating frame (with cubic and quartic terms ignored) is defined by:

$$T_{BE} = \frac{1}{2}\int_0^h m\left[\dot{u}_0^2 + \dot{v}_0^2 + \dot{w}_0^2\right] dx$$

$$\underline{+\int_0^h \frac{J_{yy}}{R}\left[\dot{u}_0\left(-\dot{v}_0' + \frac{\dot{u}_0}{R}\right) + \dot{w}_0\dot{\phi}_1\right] dx}$$

$$\underline{+\frac{1}{2}\int_0^h J_{yy}\frac{I_{yy}}{AR^2}\left(-\dot{v}_0' + \frac{\dot{u}_0}{R}\right)^2 dx}$$

$$+\frac{1}{2}\int_0^h \left[J_0 + \underline{\underline{\frac{J_{yyy}}{R} + \frac{J_{yzz}}{R}}}\right]\left(\dot{\phi}_1\right)^2 dx. \tag{5.13}$$

The terms in (5.13) with a double underline are ignored in both TR and ST approximations; the ST approximation also excludes the (shifted mass center) terms with a single underline.

The most important feature regarding the curvature approximations is that they apply only to properties of the cross-sections; the proper coupling of the displacement variables is maintained. Thus, the results for a circular beam modeled with ST circular elements converge *identically* to the results of a model using an infinite number of straight (St) elements.

The torsional constant, I_0, appears to be independent of the curvature approximation. However, the fundamental substitution used in the formulation:

$$I_0 = k_T\left(I_{20} + I_{02}\right), \tag{5.14}$$

suggests a possible increase in I_0 for EX and TR approximations assuming k_T is not a function of curvature (see Tables 14.2.2-3). However, recall that the axial rotation, ϕ_1, is defined assuming that the center of twist is coincident with the cross-sectional centroid. Curvature produces a shift in the center of twist (even for doubly-symmetric cross sections) which cannot be characterized by the displacement assumptions for engineering beams. Thus, the torsional constant will be assumed independent of curvature for the purposes of this research; (5.14) merely defines the appropriate substitution for circular beams.

The hierarchy of curvature approximations provides a means of understanding similar formulations in literature, particularly for planar problems. Filipich and Laura [58] utilized the almost classical formulation for circular BE beams with ST approximations. BE:ST formulations have also been applied to problems involving variable curvature [54,59]. It is most interesting to note that first-order analyses of in-plane bending vibrations for arches and rings typically employ an assumption of zero extension of the centroidal axis [60], namely:

$$\epsilon_\theta|_{y=0} = u_0' + \frac{v_0}{R} \cong 0, \text{ or} \tag{5.15a}$$

$$u_0' \cong -\frac{v_0}{R}. \tag{5.15b}$$

This relationship explicitly eliminates the extensional energy for ST approximations and cancels what may be interpreted as the extensional energy for TR approximations when viewed in the context of (5.11*b*). Applying this assumption to the planar terms of (5.12) produces:

$$V_{BE:ST} \cong \frac{EI_{yy}}{2} \int_0^h \left(-v_0'' - \frac{v_0}{R^2}\right)^2 dx. \tag{5.16}$$

However, (5.11*b*) shows this to be what may be considered the bending energy for BE:TR beams. Thus, assuming inextensibility for ST beams may actually

produce better approximations of in-plane bending frequencies if the extensional energy is indeed small. The validity of this assumption will be explored in Chapter 9.

Many planar formulations in the literature are hybrids of the ones derived for this research. Den Hartog's 1928 formulation [61] coupled BE:TR strain energy with BE:ST kinetic energy; it is uncertain that this was his intent but it continues to confuse researchers unfamiliar with higher-order curvature approximations [58]. Seidel and Erdelyi [62] formulated a Timoshenko ring with EX extensional and bending energies and ST shear and kinetic energies; they also applied the inextensibility assumption. Kirkhope developed two Timoshenko ring formulations, one with ST and inextensional approximations [63] and the other with what appears to be TR extensional and bending energies (he formulated these energies in terms of the Winkler-Bach constant but noted the truncated-series approximation in (5.6)), ST shear energy, and TR kinetic energy [64]. Comparisons of the two theories with experimental data [65] showed similar trends, with the ST ring being more accurate in some cases; this is not surprising based on the above discussion. Kirkhope's out-of-plane formulation for circular TI rings relied exclusively on ST approximations [66]. No formulation, for any beam type, has been found in the literature which fully utilizes the exact characterization of curvature.

6. INTRODUCTION OF GEOMETRIC NONLINEARITIES

The words of Harold Martin [67] serve as an appropriate introduction to this section:

> *Engineers by training and tradition are prone to think of nature as being essentially linear in action and behavior. This, however, is seldom the case. For the most part, it is merely good fortune when a linear theory will predict actual behavior with satisfactory accuracy over a useful range of parameters. It is therefore not surprising that there are important areas for which linear theory is totally inadequate. The geometrically nonlinear problem of structural mechanics is such an area.*
>
> *The hope of successfully grappling with nonlinear problems has long been the goal of the engineering analyst... Nonlinear theory is inevitably more complex than the corresponding linear theory. Consequently, the application of nonlinear theory to physical problems leads to mathematical problems which are usually intractable... At the present time, finite elements offer the greatest hope for solving complex nonlinear problems.*

The displacement-based energy formulations provide an excellent foundation for the inclusion of geometric nonlinearities. The terms deemed relevant for this research of engineering beams may be obtained merely by retaining the quadratic terms in the strain/displacement relationships [68,69]. This approach is often and inappropriately termed a "moderate rotation" formulation; the small rotation assumptions used to define the beam kinematics are still used in the nonlinear strain/displacement relations. Also, problems requiring the inclusion of geometric nonlinearities need not have deflections any larger than those of a

comparable linear analysis. Thus, "large displacement" is another misnomer for this type of analysis.

6.1 NONLINEAR FORMULATION FOR STRAIGHT BEAMS

The nonlinear Green's strains in a Cartesian space are defined as follows [70]:

$$\begin{aligned}\varepsilon_x &= \left[\frac{\partial u}{\partial x}\right] + \frac{1}{2}\left[\left(\frac{\partial u}{\partial x}\right)^2 + \left(\frac{\partial v}{\partial x}\right)^2 + \left(\frac{\partial w}{\partial x}\right)^2\right] \\ &\cong \left[\frac{\partial u}{\partial x}\right] + \frac{1}{2}\left[\left(\frac{\partial v}{\partial x}\right)^2 + \left(\frac{\partial w}{\partial x}\right)^2\right], \end{aligned} \tag{6.1a}$$

$$\begin{aligned}\gamma_{xy} &= \left[\frac{\partial u}{\partial y} + \frac{\partial v}{\partial x}\right] + \left[\frac{\partial u}{\partial x}\frac{\partial u}{\partial y} + \frac{\partial v}{\partial x}\frac{\partial v}{\partial y} + \frac{\partial w}{\partial x}\frac{\partial w}{\partial y}\right] \\ &\cong \left[\frac{\partial u}{\partial y} + \frac{\partial v}{\partial x}\right] + \left[\frac{\partial v}{\partial x}\frac{\partial v}{\partial y} + \frac{\partial w}{\partial x}\frac{\partial w}{\partial y}\right], \text{ and} \end{aligned} \tag{6.1b}$$

$$\begin{aligned}\gamma_{xz} &= \left[\frac{\partial w}{\partial x} + \frac{\partial u}{\partial z}\right] + \left[\frac{\partial u}{\partial z}\frac{\partial u}{\partial x} + \frac{\partial v}{\partial z}\frac{\partial v}{\partial x} + \frac{\partial w}{\partial z}\frac{\partial w}{\partial x}\right] \\ &\cong \left[\frac{\partial w}{\partial x} + \frac{\partial u}{\partial z}\right] + \left[\frac{\partial v}{\partial z}\frac{\partial v}{\partial x} + \frac{\partial w}{\partial z}\frac{\partial w}{\partial x}\right]. \end{aligned} \tag{6.1c}$$

The exclusion of quadratic terms involving $\partial u/\partial x$ is based on the assumption of small axial strains. Substituting the three-dimensional Timoshenko displacements (2.34) results in:

$$\varepsilon_x = \left[u_0' + yu_y' + zu_z'\right] + (1/2)\left[(v_0' - z\phi_1')^2 + (w_0' + y\phi_1')^2\right], \tag{6.2a}$$

$$\gamma_{xy} = \left[u_y + v_0' - z\phi_1'\right] + \left[(w_0' + y\phi_1')\,(\phi_1)\right], \text{ and} \tag{6.2b}$$

$$\gamma_{xz} = \left[u_z + w_0' + y\phi_1'\right] + \left[(v_0' - z\phi_1')\,(-\phi_1)\right]. \tag{6.2c}$$

The one-dimensional stress/strain law is again applied to the axial strain. Rearranging the shear strain terms as in (3.15):

$$\gamma_{xy} = (u_y + v_0' + w_0'\phi_1) - (z - y\phi_1)\,(\phi_1') = (\gamma_{xy})_{F_y} + (\gamma_{xy})_T, \text{ and} \tag{6.3a}$$

$$\gamma_{xz} = (u_z + w_0' - v_0'\phi_1) + (y + z\phi_1)\,(\phi_1') = (\gamma_{xz})_{F_z} + (\gamma_{xz})_T, \tag{6.3b}$$

allows for a similar application of the Timoshenko shear correction factors and Saint-Venant torsional constant in computing the strain energy.

The resulting integration of the strain energy will possess the linear terms from before (3.18) plus cubic and quartic terms involving the displacement variables and their x-derivatives. The quartic terms are assumed negligible; this not only eliminates strain energy terms from the three strains in (6.2-3) but allows e_y, e_z, and γ_{yz} to be ignored even though they are no longer identically zero. The strain energy is thus computed to be:

$$\begin{aligned} V_{TI} = \frac{E}{2}\int_0^h \Big\{ & \left[A\left(u_0'\right)^2 + I_{yy}\left(u_y'\right)^2 + I_{zz}\left(u_z'\right)^2\right] \\ & + Au_0'\left[\left(v_0'\right)^2 + \left(w_0'\right)^2\right] \\ & + \left(I_{yy} + I_{zz}\right)u_0'\left(\phi_1'\right)^2 \\ & - 2I_{zz}u_z'\left(v_0'\phi_1'\right) \\ & + 2I_{yy}u_y'\left(w_0'\phi_1'\right)\Big\}dx \\ + \frac{G}{2}\int_0^h \Big\{ & \left[Ak_y\left(u_y + v_0'\right)^2 + Ak_z\left(u_z + w_0'\right)^2 + I_0\left(\phi_1'\right)^2\right] \\ & + 2k_yA\left(u_y + v_0'\right)\left(w_0'\phi_1\right) \\ & - 2k_zA\left(u_z + w_0'\right)\left(v_0'\phi_1\right)\Big\}dx. \end{aligned} \tag{6.4}$$

Recognizing the linear terms from (3.18) and utilizing the definitions of the integrated forces and moments from Section 3.5, the strain energy may be rewritten

as:

$$V = (V)_{LINEAR}$$
$$+\frac{1}{2}\int_0^h \Big\{ F_x \left[(v_0')^2 + (w_0')^2 \right]$$
$$+\frac{F_x}{A}\left(I_{yy} + I_{zz}\right)(\phi_1')^2$$
$$-2\left(M_y v_0' + M_z w_0'\right)\phi_1'$$
$$+2\left(F_y w_0' - F_z v_0'\right)\phi_1 \Big\} dx. \qquad (6.5)$$

The first nonlinear term in (6.5) characterizes Euler buckling of beam-columns. The second term relates to the torsional buckling potential of a column. Warping rigidity, necessary for an accurate evaluation of torsional buckling for open, thin-walled sections, does not enter this formulation but its exclusion is a conservative assumption. Recall that the centroid and center of twist are assumed coincident, thus uncoupling the Euler and torsional buckling terms. The third term is associated with lateral buckling, representing the potential for moment-induced twisting in a beam. The final term represents another form of lateral buckling. All of these nonlinearities are discussed in great detail in elementary stability texts [16,71].

Equation 6.5 is purposely written without any specification of beam type. While this formulation is based on Timoshenko beams, u_y and u_z do not enter into the nonlinear terms after the integrated forces and moments are introduced. Thus, (6.5) is equally applicable to Timoshenko, Rayleigh, or Bernoulli-Euler straight beams by substituting their respective force and moment equations. Note, however, that the BE/RA shear-induced lateral buckling terms must be derived from Newtonian principles since the no-shear assumption eliminates these terms from the energy formulation. Their existence is confirmed by a comparable

NASTRAN beam formulation [72]. Recalling (1.36), the deformation-induced changes in the forces and moments may be included via the outlined iteration procedure.

6.2 NONLINEAR FORMULATION FOR CIRCULAR BEAMS

Nowhere in these theoretical formulations does the progression of complexity benefit overall understanding more than in the development of geometric nonlinearities for circular beams. The straight-beam formulation provides insight into the underlying assumptions necessary to extract the geometric nonlinearities from the strain energy computed using quadratic strains. While the stability of arches and rings has been the subject of extensive research ([73] provides an excellent compendium), this general formulation in three-dimensional space is a new development. The result of this section is an equation similar to (6.5) for circular beams.

The formulation begins with the inclusion of the quadratic terms in the strain/displacement relationships for cylindrical coordinates, namely [52]:

$$\begin{aligned}
\varepsilon_\theta &= \left[\frac{1}{r}\frac{\partial u}{\partial \theta} + \frac{v}{r}\right] + \frac{1}{2}\left[\left(\frac{1}{r}\frac{\partial u}{\partial \theta} + \frac{v}{r}\right)^2 + \left(\frac{1}{r}\frac{\partial v}{\partial \theta} - \frac{u}{r}\right)^2 + \left(\frac{1}{r}\frac{\partial w}{\partial \theta}\right)^2\right] \\
&= \left(\frac{R}{R+y}\right)\left[\frac{\partial u}{\partial x} + \frac{v}{R}\right] \\
&\quad + \frac{1}{2}\left(\frac{R}{R+y}\right)^2\left[\left(\frac{\partial u}{\partial x} + \frac{v}{R}\right)^2 + \left(\frac{\partial v}{\partial x} - \frac{u}{R}\right)^2 + \left(\frac{\partial w}{\partial x}\right)^2\right], \qquad (6.6a) \\
\gamma_{\theta r} &= \left[\frac{\partial u}{\partial r} - \frac{u}{r} + \frac{1}{r}\frac{\partial v}{\partial \theta}\right] + \left[\left(\frac{1}{r}\frac{\partial u}{\partial \theta} + \frac{v}{r}\right)\frac{\partial u}{\partial r} + \left(\frac{1}{r}\frac{\partial v}{\partial \theta} - \frac{u}{r}\right)\frac{\partial v}{\partial r} + \left(\frac{1}{r}\frac{\partial w}{\partial \theta}\right)\frac{\partial w}{\partial r}\right] \\
&= \left(\frac{R}{R+y}\right)\left[\left(1 + \frac{y}{R}\right)\frac{\partial u}{\partial y} - \frac{u}{R} + \frac{\partial v}{\partial x}\right] \\
&\quad + \left(\frac{R}{R+y}\right)\left[\left(\frac{\partial u}{\partial x} + \frac{v}{R}\right)\frac{\partial u}{\partial y} + \left(\frac{\partial v}{\partial x} - \frac{u}{r}\right)\frac{\partial v}{\partial y} + \frac{\partial w}{\partial x}\frac{\partial w}{\partial y}\right], \text{ and} \qquad (6.6b)
\end{aligned}$$

$$\gamma_{x\theta} = \left[\frac{1}{r}\frac{\partial w}{\partial \theta} + \frac{\partial u}{\partial z}\right] + \left[\frac{\partial u}{\partial z}\left(\frac{1}{r}\frac{\partial u}{\partial \theta} + \frac{v}{r}\right) + \frac{\partial v}{\partial z}\left(\frac{1}{r}\frac{\partial v}{\partial \theta} - \frac{u}{r}\right) + \frac{\partial w}{\partial z}\left(\frac{1}{r}\frac{\partial w}{\partial \theta}\right)\right]$$

$$= \left(\frac{R}{R+y}\right)\left[\frac{\partial w}{\partial x} + \left(1 + \frac{y}{R}\right)\frac{\partial u}{\partial z}\right]$$

$$+ \left(\frac{R}{R+y}\right)\left[\frac{\partial u}{\partial z}\left(\frac{\partial u}{\partial x} + \frac{v}{R}\right) + \frac{\partial v}{\partial z}\left(\frac{\partial v}{\partial x} - \frac{u}{R}\right) + \frac{\partial w}{\partial z}\frac{\partial w}{\partial x}\right]. \tag{6.6c}$$

The small axial strain assumption takes on a greater significance for circular beams. Not only does it allow for the exclusion of quadratic terms involving $(\partial u/\partial x + v/R)$, but also implies that the beam is not "short." This in turn suggests that the ST curvature approximation is sufficient to quantify the cross-sectional properties.

Note that the axial strain energy computed from (6.6*a*) will contain terms involving curvature-dependent moments of area defined by:

$$I^*_{ij} = \iint \left(\frac{R}{R+y}\right)^2 y^i z^i dy dz \quad i,j = 0,1,2,3. \tag{6.7}$$

It will be assumed for the purposes of computing the geometric nonlinearities that the ST curvature approximation may be extended such that:

$$I^*_{00} \cong A, \tag{6.8a}$$

$$I^*_{20} \cong I_{yy}, \tag{6.8b}$$

$$I^*_{02} \cong I_{zz}, \text{ and} \tag{6.8c}$$

$$I^*_{ij} \cong 0, \text{ otherwise.} \tag{6.8d}$$

Therefore, the approximate strains in terms of the Timoshenko displacement variables are:

$$\varepsilon_\theta \cong \left[u_0' + \frac{v_0}{R} + y u_y' + z\left(u_z' - \frac{\phi_1}{R}\right)\right]$$

$$+ \frac{1}{2}\left[\left(v_0' - \frac{u_0}{R} - z\left(\phi_1' + \frac{u_z}{R}\right)\right)^2 + \left(w_0' + y\phi_1'\right)^2\right], \tag{6.9a}$$

$$\gamma_{\theta r} \cong \left[u_y + v_0' - \frac{u_0}{R} - z\left(\phi_1' + \frac{u_z}{R}\right)\right] + \left[\left(w_0' + y\phi_1'\right)\left(\phi_1\right)\right], \text{ and} \tag{6.9b}$$

$$\gamma_{x\theta} \cong \left[u_x + w_0' + y\left(\phi_1' + \frac{u_x}{R}\right)\right] + \left[\left(v_0' - \frac{u_0}{R} - z\left(\phi_1' + \frac{u_x}{R}\right)\right)\left(-\phi_1\right)\right]. \tag{6.9c}$$

Note that the quadratic terms containing (y/R) in (6.9) are also assumed to be eliminated by the ST approximation, but the (z/R) terms are chosen to be maintained.

Applying the appropriate correction factors and performing the strain energy integration result in:

$$\begin{aligned} V_{TI} = \frac{E}{2}\int_0^h \Bigg\{ & \left[A\left(u_0' + \frac{v_0}{R}\right)^2 + I_{yy}\left(u_y'\right)^2 + I_{xx}\left(u_x' - \frac{\phi_1}{R}\right)^2\right] \\ & + A\left(u_0' + \frac{v_0}{R}\right)\left[\left(v_0' - \frac{u_0}{R}\right)^2 + \left(w_0'\right)^2\right] \\ & + I_{yy}\left(u_0' + \frac{v_0}{R}\right)\left(\phi_1'\right)^2 \\ & + I_{xx}\left(u_0' + \frac{v_0}{R}\right)\left(\phi_1' + \frac{u_x}{R}\right)^2 \\ & - 2I_{xx}\left(u_x' - \frac{\phi_1}{R}\right)\left(v_0' - \frac{u_0}{R}\right)\left(\phi_1' + \frac{u_x}{R}\right) \\ & + 2I_{yy}\left(u_y'\right)\left(w_0'\right)\left(\phi_1'\right)\Bigg\}dx \\ + \frac{G}{2}\int_0^h \Bigg\{ & \left[k_y A\left(u_y + v_0' - \frac{u_0}{R}\right)^2 + k_x A\left(u_x + w_0'\right)^2 + I_0\left(\phi_1' + \frac{u_x}{R}\right)^2\right] \\ & + 2k_y A\left(u_y + v_0' - \frac{u_0}{R}\right)\left(w_0'\right)\left(\phi_1\right) \\ & - 2k_x A\left(u_x + w_0'\right)\left(v_0' - \frac{u_0}{R}\right)\left(\phi_1\right)\Bigg\}dx. \end{aligned} \tag{6.10}$$

Substituting the integrated force and moment relations consistent with the ST approximation results in:

$$
\begin{aligned}
V_{TI} &= (V_{TI})_{LINEAR} \\
&+ \frac{1}{2}\int_0^h \Bigg\{ F_x \left[\left(v_0' - \frac{u_0}{R} \right)^2 + \left(w_0' \right)^2 \right] \\
&\quad + \frac{F_x}{A} \left[I_{yy} \left(\phi_1' \right)^2 + I_{zz} \left(\phi_1' + \frac{u_x}{R} \right)^2 \right] \\
&\quad - 2 \left[M_y \left(v_0' - \frac{u_0}{R} \right) \left(\phi_1' + \frac{u_x}{R} \right) + M_z \left(w_0' \right) \left(\phi_1' \right) \right] \\
&\quad + 2 \left[F_y w_0' - F_z \left(v_0' - \frac{u_0}{R} \right) \right] \left(\phi_1 \right) \Bigg\} dx,
\end{aligned}
\tag{6.11}
$$

where $(V_{TI})_{LINEAR}$ is provided by (3.33). Note that the Timoshenko rotations are present in (6.11), but with the appropriate substitution of the no-shear assumptions (3.34):

$$
\begin{aligned}
V_{BE/RA} &= (V_{BE/RA})_{LINEAR} \\
&+ \frac{1}{2}\int_0^h \Bigg\{ F_x \left[\left(v_0' - \frac{u_0}{R} \right)^2 + \left(w_0' \right)^2 \right] \\
&\quad + \frac{F_x}{A} \left[I_{yy} \left(\phi_1' \right)^2 + I_{zz} \left(\phi_1' - \frac{w_0'}{R} \right)^2 \right] \\
&\quad - 2 \left[M_y \left(v_0' - \frac{u_0}{R} \right) \left(\phi_1' - \frac{w_0'}{R} \right) + M_z \left(w_0' \right) \left(\phi_1' \right) \right] \\
&\quad + 2 \left[F_y w_0' - F_z \left(v_0' - \frac{u_0}{R} \right) \right] \left(\phi_1 \right) \Bigg\} dx,
\end{aligned}
\tag{6.12}
$$

where $(V_{BE/RA})_{LINEAR}$ is provided by (3.35).

The planar terms in the formulation of circular-beam nonlinearities are identical to those of Langhaar, Boresi, and Carver [74]. Furthermore, their analysis compared favorably with experimental results when ST-approximated geometric nonlinearities were added to the EX linear strain energy. This concept is often

used implicitly in the analysis of preloaded arches and rings [75]. Equations 6.11-12 are expressed in terms which allow for the inclusion of geometric nonlinearities regardless of which curvature approximation is used.

The buckling of arches and rings is further complicated by the assumptions made regarding post-deformation load orientation. Three approaches may be taken [76]:

1) Hydrostatic: the load maintains a normal orientation to the deformed surface.
2) Constant direction: the load is assumed to maintain the undeformed orientation. This most simple and common approach is adopted for this research due to its applicability to gravitational and centrifugal loading.
3) Centrally directed: the (pressure) load is assumed to remain directed toward the center of the arc [77].

Wempner and Kesti [78] have shown that the critical pressure for a circular ring possesses a 3/4/4.5 relationship with respect to hydrostatic/constant direction/centrally directed loading assumptions.

7. FINITE ELEMENT DISCRETIZATION FOR BEAM PROBLEMS

The previous chapters have focused on the formulation of the potential and kinetic energies for beam elements. Rotating coordinate system effects have been included explicitly and the derivation of geometric nonlinearities has been presented. So far, the derivations have centered on an individual element and have been defined in terms of the beam properties, the beam displacement variables relative to the local frame, and the position and orientation of the element relative to the inertial frame.

This chapter is devoted to the definition of the polynomial-based finite element space, namely:

$$S^{[p]}(\Upsilon, \Psi, \Delta, \{Q\}) \subset E(\Upsilon), \tag{7.1}$$

where the following definitions elaborate on this description:

$\Upsilon \equiv$ domain.

$\Psi \equiv$ beam type. The beam type is assumed to be identical for all elements in a given analysis.

$n_D(\Psi) \equiv$ number of three-dimensional displacement variables for a given beam type. Thus, $n_D = 4$ for Bernoulli-Euler and Rayleigh beams and relates to u_0, v_0, w_0 and ϕ_1, in that order; $n_D = 6$ for Timoshenko beams with the inclusion of u_y and u_z. The simplification for planar problems will be made via application of the appropriate constraints (see Section 7.6).

$\Delta \equiv$ mesh or partition. The mesh defines the division of the entire domain into subdomains or elements.

$n_E(\Delta) \equiv$ number of subdomains or elements.

$n_G(\Delta) \equiv$ number of grid points or nodes used to define the mesh.

$\Upsilon^{(k)}$ $\equiv$ domain of the kth element. This subdomain may be defined in terms of the local coordinates as:

$$\Upsilon^{(k)} = \left\{ x \mid x_A^{(k)} < x < x_B^{(k)},\ h^{(k)} = x_B^{(k)} - x_A^{(k)} \right\}, \tag{7.2}$$

where A and B refer to the ends of the beam element (see Figures 2.2-3). Note that the beam displacement variables are only functions of x and t and will be defined in the context of assumed-modes via separation of variables.

$\Upsilon^{(st)}$ $\equiv$ standard element defined as:

$$\Upsilon^{(st)} = \{ \xi \mid -1 < \xi < +1 \}. \tag{7.3}$$

$\{Q\}$ $\equiv n_E \times 1$ vector of mapping functions. $Q^{(k)}(\xi)$ maps the kth element to the standard domain. Linear mapping is used exclusively in this research, namely:

$$x = Q^{(k)}(\xi) = \left(\frac{1-\xi}{2} \right) x_A^{(k)} + \left(\frac{1+\xi}{2} \right) x_B^{(k)}, \text{ for} \tag{7.4a}$$

$$x \in \Upsilon^{(k)}. \tag{7.4b}$$

$[p]$ $\equiv n_D \times n_E$ matrix of polynomial orders. The concept of adaptive p-refinement may be seen in this context though it is not addressed. Furthermore, the polynomial orders are assumed independent of the element number for this study, namely:

$$p_{ij} \equiv p_i, \quad j = 1, 2, \ldots, n_E. \tag{7.5}$$

This in no way precludes the process of hierarchic extensions in p_i, $i = 1, 2, \ldots, n_D$. The relationship between the polynomial orders of the various displacement variables will merit future discussion. PVAEB is currently limited to $p_i \leq 9$.

$C_\ell(\Upsilon)$ $\equiv$ set of all displacement functions on Υ with bounded continuous derivatives up to order ℓ.

7.1 DEFINITION OF ELEMENTAL SHAPE FUNCTIONS

The elemental shape functions form the basis for the systematic definition of the basis functions for the finite element space. The shape functions and basis functions are *not* the same, in general. The shape functions are defined in the local frame for a single element. The basis functions will be defined in either the local or global frame and may involve a linear combination of the shape functions in conjunction with local-to-global transformations. They may indeed span more than one element in the context of local support. The distinction between these functions will become obvious through the ensuing discussion.

The beam displacement variables for each element are approximated as a linear combination of the elemental shape functions in conjunction with the element mapping (7.4) and complex harmonic response (1.16). For example, the axial displacement is approximated as:

$$\begin{aligned} u_0^{(k)}(x,t) &= u_0^{(k)}\left(Q^{(k)}(\xi),t\right) \\ &\cong \sum_{j=1}^{p_1+1} u_{0,j}^{(k)} N_j(\xi) e^{i\omega t} \\ &\cong \left\{u_{0,j}^{(k)}\right\}^T \{N_j(\xi)\}\, e^{i\omega t}, \end{aligned} \tag{7.6}$$

where $N_j(\xi)$ are the elemental shape functions and $u_{0,j}^{(k)}$ are the unknown coefficients. The elemental shape functions are chosen to be polynomials for this research. Additional objectives regarding their definition include:

1) ensuring finite strain energy,

2) producing basis functions which are complete (1.10),

3) minimizing connectivity between adjoining elements,

4) producing hierarchic elemental matrices,

5) maximizing sparseness of elemental matrices, and

6) promoting numerical stability.

The latter two desires suggest the use of orthogonal polynomials, but this conflicts with the desire for minimum connectivity. Thus, appropriate compromises must be invoked.

The issue of finite strain energy must be addressed in the context of the formulations in Chapter 3. The strain energy for Timoshenko beams (3.18,33) involves the first derivatives (in x) of all six displacement variables. Thus, all six variables must be contained in the C_0 space to ensure finite strain energy. The $N_j(\xi)$ shape functions will be chosen to be C_0-compatible such that for:

TI Beams:
$$u_0^{(k)}\left(Q^{(k)}(\xi),t\right) \cong \sum_{j=1}^{p_1+1} u_{0,j}^{(k)} N_j(\xi) e^{i\omega t}, \tag{7.7a}$$

$$v_0^{(k)}\left(Q^{(k)}(\xi),t\right) \cong \sum_{j=1}^{p_2+1} v_{0,j}^{(k)} N_j(\xi) e^{i\omega t}, \tag{7.7b}$$

$$w_0^{(k)}\left(Q^{(k)}(\xi),t\right) \cong \sum_{j=1}^{p_3+1} w_{0,j}^{(k)} N_j(\xi) e^{i\omega t}, \tag{7.7c}$$

$$\phi_1^{(k)}\left(Q^{(k)}(\xi),t\right) \cong \sum_{j=1}^{p_4+1} \phi_{1,j}^{(k)} N_j(\xi) e^{i\omega t}, \tag{7.7d}$$

$$u_y^{(k)}\left(Q^{(k)}(\xi),t\right) \cong \sum_{j=1}^{p_5+1} u_{y,j}^{(k)} N_j(\xi) e^{i\omega t}, \text{ and} \tag{7.7e}$$

$$u_z^{(k)}\left(Q^{(k)}(\xi),t\right) \cong \sum_{j=1}^{p_6+1} u_{z,j}^{(k)} N_j(\xi) e^{i\omega t}. \tag{7.7f}$$

Note that the x-derivatives of the displacement variables may be related to the ξ-derivatives of the shape functions, for example:

$$\frac{d^m}{dx^m}\left(u_0^{(k)}(Q^{(k)}(\xi),t)\right) \cong \left(\frac{2}{h^{(k)}}\right)^m \left(\sum_{j=1}^{p_1+1} u_{0,j}^{(k)} \frac{d^m N_j(\xi)}{d\xi^m} e^{i\omega t}\right), \tag{7.8}$$

or, in shorthand:

$$u_0' \cong \left(\frac{2}{h}\right) \{u_{0,j}\}^T \{N_j^*\}\, e^{i\omega t}, \tag{7.9a}$$

$$u_0'' \cong \left(\frac{2}{h}\right)^2 \{u_{0,j}\}^T \{N_j^{**}\}\, e^{i\omega t}, \text{ etc.,} \tag{7.9b}$$

where $^* \equiv d/d\xi$ and the element designation ((k) superscript) has been dropped for simplicity.

The compromise between minimum connectivity and maximum sparseness and stability for C_0 functions has been developed previously [29]. The linear interpolants serve as the first two shape functions, namely:

$$N_1(\xi) = \frac{1-\xi}{2} = \frac{P_0(\xi) - P_1(\xi)}{2}: \quad N_1(-1) = 1,\ N_1(+1) = 0; \text{ and} \tag{7.10a}$$

$$N_2(\xi) = \frac{1+\xi}{2} = \frac{P_0(\xi) + P_1(\xi)}{2}: \quad N_2(-1) = 0,\ N_2(+1) = 1; \tag{7.10b}$$

the relationship between these functions and the Legendre polynomials, $P_i(\xi)$, is noted for future reference. Thus, all of the interelement connectivities may be conveniently enforced using the linear interpolants (termed external modes) in (7.7), noting that $p_i \geq 1,\ i = 1,2,\ldots,6$, is required. Also note that $p_i = 1,\ i = 1,2,\ldots,6$, represent the lowest-order approximations typically used in h-version, TI beam elements.

Additional shape functions may be constructed to be zero at the ends (called internal modes) using Legendre polynomials. They are defined by:

$$N_j(\xi) = \sqrt{\frac{2j-3}{2}} \int_{-1}^{\xi} P_{j-2}(t)dt = \frac{1}{\sqrt{2(2j-3)}} \Big(P_{j-1}(\xi) - P_{j-3}(\xi)\Big), \text{ where} \tag{7.11a}$$

$$N_j(-1) = N_j(+1) = 0, \text{ for} \tag{7.11b}$$

$$j > 2. \tag{7.11c}$$

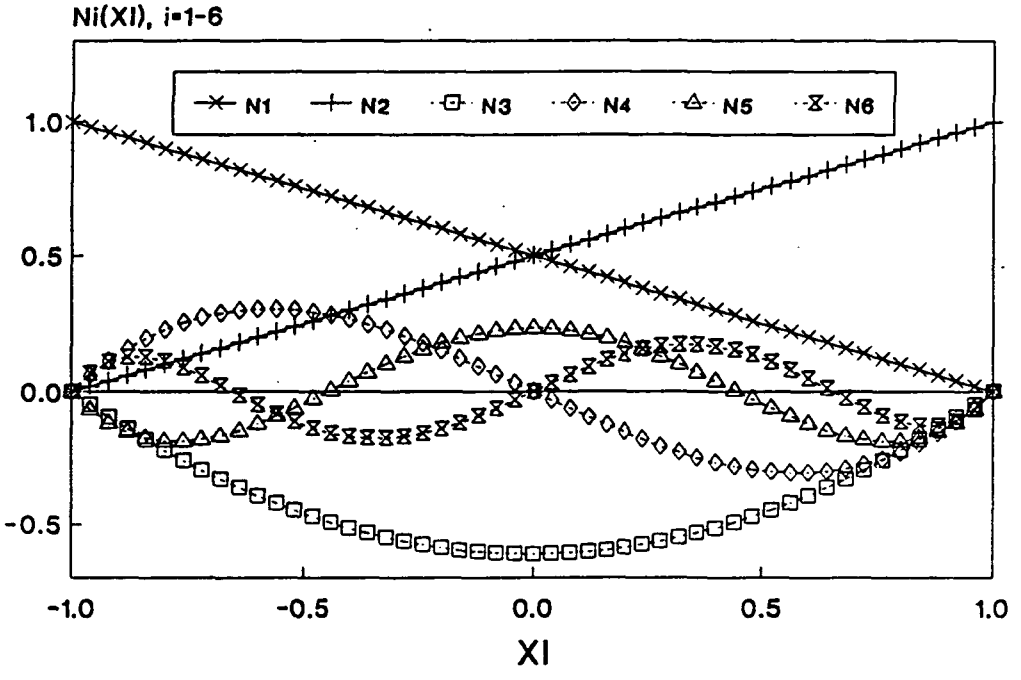

Figure 7.1 C_0-compatible elemental shape functions.

This choice of functions is certainly not unique even in the space of polynomials [23,79], but they do satisfy the stated desires for the elemental shape functions. The specification of the standard element has some effect on function selection.

Figure 7.1 illustrates the first six C_0 elemental shape functions. Of particular interest are two integrals which factor into the elemental formulations. For $i, j \leq 6$:

$$\int_{-1}^{+1} \{N_i\}\{N_j\}^T d\xi = \begin{bmatrix} \frac{2}{3} & \frac{1}{3} & \frac{-1}{\sqrt{6}} & \frac{1}{3\sqrt{10}} & 0 & 0 \\ & \frac{2}{3} & \frac{-1}{\sqrt{6}} & \frac{-1}{3\sqrt{10}} & 0 & 0 \\ & & \frac{2}{5} & 0 & \frac{-1}{5\sqrt{21}} & 0 \\ & & & \frac{2}{21} & 0 & \frac{-1}{7\sqrt{45}} \\ & & & & \frac{2}{45} & 0 \\ & \text{Symmetric} & & & & \frac{2}{77} \end{bmatrix}, \tag{7.12}$$

where, for $i \geq 3$:

$$\int_{-1}^{+1} N_i^2 d\xi = \frac{2}{(2i-1)(2i-5)}, \text{ and} \tag{7.13a}$$

$$\int_{-1}^{+1} N_i N_{i+2} d\xi = \frac{-1}{(2i-1)\sqrt{(2i-3)(2i+1)}}; \tag{7.13b}$$

also:

$$\int_{-1}^{+1} \{N_i^*\}\{N_j^*\}^T d\xi = \begin{bmatrix} \frac{1}{2} & -\frac{1}{2} & 0 & 0 & 0 & 0 \\ & \frac{1}{2} & 0 & 0 & 0 & 0 \\ & & 1 & 0 & 0 & 0 \\ & & & 1 & 0 & 0 \\ & & & & 1 & 0 \\ & \text{Symmetric} & & & & 1 \end{bmatrix}. \tag{7.14}$$

The connectivity/orthogonality compromise is apparent from the loss of bandedness in the upper left corners of these matrices. Note that the external and internal modes are mostly orthogonal to each other (refer to their definitions in terms of Legendre polynomials in (7.10-11)).

It is useful at this time to relate the coefficients in (7.7) to the displacements and rotations at the beam ends. Define:

$u_{A1}, u_{A2}, u_{A3} \equiv$ displacements at end A, (7.15a)

$u_{A4}, u_{A5}, u_{A6} \equiv$ rotations at end A, (7.15b)

$u_{B1}, u_{B2}, u_{B3} \equiv$ displacements at end B, and (7.15c)

$u_{B4}, u_{B5}, u_{B6} \equiv$ rotations at end B, (7.15d)

with respect to the local axes, x, y, and z, respectively. (7.15e)

Then, for:

TI Beams: $u_{A1} = u_{0,1}^{(k)},\ u_{A2} = v_{0,1}^{(k)},\ u_{A3} = w_{0,1}^{(k)},$ (7.16a)

$u_{A4} = \phi_{1,1}^{(k)},\ u_{A5} = u_{z,1}^{(k)},\ u_{A6} = -u_{y,1}^{(k)},$ (7.16b)

$u_{B1} = u_{0,2}^{(k)},\ u_{B2} = v_{0,2}^{(k)},\ u_{B3} = w_{0,2}^{(k)},$ (7.16c)

$u_{B4} = \phi_{1,2}^{(k)},\ u_{B5} = u_{z,2}^{(k)},\ u_{B6} = -u_{y,2}^{(k)}.$ (7.16d)

These definitions for Timoshenko beams are independent of curvature.

The strain energy formulations for Bernoulli-Euler and Rayleigh beams are derived from the Timoshenko formulations via application of the no-shear assumptions. The number of displacement variables is reduced to four with the elimination of u_y and u_z, but the resulting formulations (3.20,35) involve the second derivatives in x for v_0 and w_0. Thus, v_0 and w_0 must be contained in the C_1 space to ensure finite strain energy. The $L_j(\xi)$ shape functions will be chosen to be C_1-compatible such that for:

$$\text{BE/RA Beams:} \quad u_0^{(k)}\left(Q^{(k)}(\xi),t\right) \cong \sum_{j=1}^{p_1+1} u_{0,j}^{(k)} N_j(\xi) e^{i\omega t}, \tag{7.17a}$$

$$v_0^{(k)}\left(Q^{(k)}(\xi),t\right) \cong \sum_{j=1}^{p_2+1} v_{0,j}^{(k)} L_j(\xi) e^{i\omega t}, \tag{7.17b}$$

$$w_0^{(k)}\left(Q^{(k)}(\xi),t\right) \cong \sum_{j=1}^{p_3+1} w_{0,j}^{(k)} L_j(\xi) e^{i\omega t}, \text{ and} \tag{7.17c}$$

$$\phi_1^{(k)}\left(Q^{(k)}(\xi),t\right) \cong \sum_{j=1}^{p_4+1} \phi_{1,j}^{(k)} N_j(\xi) e^{i\omega t}. \tag{7.17d}$$

The desires in defining the $L_j(\xi)$'s are identical to those for the C_0 functions. The external modes are defined using the Hermite cubices typical of h-version codes, namely:

$$L_1(\xi) = \frac{\xi^3}{4} - \frac{3\xi}{4} + \frac{1}{2} = \frac{P_3(\xi)}{10} - \frac{3P_1(\xi)}{5} + \frac{P_0(\xi)}{2}:$$

$$L_1(-1) = 1,\ L_1^*(-1) = L_1(+1) = L_1^*(+1) = 0; \tag{7.18a}$$

$$L_2(\xi) = \frac{\xi^3}{8} - \frac{\xi^2}{8} - \frac{\xi}{8} + \frac{1}{8} = \frac{P_3(\xi)}{20} - \frac{P_2(\xi)}{12} - \frac{P_1(\xi)}{20} + \frac{P_0(\xi)}{12}:$$

$$L_2^*(-1) = 1,\ L_2(-1) = L_2(+1) = L_2^*(+1) = 0; \tag{7.18b}$$

$$L_3(\xi) = -\frac{\xi^3}{4} + \frac{3\xi}{4} + \frac{1}{2} = -\frac{P_3(\xi)}{10} + \frac{3P_1(\xi)}{5} + \frac{P_0(\xi)}{2}:$$

$$L_3(+1) = 1,\ L_3(-1) = L_3^*(-1) = L_3^*(+1) = 0; \text{ and} \tag{7.18c}$$

$$L_4(\xi) = \frac{\xi^3}{8} + \frac{\xi^2}{8} - \frac{\xi}{8} - \frac{1}{8} = \frac{P_3(\xi)}{20} + \frac{P_2(\xi)}{12} - \frac{P_1(\xi)}{20} - \frac{P_0(\xi)}{12}:$$

$$L_4^*(+1) = 1,\ L_4(-1) = L_4^*(-1) = L_4(+1) = 0. \tag{7.18d}$$

Note that $p_i \geq 3$, $i = 2,3$, is required to ensure C_1 compatibility of v_0 and w_0 and that interelement connectivity will involve these two variables *and* the first derivatives in x. Thus, the internal modes suitable for p-extensions are defined using Legendre polynomials as:

$$L_j(\xi) = \sqrt{\frac{2j-5}{2}} \int_{-1}^{\xi} \int_{-1}^{\theta} P_{j-3}(t)\,dt\,d\theta$$

$$= \frac{1}{\sqrt{2(2j-5)}} \left[\frac{P_{j-1}(\xi) - P_{j-3}(\xi)}{2j-3} + \frac{P_{j-5}(\xi) - P_{j-3}(\xi)}{2j-7} \right], \text{ where} \qquad (7.19a)$$

$$L_j(-1) = L_j^*(-1) = L_j(+1) = L_j^*(+1) = 0, \text{ for} \qquad (7.19b)$$

$$j > 4. \qquad (7.19c)$$

Again, this choice of functions is not unique [79], but it is an improvement over some that have been suggested in the literature [20,21].

Figures 7.2 and 7.3 illustrate the first eight C_1 elemental shape functions. Two integrals of interest in the formulations are, for $i,j \leq 10$:

$$\int_{-1}^{+1} \{L_i\}\{L_j\}^T d\xi =$$

$$\begin{bmatrix}
\frac{26}{35} & \frac{11}{105} & \frac{9}{35} & \frac{-13}{210} & \frac{1}{3\sqrt{10}} & \frac{-4}{45\sqrt{14}} & 0 & \frac{1}{315\sqrt{22}} & 0 & 0 \\
 & \frac{2}{105} & \frac{13}{210} & \frac{-1}{70} & \frac{1}{14\sqrt{10}} & \frac{-1}{90\sqrt{14}} & \frac{-1}{210\sqrt{18}} & \frac{1}{630\sqrt{22}} & 0 & 0 \\
 & & \frac{26}{35} & \frac{-11}{105} & \frac{1}{3\sqrt{10}} & \frac{4}{45\sqrt{14}} & 0 & \frac{-1}{315\sqrt{22}} & 0 & 0 \\
 & & & \frac{2}{105} & \frac{-1}{14\sqrt{10}} & \frac{-1}{90\sqrt{14}} & \frac{1}{210\sqrt{18}} & \frac{1}{630\sqrt{22}} & 0 & 0 \\
 & & & & \frac{2}{63} & 0 & \frac{-4}{693\sqrt{5}} & 0 & \frac{1}{693\sqrt{65}} & 0 \\
 & & & & & \frac{2}{495} & 0 & \frac{-4}{585\sqrt{77}} & 0 & \frac{1}{1287\sqrt{105}} \\
 & & & & & & \frac{6}{5005} & 0 & \frac{-4}{1155\sqrt{117}} & 0 \\
 & & \text{Symmetric} & & & & & \frac{2}{4095} & 0 & \frac{-4}{1989\sqrt{165}} \\
 & & & & & & & & \frac{2}{8415} & 0 \\
 & & & & & & & & & \frac{6}{46189}
\end{bmatrix}, \qquad (7.20)$$

where, for $i \geq 5$:

$$\int_{-1}^{+1} L_i^2\,d\xi = \frac{6}{(2i-1)(2i-3)(2i-7)(2i-9)}, \qquad (7.21a)$$

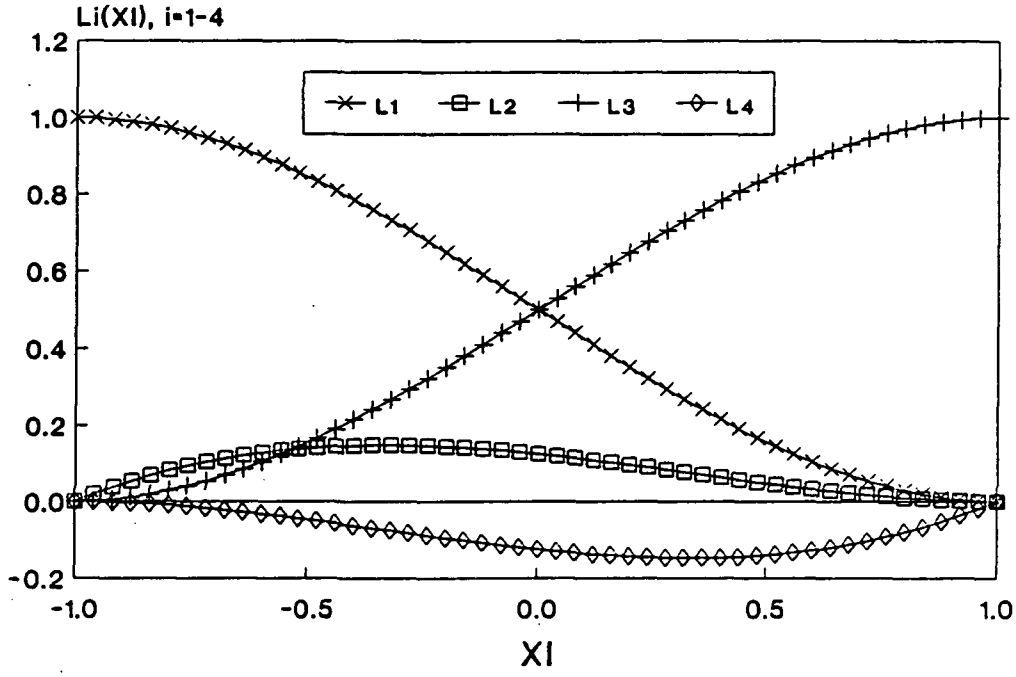

Figure 7.2 C_1-compatible elemental shape functions (external modes).

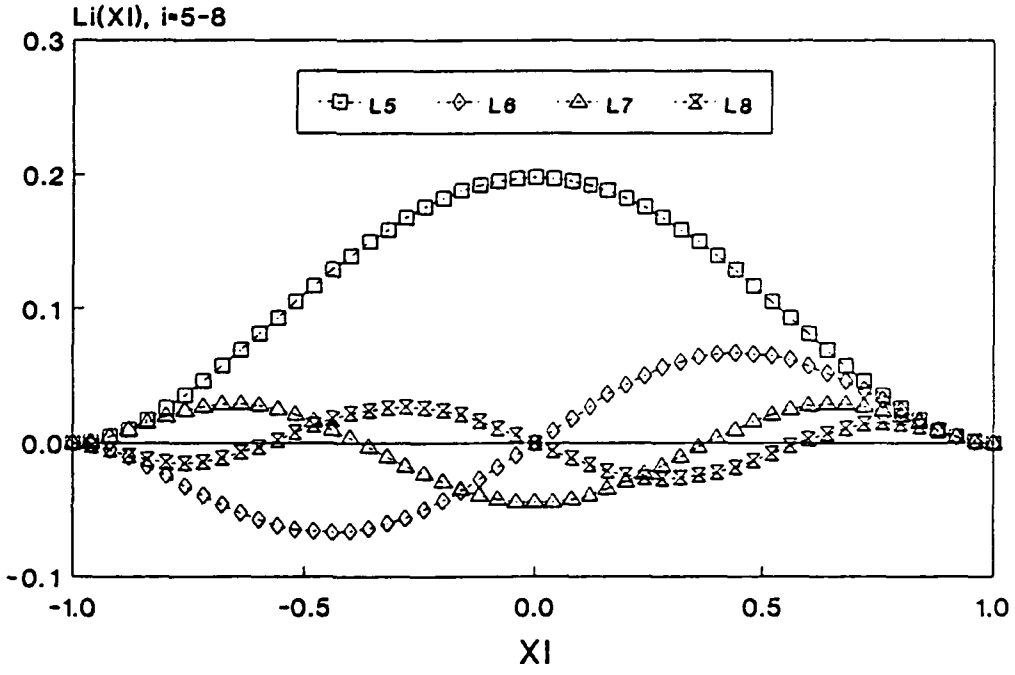

Figure 7.3 C_1-compatible elemental shape functions (internal modes).

$$\int_{-1}^{+1} L_i L_{i+2} d\xi = \frac{-4}{(2i+1)(2i-3)(2i-7)\sqrt{(2i-1)(2i-5)}}, \text{ and} \tag{7.21b}$$

$$\int_{-1}^{+1} L_i L_{i+4} d\xi = \frac{1}{(2i+1)(2i-1)(2i-3)\sqrt{(2i+3)(2i-5)}}; \tag{7.21c}$$

also:

$$\int_{-1}^{+1} \{L_i^{**}\}\{L_j^{**}\}^T d\xi = \begin{bmatrix} \frac{3}{2} & \frac{3}{4} & -\frac{3}{2} & \frac{3}{4} & 0 & 0 & 0 & 0 & 0 & 0 \\ & \frac{1}{2} & -\frac{3}{4} & \frac{1}{4} & 0 & 0 & 0 & 0 & 0 & 0 \\ & & \frac{3}{2} & -\frac{3}{4} & 0 & 0 & 0 & 0 & 0 & 0 \\ & & & \frac{1}{2} & 0 & 0 & 0 & 0 & 0 & 0 \\ & & & & 1 & 0 & 0 & 0 & 0 & 0 \\ & & & & & 1 & 0 & 0 & 0 & 0 \\ & & & & & & 1 & 0 & 0 & 0 \\ & & \text{Symmetric} & & & & & 1 & 0 & 0 \\ & & & & & & & & 1 & 0 \\ & & & & & & & & & 1 \end{bmatrix}. \tag{7.22}$$

Again, the loss of bandedness in the upper left corners of these matrices reflects the compromise between connectivity ease and pure orthogonality.

The coefficients in (7.17) involving the external modes may again be related to the displacments and rotations at the beam ends (7.15). However, curvature affects these relations for BE/RA beams; their proper definition is essential in establishing the interelement connectivity between straight and circular beam elements. Thus, for:

$$\text{BE/RA Beams: } u_{A1} = u_{0,1}^{(k)},\ u_{A2} = v_{0,1}^{(k)},\ u_{A3} = w_{0,1}^{(k)}, \tag{7.23a}$$

$$u_{A4} = \phi_{1,1}^{(k)},\ u_{A5} = \frac{-w_{0,2}^{(k)}}{h^{(k)}},\ u_{A6} = \frac{v_{0,2}^{(k)}}{h^{(k)}} - \frac{u_{0,1}^{(k)}}{R^{(k)}}, \tag{7.23b}$$

$$u_{B1} = u_{0,2}^{(k)},\ u_{B2} = v_{0,3}^{(k)},\ u_{B3} = w_{0,3}^{(k)}, \tag{7.23c}$$

$$u_{B4} = \phi_{1,2}^{(k)},\ u_{B5} = \frac{-w_{0,4}^{(k)}}{h^{(k)}},\ u_{B6} = \frac{v_{0,4}^{(k)}}{h^{(k)}} - \frac{u_{0,2}^{(k)}}{R^{(k)}}, \tag{7.23d}$$

where $R^{(k)} = \infty$ for straight beam elements.

7.2 COMPUTATION OF ELEMENTAL MATRICES

The elemental matrices for straight and circular beam elements are computed after substitution of the displacement variables in terms of the elemental shape functions. For example, the linear strain energy for BE/RA beam elements may be represented by:

$$\left(V^{(k)}_{BE/RA}\right)_{LINEAR} \cong \frac{1}{2}\left\{\begin{array}{c}\{u^{(k)}_{0,j_1}\}\\ \{v^{(k)}_{0,j_2}\}\\ \{w^{(k)}_{0,j_3}\}\\ \{\phi^{(k)}_{1,j_4}\}\end{array}\right\}^T \left[\begin{array}{cccc}[k^{(k)}_{11}] & [k^{(k)}_{12}] & [k^{(k)}_{13}] & [k^{(k)}_{14}]\\ & [k^{(k)}_{22}] & [k^{(k)}_{23}] & [k^{(k)}_{24}]\\ & & [k^{(k)}_{33}] & [k^{(k)}_{34}]\\ \multicolumn{2}{c}{\text{Symmetric}} & & [k^{(k)}_{44}]\end{array}\right] \left\{\begin{array}{c}\{u^{(k)}_{0,j_1}\}\\ \{v^{(k)}_{0,j_2}\}\\ \{w^{(k)}_{0,j_3}\}\\ \{\phi^{(k)}_{1,j_4}\}\end{array}\right\} e^{2i\omega t}, \tag{7.24}$$

where:

$$\left[\begin{array}{cccc}[k^{(k)}_{11}] & [k^{(k)}_{12}] & [k^{(k)}_{13}] & [k^{(k)}_{14}]\\ & [k^{(k)}_{22}] & [k^{(k)}_{23}] & [k^{(k)}_{24}]\\ & & [k^{(k)}_{33}] & [k^{(k)}_{34}]\\ \multicolumn{2}{c}{\text{Symmetric}} & & [k^{(k)}_{44}]\end{array}\right] \equiv [K^{(k)}], \tag{7.25}$$

is defined as the elemental stiffness matrix. Similar matrices which result from this substitution are defined as:

$[M^{(k)}] \equiv$ elemental mass matrix,

$[C^{(k)}] \equiv$ elemental Coriolis matrix,

$[K^{(k)}_S] \equiv$ elemental centrifugal softening matrix, and

$[K^{(k)}_G] \equiv$ elemental geometric nonlinearity matrix.

The following observations are made regarding the elemental matrices:

1) The dimensions of the elemental submatrices depend on the polynomial orders used to approximate the various beam displacement variables. Referring to (7.17) and (7.25), for example:

$$\dim[k^{(k)}_{ij}] = (p_i + 1) \times (p_j + 1). \tag{7.26}$$

2) All derivatives of the beam displacement variables with respect to x are converted to derivatives of the elemental shape functions with respect to ξ. Thus, the elemental matrices will involve integrals of the form:

$$\int_{-1}^{+1} C(\xi)\{A(\xi)\}\{B(\xi)\}^T d\xi, \text{ where} \tag{7.27a}$$

$$\{A(\xi)\},\ \{B(\xi)\} = \{N(\xi)\},\ \{N^*(\xi)\},\ \{L(\xi)\},\ \{L^*(\xi)\},\ \text{or}\ \{L^{**}(\xi)\}. \tag{7.27b}$$

Curvature and rotating coordinate system effects significantly increase the number of combinations of $\{A(\xi)\}$ and $\{B(\xi)\}$ in these integrals. Curvature approximations may either change or zero certain values of $C(\xi)$.

3) The constant beam properties result in constant $C(\xi)$'s in the integrals required for the elemental stiffness and mass matrices. Thus, they may be computed explicitly using tables for $\int_{-1}^{+1}\{A(\xi)\}\{B(\xi)\}^T d\xi$. Variations in position and orientation of the beam element with respect to the inertial frame mandate the use of numerical quadrature for computing $[K_S^{(k)}]$ and $[C^{(k)}]$.

4) The elemental geometric nonlinearity matrix also requires use of numerical quadrature. Note that the integrated forces and moments (see Section 3.5) depend on the approximations of the displacement variables (7.7,17). Thus, hierarchic extensions of these approximations typically produce nonhierarchic $[K_G^{(k)}]$'s.

The resulting elemental matrices for BE/RA beams are summarized in Appendix 14.3. Appendix 14.4 summarizes the elemental matrices for TI beams. This separation by beam type is mandated by the fundamental differences between the displacement variables and their approximations in terms of the elemental shape functions. The element designation ((k) superscript) has been dropped throughout the Appendices for simplicity. The elemental matrices are defined in the submatrix form as illustrated in (7.25); the dimensions of the

submatrices are implicitly defined as in (7.26). The applicability of the individual submatrix terms are listed for straight beams (St) and circular beams with straight (ST), truncated series (TR), or exact (EX) curvature approximations.

7.3 ASSEMBLY OF UNCONSTRAINED GLOBAL MATRICES

Once the elemental matrices have been computed, the global matrices are assembled by enforcing the interelement constraints. This primarily involves relating the locally defined displacements and rotations of the ends of the beam elements to the globally defined displacements and rotations of the appropriate grid points. The basis functions associated with the movements of a particular grid point will consist of a linear combination of the elemental shape functions from all elements joined at that grid point.

The global matrix assembly process involves a three-fold operation:

1) converting the external modes of the elemental matrices into displacements and rotations at the beam element ends,
2) transforming the locally defined elemental end movements to the global frame, and
3) adding the resulting transformed elemental matrices to the global matrix structure.

This procedure will be discussed in the context of the stiffness matrix. The assembly procedure is identical for all other matrices; the skew-symmetry of the Coriolis matrix poses no problem.

The elemental stiffness matrix may be arranged with respect to the following order of coefficients:

$$\left\{ \begin{matrix} \{u_E^{(k)}\} \\ \{u_I^{(k)}\} \end{matrix} \right\} = \left\{ \begin{matrix} u_{0,1}^{(k)} \\ v_{0,1}^{(k)} \\ w_{0,1}^{(k)} \\ \phi_{1,1}^{(k)} \\ u_{x,1}^{(k)} \\ u_{y,1}^{(k)} \\ u_{0,2}^{(k)} \\ v_{0,2}^{(k)} \\ w_{0,2}^{(k)} \\ \phi_{1,2}^{(k)} \\ u_{x,2}^{(k)} \\ u_{y,2}^{(k)} \\ \{u_I^{(k)}\} \end{matrix} \right\}_{TI} = \left\{ \begin{matrix} u_{0,1}^{(k)} \\ v_{0,1}^{(k)} \\ w_{0,1}^{(k)} \\ \phi_{1,1}^{(k)} \\ w_{0,2}^{(k)} \\ v_{0,2}^{(k)} \\ u_{0,2}^{(k)} \\ v_{0,3}^{(k)} \\ w_{0,3}^{(k)} \\ \phi_{1,2}^{(k)} \\ w_{0,4}^{(k)} \\ v_{0,4}^{(k)} \\ \{u_I^{(k)}\} \end{matrix} \right\}_{BE/RA}, \tag{7.28}$$

where $\{u_E^{(k)}\}$ and $\{u_I^{(k)}\}$ represent the coefficients associated with the external and internal modes, respectively. Therefore:

$$\left(V^{(k)}\right)_{LINEAR} \cong \frac{1}{2} \left\{ \begin{matrix} \{u_E^{(k)}\} \\ \{u_I^{(k)}\} \end{matrix} \right\}^T \begin{bmatrix} [K_{EE}^{(k)}] & [K_{EI}^{(k)}] \\ [K_{IE}^{(k)}] & [K_{II}^{(k)}] \end{bmatrix} \left\{ \begin{matrix} \{u_E^{(k)}\} \\ \{u_I^{(k)}\} \end{matrix} \right\}. \tag{7.29}$$

The external modes may be related to the local end displacements and rotations of the beam element. Defining:

$$\left\{ \begin{matrix} \{u_E^{(\ell)}\} \\ \{u_I^{(\ell)}\} \end{matrix} \right\} = \left\{ \begin{matrix} u_{A1} \\ u_{A2} \\ u_{A3} \\ u_{A4} \\ u_{A5} \\ u_{A6} \\ u_{B1} \\ u_{B2} \\ u_{B3} \\ u_{B4} \\ u_{B5} \\ u_{B6} \\ \{u_I^{(\ell)}\} \end{matrix} \right\}, \tag{7.30}$$

allows the elemental stiffness matrix to be defined as:

$$\left(V^{(\ell)}\right)_{LINEAR} \cong \frac{1}{2} \left\{ \begin{matrix} \{u_E^{(\ell)}\} \\ \{u_I^{(\ell)}\} \end{matrix} \right\}^T \left[\begin{matrix} [K_{EE}^{(\ell)}] & [K_{EI}^{(\ell)}] \\ [K_{IE}^{(\ell)}] & [K_{II}^{(\ell)}] \end{matrix} \right] \left\{ \begin{matrix} \{u_E^{(\ell)}\} \\ \{u_I^{(\ell)}\} \end{matrix} \right\}. \tag{7.31}$$

The (ℓ) superscript denotes the "local" description of the elemental matrices, realizing that $(V^{(k)})_{LINEAR} = (V^{(\ell)})_{LINEAR}$. Also note that $\{u_I^{(k)}\} = \{u_I^{(\ell)}\}$; thus $[K_{II}^{(k)}] = [K_{II}^{(\ell)}]$. However, the remaining three local stiffness submatrices must be derived from the elemental stiffness submatrices using the relations in (7.16) or (7.23).

The local stiffness matrix for Timoshenko beams is specified quite easily as:

$$[K^{(\ell)}]_{TI} = \left(k_{ij}^{(\ell)}\right)_{TI}$$

$$= \begin{cases} -\left(k_{ij}^{(k)}\right)_{TI} & i,j = 6,12, \\ & (i,j) \neq (6,6),(6,12),(12,6),(12,12); \\ \left(k_{ij}^{(k)}\right)_{TI} & \text{otherwise.} \end{cases} \tag{7.32}$$

This relation is valid for both straight and circular TI beams. Equation 7.23 shows two conversions which must be performed on both straight and circular BE/RA beams. These must be performed sequentially to allow the effects of the first conversion to be carried through the second conversion, but the order is not important. Therefore, performing the w_0 conversions first:

$$[K^{(\ell')}]_{BE/RA} = \left(k_{ij}^{(\ell')}\right)_{BE/RA}$$

$$= \begin{cases} -h^{(k)}\left(k_{ij}^{(k)}\right)_{BE/RA} & i,j = 5,11, \\ & (i,j) \neq (5,5),(5,11),(11,5),(11,11); \\ \left(h^{(k)}\right)^2\left(k_{ij}^{(k)}\right)_{BE/RA} & (i,j) = (5,5),(5,11),(11,5),(11,11); \\ \left(k_{ij}^{(k)}\right)_{BE/RA} & \text{otherwise.} \end{cases} \tag{7.33}$$

Then, the v_0 conversions may be performed on this intermediate matrix such that:

$$[K^{(\ell)}]_{BE/RA} = \left(k_{ij}^{(\ell)}\right)_{BE/RA}$$

$$= \begin{cases} h^{(k)} \left(k_{ij}^{(\ell')}\right)_{BE/RA} & i,j = 6,12, \\ & (i,j) \neq (6,6),(6,12),(12,6),(12,12); \\ \left(h^{(k)}\right)^2 \left(k_{ij}^{(\ell')}\right)_{BE/RA} & (i,j) = (6,6),(6,12),(12,6),(12,12); \\ \left(k_{ij}^{(\ell')}\right)_{BE/RA} & \text{otherwise.} \end{cases} \tag{7.34}$$

Circular BE/RA beams possess an additional coupling term in the local z rotation (u_6). This may be accounted for by noting the inverse relations of (7.23), namely:

$$\frac{v_{0,2}^{(k)}}{h^{(k)}} = u_{A6} + \frac{u_{A1}}{R^{(k)}}, \text{ and} \tag{7.35a}$$

$$\frac{v_{0,4}^{(k)}}{h^{(k)}} = u_{B6} + \frac{u_{B1}}{R^{(k)}}. \tag{7.35b}$$

This allows the curvature effect to be included by applying a second two-stage transformation to the matrix defined in (7.34). Thus:

$$[K^{(\ell')}]_{BE/RA:NonSt} = \left(k_{ij}^{(\ell')}\right)_{BE/RA:NonSt}$$

$$= \begin{cases} \left(k_{ij}^{(\ell)}\right)_{BE/RA} + \dfrac{\left(k_{i(j+5)}^{(\ell)}\right)_{BE/RA}}{R^{(k)}} & j = 1,7; \\ \left(k_{ij}^{(\ell)}\right)_{BE/RA} & \text{otherwise;} \end{cases} \tag{7.36}$$

then:

$$[K^{(\ell)}]_{BE/RA:NonSt} = \left(k_{ij}^{(\ell)}\right)_{BE/RA:NonSt}$$

$$= \begin{cases} \left(k_{ij}^{(\ell')}\right)_{BE/RA:NonSt} + \dfrac{\left(k_{(i+5)j}^{(\ell')}\right)_{BE/RA:NonSt}}{R^{(k)}} & i = 1,7; \\ \left(k_{ij}^{(\ell')}\right)_{BE/RA:NonSt} & \text{otherwise.} \end{cases} \tag{7.37}$$

It is important to understand that this transformation is defined in terms of matrix *structure*, not content. As seen in Appendices 14.3 and 14.4, the elemental matrices for straight and circular beams are significantly different. Conversion to the local description for circular BE/RA beams merely involves the four separate transformations in (7.33,34) and (7.36,37).

The displacements and rotations at the beam ends defined in (7.16) and (7.23) are specified in the local coordinate system. Imposing interelement connectivity using these variables is possible only if the local frames of adjoining elements coincide. However, the engineering beam elements are formulated to allow for nontangential intersections of an arbitrary number of elements. To provide for this flexibility, it is suitable to define the grid point displacements and rotations in the global frame, namely:

$$\{{}^{G}U_j\} = \begin{Bmatrix} U_{j1} \\ U_{j2} \\ U_{j3} \\ U_{j4} \\ U_{j5} \\ U_{j6} \end{Bmatrix}, \quad j = 1, 2, \cdots, n_G, \tag{7.38}$$

where U_{j1}, U_{j2}, and U_{j3} are the displacements and U_{j4}, U_{j5}, and U_{j6} are the rotations of the jth grid point with respect to the global axes, X, Y, and Z, respectively; n_G is the total number of grid points.

For a particular element, transformation of the external modes requires $[{}^{L}_{G}T^{(k)}(\xi)]$, which is known exactly from the problem geometry. Thus:

$$\begin{Bmatrix} u_{A1} \\ u_{A2} \\ u_{A3} \end{Bmatrix} = \left[{}^{L}_{G}T^{(k)}(-1)\right] \begin{Bmatrix} U_{A1} \\ U_{A2} \\ U_{A3} \end{Bmatrix}, \tag{7.39a}$$

$$\begin{Bmatrix} u_{A4} \\ u_{A5} \\ u_{A6} \end{Bmatrix} = \left[{}^{L}_{G}T^{(k)}(-1)\right] \begin{Bmatrix} U_{A4} \\ U_{A5} \\ U_{A6} \end{Bmatrix}, \tag{7.39b}$$

$$\begin{Bmatrix} u_{B1} \\ u_{B2} \\ u_{B3} \end{Bmatrix} = \left[{}^{L}_{G}T^{(k)}(+1) \right] \begin{Bmatrix} U_{B1} \\ U_{B2} \\ U_{B3} \end{Bmatrix}, \text{ and} \tag{7.39c}$$

$$\begin{Bmatrix} u_{B4} \\ u_{B5} \\ u_{B6} \end{Bmatrix} = \left[{}^{L}_{G}T^{(k)}(+1) \right] \begin{Bmatrix} U_{B4} \\ U_{B5} \\ U_{B6} \end{Bmatrix}. \tag{7.39d}$$

This allows for the definition:

$$\begin{Bmatrix} \{U_E^{(g)}\} \\ \{u_I^{(g)}\} \end{Bmatrix} = \begin{Bmatrix} U_{A1} \\ U_{A2} \\ U_{A3} \\ U_{A4} \\ U_{A5} \\ U_{A6} \\ U_{B1} \\ U_{B2} \\ U_{B3} \\ U_{B4} \\ U_{B5} \\ U_{B6} \\ \{u_I^{(g)}\} \end{Bmatrix}, \tag{7.40}$$

such that:

$$\left(V^{(g)}\right)_{LINEAR} \cong \frac{1}{2} \begin{Bmatrix} \{U_E^{(g)}\} \\ \{u_I^{(g)}\} \end{Bmatrix}^T \begin{bmatrix} [K_{EE}^{(g)}] & [K_{EI}^{(g)}] \\ [K_{IE}^{(g)}] & [K_{II}^{(g)}] \end{bmatrix} \begin{Bmatrix} \{U_E^{(g)}\} \\ \{u_I^{(g)}\} \end{Bmatrix}. \tag{7.41}$$

The (g) superscript denotes the "global" description of the elemental matrices even though $\left(V^{(g)}\right)_{LINEAR} = \left(V^{(\ell)}\right)_{LINEAR} = \left(V^{(k)}\right)_{LINEAR}$. The internal modes will again be unaffected by the transformation; thus $\{u_I^{(g)}\} = \{u_I^{(\ell)}\} = \{u_I^{(k)}\} \equiv \{u_I\}$ and $[K_{II}^{(g)}] = [K_{II}^{(\ell)}] = [K_{II}^{(k)}]$. The two-stage transformation to the global description is defined using:

$$\left[{}^{L}_{G}T^{(k)}(\xi) \right] = \left({}^{L}_{G}t^{(k)}_{mn}(\xi) \right) \quad m, n = 1, 2, 3, \tag{7.42}$$

such that:

$$[K^{(g')}] = k_{ij}^{(g')}$$

$$= \begin{cases} \sum_{m=1}^{3} k_{im}^{(\ell)} \left({}_{G}^{L}t_{mj}^{(k)}(-1) \right) & j = 1,2,3; \\ \sum_{m=1}^{3} k_{i(m+3)}^{(\ell)} \left({}_{G}^{L}t_{m(j-3)}^{(k)}(-1) \right) & j = 4,5,6; \\ \sum_{m=1}^{3} k_{i(m+6)}^{(\ell)} \left({}_{G}^{L}t_{m(j-6)}^{(k)}(+1) \right) & j = 7,8,9; \\ \sum_{m=1}^{3} k_{i(m+9)}^{(\ell)} \left({}_{G}^{L}t_{m(j-9)}^{(k)}(+1) \right) & j = 10,11,12; \\ k_{ij}^{(\ell)} & \text{otherwise.} \end{cases} \tag{7.43}$$

Then, recalling (2.21):

$$\left[{}_{G}^{L}T^{(k)}(\xi) \right]^{T} = \left[{}_{L}^{G}T^{(k)}(\xi) \right] = \left({}_{L}^{G}t_{mn}^{(k)}(\xi) \right) \quad m,n = 1,2,3, \tag{7.44}$$

allows for the definition of the second stage of the transformation as:

$$[K^{(g)}] = k_{ij}^{(g)}$$

$$= \begin{cases} \sum_{m=1}^{3} \left({}_{L}^{G}t_{im}^{(k)}(-1) \right) k_{mj}^{(g')} & i = 1,2,3; \\ \sum_{m=1}^{3} \left({}_{L}^{G}t_{(i-3)m}^{(k)}(-1) \right) k_{(m+3)j}^{(g')} & i = 4,5,6; \\ \sum_{m=1}^{3} \left({}_{L}^{G}t_{(i-6)m}^{(k)}(+1) \right) k_{(m+6)j}^{(g')} & i = 7,8,9; \\ \sum_{m=1}^{3} \left({}_{L}^{G}t_{(i-9)m}^{(k)}(+1) \right) k_{(m+9)j}^{(g')} & i = 10,11,12; \\ k_{ij}^{(g')} & \text{otherwise.} \end{cases} \tag{7.45}$$

The local-to-global transformation as defined is independent of beam type or curvature.

The global displacement (and rotation) vector may be defined as:

$$\left\{ U^{(G)} \right\} = \begin{Bmatrix} \{{}^{G}U_1\} \\ \{{}^{G}U_2\} \\ \vdots \\ \{{}^{G}U_{n_G}\} \\ \{{}^{G}U_P\} \\ \{\Sigma u_I\} \end{Bmatrix}. \tag{7.46}$$

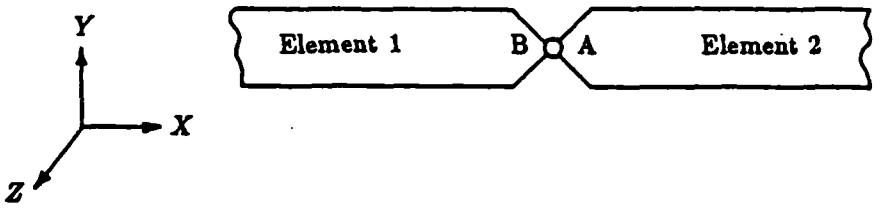

Figure 7.4 Hinge modeling via pin flag.

$\{^G U_P\}$ defines the vector of n_P globally specified degrees-of-freedom introduced through the use of pin flags [80]. Pin flags allow for the release of interelement constraints. For example, Figure 7.4 illustrates a hinge to be placed between the two beam elements to eliminate the transfer of Z-moments through the connection. This may be accomplished by flagging the sixth displacement variable (i.e., the global Z rotation defined by U_6) for end B of Element 1 *or* end A of Element 2. For the latter case, all matrix terms involving the Z rotation for end A of Element 2 would be related to the pin degree-of-freedom instead of U_6 of the connecting grid point.

The collected internal modes are defined in global displacement vector as:

$$\{\Sigma u_I\} = \begin{Bmatrix} \{u_I\}_1 \\ \{u_I\}_2 \\ \vdots \\ \{u_I\}_{n_E} \end{Bmatrix}. \tag{7.47}$$

Thus, the number of unconstrained global degrees-of-freedom is:

$$n_U = (n_G \times 6) + n_P + \sum_{j=1}^{n_E} \left(\left(\sum_{j=1}^{n_D} (p_{ij} + 1) \right) - 12 \right), \tag{7.48}$$

or, noting the restriction in (7.5):

$$n_U = (n_G \times 6) + n_P + \left(n_E \times \left(\left(\sum_{i=1}^{n_D} (p_i + 1) \right) - 12 \right) \right). \tag{7.49}$$

Note that the process of p-extension involves increases in the p_i's with n_G and n_E fixed, h-extension involves increases in n_E and n_G with the p_i's fixed, and hp-extension involves increases in all three parameters. From (7.46) and (7.47), it is seen that p-extension increases only the number of internal modes. Also, the basis functions for the finite element space are either the linear combinations of globally transformed external modes or the individual, locally defined internal modes. Thus, all linear matrices derived from p-extensions are explicitly hierarchic.

The global stiffness matrix is assembled by summing the contributions from the elemental stiffness matrices after transformation to the global description. Note that (7.41) may be defined relative to the global displacement vector as:

$$\left(V^{(g)}\right)_{LINEAR} \cong \frac{1}{2}\{U^{(G)}\}^T[\overline{K}^{(g)}]\{U^{(G)}\}. \tag{7.50}$$

The conversion from (7.41) to (7.50) merely consists of an expansion of matrix dimension; $[K^{(g)}]$ and $[\overline{K}^{(g)}]$ contain the same nonzero terms arranged in different fashions, taking into account any applicable pin flags. In addition, globally defined linear springs are allowed to connect between any grid point degree-of-freedom and ground such that:

$$V^{(SP)} = \frac{1}{2}\sum_{j=1}^{n_G}\sum_{i=1}^{6} k^{(SP)}_{(6\times(j-1)+i)}U^2_{ji}$$

$$= \frac{1}{2}\begin{Bmatrix} \{{}^GU_1\} \\ \{{}^GU_2\} \\ \vdots \\ \{{}^GU_{n_G}\} \\ \{{}^GU_P\} \\ \\ \{\Sigma u_I\} \end{Bmatrix}^T \begin{bmatrix} k^{(SP)}_1 & 0 & \dots & 0 & 0 & \dots & 0 \\ 0 & k^{(SP)}_2 & \ddots & \vdots & \vdots & & \vdots \\ \vdots & \ddots & \ddots & 0 & \vdots & & \vdots \\ 0 & \dots & 0 & k^{(SP)}_{(6\times n_G)} & 0 & \dots & 0 \\ 0 & \dots & \dots & 0 & 0 & \dots & 0 \\ \vdots & & & \vdots & \vdots & & \vdots \\ 0 & \dots & \dots & 0 & 0 & \dots & 0 \end{bmatrix} \begin{Bmatrix} \{{}^GU_1\} \\ \{{}^GU_2\} \\ \vdots \\ \{{}^GU_{n_G}\} \\ \{{}^GU_P\} \\ \\ \{\Sigma u_I\} \end{Bmatrix}$$

$$= \frac{1}{2}\{U^{(G)}\}^T[K^{(SP)}]\{U^{(G)}\}. \tag{7.51}$$

Therefore, the global stiffness matrix is:

$$[K^{(G)}] = \left[\sum_{i=1}^{n_E}[\overline{K}^{(g)}]_i + [K^{(SP)}]\right]. \tag{7.52}$$

The same assembly procedure is followed for all other matrices. The distributed mass terms summarized in Appendix 14.5 may be added directly to the global matrices with respect to the displacements and rotations of the associated grid point.

7.4 DEFINITION OF NONROTATING LOADS

The formulation of the kinetic energy for beam elements in a rotating frame introduces centrifugal load terms to the static load vector. Additional static load capabilities are developed in this section. They are defined in terms of loss of potential energy to allow direct substitution into Lagrange's equation (1.14).

7.4.1 Generalized Distributed Forces

Generalized distributed forces are defined in units of force per unit length and are assumed to be applied along the beam axis. They may be specified in the local frame:

$$\{^L f^{(k)}\} \equiv \begin{Bmatrix} f_x^{(k)} \\ f_y^{(k)} \\ f_z^{(k)} \end{Bmatrix}, \tag{7.53}$$

or in the global frame:

$$\{^G f^{(k)}\} \equiv \begin{Bmatrix} f_X^{(k)} \\ f_Y^{(k)} \\ f_Z^{(k)} \end{Bmatrix}, \tag{7.54}$$

such that:

$$\{^L f^{(k)}\} = \left[{}^L_G T^{(k)}(\xi)\right] \{^G f^{(k)}\}. \tag{7.55}$$

The loss of potential energy associated with these loads is merely:

$$\left(V_f^{(k)}\right) = -\int_0^{h^{(k)}} \left[f_x^{(k)} u_0^{(k)} + f_y^{(k)} v_0^{(k)} + f_z^{(k)} w_0^{(k)}\right] dx. \tag{7.56}$$

The (k) superscript throughout denotes the fact that distributed loads are applied on an element-by-element basis. As defined, (7.56) is applicable to both straight and circular elements of all beam types.

7.4.2 Loading by Gravity

Gravitational loading is applicable to all elements of a model. The gravitational acceleration vector is specified in the global frame:

$$\{{}^G g\} = \begin{Bmatrix} g_X \\ g_Y \\ g_Z \end{Bmatrix}, \tag{7.57}$$

such that:

$$\{{}^L g^{(k)}\} = \left[{}^L_G T^{(k)}(\xi)\right] \{{}^G g\} \equiv \begin{Bmatrix} g_x^{(k)} \\ g_y^{(k)} \\ g_z^{(k)} \end{Bmatrix}. \tag{7.58}$$

The gravitational potential energy is defined using the undeformed position of the center of mass as the datum. For straight beam elements, the gravitational potential energy is:

$$\left(V_g^{(k)}\right)_{BE/RA/TI:St} = -m^{(k)} \int_0^{h^{(k)}} \left[g_x^{(k)} u_0^{(k)} + g_y^{(k)} v_0^{(k)} + g_z^{(k)} w_0^{(k)}\right] dx. \tag{7.59}$$

Circular beam elements must take into account the shift in the mass center due to curvature. For circular Timoshenko beams:

$$\left(V_g^{(k)}\right)_{TI:NonSt} = -m^{(k)} \int_0^{h^{(k)}} \left[g_x^{(k)} \left(u_0^{(k)} + \bar{y}_m^{(k)} u_y^{(k)}\right) + g_y^{(k)} v_0^{(k)} + g_z^{(k)} \left(w_0^{(k)} + \bar{y}_m^{(k)} \phi_1^{(k)}\right)\right] dx. \tag{7.60}$$

Applying the no-shear assumption for BE/RA beams produces:

$$\left(V_g^{(k)}\right)_{BE/RA:NonSt} = -m^{(k)} \int_0^{h^{(k)}} \left[g_x^{(k)} \left(u_0^{(k)} + \bar{y}_m^{(k)} \left(\left(-v_0^{(k)}\right)' + \frac{u_0^{(k)}}{R} \right) \right) + g_y^{(k)} v_0^{(k)} + g_z^{(k)} \left(w_0^{(k)} + \bar{y}_m^{(k)} \phi_1^{(k)} \right) \right] dx. \tag{7.61}$$

Recall that $\bar{y}_m^{(k)} = 0$ for the ST curvature approximation and that $m^{(k)} \bar{y}_m^{(k)} = J_{yy}^{(k)} / R^{(k)}$ for the TR and EX curvature approximations.

7.4.3 Forces and Moments at Grid Points

Application of forces and moments at the grid points provides a powerful verification tool for the strain energy formulations by allowing comparisons with simple known solutions. The forces and moments are applied in the global frame and include the gravitational forces induced by any applicable distributed masses $(\mathcal{M}_j)$. Define:

$$\{{}^G F_j\} = \begin{Bmatrix} F_{jX} + \mathcal{M}_j g_X \\ F_{jY} + \mathcal{M}_j g_Y \\ F_{jZ} + \mathcal{M}_j g_Z \\ M_{jX} \\ M_{jY} \\ M_{jZ} \end{Bmatrix}, \tag{7.62}$$

where the j subscript denotes the grid point of application. Therefore:

$$(V_F)_j = -\{{}^G F_j\}^T \{{}^G U_j\}, \tag{7.63}$$

or:

$$(V_F) = -\begin{Bmatrix} \{{}^G F_1\} \\ \{{}^G F_2\} \\ \vdots \\ \{{}^G F_{n_G}\} \\ \{0\} \\ \{0\} \end{Bmatrix}^T \begin{Bmatrix} \{{}^G U_1\} \\ \{{}^G U_2\} \\ \vdots \\ \{{}^G U_{n_G}\} \\ \{{}^G U_P\} \\ \{\Sigma u_I\} \end{Bmatrix}$$

$$= -\{F^{(G)}\}^T \{U^{(G)}\}, \tag{7.64}$$

defines the loss of potential energy due to the applied grid point forces and moments.

7.4.4 Assembly of the Global Load Vector

The elemental load vector terms associated with the centrifugal, gravitational, and distributed forces for BE/RA and TI beam elements are listed in Appendices 14.3 and 14.4, respectively. They are presented in terms of the local displacement variables *after* substitution of their approximations as linear combinations of the elemental shape functions. From a virtual work perspective, the elemental load vector is related to the virtual change in the potential energy by:

$$\left(\delta V^{(k)}\right) \cong -\left\{\begin{array}{c}\{R_E^{(k)}\}\\ \{R_I^{(k)}\}\end{array}\right\}^T \left\{\begin{array}{c}\{\delta u_E^{(k)}\}\\ \{\delta u_I^{(k)}\}\end{array}\right\}, \tag{7.65}$$

where the external and internal modes are separated in accordance with (7.28). Thus, the elemental load vectors must be transformed to a global description using a process similar to that used for the elemental matrices. Only then may they be summed to produce the global load vector.

Referring to (7.30), the local description of the virtual change in potential energy is:

$$\{\delta V^{(\ell)}\} \cong -\left\{\begin{array}{c}\{R_E^{(\ell)}\}\\ \{R_I^{(\ell)}\}\end{array}\right\}^T \left\{\begin{array}{c}\{\delta u_E^{(\ell)}\}\\ \{\delta u_I^{(\ell)}\}\end{array}\right\}, \tag{7.66}$$

where:

$$\begin{aligned}\{R^{(\ell)}\}_{TI} &= \left(r_i^{(\ell)}\right)_{TI}\\ &= \begin{cases} -\left(r_i^{(k)}\right)_{TI} & i = 6, 12;\\ \left(r_i^{(k)}\right)_{TI} & \text{otherwise;}\end{cases}\end{aligned} \tag{7.67}$$

$$\{R^{(\ell)}\}_{BE/RA} = \left(r_i^{(\ell)}\right)_{BE/RA}$$

$$= \begin{cases} -h^{(k)}\left(r_i^{(k)}\right)_{BE/RA} & i = 5, 11; \\ h^{(k)}\left(r_i^{(k)}\right)_{BE/RA} & i = 6, 12; \\ \left(r_i^{(k)}\right)_{BE/RA} & \text{otherwise; and} \end{cases} \tag{7.68}$$

$$\{R^{(\ell)}\}_{BE/RA:NonSt} = \left(r_i^{(\ell)}\right)_{BE/RA:NonSt}$$

$$= \begin{cases} \left(r_i^{(\ell)}\right)_{BE/RA} + \dfrac{\left(r_{(i+5)}^{(\ell)}\right)_{BE/RA}}{R^{(k)}} & i = 1, 7; \\ \left(r_i^{(\ell)}\right)_{BE/RA} & \text{otherwise.} \end{cases} \tag{7.69}$$

Then, the global description may be defined using (7.40) as:

$$\{\delta V^{(g)}\} \cong -\begin{Bmatrix} \{R_E^{(g)}\} \\ \{R_I^{(g)}\} \end{Bmatrix}^T \begin{Bmatrix} \{\delta U_E^{(g)}\} \\ \{\delta u_I^{(g)}\} \end{Bmatrix}, \tag{7.70}$$

where, using (7.44):

$$\{R^{(g)}\} = r_i^{(g)}$$

$$= \begin{cases} \sum_{m=1}^{3} \left({}^{G}_{L}t_{im}^{(k)}(-1)\right) r_m^{(\ell)} & i = 1, 2, 3; \\ \sum_{m=1}^{3} \left({}^{G}_{L}t_{(i-3)m}^{(k)}(-1)\right) r_{(m+3)}^{(\ell)} & i = 4, 5, 6; \\ \sum_{m=1}^{3} \left({}^{G}_{L}t_{(i-6)m}^{(k)}(+1)\right) r_{(m+6)}^{(\ell)} & i = 7, 8, 9; \\ \sum_{m=1}^{3} \left({}^{G}_{L}t_{(i-9)m}^{(k)}(+1)\right) r_{(m+9)}^{(\ell)} & i = 10, 11, 12; \\ r_i^{(\ell)} & \text{otherwise.} \end{cases} \tag{7.71}$$

Finally, (7.70) may be redefined with respect to the global (virtual) displacement vector such that:

$$\{\delta V^{(g)}\} \cong -\{\overline{R}^{(g)}\}^T \{\delta U^{(G)}\}. \tag{7.72}$$

Therefore, the assembled global load vector is defined by (recall (7.64)):

$$\{R^{(G)}\} = \left\{ \sum_{i=1}^{n_E} \{\overline{R}^{(e)}\}_i + \{F^{(G)}\} \right\}, \tag{7.73}$$

such that:

$$\{\delta V^{(G)}\} = -\{R^{(G)}\}^T \{\delta U^{(G)}\}. \tag{7.74}$$

7.5 COMMENTS REGARDING CIRCULAR BEAM ELEMENTS

The formulation and discretization of circular beam elements have been developed in explicit detail in this and previous chapters. Coupling of the displacement variables exist in the strain energy formulations and no-shear assumptions presented in Chapter 3. The global description of the elemental matrices for circular BE/RA beams is also affected by coupling. Except for some quadratic strain terms in the formulation of circular-beam geometric nonlinearities, no assumptions regarding the "shallowness" of curvature are made. The curvature approximations of Chapter 5 simplify the computation of beam properties but maintain the coupling of displacement variables. Inextensibility assumptions are discussed but never applied to the formulations.

The preceding paragraph provides the necessary framework for discussing the literature regarding circular beam elements, particularly arch elements. The words of Babu and Prathap [81] provide a useful introduction to the discussion:

> *Early attempts to derive curved beam and shell elements in a curvilinear system were dramatically unsuccessful. This was wrongly attributed to the failure of these elements to recover strain-free rigid body displacement modes in a curvilinear coordinate description. Recent evidence points to a "membrane locking" phenomenon that arises when constrained strain*

fields corresponding to inextensional bending are not "consistently" recovered.

The issue of rigid body modes is significant to the present formulation. The polynomial-based external modes in (7.7) or (7.17) will not represent all of the rigid body motions for circular beam elements (but will for straight elements) except in the limit as $h \to 0$. However, inclusion of internal modes via p-extension allow the rigid body modes to be recovered within the context of energy minimization.

The locking problem is more abstract. Strictly speaking, "locking" is the inability of a finite element formulation *and* discretization to converge to the exact solution via extension. The shear locking described in [82] provides a classic example. Often, this terminology is applied to problems that do converge to the exact solution but at a very slow rate. Exotically-named techniques such as hybrid and mixed formulations [83], reduced or selective integration [84], penalty relaxation [85], and field-consistent strain interpolation [86] have been introduced to compensate for shortcomings in the formulation and/or discretization and to improve convergence in problems experiencing "pseudo-locking."

In a sense, p-extension may be considered an addition to this list of techniques. However, p-extension will not relieve locking problems introduced by the formulation. Experience gained from this research suggests that the potential for locking is, at the very least, enhanced by the use of simplified formulations. In particular, ignoring the coupling of displacement variables during any stage leading to the global finite element matrices or applying inextensibility assumptions *will* produce locking-type phenomena. The distinction between errors of idealization and errors of discretization is significant in understanding the source

of locking. No locking problems have been encountered utilizing the formulations presented here in conjunction with p-extensions.

The issue of poor rates of convergence merits further discussion. Previous arch studies have shown that better accuracy could be obtained with straight elements as opposed to (ST) circular elements using the minimum polynomial orders in h-extensions [81]. This observation is made even more significant by the additional mapping-induced errors in straight-element models. These findings were confirmed using the formulations of this investigation; thus, some pseudo-locking phenomena are present. A similar comparison between h-extensions of straight beams versus p-extensions of circular beams is just as enlightening. In terms of degrees-of-freedom, the initially better accuracy of the low-dof straight-beam models is quickly surpassed by the circular-beam models due to the superior convergence rate of p-extensions. Typically, circular beams require higher p-levels than straight beams for comparable accuracy, but the rates of convergence have been found to be quite similar. Separate specification of the polynomial orders for straight and circular beam elements is an obvious first step in adaptive p-refinement.

7.6 APPLICATION OF HOMOGENEOUS BOUNDARY CONDITIONS

The unconstrained global matrices are defined in the space of $S(\Upsilon) \subset E(\Upsilon)$. In the absence of springs, this implies that the global stiffness matrix in (7.52) is either explicitly singular or approaches singularity as $p_i \to \infty$, $i = 1, 2, \ldots, n_D$. Thus, the application of geometric boundary conditions not only restricts the space to $\tilde{S}(\Upsilon) \subset \tilde{E}(\Upsilon)$ but also provides for the elimination of rigid body motions which make the stiffness matrix singular. Springs may serve the same purpose, but the emphasis in this section is on enforcing the geometric boundary conditions.

The geometric boundary conditions are assumed homogeneous for this development. Furthermore, they are assumed to involve enforcing zero global displacements and/or rotations at grid points. Thus, the global displacement vector in (7.46) may be partitioned into:

$$\{U^{(G)}\} = \begin{Bmatrix} \{U_D^{(G)}\} \\ \{0\} \end{Bmatrix}, \tag{7.75}$$

where $\{U_D^{(G)}\}$ is the vector of the remaining dependent coefficients. Defining n_C as the number of constrained degrees-of-freedom, $\{U_D^{(G)}\}$ contains n terms where (see (7.49)):

$$n = n_U - n_C. \tag{7.76}$$

The dimension, n, represents the number of degrees-of-freedom cited for all problems in this report.

Partitioning the global stiffness matrix and load vector consistent with (7.75) produces:

$$\begin{bmatrix} [K_{DD}^{(G)}] & [K_{DC}^{(G)}] \\ [K_{CD}^{(G)}] & [K_{CC}^{(G)}] \end{bmatrix} \begin{Bmatrix} \{U_D^{(G)}\} \\ \{0\} \end{Bmatrix} = \begin{Bmatrix} \{R_D^{(G)}\} \\ \{R_C^{(G)}\} + \{F_C^{(G)}\} \end{Bmatrix}, \tag{7.77}$$

where $\{F_C^{(G)}\}$ are the resultant generalized forces induced by the constraints. The static solution is obtained from:

$$\left[K_{DD}^{(G)}\right] \left\{U_D^{(G)}\right\} = \left\{R_D^{(G)}\right\}, \tag{7.78}$$

and the constraint forces may be obtained after solution for $\{U_D^{(G)}\}$ via:

$$\left\{F_C^{(G)}\right\} = \left[K_{CD}^{(G)}\right] \left\{U_D^{(G)}\right\} - \left\{R_C^{(G)}\right\}. \tag{7.79}$$

Inclusion of the centrifugal softening and geometric nonlinearity matrices and the centrifugal load vector poses no problems for this partitioning scheme.

Application of geometric boundary conditions to free-response eigenproblems follows a similar procedure. Partitioning of the complex eigenproblem may be represented by:

$$\left[\begin{bmatrix} [K_{DD}^{(G)}] & [K_{DC}^{(G)}] \\ [K_{CD}^{(G)}] & [K_{CC}^{(G)}] \end{bmatrix} + i\omega \begin{bmatrix} [C_{DD}^{(G)}] & [C_{DC}^{(G)}] \\ [C_{CD}^{(G)}] & [C_{CC}^{(G)}] \end{bmatrix} - \omega^2 \begin{bmatrix} [M_{DD}^{(G)}] & [M_{DC}^{(G)}] \\ [M_{CD}^{(G)}] & [M_{CC}^{(G)}] \end{bmatrix}\right] \begin{Bmatrix} \{U_D^{(G)}\} \\ \{0\} \end{Bmatrix} = \begin{Bmatrix} \{0\} \\ \{F_C^{(G)}\} \end{Bmatrix}. \tag{7.80}$$

Solution of the constrained eigenproblem:

$$\left[[K_{DD}^{(G)}] + i\omega[C_{DD}^{(G)}] - \omega^2[M_{DD}^{(G)}]\right] \left\{U_D^{(G)}\right\} = \{0\}, \tag{7.81}$$

leads to the solution of the dynamic constraint forces:

$$\left\{F_C^{(G)}\right\} = \left[[K_{CD}^{(G)}] + i\omega[C_{CD}^{(G)}] - \omega^2[M_{CD}^{(G)}]\right] \left\{U_D^{(G)}\right\}, \tag{7.82}$$

or:

$$\left\{f_C^{(G)}\right\} = \left\{F_C^{(G)}\right\} e^{i\omega t}. \tag{7.83}$$

The constraint forces in (7.79) and (7.82,83) may be derived from the integrated forces and moments of the beam elements as defined in Section 3.5. However, the constraint forces are derived directly from the energy-based matrix formulation and, thus, possess superior convergence in comparison to the integrated forces and moments approach [87]. Using the principle of virtual work, the matrix formulation provides for the computation of "super-convergent" forces and moments at the ends of any beam element. Defining:

$$\left\{F_E^{(e)}\right\} = \begin{Bmatrix} F_{Ax} \\ F_{Ay} \\ F_{Az} \\ M_{Ax} \\ M_{Ay} \\ M_{Az} \\ F_{Bx} \\ F_{By} \\ F_{Bz} \\ M_{Bx} \\ M_{By} \\ M_{Bz} \end{Bmatrix}, \tag{7.84}$$

and recalling (7.30), (7.31), and (7.66), this computation for a linear static problem takes the form:

$$\left\{F_E^{(\ell)}\right\} = \left[\left[K_{EE}^{(\ell)}\right]\left[K_{EI}^{(\ell)}\right]\right]\left\{\begin{matrix}\{u_E^{(\ell)}\}\\ \{u_I^{(\ell)}\}\end{matrix}\right\} - \left\{R_E^{(\ell)}\right\}. \tag{7.85}$$

$\{u_E^{(\ell)}\}$ and $\{u_I^{(\ell)}\}$ are known via inverse transformation of the appropriate terms from the global solution vector. Application to linear eigenproblems is apparent; however, nonlinear problems require the inclusion of deformation-dependent terms which will not be developed as part of this research.

Homogeneous constraints coupled with the fixing of certain p_i's provide a simple means for performing planar analyses using the three-dimensional formulations. Referring to the discussion in Section 2.3, in-plane responses may be evaluated by the specification:

$$\text{Constrain}: \quad U_{j3}, U_{j4}, U_{j5}, \quad j = 1, 2, \ldots, n_G, \text{ and} \tag{7.86a}$$

$$\begin{aligned}\text{Fix}: \quad & p_3 = p_4 = p_6 = 1, \text{ for TI Beams, or} \\ & p_3 = 3, \; p_4 = 1, \text{ for BE/RA Beams.}\end{aligned} \tag{7.86b}$$

Out-of-plane responses characterized by (2.35) result from the specification:

$$\text{Constrain}: \quad U_{j1}, U_{j2}, U_{j6}, \quad j = 1, 2, \ldots, n_G, \text{ and} \tag{7.87a}$$

$$\begin{aligned}\text{Fix}: \quad & p_1 = p_2 = p_5 = 1, \text{ for TI Beams, or} \\ & p_1 = 1, \; p_2 = 3, \text{ for BE/RA Beams.}\end{aligned} \tag{7.87b}$$

Again, these specifications assume that the entire model lies in the global XY-plane and does not involve Coriolis coupling.

It is desirable at times to solve eigenproblems possessing rigid body modes. While this implies a singular (positive semidefinite) global stiffness matrix, the

global mass matrix (as derived from the quadratic form) is always positive definite. Thus, the stiffness matrix may be made positive definite by adding to it a positively scaled mass matrix. This process is known as shifting, and it is also used to improve the rate of convergence for iterative eigensolvers [14]. Starting with the singular eigenproblem:

$$[[K] - \omega^2[M]]\,\{U\} = 0, \tag{7.88}$$

the shifted eigenproblem is defined using:

$$[\hat{K}] \equiv [K] + \alpha[M], \tag{7.89}$$

where α is a positive constant. The shifted eigenproblem is:

$$\left[[\hat{K}] - \omega_\alpha^2[M]\right]\,\{U_\alpha\} = 0, \tag{7.90}$$

where the relationship between (7.88) and (7.90) is simply:

$$\omega^2 = \omega_\alpha^2 - \alpha, \text{ and} \tag{7.91a}$$

$$\{U\} = \{U_\alpha\}. \tag{7.91b}$$

The shifting procedure is limited to linear, nonrotating eigenproblems for this investigation. Rotating coordinate system effects and/or geometric nonlinearities may be included with the appropriate assumptions and some algorithmic manipulations [39,75].

8. THE BENEFITS OF HIERARCHIC p-EXTENSIONS

The benefits of p-version finite elements are best discussed in the context of a sample problem. The intent here is not to analyze a particularly difficult system. Rather, a very simple problem is used so that comparisons with the known exact solution may be made. Therefore, a nonrotating, straight, uniform, cantilever, Bernoulli-Euler beam will be evaluated for beam flexure. The problem is illustrated in Figure 8.1. The beam properties are chosen for ease of analysis:

$$m = EI = L \equiv 1. \tag{8.1}$$

The emphasis of this investigation is dynamics, but a few comments regarding beam statics are in order. If static point forces and moments of arbitrary direction are applied to the free end of the cantilever beam in Figure 8.1, *exact* results for BE/RA beams are obtained using $p_1 = p_4 = 1$ and $p_2 = p_3 = 3$, i.e., the minimum p-levels allowed. Exact results for TI elements require $p_1 = p_4 = 1$, $p_2 = p_3 = 3$, and $p_5 = p_6 = 2$ for the formulations used in this research. Thus, additional degrees-of-freedom are required to characterize the shear energy, and the minimum p-levels for Timoshenko beams ($p_i = 1,\ i = 1,2,\ldots,6$) are not sufficient for evaluating even the simplest of problems. Different formulations of h-version TI beam elements have eliminated the need for the additional degrees-of-freedom [17,50], but they are not easily extended to higher p-levels and make the inclusion of rotating coordinate system effects difficult.

8.1 CONVERGENCE RATES FOR EXTENSIONS

The exact eigensolution for the problem in Figure 8.1 using BE beams and (8.1) is:

$$w_n(x,t) = W_n(x)e^{i\omega_n t}, \text{ where} \tag{8.2a}$$

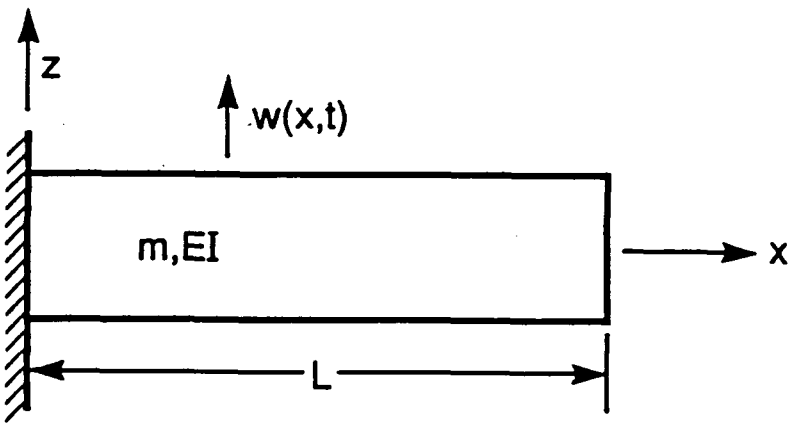

Figure 8.1 Cantilever beam sample problem.

$$W_n(x) = (\cosh \beta_n x - \cos \beta_n x) - \left(\frac{\cosh \beta_n + \cos \beta_n}{\sinh \beta_n + \sin \beta_n}\right)(\sinh \beta_n x - \sin \beta_n x), \tag{8.2b}$$

$$\cos \beta_n = \frac{-1}{\cosh \beta_n}, \text{ and} \tag{8.2c}$$

$$\omega_n = \beta_n^2. \tag{8.2d}$$

The n subscript represents the nth positive value of β which satisfies (8.2c). It is obvious that exact finite element solutions are not possible using polynomial elemental shape functions but may only be approached via extension. In comparing the finite element solutions to the exact solution, an error condition may be defined as:

$$e = \left|\frac{(*_{EX} - *_{FE})}{*_{EX}}\right|, \tag{8.3}$$

where the $*$ represents the various parameters which may be compared. For this analysis, the compared values are:

$\omega_n \equiv$ natural frequency,

$W_n(L) \equiv$ displacement at $x = L$,

$W_n'(L) \equiv$ rotation at $x = L$,

$M(0) = EIW_n''(0) \equiv$ moment at $x = 0$,

$F(0) = EIW_n'''(0) \equiv$ shear force at $x = 0$,

$M_C \equiv$ moment at $x = 0$ from constraint equation, and

$F_C \equiv$ shear force at $x = 0$ from constraint equation.

The eigenvectors are mass-normalized to provide consistent scaling between the various models.

The strain and kinetic energies for this simplified problem are:

$$V = \frac{EI}{2}\int_0^L (w'')^2\,dx, \text{ and} \tag{8.4a}$$

$$T = \frac{m}{2}\int_0^L (\dot{w})^2\,dx. \tag{8.4b}$$

Two different extension techniques are utilized for this analysis. The h-extension method involves increasing the number of uniform elements with $p_3 = 3$. Thus:

$$\Upsilon^{(k)} = \left\{ x \;\middle|\; \tfrac{(k-1)}{n_E} L < x < \tfrac{k}{n_E} L, \text{ or} \right.$$
$$h^{(k)} = \tfrac{L}{n_E} \equiv h, \text{ for}$$
$$\left. k = 1, 2, \ldots, n_E \right\}. \tag{8.5}$$

Therefore (see (7.20,22)):

$$V^{(k)} \cong \frac{1}{2}\left\{w_{0,i}^{(k)}\right\}^T \left[\frac{8EI}{h^3}\int_{-1}^{+1} \{L_i^{**}\}\{L_j^{**}\}^T\,d\xi\right]\left\{w_{0,j}^{(k)}\right\} e^{2i\omega t}, \text{ and} \tag{8.6a}$$

$$T^{(k)} \cong \frac{1}{2}\left\{w_{0,i}^{(k)}\right\}^T \left[\frac{mh}{2}\int_{-1}^{+1} \{L_i\}\{L_j\}^T\,d\xi\right]\left\{w_{0,j}^{(k)}\right\} e^{2i\omega t}, \text{ where} \tag{8.6b}$$

$$i, j \le 4, \tag{8.6c}$$

for the h-extension models. Interelement connectivity is enforced by equating (see (7.23)):

$$w_{0,3}^{(k)} = w_{0,1}^{(k+1)}, \text{ and} \tag{8.7a}$$

$$\frac{w_{0,4}^{(k)}}{h} = \frac{w_{0,2}^{(k+1)}}{h}, \text{for} \tag{8.7b}$$

$$k = 1, 2, \ldots, (n_E - 1)\,. \tag{8.7c}$$

The clamped boundary condition at $x = 0$ implies:

$$w_{0,1}^{(1)} = \frac{w_{0,2}^{(1)}}{h} = 0. \tag{8.8}$$

The resulting number of degrees-of-freedom for the h-version models is:

$$n_h = n_E \times 2, \tag{8.9}$$

where the h subscript denotes the h-extension procedure.

The p-extension models contain a single element ($h = L$) with increasing polynomial order up to $p_3 = 15$. The strain and potential energies are approximated as in (8.6a) and (8.6b), with $i, j \leq (p_3 + 1)$. The clamped boundary condition is enforced as in (8.8), but the number of degrees-of-freedom is:

$$n_p = p_3 - 1. \tag{8.10}$$

The p subscript merely denotes the p-extension models for this problem.

Figures 8.2 and 8.3 display the convergence of the various first-mode parameters as a function of degrees-of-freedom for the h- and p-extension models, respectively. The superiority of the p-version finite elements is quite easily seen; the linear nature of the log(e) versus degrees-of-freedom implies exponential rates of convergence for this class of problems, that is:

$$e \cong C\exp(-\beta n_p), \tag{8.11}$$

where C and β are constants depending on the problem parameter. The (asymptotic) convergence rate for the h-version models is known to be algebraic [29], namely:

$$e \cong C n_h^{-\beta}. \tag{8.12}$$

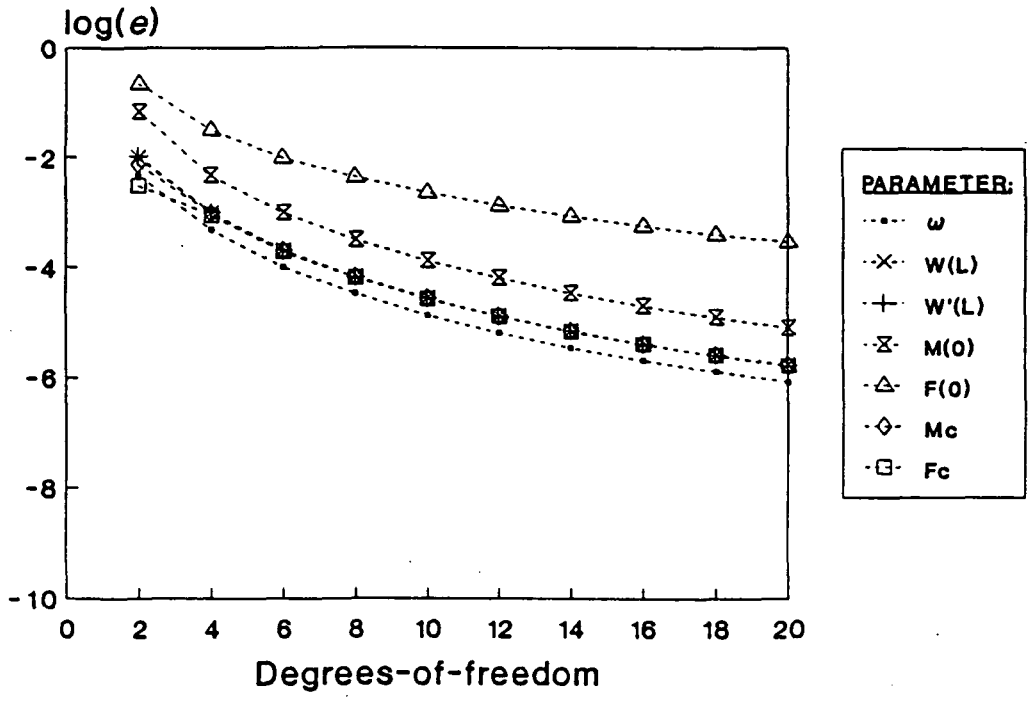

Figure 8.2 Convergence of first-mode cantilever parameters for h-extensions.

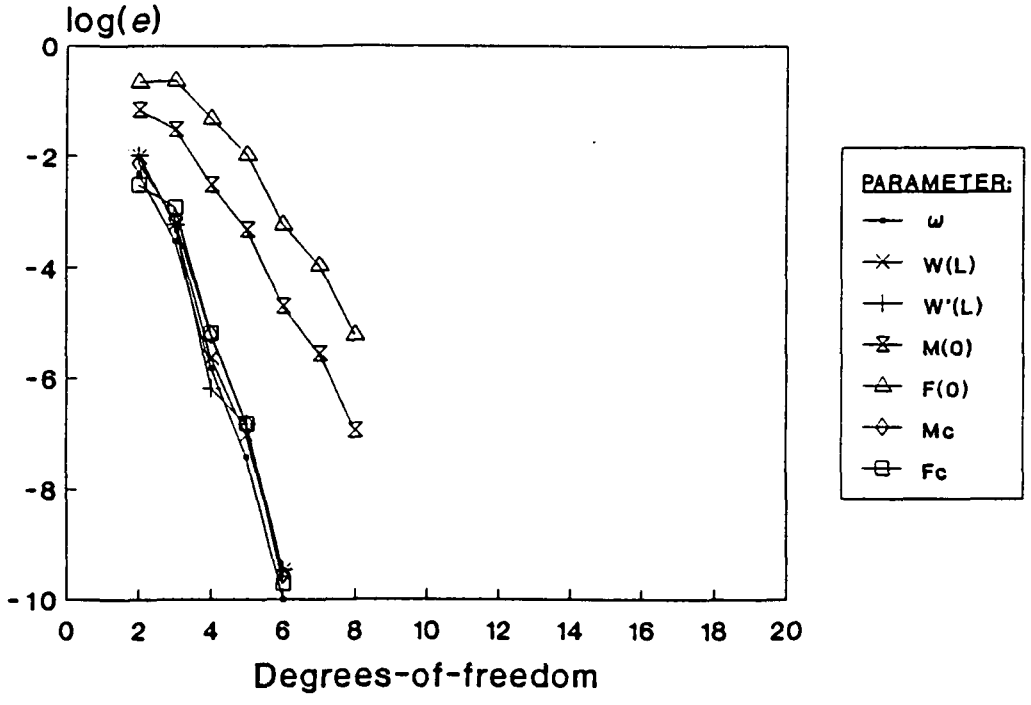

Figure 8.3 Convergence of first-mode cantilever parameters for p-extensions.

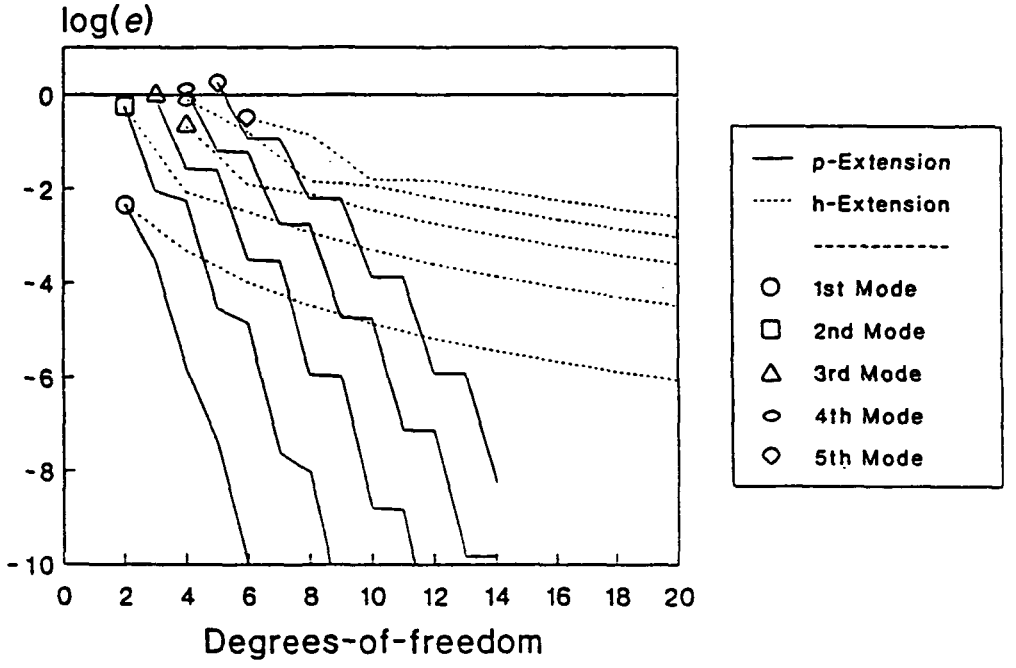

Figure 8.4 Convergence of the first five cantilever natural frequencies.

The super-convergence of the clamped force and moment from the constraint equations is clearly seen in Figures 8.2 and 8.3. The higher-order derivatives required in computing $M(0)$ and $F(0)$ produce less accurate results which are not necessarily monotonic.

Figure 8.4 exhibits the convergence of the first five natural frequencies versus the number of degrees-of-freedom for both models. Although accuracy decreases with increasing natural frequency, exponential rates of convergence still exist for the higher natural frequencies of the p-version models. The stepped convergence, particularly in the p-extension results, is due to the symmetric/antisymmetric bias of the various modes. A summary of the p- versus h-extension comparison is provided in Table 8.1.

The eigenvalues and eigenvectors in this analysis are obtained using the threshold Jacobian method as outlined in [14]. This transformation technique

Table 8.1 Minimum number of degrees-of-freedom for one percent error in cantilever parameters.

Mode	1		2		3		4	
Extension	p	h	p	h	p	h	p	h
Parameter:								
ω	2	2	3	4	6	8	7	12
$W(L)$	2	2	5	4	6	10	7	14
$W'(L)$	3	4	5	6	6	10	7	14
$M(0)$	4	4	6	8	7	14	NA	20
$F(0)$	6	6	7	14	NA	NA	NA	NA
M_C	2	2	3	4	6	10	7	14
F_C	2	2	3	4	6	10	7	14

NA $\equiv$ *not available*

Table 8.2 Number of Jacobian rotations versus degrees-of-freedom for p- and h-extensions.

Number of DOF's	Number of Rotations	
	p-Extension	h-Extension
2	1	1
3	7	
4	18	22
5	32	
6	49	67
7	73	
8	107	142
9	139	
10	182	266

uses successive rotations to iteratively diagonalize both the stiffness and mass matrices and solve for *all* of the eigenvalues and eigenvectors. The computational effort is a function of the number of degrees-of-freedom and the number of rotations required to satisfy the convergence criterion. Table 8.2 compares the number of Jacobian rotations versus the number of degrees-of-freedom for the cantilever problem with p- and h-extensions. Based on these results, the p-version finite element method is also superior in terms of computational efficiency.

It is instructive to note that a similar analysis exists in the literature [21]. The analysis presented here differs from that of the cited reference in the definition of the standard element and of the elemental shape functions used to define the internal modes. While this leads to different eigenvectors, the resulting eigenvalues and eigenfunctions are identical for the two formulations (see (1.8)). Thus, the solution depends on the finite element space but *not* on the basis functions which define the space. The resulting matrices in [21] are less sparse than those presented here. However, there is no appreciable difference between the two formulations in terms of Jacobian rotations versus degrees-of-freedom since the Jacobian method destroys the sparse nature of the matrices. This observation suggests that sparse matrices are not the primary reason for the results in Table 8.2. Other eigensolvers which capitalize on matrix sparseness (in terms of storage and computational effort) will still benefit from the present formulation.

8.2 SEQUENTIAL EIGENSOLUTIONS FOR HIERARCHIC EXTENSIONS

The hierarchic nature of the matrices resulting from p-extensions lends itself to algorithmic enhancements within the eigensolver. With respect to the Jacobian method, the eigenvectors from a lower p-level can be used to partially diagonalize the matrices before additional rotations are performed. This procedure begins with the generic eigenproblem:

$$\left[[K^{(p)}] - \omega^2[M^{(p)}]\right]\{U\} = 0, \tag{8.13}$$

resulting in the eigenvalues:

$$\omega_1^{(p)}, \omega_2^{(p)}, \ldots, \omega_{n_p}^{(p)}, \tag{8.14}$$

and corresponding eigenvectors:

$$\left[U^{(p)}\right] = \left[\left\{U_1^{(p)}\right\}, \left\{U_2^{(p)}\right\}, \ldots, \left\{U_{n_p}^{(p)}\right\}\right]. \tag{8.15}$$

Recall the fundamental orthogonality condition for discrete systems [11]:

$$\left[U^{(p)}\right]^T \left[K^{(p)}\right] \left[U^{(p)}\right] = \left[\overline{k}_{ij}^{(p)} \delta_{ij}\right], \text{ and} \tag{8.16a}$$

$$\left[U^{(p)}\right]^T \left[M^{(p)}\right] \left[U^{(p)}\right] = \left[\overline{m}_{ij}^{(p)} \delta_{ij}\right], \tag{8.16b}$$

where δ_{ij} is the Kronecker delta and:

$$\omega_i^{(p)} = \sqrt{\overline{k}_{ii}^{(p)} \Big/ \overline{m}_{ii}^{(p)}}. \tag{8.17}$$

Mass normalization merely implies scaling of the eigenvectors such that:

$$\overline{m}_{ii}^{(p)} \equiv 1, \text{ and} \tag{8.18a}$$

$$\overline{k}_{ii}^{(p)} = \left(\omega_i^{(p)}\right)^2. \tag{8.18b}$$

Hierarchic p-extensions allow for the generic partitioning:

$$\left[K^{(p+1)}\right] = \begin{bmatrix} [K^{(p)}] & [K_{12}] \\ [K_{21}] & [K_{22}] \end{bmatrix}, \text{ and} \tag{8.19a}$$

$$\left[M^{(p+1)}\right] = \begin{bmatrix} [M^{(p)}] & [M_{12}] \\ [M_{21}] & [M_{22}] \end{bmatrix}. \tag{8.19b}$$

Then, defining the estimated eigenvectors as:

$$\left[\hat{U}^{(p+1)}\right] \cong \begin{bmatrix} [U^{(p)}] & [0] \\ [0] & [I] \end{bmatrix}, \tag{8.20}$$

allows for the partial diagonalization:

$$\left[\hat{U}^{(p+1)}\right]^T \left[K^{(p+1)}\right] \left[\hat{U}^{(p+1)}\right] = \begin{bmatrix} [\overline{k}_{ij}^{(p)} \delta_{ij}] & [U^{(p)}]^T [K_{12}] \\ [K_{21}][U^{(p)}] & [K_{22}] \end{bmatrix}, \text{ and} \tag{8.21a}$$

$$\left[\hat{U}^{(p+1)}\right]^T \left[M^{(p+1)}\right] \left[\hat{U}^{(p+1)}\right] = \begin{bmatrix} [\overline{m}_{ij}^{(p)} \delta_{ij}] & [U^{(p)}]^T [M_{12}] \\ [M_{21}][U^{(p)}] & [M_{22}] \end{bmatrix}. \tag{8.21b}$$

Table 8.3 Comparison of computational effort for nonsequential and sequential solutions to p-extensions for the cantilever problem.

p-Level	Number of DOF's	Number of Jacobian Rotations			
		Nonsequential		Sequential	
		Incremental	Total	Incremental	Total
3	2	1	1	1	1
4	3	7	8	6	7
5	4	18	26	14	21
6	5	32	58	22	43
7	6	49	107	32	75
8	7	73	180	47	122
9	8	107	287	58	180

Additional Jacobian rotations may then be performed to complete the diagonalization of the $(p+1)$-approximation.

Table 8.3 compares this sequential approach to the nonsequential technique of solving each p-level independently. The number of Jacobian rotations is smaller for the sequential approach at every p-level except for the $p_3 = 3$ starting case. However, 68 percent more rotations are required to solve through $p_3 = 9$ sequentially than to solve the $p_3 = 9$ case independently. This is not wasted effort; convergence information provided by the hierarchic solutions allow for the estimation of discretization errors (see Section 8.5). Additionally, convergence at the lower p-levels may be sufficient to allow the solution sequence to be terminated at $p_3 < 9$.

8.3 COMMENTS ON SOLUTION TECHNIQUES FOR EIGENPROBLEMS

Variations of the Jacobian eigensolver discussed in the previous sections are used extensively for eigenproblems possessing a limited number of degrees-of-freedom. Barring numerical instabilities, this method is absolutely robust in

obtaining *all* of the eigenvalues and eigenvectors for a given system. The procedure for sequential solutions of hierarchic extensions has been outlined and generalization to complex eigenproblems is not difficult. However, the number of operations required for solution is on the order of n^3 [14]. Furthermore, the full matrices (at least the terms along the diagonal and above for matrices possessing symmetry) must be stored due to the loss of sparseness produced by the successive Jacobian rotations. Besides, only a small number of the lowest or highest eigenvalue/vector's may be of practical interest.

Developments in the field of eigensolution techniques focus on eliminating these shortcomings. The computer age has spawned renewed interest in this field, and improvements are occurring at a rapid pace. Though it is not the intent of this research to contribute to these developments, a brief discussion of the eigensolvers used in this investigation is in order.

The subspace iteration method is incorporated into PVAEB for the evaluation of large, nonrotating eigenproblems. A thorough discussion of the technique is provided in [14], and the eigensolver subroutines are adapted from those provided in the cited reference. Subspace iteration is fundamentally a block (i.e., more than one vector iterated simultaneously) vector iteration scheme for determining the lowest r eigenvalue/vector's of an n-dimensional eigenproblem, where $r \ll n$. The constrained, global stiffness and mass matrices may be stored in "skyline" format [88] to capitalize on their sparse nature.

The iteration procedure begins with an estimate of the lowest r eigenvectors of $[[K] - \omega^2[M]]\,\{U\} = \{0\}$, namely:

$$[U]_1 = [\{U_1\}, \{U_2\}, \ldots, \{U_r\}]_1. \tag{8.22}$$

Then, the block iteration proceeds by solving:

$$[\overline{U}]_{j+1} = [K]^{-1}[M][U]_j, \tag{8.23}$$

such that:

$$[\overline{K}]_{j+1} = [\overline{U}]^T_{j+1}[K][\overline{U}]_{j+1}, \text{ and} \tag{8.24a}$$

$$[\overline{M}]_{j+1} = [\overline{U}]^T_{j+1}[M][\overline{U}]_{j+1}, \tag{8.24b}$$

where $[\overline{K}]_{j+1}$ and $[\overline{M}]_{j+1}$ may be viewed as projections to the r-dimensional space. Solution of the projected eigenproblem (via the Jacobian method):

$$[[\overline{K}]_{j+1} - \omega^2_{j+1}[\overline{M}]_{j+1}]\,\{Q\}_{j+1} = \{0\}, \tag{8.25}$$

results in an improved estimate of eigenvectors:

$$[U]_{j+1} = [\overline{U}]_{j+1}[Q]_{j+1}. \tag{8.26}$$

As stated in [14], $[U]_{j+1}$ *theoretically* converges to the lowest r eigenvectors as $j \to \infty$ with the corresponding eigenvalues coming from the solution of (8.25), *provided* that the starting vectors are not orthogonal to one of the desired eigenvectors. In practice, however, this is not the case. "Stiff" systems produce algorithmic instabilities as all eigenvectors in the block attempt to converge to the lowest eigenvector. Furthermore, some of the lowest r eigenvectors may be missed even with acceptable starting vectors. The latter condition may be checked utilizing the Sturm sequence property [14]. Performing Gauss factorization of the form:

$$[[K] - \mu[M]] = [L][D][L]^T, \tag{8.27}$$

where $[L]$ and $[D]$ are lower triangular and diagonal matrices, respectively, produces η negative elements in $[D]$ where η is the number of eigenvalues ($\lambda = \omega^2$) less than μ.

Another significant difference between the subspace iteration and Jacobian methods involves the determination of convergence. Off-diagonal matrix terms are checked in the Jacobian procedure for satisfaction of the orthogonality condition in (8.16) to some acceptable tolerance. The subspace iteration method as implemented simply checks the change in the eigenvalues after each iteration. For problems with repeated or similar eigenvalues, the convergence rate may be slow enough to satisfy the tolerance criterion even though the eigenvalue/vector pair is not accurate. A convenient error check for this condition involves computing:

$$\epsilon = \frac{\left\| \left[[K] - \omega_{j+1}^2 [M] \right] \{U\}_{j+1} \right\|_2}{\left\| [K] \{U\}_{j+1} \right\|_2}, \tag{8.28}$$

for each eigenpair, where $\| * \|_2$ represents the Euclidean vector norm [14]. Typically, an accuracy of $10^{-2\ell}$ for the eigenvalue produces an accuracy of $10^{-\ell}$ for the eigenvector with respect to this error norm. Convergence for the subspace iteration method may be enhanced by using q iteration vectors where $r < q \ll n$. In practice:

$$q = \min(2r, r + 8), \tag{8.29}$$

has been used extensively. Additional refinements to the basic subspace iteration algorithm have been implemented to improve convergence and to make the procedure more robust [89].

The selection of the starting eigenvectors in (8.22) has a significant effect on the number of subspace iterations required for convergence. Hierarchic extensions again provide a most beneficial approach for sequential eigensolutions. Recalling (8.19-20) and (8.22), the starting eigenvectors may be defined as:

$$\left[U^{(p+1)}\right]_1 = \left[\left\{ \begin{Bmatrix} U_1^{(p)} \\ \{0\} \end{Bmatrix} \right\}, \left\{ \begin{Bmatrix} U_2^{(p)} \\ \{0\} \end{Bmatrix} \right\}, \ldots, \left\{ \begin{Bmatrix} U_r^{(p)} \\ \{0\} \end{Bmatrix} \right\} \right]. \tag{8.30}$$

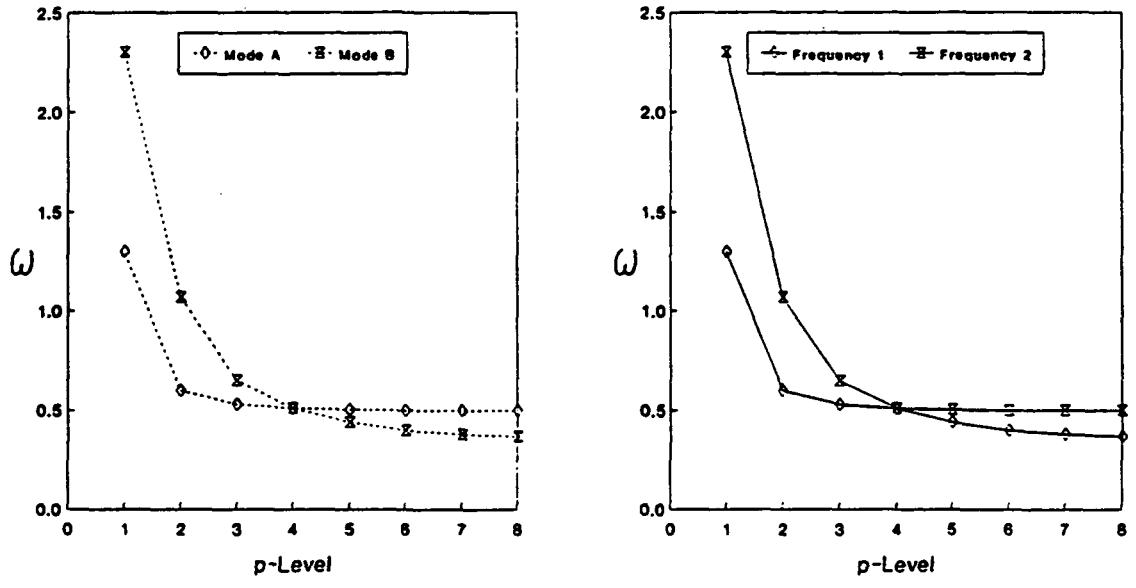

Mode Tracking Frequency Tracking

Figure 8.5 Extension-induced crossing of approximate natural frequencies.

Using q iteration vectors as in (8.29) causes no difficulty. A sample of this approach in Chapter 11 shows that hierarchic extensions can improve robustness as well as convergence. However, a minor problem exists when the natural frequencies of different modes cross during the p-extensions. This phenomenon is illustrated in Figure 8.5. Locking onto Mode A at the low p-levels may induce failure in the Sturm sequence check (8.27) at the higher p-levels. This causes a problem only if the crossing modes occur near the r-boundary of desired eigenpairs and can usually be overcome by either increasing or decreasing r.

A major criticism of subspace iteration is that $[U]_j$ is overwritten by $[U]_{j+1}$ at each step. The Lanczos method, stated in the simplest of terms, uses *all* of the $[U]_j$, $j = 1, 2, \ldots$ in the estimation of the lowest eigenpairs [90]. Though block versions do exist, the Lanczos method is typically implemented using a single iteration vector [91]. Comparisons with subspace iteration have demonstrated the superiority of the Lanczos procedure [92], and continued algorithmic refinements

in the past few decades have made this technique sufficiently robust for practical use.

Mention of the Lanczos method is mandated by its successful application to gyroscopic systems [93]. A single-vector Lanczos solver is incorporated into PVAEB for problems involving rotating coordinate system effects based on an adaptation of software graciously provided by Dr. O. A. Bauchau. A state variable formulation is used, namely:

$$\left[\begin{bmatrix}[M] & [0]\\ [0] & [K]\end{bmatrix} - i\omega \begin{bmatrix}[0] & [M]\\ -[M] & -[C]\end{bmatrix}\right] \begin{Bmatrix} i\omega\{U\} \\ \{U\}\end{Bmatrix} = \begin{Bmatrix}\{0\}\\ \{0\}\end{Bmatrix}, \tag{8.31}$$

but the individual $(n \times n)$ submatrices are still stored in skyline format and complex arithmetic is avoided entirely. The Sturm sequence check (8.27) and error condition (8.28) are easily generalized to complex eigenproblems [94]. However, the single-vector implementation precludes enhancement from sequential solutions of hierarchic extensions.

8.4 COMMENTS ON MATRIX REDUCTION VIA STATIC CONDENSATION

From the user's perspective, p-version finite elements allow for the use of the minimum number of elements necessary to capture the problem geometry. Improvements to the approximate solution may be obtained by increasing the order of the polynomial displacement approximations as opposed to increasing the number of elements in h-version models. This difference is particularly useful for combined static/dynamic analyses for three reasons:

1) the superior convergence properties of p-version finite elements have already been demonstrated,
2) the added computational complexity of eigenproblems versus static problems severely restricts the allowable number of dynamic degrees-of-freedom, and

3) accurate estimates of the lowest natural frequencies typically do not require a large number of degrees-of-freedom.

Historically, static condensation procedures [95] have been used to reduce the number of h-version degrees-of-freedom to an acceptable level for dynamic analysis. The fundamental assumption of these methods is that the inertial loads may be ignored while reducing the number of degrees-of-freedom without much effect on the accuracy of the lowest natural frequencies and mode shapes. Significant insight, both general and problem-specific, is required for successful utilization of static condensation methods, and refinements of these techniques continue [96] in spite of the dramatic improvements in eigensolvers. Since static condensation is still used in engineering practice, it is instructive to discuss p-extensions from this perspective.

Starting from the homogeneous static matrix equation:

$$[K]\{U\} = \{0\}, \tag{8.32}$$

partial Gaussian elimination of the first q unknown displacements may be represented by [97]:

$$\begin{bmatrix} [I] & -[\overline{T}] \\ [0] & [\overline{K}] \end{bmatrix} \begin{Bmatrix} \{U_q\} \\ \{U_r\} \end{Bmatrix} = \{0\}, \tag{8.33}$$

where $\{U_r\}$ are the remaining independent displacements. Thus:

$$\begin{Bmatrix} \{U_q\} \\ \{U_r\} \end{Bmatrix} = \begin{bmatrix} [\overline{T}] \\ [I] \end{bmatrix} \{U_r\}, \text{ or} \tag{8.34a}$$

$$\{U\} = [T]\{U_r\}. \tag{8.34b}$$

In this form, the reduced stiffness matrix may be written as:

$$[\overline{K}] = [T]^T[K][T]. \tag{8.35}$$

Table 8.4 Effect of static condensation on errors for the first-mode cantilever parameters of 8-dof models.

Case Number	1	2	3	4	5
Number of Elements	1	4	8	8	4
Polynomial Order	9	3	3	3	9
Condensation†	N	N	E2	D	E
Parameter:	log(e)				
ω	<-10	-4.49	-4.49	-5.45	-4.49
$W(L)$	<-10	-4.18	-4.18	-5.16	-4.18
$W'(L)$	<-10	-4.18	-4.18	-3.39	-4.18
$M(0)$	-6.95	-3.51	-3.51	-4.83	-3.51
$F(0)$	-5.22	-2.36	-2.36	-5.31	-2.36
M_C	<-10	-4.19	-3.54	-4.41	-4.19
F_C	<-10	-4.19	-2.42	-3.25	-4.19

†*Condensation Legend*:
N ≡ *no condensation*,
E ≡ *condensed to nodal displacements and rotations (external modes)*,
E2 ≡ *condensed to displacements and rotations at every other node, and* D ≡ *condensed to nodal displacements only.*

For the nonrotating eigenproblem, the same transformation may be applied to the mass matrix such that:

$$[\overline{M}] = [T]^T[M][T]. \tag{8.36}$$

Therefore:

$$[[\overline{K}] - \omega^2[\overline{M}]]\,\{U_r\} = \{0\}, \tag{8.37}$$

defines the statically condensed eigenproblem.

Table 8.4 presents various analyses of the cantilever sample problem utilizing static condensation. All five cases result in an 8-dof eigenproblem for consistent comparisons. Case 1 (single element, $p_3 = 9$) and Case 2 (four elements, $p_3 = 3$) do not involve static condensation. Case 3 contains eight $p_3 = 3$ elements with condensed degrees-of-freedom identical to those of Case 2. The Case 3 results are identical to the Case 2 results except for increased errors in the generalized

constraint forces. Further increases in the number of elements while maintaining the same condensed dof's will result in:

$$M_C \rightarrow M(0), \text{ and} \tag{8.38a}$$

$$F_C \rightarrow F(0), \tag{8.38b}$$

thus imposing poorer convergence characteristics on the generalized constraint forces (see Figures 8.2-3).

Case 4 utilizes the often-used assumption of ignoring rotational degrees-of-freedom. While this produces an improved estimate of the natural frequency when compared to Case 2, errors in the other parameters are both better and worse without any consistent pattern. The Case 4 results are still inferior to those obtained by using a higher-order polynomial approximation (Case 1).

Case 5 involves condensing the internal modes out of a four-element, $p_3 = 9$ model. The Case 5 results are identical to those for Case 2. Mathematically, the process of static p-condensation for this problem results in:

$$[\overline{T}] = [0]; \tag{8.39}$$

that is, the transformation matrix between internal modes and external modes is null for straight beam elements with uniform properties. However, this condition is due to the particular structure of the stiffness matrix (see (8.6*a*) and (7.22)) and does *not* generalize to problems involving tapered elements, circular elements, rotating coordinate effects, and/or geometric nonlinearities. This is a moot point since p-condensation is never used in practice. Rather, analysis begins with the lowest p-level and extends to higher polynomial orders until suitable convergence of the natural frequencies and point functionals is attained. Table 8.4 clearly demonstrates the superiority of the p-extension philosophy when compared to static condensation.

8.5 *A POSTERIORI* ESTIMATION OF DISCRETIZATION ERRORS

The quantification of discretization errors is an important development in the p-version technology. For static analyses, the strain energy forms the basis for the estimation of errors. Previous studies, summarized in [29], have used the assumption of asymptotic algebraic convergence in the error estimation, namely:

$$V_{EX} - V_p \cong C n_p^{-\beta}. \tag{8.40}$$

V_{EX} is the exact strain energy while V_p denotes the computed strain energy for the generic polynomial order, p, using n_p degrees-of-freedom, that is:

$$V_p = \frac{1}{2} \left\{ U^{(p)} \right\}^T \left[K^{(p)} \right] \left\{ U^{(p)} \right\}. \tag{8.41}$$

The generic stiffness matrix in (8.41) may include the effects of geometric non-linearities and centrifugal softening (recall that centrifugal softening terms are derived from the kinetic energy formulation). β in (8.40) is typically referred to as the rate of convergence or convergence exponent.

The exact strain energy is generally unknown, but it can be estimated from finite element solutions in the asymptotic range as:

$$V_{EX} \cong \frac{V_p n_p^{\beta} - V_{p-1} n_{p-1}^{\beta}}{n_p^{\beta} - n_{p-1}^{\beta}}. \tag{8.42}$$

Given three successive finite element solutions, β may be estimated by solving for it from the relation:

$$\frac{V_p - V_{p-1}}{n_{p-1}^{-\beta} - n_p^{-\beta}} = \frac{V_{p-1} - V_{p-2}}{n_{p-2}^{-\beta} - n_{p-1}^{-\beta}}. \tag{8.43}$$

The error is defined in terms of the energy norm:

$$\| v \|_{E(\tau)} \equiv \sqrt{V}, \tag{8.44}$$

such that the relative error in energy norm is defined by:

$$e_{\mathcal{V}} \equiv \frac{\|\mathcal{V}_{EX} - \mathcal{V}_{FE}\|_{E(\Upsilon)}}{\|\mathcal{V}_{EX}\|_{E(\Upsilon)}}. \tag{8.45}$$

A similar estimation procedure is used for eigenproblems. Recalling (8.16-18), the relationship between the strain energy and the square of the natural frequencies is quite apparent. Estimation of the exact natural frequencies may be obtained by substituting the squared natural frequencies for the strain energy in (8.42-43). The relative error in natural frequencies is defined as:

$$e_{\omega} \equiv \left| \frac{(\omega_{EX} - \omega_{FE})}{\omega_{EX}} \right|, \tag{8.46}$$

for the purposes of this study.

Estimation of discretization errors by the above relations is not always well-behaved for the problems in this investigation. The symmetric/antisymmetric biasing seen in Figure 8.4 may occur in the strain energy as well as in the natural frequencies. Better error estimates for problems with biasing are easily obtained by increasing the polynomial order by two for each extension. Based on this approach, (abridged) error estimates for the first five cantilever frequencies are displayed in Table 8.5. Convergence rates and error estimates are presented with respect to each p-level (running) and the highest p-level (cumulative), which is $p_3 = 15$ for the sample problem. The running estimates are typically, though not necessarily, conservative compared to the cumulative estimates.

Two other difficulties regarding error estimates exist in the problems studied. Since frequency tracking is used, crossing modes as illustrated in Figure 8.5 will produce erroneous estimates about the crossover point. Crossover typically occurs at the lower p-levels, and verification of convergence may involve at least three extensions beyond the crossover point. A more significant problem is the

Table 8.5 Error estimates for cantilever natural frequencies (abridged).

#DOF	OMEGA # 1	EXTRAPOLATED OMEGA	DELTA OMEGA	CONVERGENCE EXPONENT RUNNING	CONVERGENCE EXPONENT CUMULATIVE	% EST. ERROR IN OMEGA RUNNING	% EST. ERROR IN OMEGA CUMULATIVE
2	0.35327315428368E+01	0.00000000000000E+00	0.00000000E+00	0.0000	0.0000	0.0000	0.4754
4	0.35160206804338E+01	0.35104327153595E+01	-0.16710862E-01	2.0000	11.5962	0.1592	0.0002
6	0.35160152687861E+01	0.35160152189402E+01	-0.54116477E-05	11.5831	24.2887	0.0000	0.0000

#DOF	OMEGA # 2	EXTRAPOLATED OMEGA	DELTA OMEGA	CONVERGENCE EXPONENT RUNNING	CONVERGENCE EXPONENT CUMULATIVE	% EST. ERROR IN OMEGA RUNNING	% EST. ERROR IN OMEGA CUMULATIVE
2	0.34806893108208E+02	0.00000000000000E+00	0.00000000E+00	0.0000	0.0000	0.0000	57.9655
4	0.22157831407518E+02	0.15836226011792E+02	-0.12649062E+02	2.0000	7.0574	39.9186	0.5598
6	0.22034797791240E+02	0.22027038980211E+02	-0.12303362E+00	6.9736	14.8007	0.0352	0.0014
8	0.22034491767814E+02	0.22034487331221E+02	-0.30602343E-03	14.7669	25.4383	0.0000	0.0000

#DOF	OMEGA # 3	EXTRAPOLATED OMEGA	DELTA OMEGA	CONVERGENCE EXPONENT RUNNING	CONVERGENCE EXPONENT CUMULATIVE	% EST. ERROR IN OMEGA RUNNING	% EST. ERROR IN OMEGA CUMULATIVE
4	0.63346583541580E+02	0.00000000000000E+00	0.00000000E+00	0.0000	0.0000	0.0000	2.6733
6	0.61716292816021E+02	0.60380375296969E+02	-0.16302907E+01	2.0000	11.0311	2.2125	0.0309
8	0.61697282501193E+02	0.61696426873814E+02	-0.19010315E-01	10.9325	19.5899	0.0014	0.0001
10	0.61697214510207E+02	0.61697213632417E+02	-0.67990985E-04	19.5504	29.3863	0.0000	0.0000

#DOF	OMEGA # 4	EXTRAPOLATED OMEGA	DELTA OMEGA	CONVERGENCE EXPONENT RUNNING	CONVERGENCE EXPONENT CUMULATIVE	% EST. ERROR IN OMEGA RUNNING	% EST. ERROR IN OMEGA CUMULATIVE
4	0.28159625332748E+03	0.00000000000000E+00	0.00000000E+00	0.0000	0.0000	0.0000	132.9130
6	0.12838933516044E+03	0.00000000000000E+00	-0.15320692E+03	0.0000	8.7439	0.0000	6.1930
8	0.12111671135271E+03	0.12042584751742E+03	-0.72726238E+01	8.6010	12.4474	0.5737	0.1777
10	0.12090406677858E+03	0.12088928898110E+03	-0.21264457E+00	12.2547	20.6357	0.0122	0.0018
12	0.12090192490536E+03	0.12090187312807E+03	-0.21418732E-02	20.5482	30.0850	0.0000	0.0000

#DOF	OMEGA # 5	EXTRAPOLATED OMEGA	DELTA OMEGA	CONVERGENCE EXPONENT RUNNING	CONVERGENCE EXPONENT CUMULATIVE	% EST. ERROR IN OMEGA RUNNING	% EST. ERROR IN OMEGA CUMULATIVE
6	0.22355138739963E+03	0.00000000000000E+00	0.00000000E+00	0.0000	0.0000	0.0000	11.8543
8	0.20109457572248E+03	0.16786365593430E+03	-0.22456812E+02	2.0000	10.4578	19.7964	0.6180
10	0.19988582726835E+03	0.19974594538459E+03	-0.12087485E+01	10.1686	17.2637	0.0700	0.0132
12	0.19985976653629E+03	0.19985856092016E+03	-0.26060732E-01	17.1056	25.7638	0.0006	0.0001
14	0.19985953118071E+03	0.19985952666025E+03	-0.23535557E-03	25.7638	25.7638	0.0000	0.0000

possible loss of monotonic convergence brought about by geometric nonlinearities. When this is sensed, the convergence rate is assumed quadratic ($\beta \equiv 2$) so that a two-point estimate may be generated from (8.42). Table 8.5 shows that the quadratic estimator is also used to produce error estimates after a single extension. The single-extension quadratic estimate for the fourth mode is not listed since the estimated exact natural frequency is negative. The quadratic estimator is also used when the general algebraic estimation logic fails, thus making the entire estimation procedure quite robust. Problems with biasing and/or crossovers will usually invoke the quadratic estimator.

9. SOLUTIONS FOR CIRCULAR BEAMS AND RINGS

The formulation of circular beam elements with the provision for variable-order polynomial approximation of the displacement variables provides a new and valuable analytical capability. This chapter is devoted to demonstrating the use of these elements and to compare the finite element solutions with theoretical and experimental results from the literature. The significance of the various beam types and curvature approximations will be explored in detail. Refer to Appendix 14.1 for interpretation of the PVAEB inputs for the various models.

9.1 EXTENSION GUIDELINES FOR CIRCULAR ELEMENTS

As mentioned in Chapter 8, exact static solutions for straight beams with point loading may be obtained using $p_1 = p_4 = 1$ and $p_2 = p_3 = 3$ for BE/RA elements, and in addition, $p_5 = p_6 = 2$ for TI elements. The implementation of p-version circular beam elements is complicated by two factors:

1) the circular geometry induces coupling of the displacement variables within the elemental formulations, and
2) the polynomial-based shape functions do not identically characterize all of the (strain-free) rigid body motions for circular elements.

Therefore, investigation into the appropriate interrelationships between the polynomial orders used to approximate the various displacement variables for circular beam elements is warranted.

It is easy to understand that no definitive set of guidelines for these interrelationships may be established. Indeed, the optimal choice of polynomial orders which minimize, for example, the error in strain energy for a particular number of degrees-of-freedom, is different for every problem. The relative contributions of extension, bending, torsion, and shear to the total strain energy will affect

the optimal path of p-extensions, as will the introduction of rotating coordinate system effects and/or geometric nonlinearities. The concept of adaptive p-refinement will merit considerable research and development in the future.

In the most general sense, rotations may be viewed as derivatives of the displacements. Thus, one simple hypothesis is to assume the polynomials used to approximate the displacement variables (u_0, v_0, and w_0) to be the same order and one order greater than those used to approximate the rotation variables (ϕ_1, and u_y and u_z for TI beams). Similar arguments have been applied to straight and circular h-version Timoshenko beam elements to circumvent locking problems [23,81].

This section documents benchmark studies into polynomial order optimization for circular beam elements. In-plane and out-of-plane (uncoupled) linear static analyses will be performed using both Bernoulli-Euler and Timoshenko beam idealizations and primarily using the ST curvature approximation (to facilitate comparisons with analytic solutions). The optimal path of p-extensions will be compared to that proposed by the simple hypothesis.

9.1.1 In-Plane Static Analysis of a Pinched Circular Ring

A three-inch thick (t) by three-inch deep (ℓ) steel ring with a ten-inch mean radius (R) subjected to a one hundred pound pinching load (W) is evaluated for its planar response. The single-element half-ring model is illustrated in Figure 9.1. Note that an appropriately constrained quarter-ring model could be used to analyze the pinched-ring problem, but the half ring has been chosen as a more exacting test of the PVAEB program. This problem is particularly beneficial for verifying the proper coupling of displacement variables for deeply curved

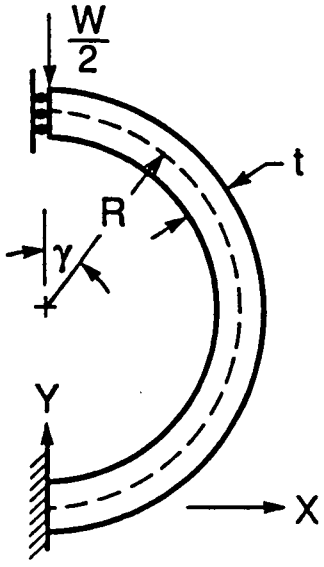

Figure 9.1 Pinched ring sample problem.

Table 9.1 PVAEB sample input for the pinched ring.

```
TITLE = 3" X 3" RECTANGULAR STEEL PINCHED RING, RADIUS = 10"
SUBTITLE = SINGLE-ELEMENT (HALF-RING) MODEL
$
BEAM = BE  $ NOTE: PROVISIONS FOR 'TI' BEAM ARE INCLUDED.
CIRC = ST  $ NOTE: PROVISIONS FOR 'TR' OR 'EX' APPROXIMATIONS ARE INCLUDED.
ANALYSIS = ST
LOAD = 100
SPC = 100
$
SEGLODISP = LO
SEFORCE = LO
ECHO = AL
REPORT
$
SUBCASE
 BRP = 9,9,3,1
 TIP = 9,9,1,1,8,1
$
BEGINBULK
$
GRID, 1, 0.,  0., 0., 123456
GRID, 2, 0., 20., 0.
$
CBARC, 1, 1, 2, 1, 1., 0., 0., 10.
CBARI, 1, 1, 10
$
PBARC, 1, 2, 9., 6.75, 6.75, 11.390625, .8333333333333, .8333333333333, +P1
+P1, 0., 0., 0., 10., 9.0684261562, 6.8426156188, , , +P2
+P2, 6.8013196171, -.68426156188, 0., 0., , , , , +P3
+P3, -1.5, 0., 1.5, 0., 0., -1.5, 0., 1.5
$
MAT, 2, 30000000., 12000000., , 7.35E-4
$
$ IN-PLANE LOADS AND CONSTRAINTS
LOAD, 100, 1., 0.5, 2
FORCE, 2, 2, -100., 0., 1., 0.
SPCADD, 100, 100
SPC, 100, 13456, 2
$
ENDDATA
```

problems regardless of the curvature approximation. Table 9.1 provides a sample of the PVAEB input for this problem.

For the ST curvature approximation, the exact force and moment distributions are known to be [98]:

$$F_x = -\frac{W}{2}\sin\gamma, \tag{9.1a}$$

$$F_y = \frac{W}{2}\cos\gamma, \text{ and} \tag{9.1b}$$

$$M_z = WR\left(\frac{1}{\pi} - \frac{\sin\gamma}{2}\right), \tag{9.1c}$$

with respect to the local beam axes (see Figure 3.3 and Section 3.5). The bending, extensional, and shear strain energies for the half ring are defined by:

$$V_B \equiv \int_0^\pi \frac{M_z^2 R}{2EI_{yy}}d\gamma, \tag{9.2a}$$

$$V_E \equiv \int_0^\pi \frac{F_x^2 R}{2EA}d\gamma, \text{ and} \tag{9.2b}$$

$$V_S \equiv \int_0^\pi \frac{F_y^2 R}{2Gk_yA}d\gamma, \tag{9.2c}$$

respectively. Therefore:

$$\begin{aligned} V_B &= \frac{W^2R^3}{2EI_{yy}}\left(\frac{\pi}{8} - \frac{1}{\pi}\right) \\ &= 0.00183677 \text{ in}-\text{lb}_\text{f}, \end{aligned} \tag{9.3a}$$

$$\begin{aligned} V_E &= \frac{\pi W^2 R}{16EA} \\ &= 0.00007272 \text{ in}-\text{lb}_\text{f}, \text{ and} \end{aligned} \tag{9.3b}$$

$$\begin{aligned} V_S &= \frac{\pi W^2 R}{16Gk_yA} \\ &= 0.00021817 \text{ in}-\text{lb}_\text{f}, \end{aligned} \tag{9.3c}$$

for the particular problem parameters, where:

$$\begin{aligned} V_{BE:ST} &= V_B + V_E \\ &= \frac{1}{2}\int_0^{\pi R}\left[EI_{yy}\left(-v_0'' + \frac{u_0'}{R}\right)^2 + EA\left(u_0' + \frac{v_0}{R}\right)^2\right]dx, \end{aligned} \tag{9.4a}$$

and:

$$V_{TI:ST} = V_B + V_E + V_S$$
$$= \frac{1}{2}\int_0^{\pi R}\left[EI_{yy}\left(u_y'\right)^2 + EA\left(u_0' + \frac{v_0}{R}\right)^2 + Gk_yA\left(u_y + v_0' - \frac{u_0}{R}\right)^2\right]dx. \quad (9.4b)$$

Invoking the TR or EX curvature approximation significantly complicates the strain energy equations. Terms containing coupled products of the forces and moments result primarily from the curvature-induced shift in the neutral axis of bending. Furthermore, this neutral axis shift produces changes in the bending moment distribution itself.

The Bernoulli-Euler beam idealization is defined completely in terms of the displacement variables, u_0 and v_0, and their respective orders of polynomial approximation, p_1 and p_2. The number of degrees-of-freedom for the single-element PVAEB model is:

$$n_{BE} = p_1 + p_2 - 3, \quad (9.5)$$

where the BE subscript merely denotes the Bernoulli-Euler idealization. Table 9.2 displays the log of the error in energy norm (8.45) for the complete range of polynomial orders for p_1 and p_2. The underlined values correspond to the minimum error for $n_{BE} = 1$ through $n_{BE} = 15$. The proposed hypothesis that $p_1 = p_2 \equiv p$ produces the minimum error is correct for $p \geq 4$. Also note that no change in strain energy occurs for $p_1 > p_2 + 1$ (using $p_1 = p_2 + 1 \equiv p$ has proven beneficial for h-version circular elements [99]).

The Timoshenko beam idealization possesses an additional displacement variable, u_y, approximated by the polynomial order p_5. The number of dof's for the TI model is:

$$n_{TI} = p_1 + p_2 + p_5 - 2. \quad (9.6)$$

Table 9.2 Log(e_V) for BE:ST analyses of the pinched ring.

		p_2						
		3	4	5	6	7	8	9
p_1	1	-0.06751	-0.09396	-0.11157	-0.11862	-0.11991	-0.11996	-0.11996
	2	-0.08365	-0.15801	-0.15898	-0.18029	-0.18030	-0.18049	-0.18049
	3	-0.08365	-0.59259	-0.63416	-0.71977	-0.72020	-0.72565	-0.72578
	4	-0.08391	-0.66870	-0.66929	-0.77101	-0.77103	-0.77767	-0.77767
	5	-0.08391	-2.08584	-2.11807	-3.24350	-3.25653	-3.28729	-3.28829
	6	-0.08391	-2.08584	-2.12351	-3.32438	-3.32514	-3.36140	-3.36140
	7	-0.08391	-2.08584	-2.12351	-5.07120	-5.11538	-6.80015	-6.80459
	8	-0.08391	-2.08584	-2.12351	-5.07120	-5.11686	-6.87845	-6.87911
	9	-0.08391	-2.08584	-2.12351	-5.07120	-5.11686	-8.72616	-8.77511

Note: underlined values represent the minimum error for a given n_{BE}.

Since the pinched-ring strain energy is dominated by bending (9.3), one might be led to believe that increasing the polynomial order for u_y is most effective in reducing the error in energy norm (see (9.4*b*)); in fact, the opposite is true. Table 9.3 compares the optimal extension path to the proposed path of $p_1 = p_2 = p_5 + 1 \equiv p$. Except for $n_{TI} = 6$, the minimum error is produced by $p_5 \leq \min(p_1, p_2)$. Thus, the coupling of the displacement variables in the extensional and shear strain energies has a significant effect on the optimal path of p-extensions even for problems dominated by bending.

Table 9.3 Log(e_v) for TI:ST analyses of the pinched ring.

	Optimal Extension Path				Proposed Extension Path			
n_{TI}	p_1	p_2	p_5	log(e_v)	p_1	p_2	p_5	log(e_v)
3	2	2	1	-0.13272	2	2	1	-0.13272
4	3	2	1	-0.18097				
5	3	3	1	-0.19002				
6	3	2	3	-0.25286	3	3	2	-0.19003
7	3	3	3	-0.27750				
8	3	4	3	-0.63996				
9	4	4	3	-0.72301	4	4	3	-0.72301
10	5	4	3	-2.24801				
11	5	5	3	-2.37079				
12	5	6	3	-2.78956	5	5	4	-2.37233
13	6	6	3	-2.82174				
14	5	6	5	-3.27432				
15	6	6	5	-3.36592	6	6	5	-3.36592
16	7	6	5	-5.45383				
17	7	7	5	-5.55564				
18	7	8	5	-6.14746	7	7	6	-5.55578
19	8	8	5	-6.16554				
20	7	8	7	-6.82335				
21	8	8	7	-6.91357	8	8	7	-6.91357
22	9	8	7	-9.28994				
23	9	9	7	-9.38162				
24	-	-	-	-	9	9	8	-9.38165

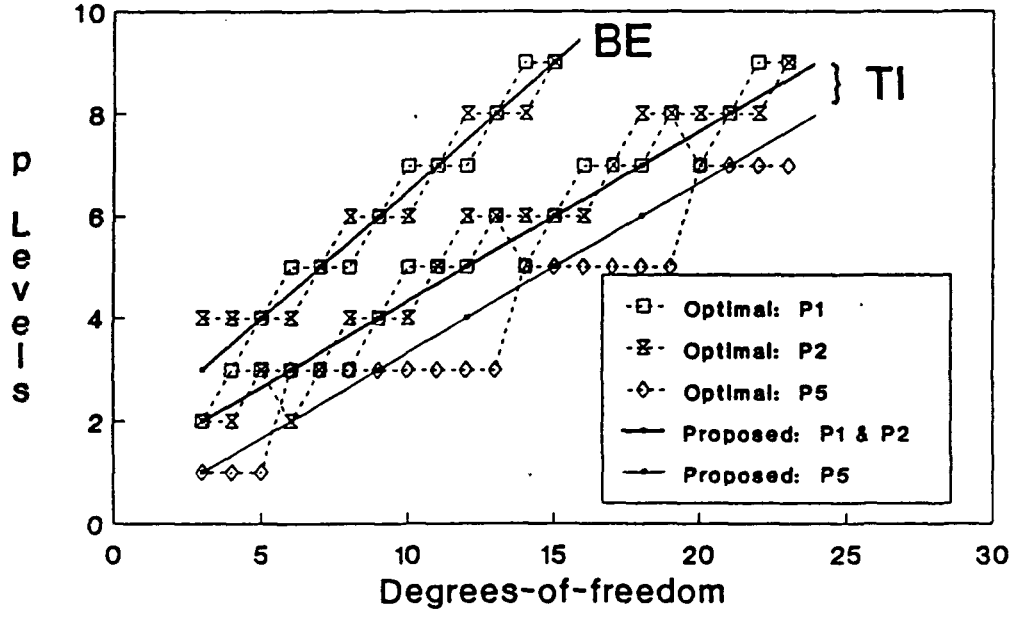

Figure 9.2 Optimal and proposed extension paths for the pinched ring.

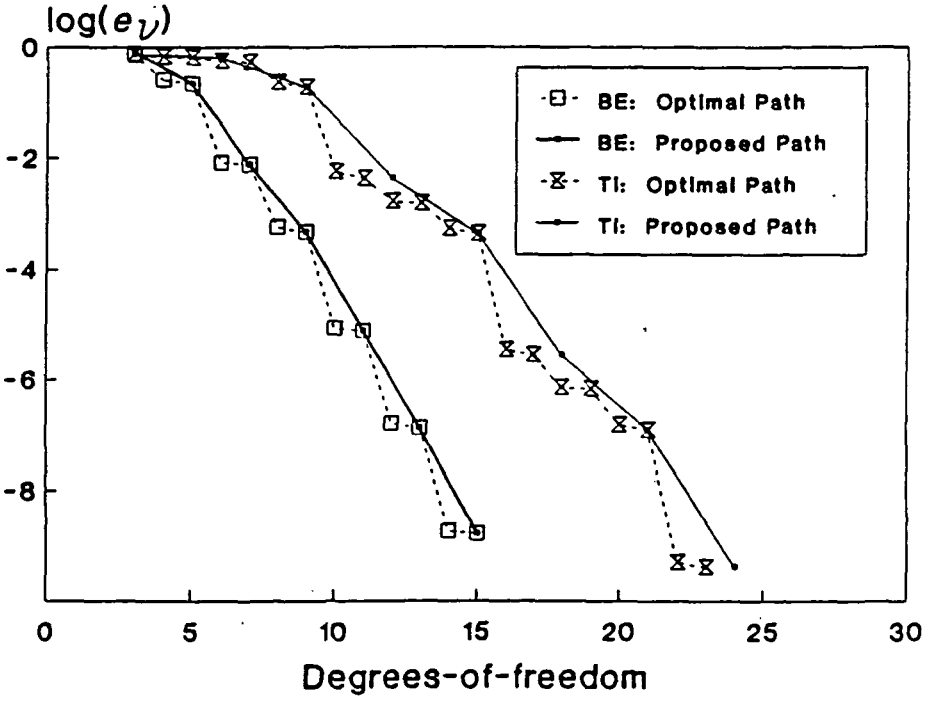

Figure 9.3 Convergence of $\log(e_\nu)$ for the pinched ring.

Figure 9.2 compares the p-levels producing the minimum error in energy norm to the hypothesized extension path for the BE and TI beam idealizations. The proposed path for BE extensions is most acceptable for the pinched ring. Choosing $p_1 = p_2 = p_5 + 2 \equiv p$ would correlate better with the optimal path for the TI idealization of this particular problem, but the selection of $p_1 = p_2 = p_5 + 1 \equiv p$ provides an acceptable rule-of-thumb. Figure 9.3 displays the convergence of the error in energy norm for the various beam types and extension paths. In all cases, (asymptotic) exponential rates of convergence (8.11) are seen to exist for p-extensions of circular beam elements.

A collection of PVAEB results for the pinched-ring problem is presented in Table 9.4. The values at $p = \infty$ for the ST curvature approximations are computed from (9.1-4). In addition, the vertical deflection at the top of the ring (Δ_{Y_T}) and the horizontal deflection at the mid-span of the ring (Δ_{X_M}) are analytically defined by [98]:

$$(\Delta_{Y_T})_{BE:ST} = -\eta R \left(\frac{\pi(1+\alpha)}{4} - \frac{2}{\pi} \right), \tag{9.7a}$$

$$(\Delta_{Y_T})_{TI:ST} = -\eta R \left(\frac{\pi(1+\alpha+\beta)}{4} - \frac{2}{\pi} \right), \tag{9.7b}$$

$$(\Delta_{X_M})_{BE:ST} = \eta R \left(\frac{1}{\pi} - \frac{(1+\alpha)}{4} \right), \text{ and} \tag{9.7c}$$

$$(\Delta_{X_M})_{TI:ST} = \eta R \left(\frac{1}{\pi} - \frac{(1+\alpha-\beta)}{4} \right), \tag{9.7d}$$

where:

$$\eta \equiv \frac{WR^2}{EI_{yy}}, \tag{9.8a}$$

$$\alpha \equiv \frac{I_{yy}}{AR^2}, \text{ and} \tag{9.8b}$$

$$\beta \equiv \frac{EI_{yy}}{Gk_yAR^2}. \tag{9.8c}$$

Table 9.4 PVAEB results for the pinched ring.

p[1]	Beam Type	CA[2]	Strain Energy (in-lb$_f$)	Top				Mid-Span			
				F_{x_T} (lb$_f$)	F_{y_T} (lb$_f$)	M_{z_T} (in-lb$_f$)	Δ_{Y_T} (μin)	F_{x_M} (lb$_f$)	F_{y_M} (lb$_f$)	M_{z_M} (in-lb$_f$)	Δ_{X_M} (μin)
3	BE	ST	.00005861	-25.316	.002378	.037354	-2.34445	-31.6501	.002378	0.00000	-1.1722
4	BE	ST	.00117836	249.225	43.6372	219.511	-47.1346	54.8861	-.856862	-104.643	18.4128
5	BE	ST	.00188050	-2.0851	85.8377	374.215	-75.2202	-47.6753	-.191589	-158.504	30.6988
6	BE	ST	.00190768	-19.158	50.7484	320.413	-76.3073	-43.7822	-.082006	-180.039	32.6535
7	BE	ST	.00190946	-.05905	47.0806	316.134	-76.3785	-49.9293	-.002551	-180.983	32.7827
8	BE	ST	.00190949	.377962	49.9906	318.293	-76.3797	-49.8947	-.001715	-181.676	32.8067
9	BE	ST	.00190949	.002098	50.0850	318.347	-76.3797	-49.9990	-.000018	-181.680	32.8072
∞[3]	BE	ST	.00190949	0.	50.	318.310	-76.3797	-50.	0.	-181.690	32.8074
9	BE	TR	.00189528	.002098	50.0847	315.977	-75.8111	-49.9990	-.000036	-184.049	32.5629
9	BE	EX	.00187041	.002119	50.0847	315.945	-74.8164	-49.9990	-.000036	-184.082	32.1065
1	TI	ST	.00004014	-43.354	4.59998	0.00000	-1.60570	-21.6769	4.59998	0.00000	-.80285
2	TI	ST	.00014752	-79.399	48.4955	0.00000	-5.90071	-5.22458	-4.01875	0.00000	-.19350
3	TI	ST	.00026722	18.6137	78.2181	.160920	-10.6890	-44.5495	-1.53682	0.00000	0.94040
4	TI	ST	.00139862	239.368	81.7531	214.922	-55.9446	50.2661	-4.62014	-107.435	20.2391
5	TI	ST	.00210964	-4.0474	22.5026	343.805	-84.3857	-48.3517	-.450736	-170.703	34.1929
6	TI	ST	.00212583	-18.798	48.1844	321.020	-85.0331	-43.8973	-.156486	-180.065	35.4028
7	TI	ST	.00212765	.076551	50.8873	317.648	-85.1059	-49.9697	-.005791	-181.473	35.5710
8	TI	ST	.00212766	.377202	50.0287	318.281	-85.1063	-49.8948	-.001777	-181.676	35.5843
9	TI	ST	.00212766	-.00071	49.9875	318.318	-85.1063	-49.9997	-.000040	-181.688	35.5850
∞[3]	TI	ST	.00212766	0.	50.	318.310	-85.1063	-50.	0.	-181.690	35.5851
9	TI	TR	.00211182	-.00071	49.9875	315.949	-84.4728	-49.9997	-.000040	-184.057	35.3201
9	TI	EX	.00208693	-.00070	49.9877	315.916	-83.4772	-49.9997	-.000040	-184.090	34.8634

[1] Refers to the polynomial order (p) for u_0 and v_0. For TI beams, the polynomial order for u_y is $\max(1, p-1)$.

[2] CA $\equiv$ curvature approximation.

[3] Computed from analytic solution [98].

The displacements in (9.7) are written such that the contributions due to the extensional and shear energies are represented by the factors, α and β, respectively.

As seen in the table, the strain energy and top deflection have converged to six significant digits at $p = 8$ for both BE:ST and TI:ST idealizations. The mid-span displacement is slightly less accurate at any particular p-level. The forces and moments computed using the integral method of Section 3.5 are least accurate, but convergence to the analytic solution is still most apparent. Grid point forces and moments computed using the principle of virtual work (7.84-85) produce accuracies on the same order as the strain energy. However, mid-span values for the single-element model cannot be computed in this manner.

Table 9.4 also displays results using the TR and EX curvature approximations. Note the decrease in strain energy and deflections as the accuracy of the curvature-dependent moments of area (I_{ij}'s) increases. The axial and shear force distributions are seen to remain unchanged, but the listed bending moments do show the effects of the shift in the neutral axis of bending.

9.1.2 Out-of-Plane Static Analysis of a Semicircular Beam

The model used to evaluate out-of-plane response is illustrated in Figure 9.4. The physical properties of the semicircular beam are identical to those of the pinched ring. The differences between the two models involve changes in the constraints and force (P) applied at the top grid point. These changes are easily seen by comparing the PVAEB input for the semicircular beam in Table 9.5 to that of the pinched ring in Table 9.1 (these two models may be combined into a single PVAEB input deck, with the LOAD and SPC cards in the case control dictating the analysis to be performed). Note that the force is oriented to isolate the out-of-plane response such that w_0, ϕ_1, and u_z (TI beams only)

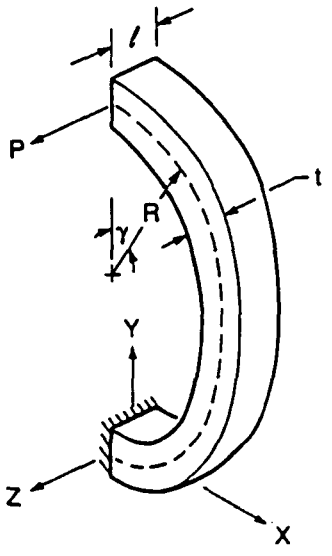

Figure 9.4 Semicircular beam sample problem.

Table 9.5 PVAEB sample input for the semicircular beam.

```
TITLE = 3" X 3" RECTANGULAR STEEL SEMICIRCULAR BEAM, RADIUS = 10"
SUBTITLE = SINGLE-ELEMENT MODEL WITH OUT-OF-PLANE LOADING
$
BEAM = BE  $ NOTE: PROVISIONS FOR 'TI' BEAM ARE INCLUDED.
CIRC = ST  $ NOTE: PROVISIONS FOR 'TR' OR 'EX' APPROXIMATIONS ARE INCLUDED.
ANALYSIS = ST
LOAD = 200
SPC = 200
$
SEGLODISP = LO
SEFORCE = LO
ECHO = AL
REPORT
$
SUBCASE
 BRP = 1,3,9,8
 TIP = 1,1,9,8,1,8
$
BEGINBULK
$
GRID, 1, 0.,  0., 0., 123456
GRID, 2, 0., 20., 0.
$
CBARC, 1, 1, 2, 1, 1., 0., 0., 10.
CBARI, 1, 1, 10
$
PBARC, 1, 2, 9., 6.75, 6.75, 11.390625, .8333333333333, .8333333333333, +P1
+P1, 0., 0., 0., 10., 9.0684261562, 6.8426156188, , , +P2
+P2, 6.8013196171, -.68426156188, 0., 0., , , , , +P3
+P3, -1.5, 0., 1.5, 0., 0., -1.5, 0., 1.5
$
MAT, 2, 30000000., 12000000., , 7.35E-4
$
$ OUT-OF-PLANE LOADS AND CONSTRAINTS
LOAD, 200, 1., 1., 3
FORCE, 3, 2, 100., 0., 0., 1.
SPCADD, 200, 200
SPC, 200, 126, 2
$
ENDDATA
```

are the displacement variables of concern (see (2.35)). These three variables are approximated in PVAEB by the polynomial orders, p_3, p_4, and p_6, respectively.

The ST curvature approximation again provides a known analytic solution to the problem; thus [98]:

$$F_z = -P, \tag{9.9a}$$

$$M_y = -PR\sin\gamma, \text{ and} \tag{9.9b}$$

$$T = PR(1-\cos\gamma), \tag{9.9c}$$

with respect to the local beam axes (see Figure 3.3 and Section 3.5). Strain energy results from bending, torsion, and shear, namely:

$$V_B = \int_0^\pi \frac{M_y^2 R}{2EI_{zz}} d\gamma, \tag{9.10a}$$

$$V_T = \int_0^\pi \frac{T^2 R}{2GI_0} d\gamma, \text{ and} \tag{9.10b}$$

$$V_S = \int_0^\pi \frac{F_z^2 R}{2Gk_z A} d\gamma, \tag{9.10c}$$

respectively. Therefore:

$$V_B = \frac{\pi P^2 R^3}{4EI_{zz}}$$

$$= 0.038785 \text{ in}-\text{lb}_f, \tag{9.11a}$$

$$V_T = \frac{3\pi P^2 R^3}{4GI_0}$$

$$= 0.172378 \text{ in}-\text{lb}_f, \text{ and} \tag{9.11b}$$

$$V_S = \frac{\pi P^2 R}{2Gk_z A}$$

$$= 0.001745 \text{ in}-\text{lb}_f, \tag{9.11c}$$

for the particular problem parameters, where:

$$V_{BE:ST} = V_B + V_T$$

$$= \frac{1}{2}\int_0^{\pi R} \left[EI_{zz}\left(-w_0'' - \frac{\phi_1}{R}\right)^2 + GI_0\left(\phi_1' - \frac{w_0'}{R}\right)^2 \right] dx, \tag{9.12a}$$

Table 9.6 Log(e_V) for BE:ST analyses of the semicircular beam.

		p_3						
		3	4	5	6	7	8	9
p_4	1	-0.38731	-0.38909	-0.38949	-0.38949	-0.38949	-0.38949	-0.38949
	2	-0.71608	-1.33939	-1.34608	-1.34900	-1.34900	-1.34900	-1.34900
	3	-0.76485	-1.54632	-1.59769	-1.60275	-1.60278	-1.60278	-1.60278
	4	-0.77607	-2.24710	-2.59942	-3.73196	-3.73632	-3.73754	-3.73754
	5	-0.77649	-2.25853	-2.61939	-4.13882	-4.16756	-4.17086	-4.17087
	6	-0.77651	-2.26291	-2.62948	-5.15656	-5.63436	-7.06259	-7.06508
	7	-0.77651	-2.26292	-2.62950	-5.16352	-5.64542	-7.54950	-7.56742
	8	-0.77651	-2.26292	-2.62951	-5.16554	-5.65158	-8.79127	-9.32191
	9	-0.77651	-2.26292	-2.62951	-5.16554	-5.65159	-8.79552	-9.32898

Note: underlined values represent the minimum error for a given n_{BE}.

and:

$$V_{TI:ST} = V_B + V_T + V_S$$
$$= \frac{1}{2}\int_0^{\pi R}\left[EI_{zz}\left(u_z' - \frac{\phi_1}{R}\right)^2 + GI_0\left(\phi_1' + \frac{u_z}{R}\right)^2 + Gk_zA\left(u_z + w_0'\right)^2\right]dx. \qquad (9.12b)$$

The number of degrees-of-freedom for the one-element Bernoulli-Euler idealization is:

$$n_{BE} = p_3 + p_4 - 1. \qquad (9.13)$$

Table 9.6 displays the log of the error in energy norm as a function of p_3 and p_4. Again, the underlined values represent the minimum error for $n_{BE} = 3$ through $n_{BE} = 16$. Note that the proposed path of $p_3 = p_4 + 1 \equiv p$ minimizes the error

Table 9.7 Log(e_V) for TI:ST analyses of the semicircular beam.

	Optimal Extension Path				Proposed Extension Path			
n_{TI}	p_3	p_4	p_6	log(e_V)	p_3	p_4	p_6	log(e_V)
4	2	1	1	-0.33859	2	1	1	-0.33859
5	2	2	1	-0.60927				
6	2	2	2	-0.61766				
7	3	2	2	-0.72008	3	2	2	-0.72008
8	3	2	3	-0.77599				
9	4	2	3	-1.34305				
10	4	3	3	-1.54995	4	3	3	-1.54995
11	4	4	3	-2.25069				
12	4	4	4	-2.32909				
13	5	4	4	-2.60300	5	4	4	-2.60300
14	5	4	5	-2.83021				
15	6	4	5	-3.73554				
16	6	5	5	-4.14239	6	5	5	-4.14239
17	6	6	5	-5.16014				
18	6	6	6	-5.35686				
19	7	6	6	-5.63793	7	6	6	-5.63793
20	7	6	7	-6.04041				
21	8	6	7	-7.06616				
22	8	7	7	-7.55307	8	7	7	-7.55307
23	8	8	7	-8.79469				
24	8	8	8	-9.08481				
25	9	8	8	-9.32499	9	8	8	-9.32499
26	9	8	9	-9.88446				

for all allowable p. Unlike p_1 and p_2 for the pinched-ring problem, p_3 and p_4 are independent in that the strain energy will continue to change indefinitely from extensions of either polynomial order. Table 9.7 compares the optimal extension path to the hypothesized path for the Timoshenko semicircular beam, where:

$$n_{TI} = p_3 + p_4 + p_6. \tag{9.14}$$

The proposed path of $p_3 = p_4 + 1 = p_6 + 1 \equiv p$ coincides exactly with the optimal path for this particular problem.

The optimal and proposed extension paths for both BE and TI analyses are illustrated in Figure 9.5. Figure 9.6 displays the convergence of the error in energy norm for the semicircular beam problem. Again, exponential convergence in the asymptotic region is evident.

Selected PVAEB output for the semicircular beam is presented in Table 9.8. For the ST approximation, the displacement and rotations at the top of the semicircular beam with respect to the global frame are [98]:

$$(\Delta_{Z_T})_{BE:ST} = \frac{\pi}{2}\eta R(3+\alpha), \tag{9.15a}$$

$$(\Delta_{Z_T})_{TI:ST} = \frac{\pi}{2}\eta R(3+\alpha+2\beta), \tag{9.15b}$$

$$(\theta_{X_T})_{BE/TI:ST} = \frac{\pi}{2}\eta(1+\alpha), \text{ and} \tag{9.15c}$$

$$(\theta_{Y_T})_{BE/TI:ST} = 2\eta, \tag{9.15d}$$

where:

$$\eta \equiv \frac{PR^2}{GI_0}, \tag{9.16a}$$

$$\alpha \equiv \frac{GI_0}{EI_{zz}}, \text{ and} \tag{9.16b}$$

$$\beta \equiv \frac{I_0}{k_z AR^2}. \tag{9.16c}$$

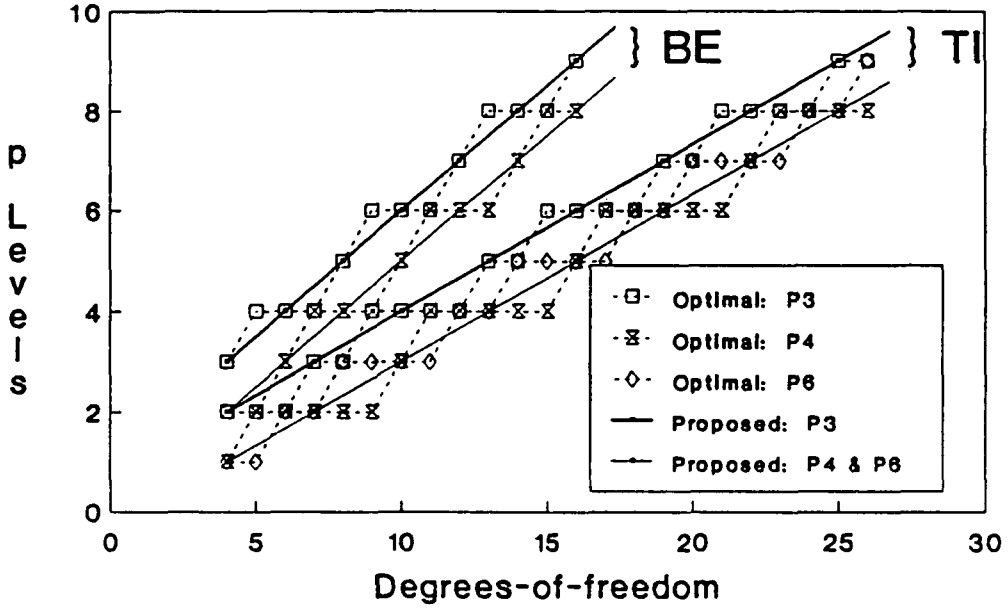

Figure 9.5 Optimal and proposed extension paths for the semicircular beam.

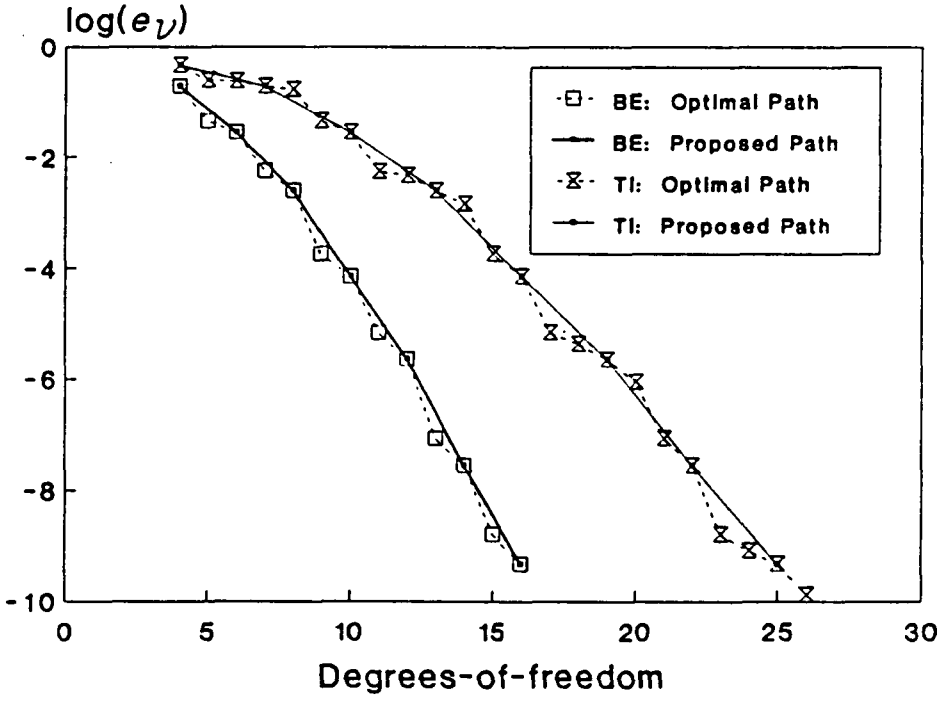

Figure 9.6 Convergence of $\log(e_v)$ for the semicircular beam.

Table 9.8 PVAEB results for the semicircular beam.

p[1]	Beam Type	CA[2]	Strain Energy (in-lb$_f$)	Top				Mid-Span		Bottom		
				T_T (in-lb$_f$)	Δ_{Z_T} (μin)	θ_{X_T} (μrad)	θ_{Y_T} (μrad)	M_{y_M} (in-lb$_f$)	T_M (in-lb$_f$)	F_{z_B} (lb$_f$)	M_{y_B} (in-lb$_f$)	T_B (in-lb$_f$)
3	BE	ST	.137767	-114.8	2755.34	86.7889	121.437	-35.9283	1005.65	-319.422	-1826.	1019.46
4	BE	ST	.199330	-758.6	3986.60	173.744	145.881	-864.006	1010.19	-289.383	-482.3	2589.36
5	BE	ST	.210102	9.9914	4202.05	190.774	146.084	-866.827	1021.74	90.1484	298.45	2106.12
6	BE	ST	.211133	52.720	4222.65	192.437	146.321	-996.458	1000.92	-76.5442	21.994	1951.94
7	BE	ST	.211162	-.2986	4223.25	192.487	146.319	-996.003	1000.53	-116.005	-12.04	1997.01
8	BE	ST	.211163	-1.230	4223.27	192.489	146.319	-999.954	1000.01	-100.786	-.4097	2001.17
9	BE	ST	.211163	.00424	4223.27	192.489	146.319	-999.943	1000.01	-99.5366	.20271	2000.04
∞[3]	BE	ST	.211163	0.	4223.27	192.489	146.319	-1000.	1000.	-100.	0.	2000.
9	BE	TR	.211163	.00424	4223.27	192.489	146.319	-999.943	1000.01	-99.5366	.20271	2000.04
9	BE	EX	.210871	.00409	4217.41	191.904	146.319	-999.942	1000.01	-99.5343	.20370	2000.04
1	TI	ST	.006565	87.323	131.306	.790187	6.13699	-31.5570	45.3805	-376.165	-39.56	3.43802
2	TI	ST	.062411	1099.1	1248.23	9.94557	77.2423	-397.188	571.175	-100.000	-497.9	43.2722
3	TI	ST	.139513	-114.8	2790.25	86.7890	121.438	-35.9283	1005.65	-100.000	-1826.	1019.46
4	TI	ST	.201075	-758.6	4021.50	173.744	145.881	-864.006	1010.19	-100.000	-482.3	2589.36
5	TI	ST	.211848	9.9914	4236.95	190.774	146.084	-866.827	1021.74	-100.000	298.45	2106.12
6	TI	ST	.212878	52.720	4257.56	192.437	146.321	-996.458	1000.92	-100.000	21.994	1951.94
7	TI	ST	.212908	-.2986	4258.15	192.487	146.319	-996.003	1000.53	-100.000	-12.04	1997.01
8	TI	ST	.212909	-1.230	4258.17	192.489	146.319	-999.954	1000.01	-100.000	-.4097	2001.17
9	TI	ST	.212909	.00424	4258.17	192.489	146.319	-999.943	1000.01	-100.000	.20271	2000.04
∞[3]	TI	ST	.212909	0.	4258.17	192.489	146.319	-1000.	1000.	-100.	0.	2000.
9	TI	TR	.212896	.00424	4257.91	192.489	146.319	-999.943	1000.01	-100.000	.20271	2000.04
9	TI	EX	.212603	.00409	4252.06	191.904	146.319	-999.942	1000.01	-100.000	.20370	2000.04

(1) Refers to the polynomial order (p) for w_0. The polynomial order for ϕ_1, and u_x for TI beams, is $\max(1, p-1)$.

(2) CA $\equiv$ curvature approximation.

(3) Computed from analytic solution [98].

The displacement and rotations are defined from a torsion-dominant perspective, with α and β serving as corrections for bending and shear, respectively.

The strain energies for both BE and TI idealizations have converged to six significant digits by $p = 8$. Recall that this same observation was made for the pinched-ring problem. Thus, the similar convergence characteristics for the in-plane and out-of-plane responses confirm:

$$p_1 = p_2 = p_3 = p_4 + 1 \equiv p \text{ for BE/RA beams, and} \tag{9.17a}$$

$$p_1 = p_2 = p_3 = p_4 + 1 = p_5 + 1 = p_6 + 1 \equiv p \text{ for TI beams,} \tag{9.17b}$$

as useful guidelines for the p-extension process for general three-dimensional problems. Generic references to p in the remainder of this text will be based on these guidelines. The optimal relationship between the in-plane and out-of-plane polynomial orders is understood to be problem specific.

The displacement and rotations at the top of the beam converge on the same order as the strain energy. The forces and moments are again slowest to converge, but note that the bottom shear force (F_{Z_B}) is exact for the TI idealization when $p_3 = p_6 + 1 \geq 2$ (actually, the constant shear force is exactly characterized over the entire beam span). This result occurs since the derivative of w_0 only enters the shear energy relation for TI beams (see (9.12b)).

The out-of-plane response is less affected by curvature approximation. This is primarily due to the assumption that I_0 is independent of curvature. Forces and moments are seen to converge to the distributions in (9.9) regardless of the curvature approximation used. Minor changes in the displacements and rotations occur as the effects of:

$$(I_{00})_{EX} \cong (A + I_{yy}/R^2)_{TR} \cong (A)_{ST}, \text{ and} \tag{9.18a}$$

$$(I_{02})_{EX} \cong (I_{zz})_{TR/ST}, \tag{9.18b}$$

are introduced.

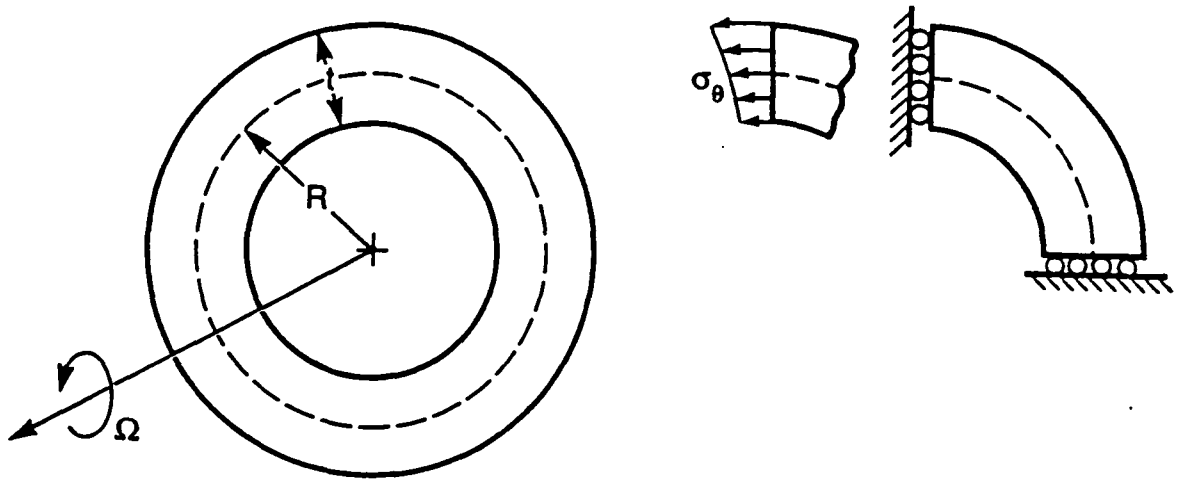

Figure 9.7 Rotating ring sample problem and PVAEB quarter-ring model.

9.2 EFFECT OF CURVATURE APPROXIMATION ON A ROTATING RING

A new and rational hierarchy of curvature approximations for the cross-sectional properties of circular beam elements has been presented in Chapter 5. This section focuses on a classical static problem which allows the effect of these approximations to be quantified. Figure 9.7 illustrates a thin ring rotating in the plane of the ring about its center. The quarter-ring finite element model is also displayed in the figure. This problem is advantageous due to its uniform radial (local y) displacement. Therefore:

1) zero static shear strain isolates the curvature effect from any shear energy assumption,
2) centrifugal load vector terms are entirely translational, thus eliminating the effect of Bernoulli-Euler assumptions, and
3) exact (no discretization error) finite element solutions may be obtained using the two degree-of-freedom PVAEB model detailed in Table 9.9 (adjusted for various t/R).

Table 9.9 PVAEB sample input for the rotating ring.

```
TITLE = ROTATING RING PROBLEM
SUBTITLE = t/R = 0.25
$
BEAM = BE
CIRC = ST  $ NOTE: PROVISIONS FOR 'TR' OR 'EX' APPROXIMATIONS ARE INCLUDED.
ANALYSIS = ST
LOAD = 100
NOSOFT  $ NOTE: CENTRIFUGAL SOFTENING IS EXCLUDED FOR CLASSICAL SOLUTION COMPARISON.
$
SEFORCE = AL
SESTRESS = AL
$
SUBCASE
 BRP = 1,3,3,1
$
BEGINBULK
$
GRID, 1, 1., 0., 0., 23456
GRID, 2, 0., 1., 0., 13456
GRID, 3, 0., 0., 0., 123456  $ NOTE: ORIGIN IS DEFINED FOR RFORCE APPLICATION.
$
CBARC, 1, 1, 1, 2, 1., 0., 0., 1.
CBARI,  1,   2,   4
$
PBARC, 1, 2, .25, .0013020833333, .020833333333, .0043882878621, , , +P1
+P1, 0., 0., 0., 1., .25131442828, .0013144282809, , , +P2
+P2, .020942869023, -.0013144282809, 0., 0., , , , , +P3
+P3, -.125, 0., .125, 0., 0., 0.
$
MAT, 2, 30000000., , .3, 7.35E-4
$
LOAD, 100, 1., 1., 7
RFORCE, 7, 3, 1., 0., 0., 1.
$
ENDDATA
```

Thus, the planar effects of the curvature approximations may be evaluated in terms of the tangential stress, σ_θ, and the integrated axial force, F_z.

The classical two-dimensional plane-stress solution for the rotating ring is:

$$(\sigma_\theta)_{2D} = \rho\Omega^2 \left(\frac{3+\nu}{8}\right)\left[R_i^2 + R_o^2 + \frac{R_i^2 R_o^2}{r^2} - \left(\frac{1+3\nu}{3+\nu}\right) r^2\right], \tag{9.19}$$

where R_i and R_o are the inner and outer radii, respectively, and $R_i \le r \le R_o$. In terms of the finite element variables:

$$y = r - R, \quad -\frac{t}{2} \le y \le \frac{t}{2}. \tag{9.20}$$

The tangential stress may be nondimensionalized such that:

$$(\overline{\sigma}_\theta)_{2D} = \frac{(\sigma_\theta)_{2D}}{\rho\Omega^2 R^2}. \tag{9.21}$$

Comparisons with the finite element solutions are made at the inner, outer, and mean radii, thus:

$$(\overline{\sigma}_\theta)_{2D}\Big|_{R_i} = \left[1 + \left(\frac{1+\nu}{2}\right)\left(\frac{t}{R}\right) + \left(\frac{1}{4}\right)\left(\frac{t}{R}\right)^2\right] = (\overline{\sigma}_\theta)_{\max}, \tag{9.22a}$$

$$(\overline{\sigma}_\theta)_{2D}\Big|_{R_o} = \left[1 - \left(\frac{1+\nu}{2}\right)\left(\frac{t}{R}\right) + \left(\frac{1}{4}\right)\left(\frac{t}{R}\right)^2\right], \text{ and} \tag{9.22b}$$

$$(\overline{\sigma}_\theta)_{2D}\Big|_{R} = \left[1 + \left(\frac{3+\nu}{128}\right)\left(\frac{t}{R}\right)^4\right]. \tag{9.22c}$$

The normalized axial force for the classical solution is merely:

$$(\overline{F}_z)_{2D} = \frac{1}{A}\iint (\overline{\sigma}_\theta)_{2D}\, dydz = \frac{(F_z)_{2D}}{\rho\Omega^2 R^2 t\ell}$$

$$= \left[1 + \left(\frac{1}{12}\right)\left(\frac{t}{R}\right)^2\right]. \tag{9.23}$$

Note that the classical solution does not include centrifugal softening effects and that the radial stress:

$$(\sigma_r)_{2D} = \rho\Omega^2\left(\frac{3+\nu}{8}\right)\left(R_i^2 + R_o^2 - \frac{R_i^2 R_o^2}{r^2} - r^2\right), \tag{9.24}$$

is entirely ignored by the circular beam formulations.

The normalized tangential stress derived from the circular beam formulations for the exact (EX) characterization of curvature is defined by:

$$(\overline{\sigma}_\theta)_{EX,No[K_s]} = \left(\frac{1+\bar{y}_m/R}{1+Z}\right)\left(\frac{R}{R+y}\right), \tag{9.25}$$

where $\bar{y}_m = I_{yy}/AR$ is the curvature-induced shift in the mass center (2.13) and Z is the Winkler-Bach constant (5.3). The rectangular cross section of the ring results in:

$$\bar{y}_m = \frac{t^2}{12R}. \tag{9.26}$$

The truncated series (TR) approximation produces $Z \cong I_{yy}/AR^2 = \bar{y}_m/R$; thus:

$$(\overline{\sigma}_\theta)_{TR,No[K_s]} = \left(\frac{R}{R+y}\right). \tag{9.27}$$

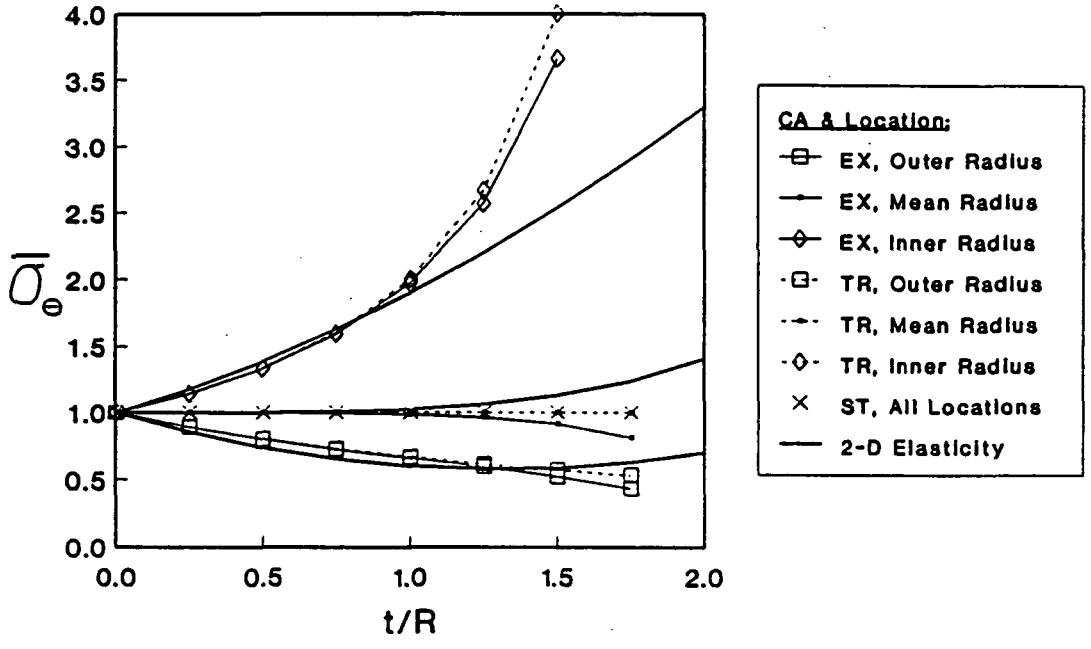

Figure 9.8 Comparison of tangential stresses for the rotating ring.

The straight (ST) curvature approximation assumes $R/(R+y) \cong 1$ and $Z = \bar{y}_m/R \cong 0$, or:

$$(\overline{\sigma}_\theta)_{ST,No[K_s]} = 1. \tag{9.28}$$

Figure 9.8 compares the normalized tangential stresses from the various curvature approximations to those from the classical solution ($\nu = 0.3$) as a function of t/R. The insensitivity to radial variation for the ST approximation severely limits its usefulness in characterizing the stresses. The TR and EX curvature approximations generate quite similar results. Both produce less than twelve percent error for all stresses and less than six percent error in the peak stress for $t/R \leq 1$. Breakdown of the assumptions inherent to the formulation of engineering beams occurs before differences between the TR and EX characterizations become significant. This observation is most useful in light of the relative ease by which the TR approximation is generated.

Comparisons of the normalized axial forces are just as enlightening. The ST approximation produces:

$$(\overline{F}_z)_{ST,No[K_s]} = 1, \tag{9.29}$$

while the TR and EX idealizations both produce:

$$(\overline{F}_z)_{TR,No[K_s]} = (\overline{F}_z)_{EX,No[K_s]} = \left[1 + \left(\frac{1}{12}\right)\left(\frac{t}{R}\right)^2\right]$$
$$= (\overline{F}_z)_{2D}. \tag{9.30}$$

Therefore, the integrated axial force emanating from the circular beam formulation agrees exactly with the classical solution as long as the curvature approximation properly accounts for the shift in the center of mass. The ST approximation induces less than five percent error in axial force for $t/R \leq 0.8$ although errors in the tangential stress may be over fifty percent.

PVAEB includes centrifugal softening effects unless the NOSOFT option is explicitly invoked (see Table 9.9). Thus, the validity of ignoring centrifugal softening may be tested. For the rotating-ring problem, softening effects result in:

$$\overline{\sigma}_\theta = C_{[K_s]}\,(\overline{\sigma}_\theta)_{No[K_s]} \quad \text{and} \tag{9.31a}$$

$$\overline{F}_z = C_{[K_s]}\,(\overline{F}_z)_{No[K_s]}, \tag{9.31b}$$

where:

$$C_{[K_s]} = \left[1 - \frac{\rho\Omega^2 R^2}{E(1+Z)}\right]^{-1}, \tag{9.32}$$

is the centrifugal softening correction factor. Therefore, centrifugal softening may be ignored in the rotating-ring problem only if $(\rho\Omega^2 R^2)/[E(1+Z)] \ll 1$, with Z depending on the chosen approximation for curvature.

9.3 EIGENSOLUTIONS FOR RINGS

The previous sections of this chapter explore the significance of beam type and curvature approximation for a collection of static circular-beam problems. The interrelationship *between* beam type and curvature approximation merits additional investigation, as does their applicability to dynamic problems. As seen in the previous section, the underlying assumptions of the engineering beam formulation must be considered in this study.

These issues may be addressed collectively in the eigenanalysis of circular rings. Numerous theoretical formulations may be gleaned from the literature for comparison, and they are complemented by an impressive assemblage of experimental data. The experimental results of Kuhl [65] are commonly cited and provide a nearly complete characterization of natural frequencies for nonrotating steel circular rings with rectangular ($t \times \ell$) cross-sections. These data will serve as the basis for comparison in this investigation.

Figure 9.9 illustrates a sampling of the ring modes experimentally determined in the Kuhl study. Figure 9.9*a* depicts the zeroth extensional mode, or "breathing" mode. Figures 9.9*b* and 9.9*c* portray the first and second extensional modes, respectively. For thin rings, the extensional natural frequencies may be computed using [100]:

$$(\hat{\omega}_n)_E = \sqrt{n^2+1}\,\sqrt{\frac{EA}{mR^2}}, \quad n = 0, 1, 2, \ldots, \tag{9.33}$$

where the $\hat{}$ denotes the use of thin-ring assumptions and the E subscript designates extensional frequencies. Naturally, formulations utilizing inextensibility assumptions cannot predict the extensional modes. Figure 9.9*d* represents the

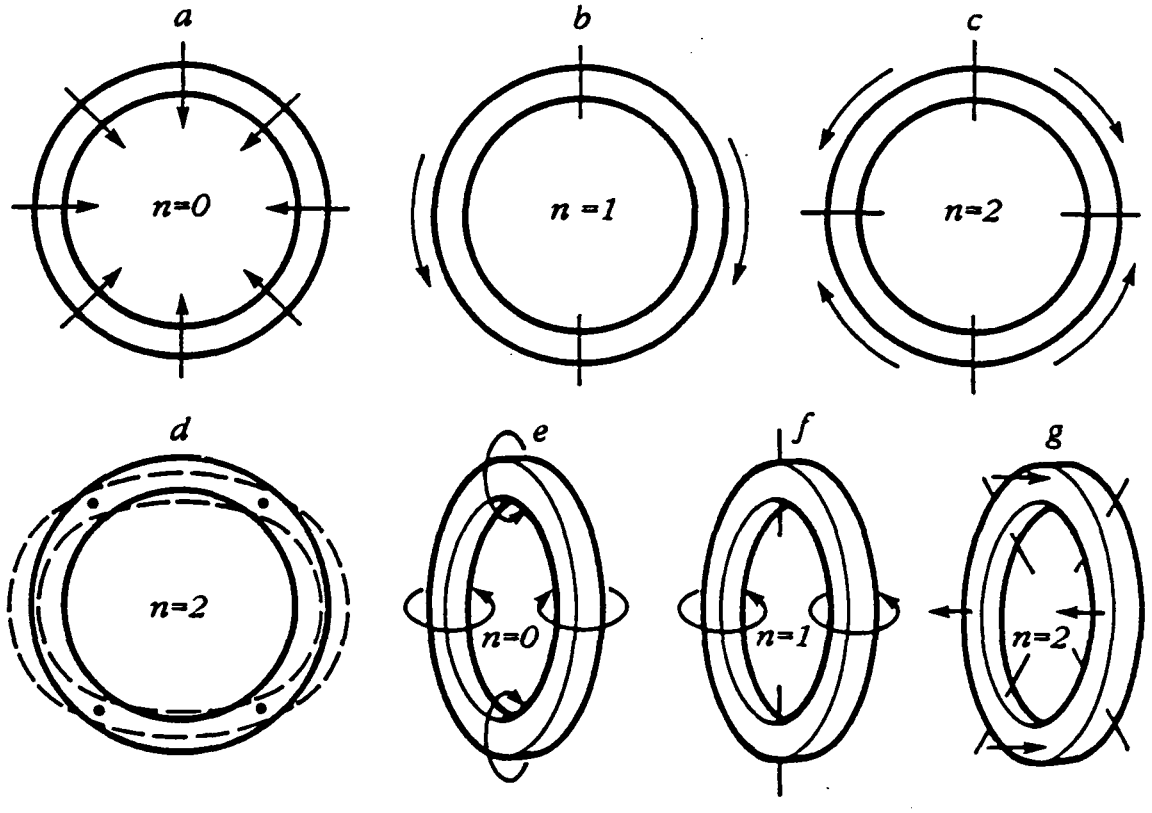

Figure 9.9 Sampling of ring vibrational modes.

second in-plane bending mode. Thin-ring (inextensibility) assumptions result in the in-plane bending frequencies [100]:

$$(\hat{\omega}_n)_{IB} = \frac{n(n^2-1)}{\sqrt{n^2+1}} \sqrt{\frac{EI_{yy}}{mR^4}}, \quad n = 2, 3, 4, \ldots \tag{9.34}$$

Without rotating coordinate system effects, the extensional and in-plane bending frequencies may be extracted from planar PVAEB analyses as discussed in Sections 2.3 and 7.6 (see (7.86)).

Out-of-plane modes include the zeroth and first torsional modes illustrated in Figures 9.9*e* and 9.9*f*, respectively, and the second out-of-plane bending mode

depicted in Figure 9.9*g*. The analytic thin-ring natural frequencies for these modes are [100]:

$$(\hat{\omega}_n)_T = \sqrt{n^2 + \frac{EI_{zz}}{GI_0}} \sqrt{\frac{GI_0}{J_0 R^2}}, \quad n = 0, 1, 2, \ldots, \tag{9.35}$$

and:

$$(\hat{\omega}_n)_{OB} = \frac{n(n^2-1)}{\sqrt{n^2 + \frac{EI_{zz}}{GI_0}}} \sqrt{\frac{EI_{zz}}{mR^4}}, \quad n = 2, 3, 4, \ldots \tag{9.36}$$

The out-of-plane response may be isolated in PVAEB analyses by invoking the conditions in (7.87). Unlike the in-plane motions, where the extensional and bending relations are explicitly independent in the thin-ring limit, the out-of-plane frequencies (except $(\hat{\omega}_0)_T$) involve coupling of the bending stiffness, I_{zz}, and torsional stiffness, I_0.

Comparisons for all frequencies of interest will be presented in nondimensional form with respect to the thin-ring values; that is:

$$\overline{\omega}_n \equiv \frac{\omega_n}{\hat{\omega}_n}. \tag{9.37}$$

In addition, comparisons with the Kuhl data will be stated in terms of frequency error, defined by:

$$e \equiv \frac{(\omega_n)_{\text{Analysis}} - (\omega_n)_{\text{Kuhl}}}{(\omega_n)_{\text{Kuhl}}}. \tag{9.38}$$

Excluding the use of absolute values in this relation allows the sign as well as the magnitude of the frequency error to be quantified.

9.3.1 In-Plane Ring Frequencies

Kuhl's experimental determination of the in-plane frequencies involved two primary sets of rings. The first seven in-plane bending frequencies were extracted for a set of 17 rings of variable thickness (t) while maintaining constant outer

radius (R_o = 45.00 mm), depth (ℓ = 4.0 mm) and material properties ($c \equiv \sqrt{E/\rho}$ = 5145 m/sec, $\nu \cong 0.29$). The zeroth extensional frequency was also experimentally determined for this set of rings. The five lowest extensional frequencies were obtained for a second set of 13 rings of variable thickness with R_o = 57.50 mm, ℓ = 3.0 mm, c = 5180 m/sec, and $\nu \cong 0.29$.

The Kuhl data for the extensional frequencies of the second set of rings may be nondimensionalized in terms of the zeroth extensional frequency, namely:

$$(\tilde{\omega}_n)_E \equiv \frac{(\omega_n)_E}{(\omega_0)_E}. \tag{9.39}$$

Thus, variations in $c \equiv \sqrt{E/\rho}$ may be isolated from those induced by t/R. Furthermore, a sufficiently accurate estimation of the actual extensional frequencies for the first set of rings may be obtained using the zeroth extensional frequencies from the first ring set and t/R-interpolations of the (9.39) ratios from the second ring set.

PVAEB models with provisions for the various idealizations in beam type and curvature approximation are thus established to match properties of the first set of Kuhl rings above. Table 9.10 provides a sample of the four-element PVAEB input. Note the use of the planar restrictions of (7.86). Also note the shift in the stiffness matrix to allow for rigid body motions (i.e., RBM = 100. in the case control, see (7.88-91) and Table 14.1.1). The mean radius (R) and cross-sectional properties must be adjusted for the various thicknesses of the Kuhl rings.

Figure 9.10 illustrates the PVAEB planar frequencies of the various modes as a function of t/R. A TI:EX idealization is used for the frequencies in this figure with $p = 9$. The in-plane bending frequencies all emanate from the origin while the extensional frequencies approach nonzero thin-ring values as $t/R \to 0$. Note the crossing of the zeroth and first extensional frequencies at $t/R \cong 1.25$. Also

Table 9.10 PVAEB sample input for in-plane analyses of the Kuhl rings.

```
TITLE = Kuhl Ring:  Ro=45mm, t/Ro=.6667: t/R=1.0; l=4mm, nu=.29, c=5145m/s.
SUBTITLE = In-plane analysis
$
BEAM = BE  $ Note: Provisions for 'RA' and 'TI' beams are included.
CIRC = ST  $ Note: Provisions for 'TR' and 'EX' approximations are included.
ANALYSIS = RE
NUMEIG = 40
RBM = 100.
SEQ
JACOBI
$
ECHO = CC
ERREST
REPORT
$
SUBCASE
 BRP = 3,3,3,1
 TIP = 3,3,1,1,2,1
SUBCASE
 BRP = 4,4,3,1
 TIP = 4,4,1,1,3,1
SUBCASE
 BRP = 5,5,3,1
 TIP = 5,5,1,1,4,1
SUBCASE
 BRP = 6,6,3,1
 TIP = 6,6,1,1,5,1
SUBCASE
 BRP = 7,7,3,1
 TIP = 7,7,1,1,6,1
SUBCASE
 BRP = 8,8,3,1
 TIP = 8,8,1,1,7,1
SUBCASE
 BRP = 9,9,3,1
 TIP = 9,9,1,1,8,1
 DELOCDISP
$
BEGINBULK
$
$  R = Ro*(1-(t/Ro)/2) (meters).
GRID,   1,  .030,    0.,    0.,  345
GRID,   2,    0.,  .030,    0.,  345
GRID,   3, -.030,    0.,    0.,  345
GRID,   4,    0., -.030,    0.,  345
$
CBARC,  1,   1,   1,   2,   1.,   0.,   0.,  .030
CBARC,  2,   1,   2,   3,  -1.,   0.,   0.,  .030
CBARC,  3,   1,   3,   4,  -1.,   0.,   0.,  .030
CBARC,  4,   1,   4,   1,   1.,   0.,   0.,  .030
CBARI,  1,   4,   10
$
$  t/R = (t/Ro)/(1-(t/Ro)/2).
PBARC, 1, 2, .00012, 9.E-9, 1.6E-10, 5.8624141590E-10, .83333333333, .83333333333, +P1
+P1, 0., 0., 0., .03, .00013183347464, 1.0650127176E-8, , , +P2
+P2, 1.7577796619E-10, -3.5500423921E-7, 0., 0., , , , , +P3
+P3, -.015, 0., .015, 0., 0., -.002, 0., .002
$
$  E(steel) = 2.0E11 N/m**2; rho (kg/m**3) adjusted to match c=sqrt(E/rho).
MAT, 2, 2.0E11, , .29, 7.555430891E3
$
ENDDATA
```

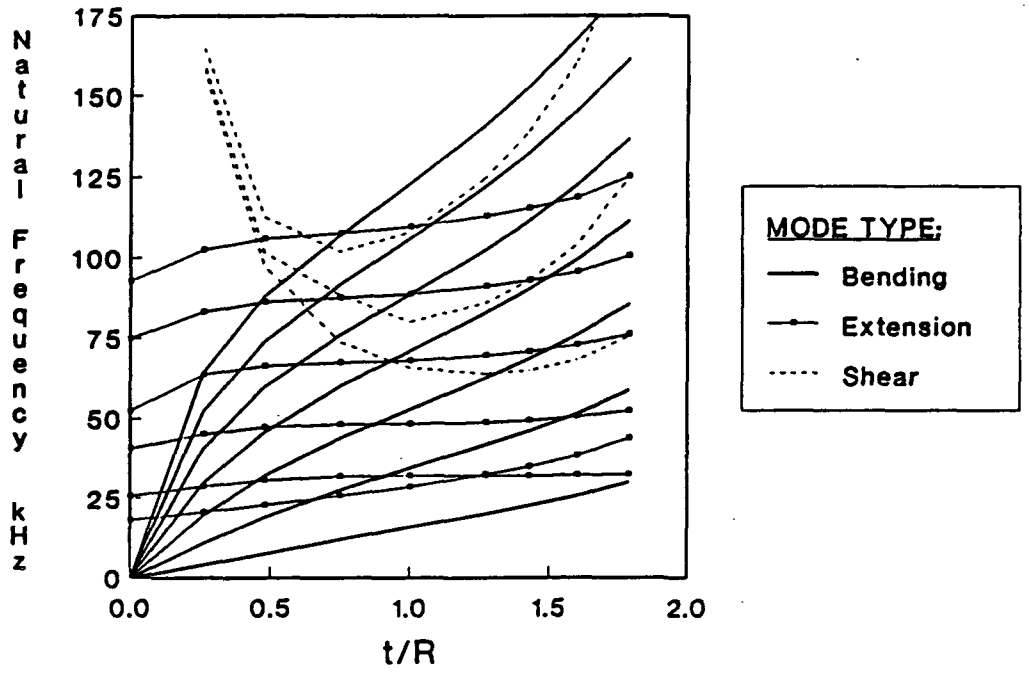

Figure 9.10 Ring in-plane frequencies versus t/R (TI:EX idealization).

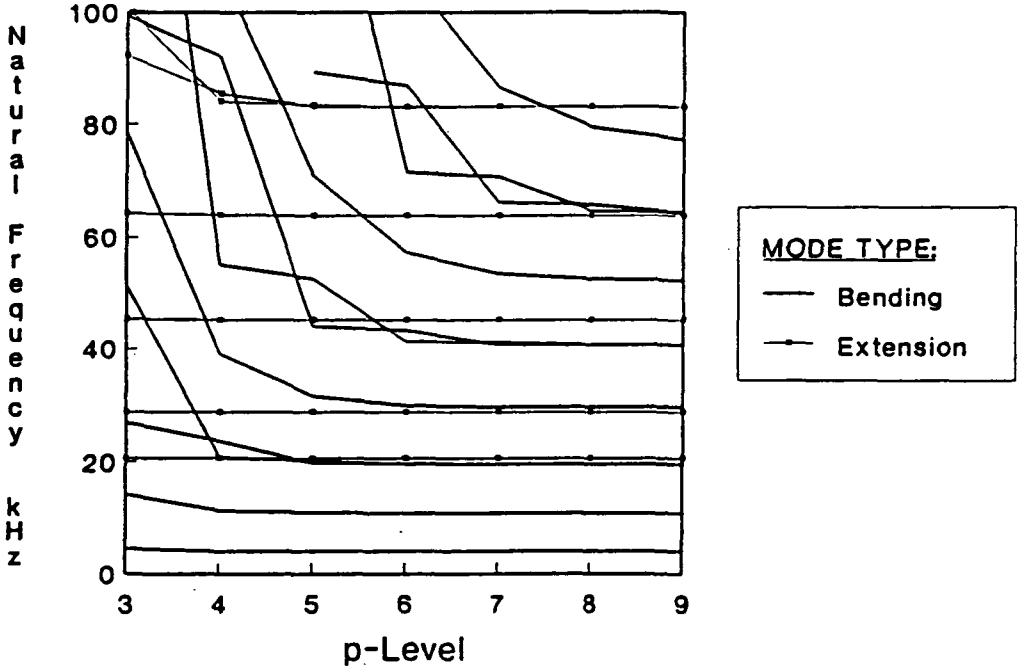

Figure 9.11 Convergence of ring in-plane frequencies for $t/R = 0.261$.

note that shear modes are present *only* in analyses utilizing TI beams. Shear frequencies are infinite in the thin-ring limit and were not quantified in the Kuhl study. Their presence is noted but not explored beyond this point.

Figure 9.11 plots the convergence of the PVAEB planar frequencies as a function of p-level for a TI:EX ring with $t/R = 0.261$. By $p = 9$, the maximum discretization error in the first five extensional and first seven bending frequencies is less than 0.1 percent. This accuracy is only slightly affected by t/R, beam type, or curvature approximation. Except for the zeroth extensional (and shear) mode, all modes shown possess dual eigenvalues. The repeated natural frequencies for $n = 1,3,5,\ldots$ are identical for all p-levels, while those for $n = 2,4,6,\ldots$ exhibit symmetric/antisymmetric biasing but converge to the same value via extension. Recalling the discussion in Section 8.5, it is obvious from this figure that the logic necessary to perform mode tracking for error estimates would be most difficult to develop (see Figure 8.5).

Planar PVAEB analyses produce three rigid body modes which are not represented in the figure. The zero frequency for global Z-rotation is identically characterized by the polynomial-based finite element ring model situated in the global XY-plane. The rigid body motions corresponding to global X- and Y-displacements are only approximately represented. However, the computed natural frequencies for these motions are already reduced to 0.1 Hertz by $p = 6$ for the four-element model.

Comparisons of the second and third in-plane bending frequencies are presented in Figures 9.12 and 9.13, respectively. Coupling of bending, extension, and shear produces departures from the thin-ring values for all idealizations. In particular, note the BE:ST results; the only difference between this characterization and the thin-ring theory is the inclusion of extensional strain energy, and

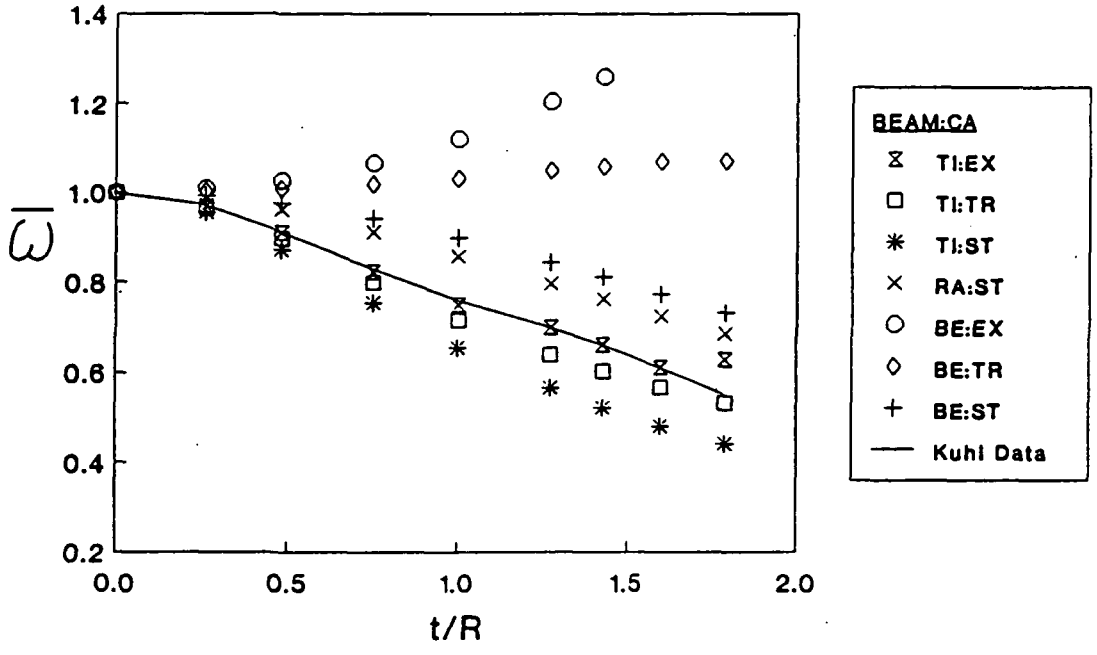

Figure 9.12 Second ring in-plane bending frequency comparison.

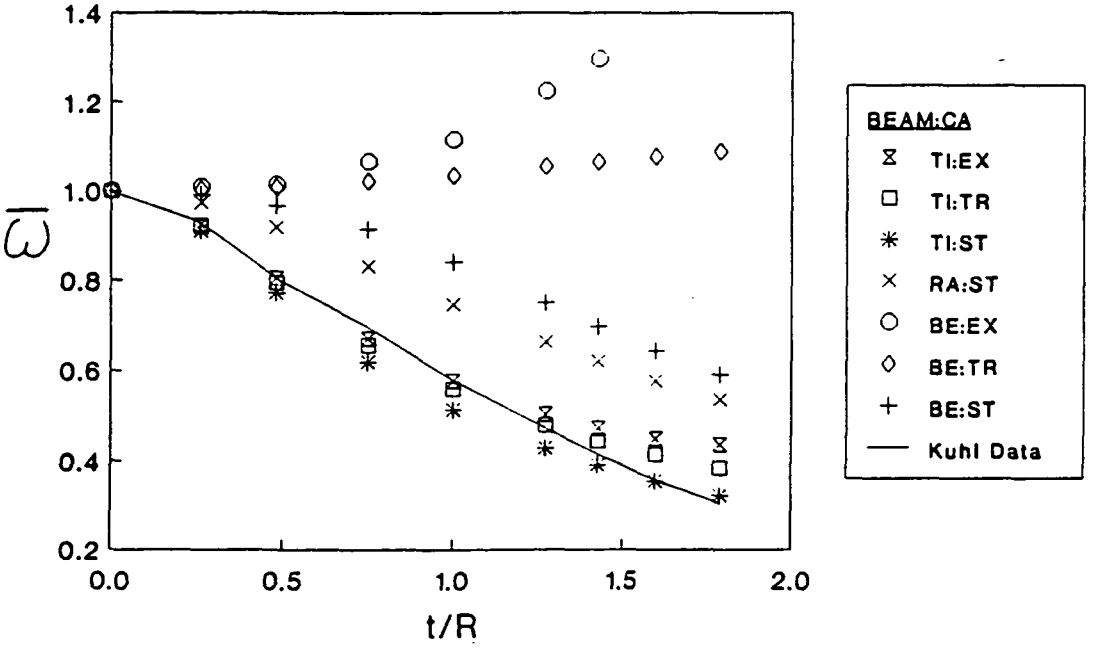

Figure 9.13 Third ring in-plane bending frequency comparison.

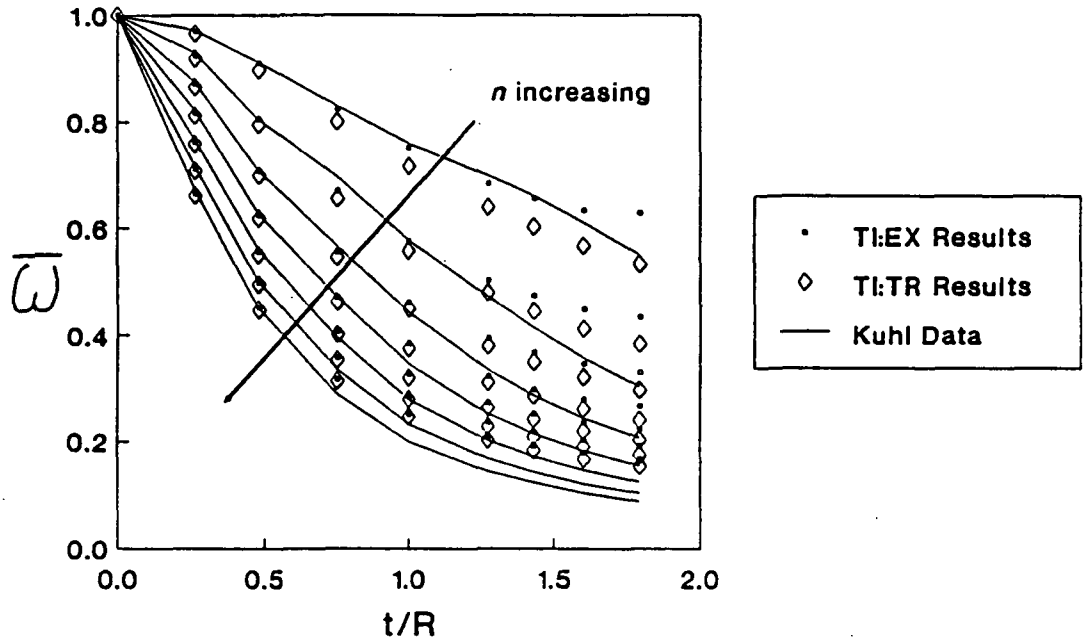

Figure 9.14 Ring in-plane bending frequency comparison.

this improves the analytical accuracy when compared to the Kuhl data. Thus, inextensibility assumptions as discussed in Chapter 5 merely place further restrictions on the applicable range of t/R.

The effect of curvature approximation varies significantly with beam type. Curvature approximation produces the most dramatic and surprising effect on Bernoulli-Euler beams. One might assume that improvements in the characterization of beam properties (I_{ij}'s) would naturally reduce the frequency error. However, the BE beam results prove that this is not necessarily true, and Rayleigh beams exhibit the same trend. TR and EX curvature approximations reduce the in-plane bending frequency error *only* for Timoshenko beams.

Figure 9.14 compares TI:TR and TI:EX results with the Kuhl data for the first seven (n = 2-8) in-plane bending frequencies. Differences between the TR and EX curvature approximations are seen to diminish with increasing mode number.

Breakdown of the engineering beam assumptions occurs as t/R increases and actually makes the TR approximation the more accurate assumption for large t/R.

Tables 9.11 and 9.12 present comparisons of in-plane bending frequency errors for a variety of analyses in the literature and PVAEB. Recall that Gardner and Bert incorporated warping terms into their cross-sectional displacements; their "simplified theory" excludes rotatory inertia effects [36]. Kirkhope's formulations were discussed relative to the present hierarchy of curvature approximations in Chapter 5, with the "inextensible theory" being a simplified version of his "full theory" in [64]. Except for the use of ST shear energy, Kirkhope's full theory is believed to coincide with the TI:TR formulation in PVAEB. Ambati, Bell, and Sharp provide a useful collection of tabulated values based on two-dimensional (plane-stress) elasticity theory [101]. The TI:EX idealization produces the most consistent accuracy for the PVAEB results, particularly in the range where the engineering beam formulation is applicable.

The previously cited investigation by Seidel and Erdelyi [77] merits further discussion. Their comparisons with the Kuhl data suggested a much smaller range of t/R for which engineering beam assumptions are acceptable. However, this conclusion was due to an erroneous nondimensionalization of the Kuhl data, which were originally presented in terms of t/R_o. This same error has propagated to at least one other study [102]; Kirkhope recognized a problem in their comparisons but did not elaborate [64]. The analytical results of Seidel and Erdelyi are consistent with the present findings.

Comparisons for the zeroth extensional frequency in Figure 9.15 exhibit an independence to beam type. This "breathing" motion involves neither shear nor rotational energy terms, much like the rotating ring problem in Section 9.2.

Table 9.11 Comparison of solutions for in-plane bending frequencies of a rectangular steel ring $(t/R = 0.479)$.

	Mode Number						
	2	3	4	5	6	7	8
Kuhl Experimental Frequency (kHz)	7.635	19.06	32.15	46.05	60.40	74.20	88.00
Percent Error:							
Thin Ring Theory [100]:	10.	24.	41.	59.	78.	100.	122.
Gardner and Bert [36]:							
Simplified Theory	-3.8	-2.3	-1.3	-1.0	-1.2	-0.6	-0.3
Full Theory	-3.6	-3.2	-3.0	-3.1	-3.3	-2.7	-2.2
Kirkhope [63,64]:							
Very Simple Theory	-1.4	0.3	1.2	1.2	0.8	1.1	1.3
Inextensible Theory	-0.2	-0.1	-0.4	-0.9	-1.5	-1.1	-0.8
Full Theory	-0.5	-0.4	-0.6	-1.0	-1.6	-1.1	-0.9
Ambati, et al. [101]:							
Elasticity Theory	1.7	0.5	0.1	-1.0	-	-	-
Watson:							
BE:ST	7.0	20.	35.	51.	66.	79.	-
TI:TR	-1.7	-1.3	-1.2	-1.3	-1.7	-1.1	-0.7
TI:EX	-0.3	-0.1	-0.2	-0.5	-1.0	-0.5	-0.1

Table 9.12 Comparison of solutions for in-plane bending frequencies of a rectangular steel ring ($t/R = 0.750$).

	Mode Number						
	2	3	4	5	6	7	8
Kuhl Experimental Frequency (kHz)	12.07	28.65	44.75	60.20	73.90	86.30	97.95
Percent Error:							
Thin Ring Theory [100]:	20.	44.	76.	112.	153.	198.	246.
Gardner and Bert [36]:							
Simplified Theory	-7.7	-8.9	-6.3	-4.0	-0.6	3.1	6.4
Full Theory	-6.7	-8.8	-6.6	-4.4	-1.0	2.7	6.0
Kirkhope [63,64]:							
Very Simple Theory	-4.2	-5.5	-3.3	-1.6	1.5	4.7	7.8
Inextensible Theory	-1.4	-4.7	-3.5	-2.1	0.8	4.1	7.2
Full Theory	-1.8	-5.1	-3.8	-2.2	0.7	4.0	7.1
Ambati, et al. [101]:							
Elasticity Theory	0.9	-3.0	-3.3	-3.8	-	-	-
Watson:							
BE:ST	13.	31.	54.	72.	84.	92.	-
TI:TR	-3.7	-5.9	-3.9	-1.8	1.5	5.2	8.2
TI:EX	-0.9	-3.8	-2.2	-0.4	2.7	6.2	9.2

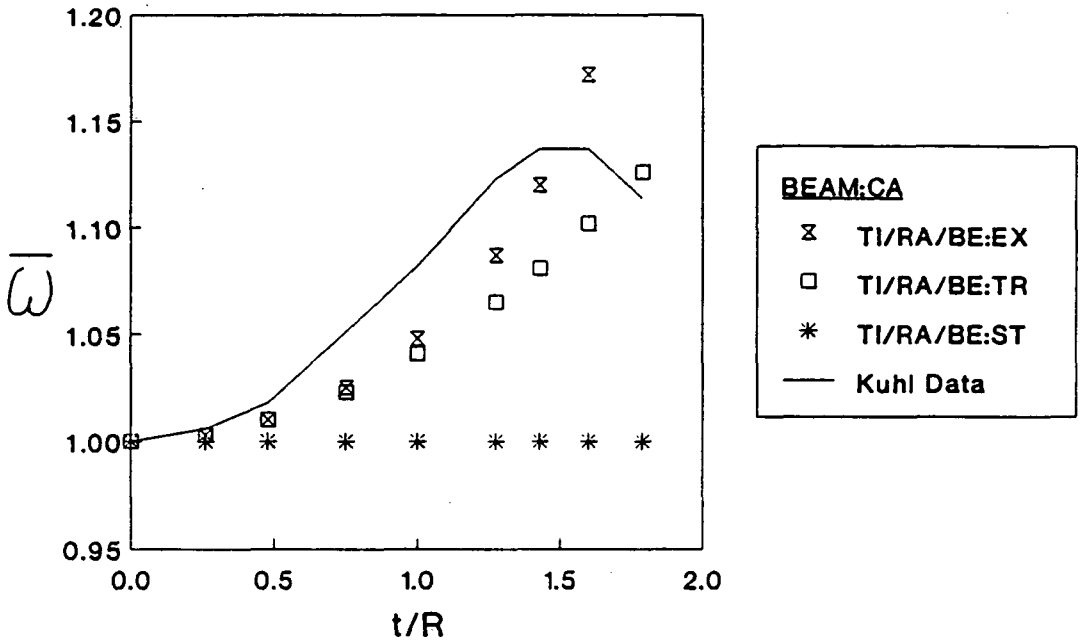

Figure 9.15 Zeroth ring extensional frequency comparison.

Changes in the predicted frequency depend entirely on the characterization of I_{00}, with $\bar{y}_m$ having no effect. The ST curvature approximation is seen to coincide exactly with the thin-ring theory. The TR and EX approximations improve the frequency prediction, produce similar results for low t/R, and differ significantly only in the region ($t/R > 1$) where breakdown of the engineering beam assumptions occurs for the rotating ring in Section 9.2.

Figures 9.16 and 9.17 display frequency comparisons for the first and second extensional modes, respectively. Again, beam type induces changes in the predicted values due to the coupling of extension, bending, and shear. These changes are dominated by the inclusion of rotational kinetic energy (compare RA:ST and BE:ST results) rather than the inclusion of shear strain energy (compare TI:ST and RA:ST results). Note from Figures 9.12-13 that the effect of the no-shear assumption is more significant for the predicted in-plane bending frequencies.

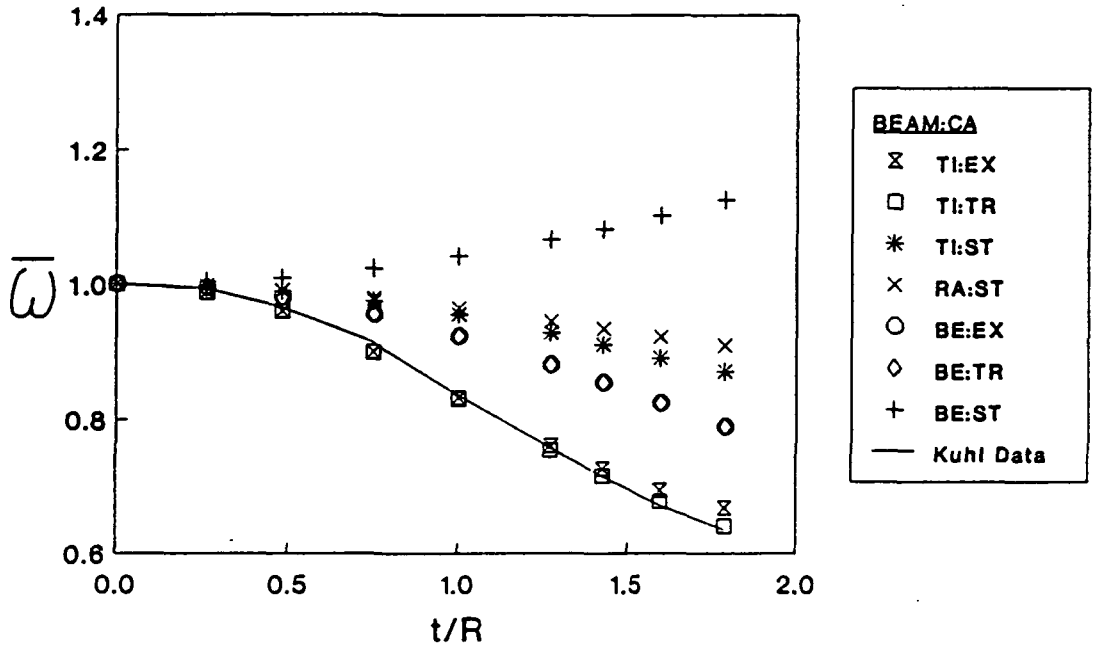

Figure 9.16 First ring extensional frequency comparison.

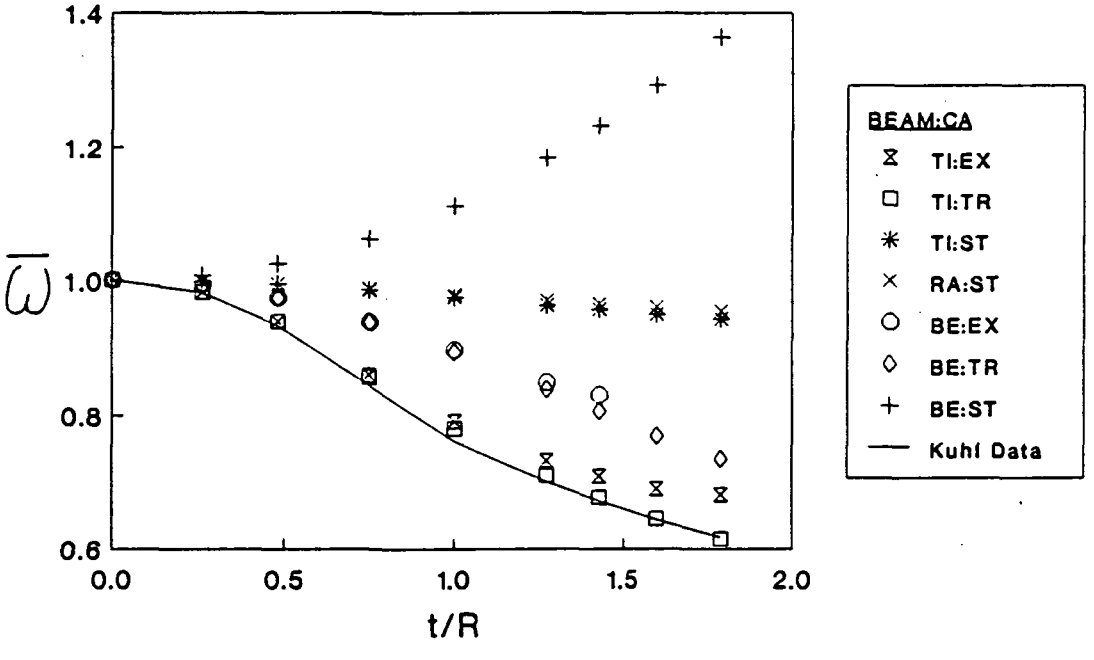

Figure 9.17 Second ring extensional frequency comparison.

Table 9.13 Comparison of solutions for extensional frequencies of a rectangular steel ring.

	Mode Number				
	0	1	2	3	4
$t/R = 0.479$: Kuhl Experimental Frequency (kHz)	22.95	30.80*	47.05*	65.50*	83.91*
Percent Error:					
Thin Ring Theory [100]:	-1.7	3.6	7.2	8.9	11.
Ambati, et al. [101]:					
Elasticity Theory	0.4	0.5	0.1	-0.2	-
Watson:					
BE:ST	-1.7	4.5	9.9	13.	16.
TI:TR	-0.8	-0.6	0.6	1.4	2.5
TI:EX	-0.7	-0.6	0.7	1.4	2.6
$t/R = 0.750$: Kuhl Experimental Frequency (kHz)	26.30	32.35*	47.29*	64.80*	82.32*
Percent Error:					
Thin Ring Theory [100]:	-4.9	9.4	18.	22.	25.
Ambati, et al. [101]:					
Elasticity Theory	0.0	-0.2	-0.4	-0.5	-
Watson:					
BE:ST	-4.9	12.	26.	34.	43.
TI:TR	-2.7	-1.6	1.4	3.3	5.2
TI:EX	-2.5	-1.5	1.8	3.9	6.0

* Obtained via three-point Lagrangian interpolation using data from rings with different t/R's.

The effects of curvature approximation on the extensional modes also differ from those exhibited by the bending modes. The BE:ST idealization is seen to produce even less accurate frequency predictions than the thin-ring theory ($\bar{\omega} \equiv 1$). TR and EX approximations reduce the frequency error for all beam types. The TR curvature approximation is typically more accurate for the high range of t/R. Table 9.13 provides additional comparisons of frequency error for the extensional frequencies (these were not reported by either Gardner and Bert or Kirkhope).

9.3.2 Out-of-Plane Ring Frequencies

A third set of 11 rings was used by Kuhl to experimentally determine the out-of-plane ring response. Again, the thickness was varied while maintaining $R_o = 45.00$ mm constant. The ring cross sections were square ($\ell = t$) and the ring material properties were $c = 5170$ m/sec and $\nu \cong 0.29$. Experimental data exist for the first seven out-of-plane bending frequencies and the first six torsional frequencies, but are limited to $t/R \leq 1.130$.

A significant concern in the PVAEB formulations was the relative benefit of curvature approximation on the out-of-plane response. Recall from Chapter 5 that the torsional constant is assumed independent of curvature (that is, the ST approximation is *always* used in defining I_0) to be consistent with the assumptions for the axial rotation, ϕ_1. However, the curvature-dependent moments of area, I_{ij}, and the curvature-induced shift in the center of mass, $\bar{y}_m$, are retained. A sample of the four-element PVAEB models used in this out-of-plane study is detailed in Table 9.14.

Table 9.14 PVAEB sample input for out-of-plane analyses of the Kuhl rings.

```
TITLE = Kuhl Ring:  Ro = 45mm, t/Ro=.6667: t/R=1.0; l=t, nu=.29, c=5170m/s.
SUBTITLE = Out-of-plane analysis
$
BEAM = BE  $ Note: Provisions for 'RA' and 'TI' beams are included.
CIRC = ST  $ Note: Provisions for 'TR' and 'EX' approximations are included.
ANALYSIS = RE
NUMEIG = 40
RBM = 100.
SEQ
JACOBI
$
ECHO = CC
ERREST
REPORT
$
SUBCASE
 BRP = 1,3,3,2
 TIP = 1,1,3,2,1,2
SUBCASE
 BRP = 1,3,4,3
 TIP = 1,1,4,3,1,3
SUBCASE
 BRP = 1,3,5,4
 TIP = 1,1,5,4,1,4
SUBCASE
 BRP = 1,3,6,5
 TIP = 1,1,6,5,1,5
SUBCASE
 BRP = 1,3,7,6
 TIP = 1,1,7,6,1,6
SUBCASE
 BRP = 1,3,8,7
 TIP = 1,1,8,7,1,7
SUBCASE
 BRP = 1,3,9,8
 TIP = 1,1,9,8,1,8
 DELOCDISP
$
BEGINBULK
$
$  R = Ro*(1-(t/Ro)/2) (meters).
GRID,    1,  .030,    0.,    0.,  126
GRID,    2,    0.,  .030,    0.,  126
GRID,    3, -.030,    0.,    0.,  126
GRID,    4,    0., -.030,    0.,  126
$
CBARC,  1,   1,   1,   2,   1.,   0.,   0.,  .030
CBARC,  2,   1,   2,   3,  -1.,   0.,   0.,  .030
CBARC,  3,   1,   3,   4,  -1.,   0.,   0.,  .030
CBARC,  4,   1,   4,   1,   1.,   0.,   0.,  .030
CBARI,  1,   4,   10
$
$  t/R = (t/Ro)/(1-(t/Ro)/2).
PBARC, 1, 2, .0009, 6.75E-8, 6.75E-08, 1.139E-7, .83333333333, .83333333333, +P1
+P1, 0., 0., 0., .03, .00098875105980, 7.9875953821E-8, , , +P2
+P2, 7.4156329485E-8, -2.6625317940E-06 , 0., 0., , , , , +P3
+P3, -.015, 0., .015, 0., 0., -.015, 0., .015
$
$  E(steel) = 2.0E11 N/m**2; rho (kg/m**3) adjusted to match c=sqrt(E/rho).
MAT, 2, 2.0E11, , .29, 7.482537628E3
$
ENDDATA
```

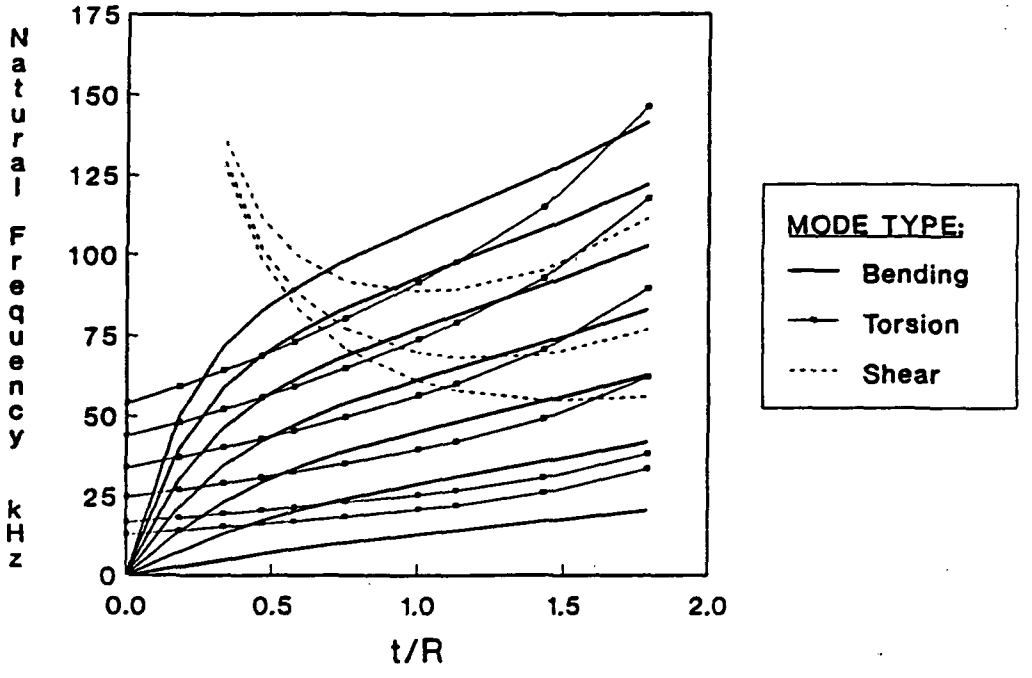

Figure 9.18 Ring out-of-plane frequencies versus t/R (TI:EX idealization).

Figure 9.18 illustrates the out-of-plane frequencies for the TI:EX idealization as a function of t/R. Note the similarities with the in-plane response:

1) bending frequencies emanate from the origin while torsional frequencies approach nonzero thin-ring values as $t/R \to 0$ (however, the zeroth and first torsional frequencies do not cross as do their extensional counterparts);
2) the presence of Timoshenko shear modes is again noted though not explored;
3) all modes with mode number, n, greater than zero have repeated roots, with even modes ($n = 2, 4, 6, \ldots$) possessing symmetric/antisymmetric biasing; and
4) rigid body motion corresponding to global Z-displacement is identically characterized at any p-level, while rigid body rotations about the global X- and Y-axes are only satisfied as $p \to \infty$ (but by $p = 6$, the computed frequencies are 0.8 Hertz).

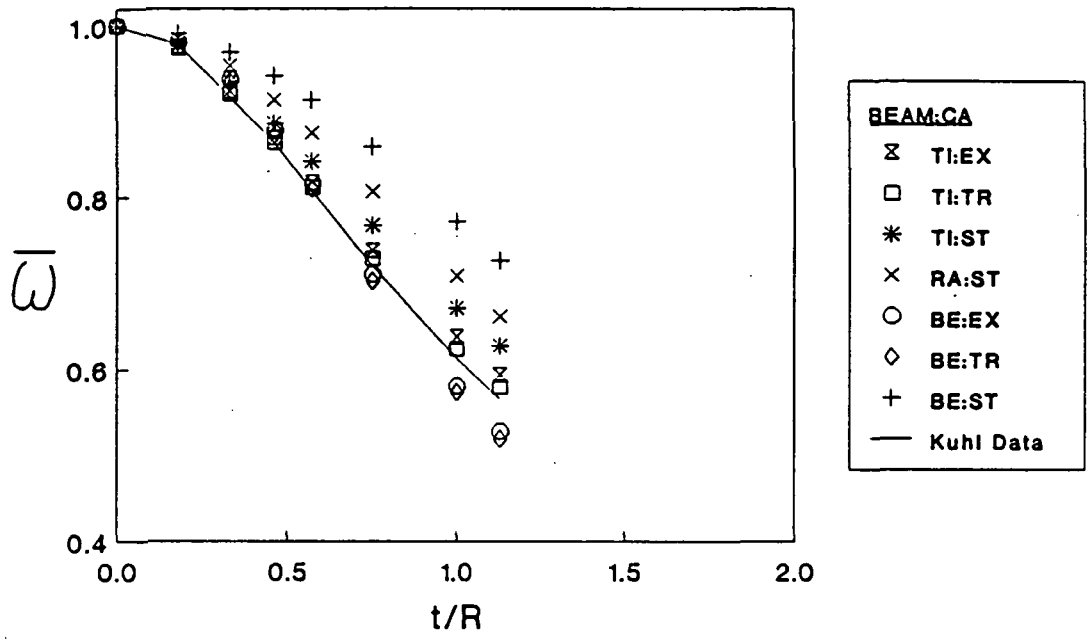

Figure 9.19 Second ring out-of-plane bending frequency comparison.

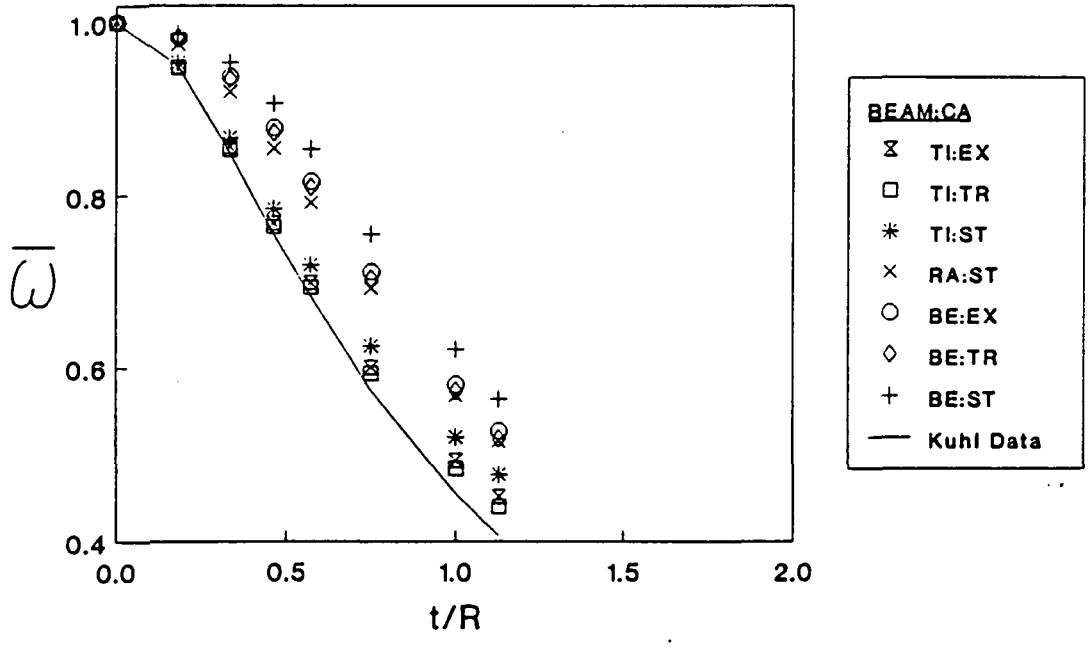

Figure 9.20 Third ring out-of-plane bending frequency comparison.

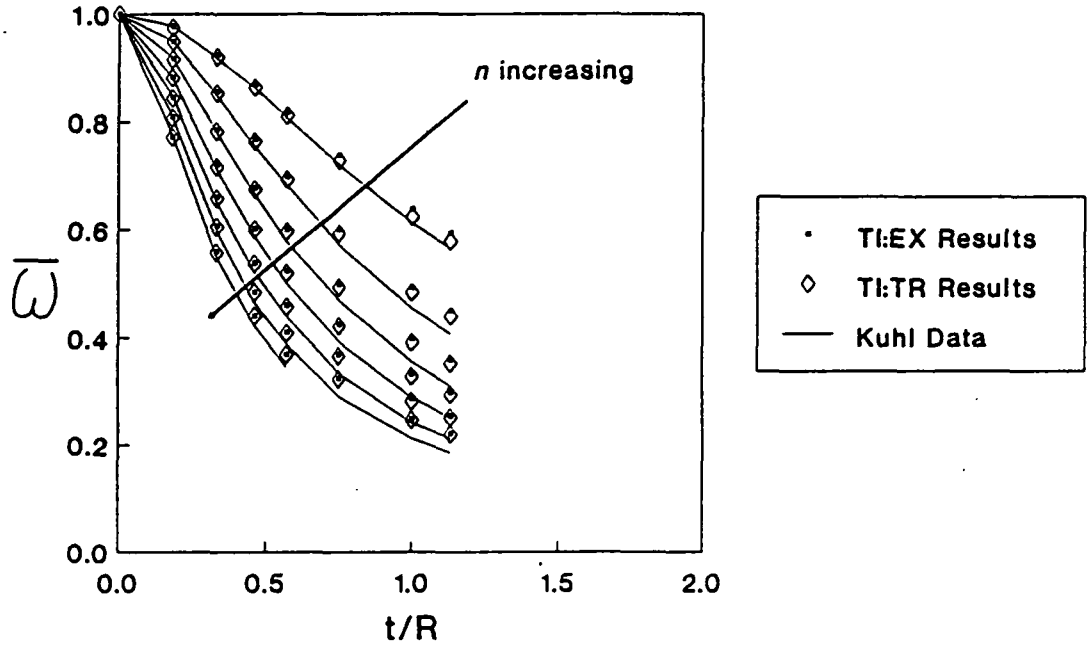

Figure 9.21 Ring out-of-plane bending frequency comparison.

Along with improvements in computational efficiency, another benefit of separating the in-plane and out-of-plane responses (when possible) is the simplification in data management. Visualizing Figures 9.10 and 9.18 combined into a single plot illustrates this point.

Figures 9.19 and 9.20 display frequency comparisons for the first and second out-of-plane bending modes, respectively. Inclusion of rotational kinetic energy and shear strain energy improves the frequency prediction by roughly the same amount (compare BE:ST, RA:ST, and TI:ST results). The effect of utilizing non-ST curvature approximations is vastly different for the two modes when Bernoulli-Euler (and Rayleigh) beams are used, further reducing the credibility of these combinations. As seen in Figure 9.21, the difference between the TR and EX approximations again diminishes with increasing mode number for TI

Table 9.15 Comparison of solutions for out-of-plane bending frequencies of a rectangular steel ring $(\ell = t)$.

	Mode Number						
	2	3	4	5	6	7	8
$t/R = 0.181$: Kuhl Experimental Frequency (kHz)	2.605	7.330	13.75	21.45	30.40	40.05	50.45
Percent Error:							
Thin Ring Theory [100]:	2.2	5.3	8.8	13.	18.	23.	29.
Kirkhope [66]:	0.1	0.4	0.2	0.5	-0.1	-0.1	-0.3
Watson:							
BE:ST	1.3	3.9	7.1	11.	15.	20.	25.
TI:ST	0.1	0.4	0.2	0.5	-0.1	0.0	-0.1
TI:TR	-0.4	-0.2	-0.4	-0.1	-0.7	-0.6	-0.7
TI:EX	-0.3	-0.1	-0.2	0.0	-0.6	-0.5	-0.7
$t/R = 0.462$: Kuhl Experimental Frequency (kHz)	6.620	16.79	28.70	41.20	53.95	66.10	79.20
Percent Error:							
Thin Ring Theory [100]:	16.	32.	50.	70.	91.	115.	136.
Kirkhope [66]:	2.5	3.8	4.0	4.7	5.2	6.8	6.6
Watson:							
BE:ST	9.0	20.	29.	33.	32.	30.	24.
TI:ST	2.6	3.8	4.0	4.7	5.2	6.9	6.8
TI:TR	-0.1	1.0	1.2	1.8	2.3	3.8	3.7
TI:EX	0.5	1.5	1.7	2.2	2.7	4.1	3.9

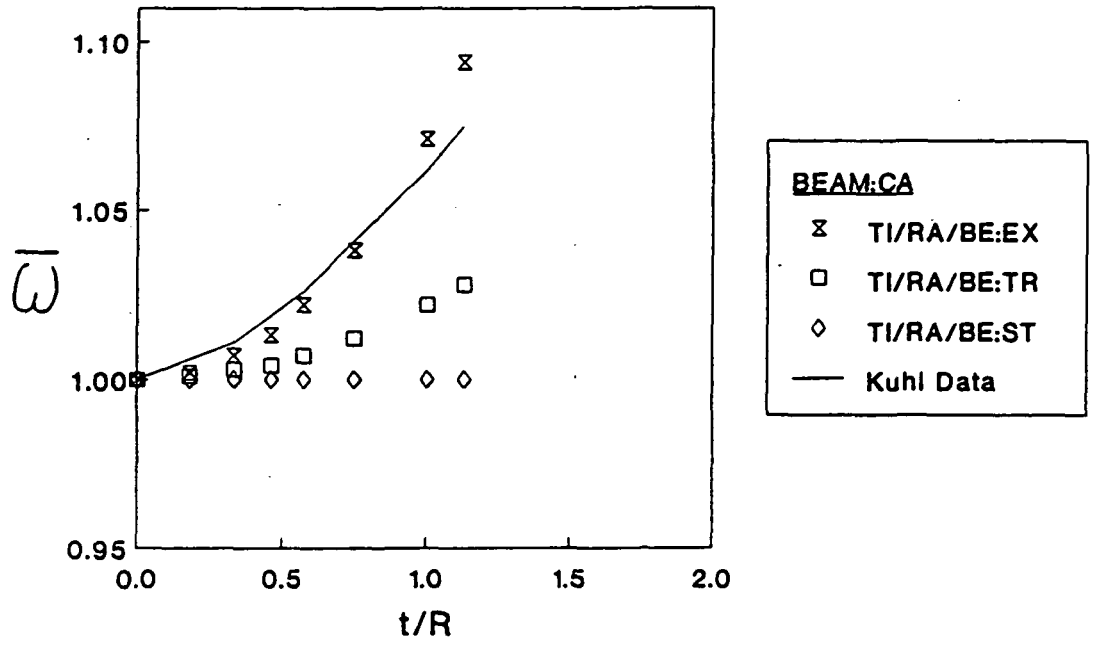

Figure 9.22 Zeroth ring torsional frequency comparison.

beams. The TR simplification generally correlates better with the Kuhl data over the full range of t/R, however.

Table 9.15 presents frequency error comparisons for the out-of-plane bending frequencies of two Kuhl rings. Kirkhope's values were generated from his TI:ST formulation and agree well with the equivalent PVAEB results. It is doubtful that he used $c = 5141$ m/sec as stated in his report [65]; this value differs from Kuhl's by -0.6 percent. Also, Kirkhope erroneously labeled his results with higher values of t/R, thus overstating the applicability of his theory to "thick" rings.

The zeroth torsional mode is similar to the zeroth extensional mode in its independence to beam type. Figure 9.22 compares the predicted and experimental frequencies for the mode. This is the only mode where the utilization of exact $I_{i,j}$'s produces a significant improvement over the truncated series approximation. The TR approximation still improves the accuracy of the frequency prediction in

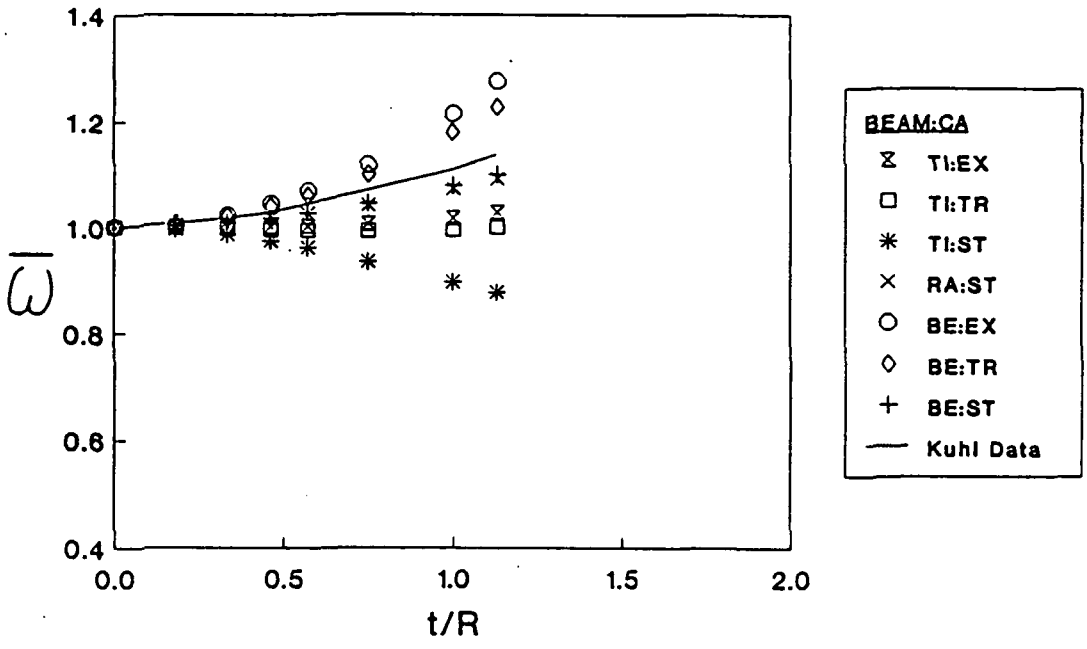

Figure 9.23 First ring torsional frequency comparison.

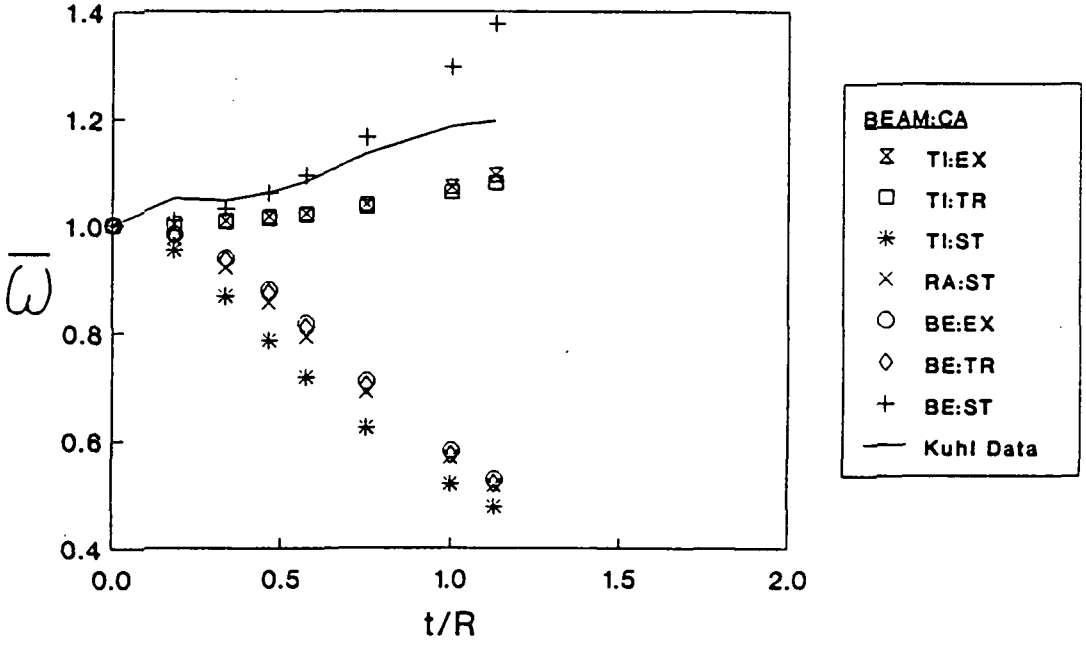

Figure 9.24 Second ring torsional frequency comparison.

Table 9.16 Comparison of solutions for torsional frequencies of a rectangular steel ring $(\ell = t)$.

	Mode Number					
	0	1	2	3	4	5
$t/R = 0.181$: Kuhl Experimental Frequency (kHz)	14.18	18.28	28.20	37.75	48.85	60.15
Percent Error:						
Thin Ring Theory [100]:	-0.6	-0.8	-4.9	-1.9	-2.2	-2.3
Kirkhope [66]:	-	-	-5.3	-2.2	-2.4	-2.5
Watson:						
BE:ST	-0.6	-0.5	-4.0	-0.6	-0.6	-0.5
TI:ST	-0.6	-1.2	-5.2	-2.1	-2.3	-2.4
TI:TR	-0.5	-0.8	-4.7	-1.5	-1.7	-1.7
TI:EX	-0.4	-0.8	-4.6	-1.5	-1.7	-1.7
$t/R = 0.462$: Kuhl Experimental Frequency (kHz)	16.22	21.05	32.15	45.00	58.65	72.25
Percent Error:						
Thin Ring Theory [100]:	-1.8	-2.8	-5.8	-7.1	-8.0	-8.2
Kirkhope [66]:	-	-	-7.8	-8.4	-8.9	-8.8
Watson:						
BE:ST	-1.8	-1.0	-0.1	2.4	7.1	17.
TI:ST	-1.9	-5.3	-7.8	-8.3	-8.8	-8.7
TI:TR	-1.4	-3.1	-4.6	-4.8	-5.2	-5.0
TI:EX	-0.6	-2.7	-4.4	-4.7	-5.1	-4.9

comparison with (thin-ring) ST values in spite of the ST-approximated torsional constant.

Figures 9.23 and 9.24 display frequency comparisons for the first and second torsional modes, respectively. The BE:ST predictions are quite good for these modes and much more accurate than the TI:ST values. Use of the TR and EX approximations are again seen to be detrimental in conjunction with BE beams but are necessary for reasonable TI beam predictions. Figure 9.24 shows an apparent discrepancy in the Kuhl data for the second torsional frequency at $t/R = 0.181$. This may also be seen in the frequency error summary in Table 9.16. Again, the (mislabeled) Kirkhope results in this table are virtually identical to the TI:ST values from PVAEB.

9.3.3 Appraisal of Engineering Beam Formulations for Ring Eigenproblems

The collection of PVAEB analyses in this section and their comparison with the Kuhl experimental data allow a definitive assessment of their applicability. Bernoulli-Euler and Rayleigh beam idealizations are appropriate for only the lowest frequencies of thin rings ($t/R \to 0$). The use of TR and EX curvature approximations with BE/RA beams is discouraged. TI:TR and TI:EX idealizations nearly always reduce the frequency error for $t/R < 1$ in comparison with TI:ST results.

Frequency errors (9.38) for TI:TR and TI:EX formulations are plotted for the in-plane bending, extensional, out-of-plane bending, and torsional modes in Figures 9.25-32. The TR and EX results for each mode type are grouped for ease of comparison. The general trend is that the TI:EX idealization is slightly more accurate for low t/R but becomes more erroneous when coupled with the breakdown of engineering beam assumptions. For all practical purposes, TI:TR

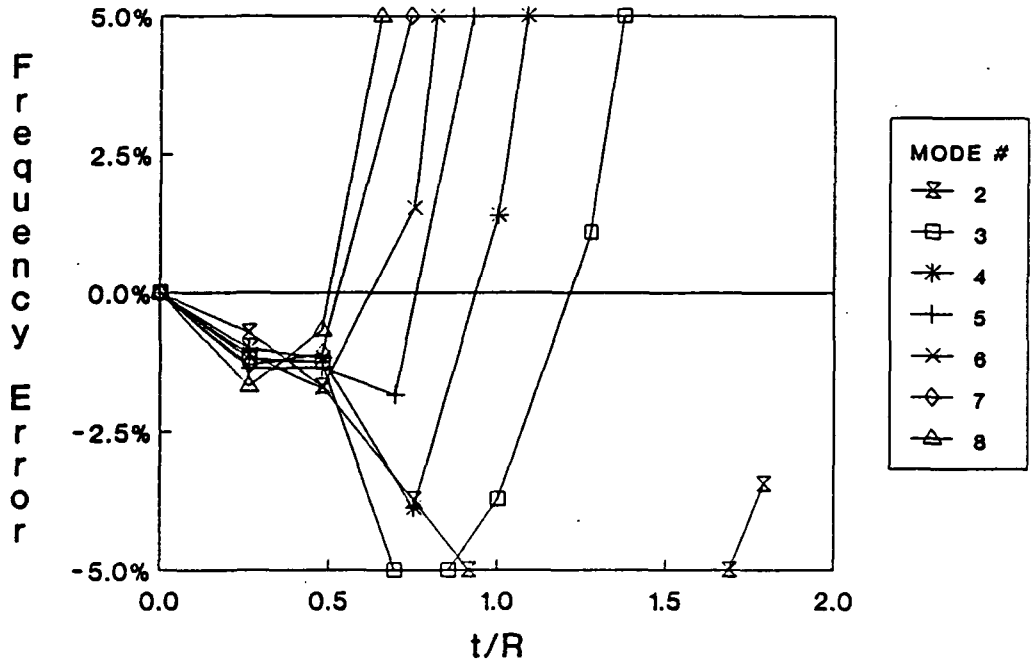

Figure 9.25 TI:TR ring in-plane bending frequency errors.

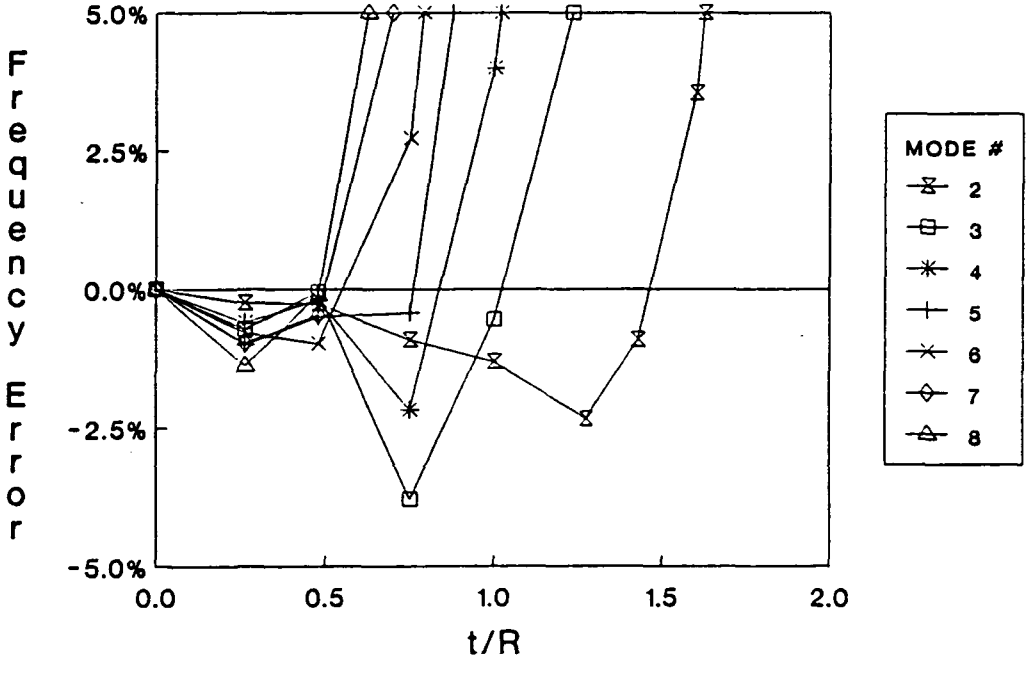

Figure 9.26 TI:EX ring in-plane bending frequency errors.

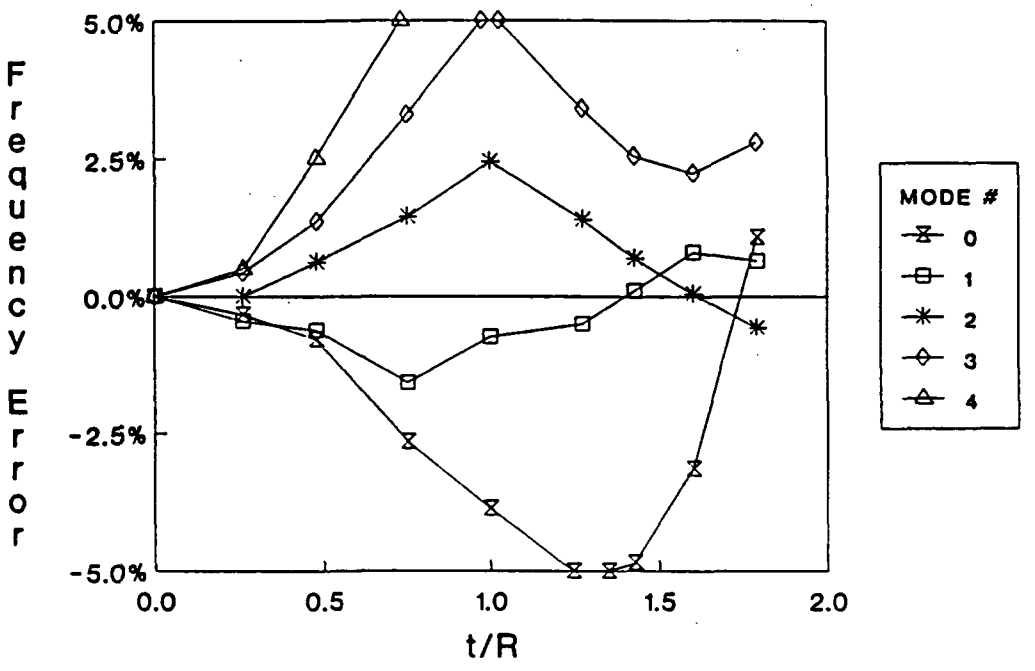

Figure 9.27 TI:TR ring extensional frequency errors.

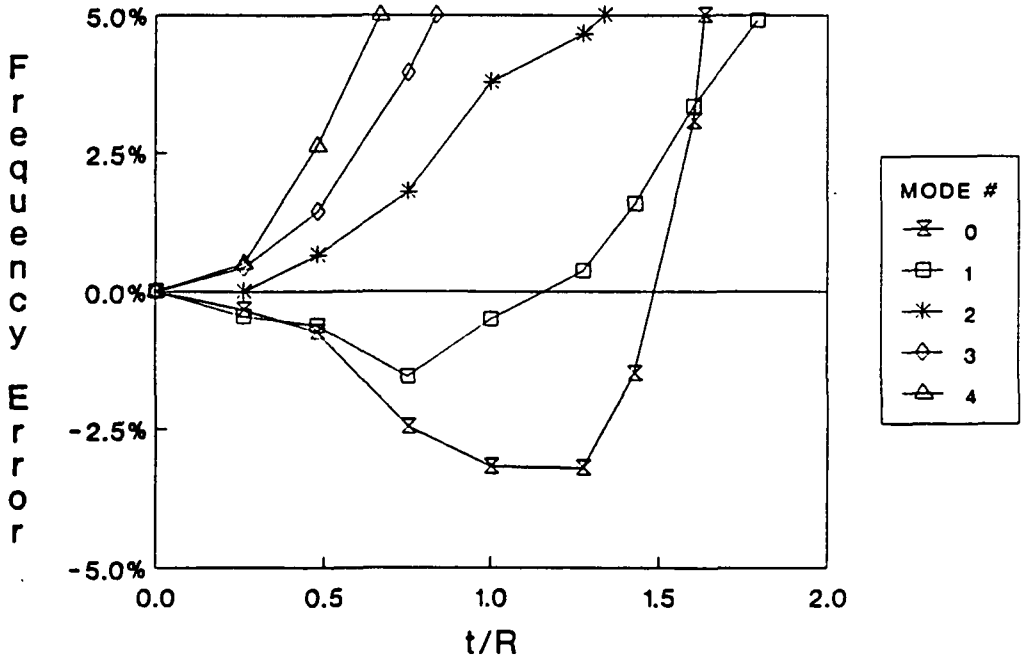

Figure 9.28 TI:EX ring extensional frequency errors.

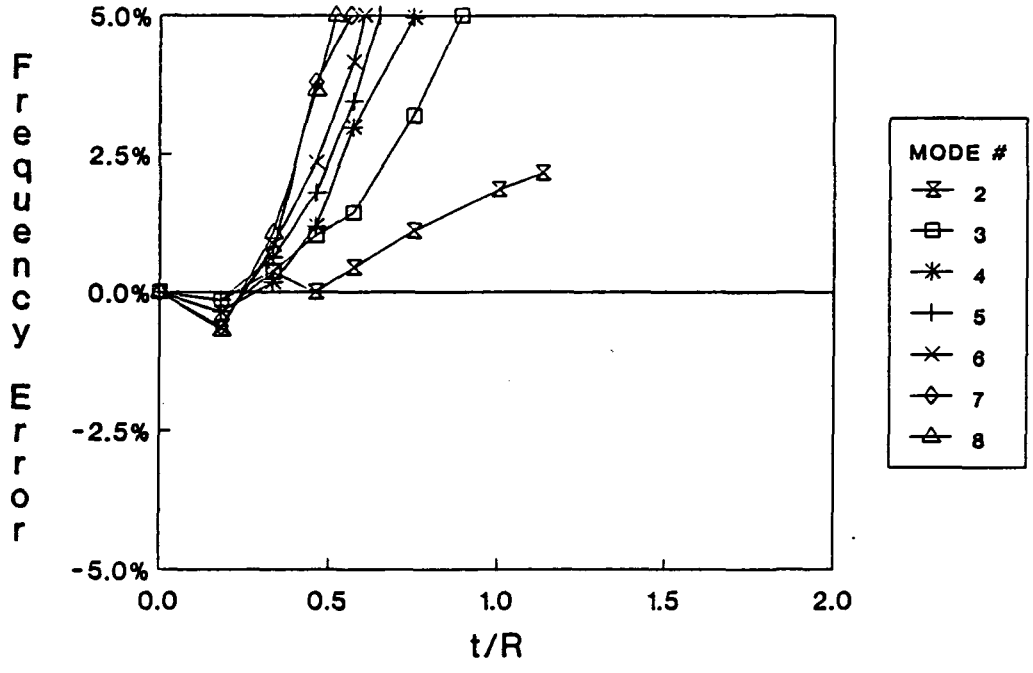

Figure 9.29 TI:TR ring out-of-plane bending frequency errors.

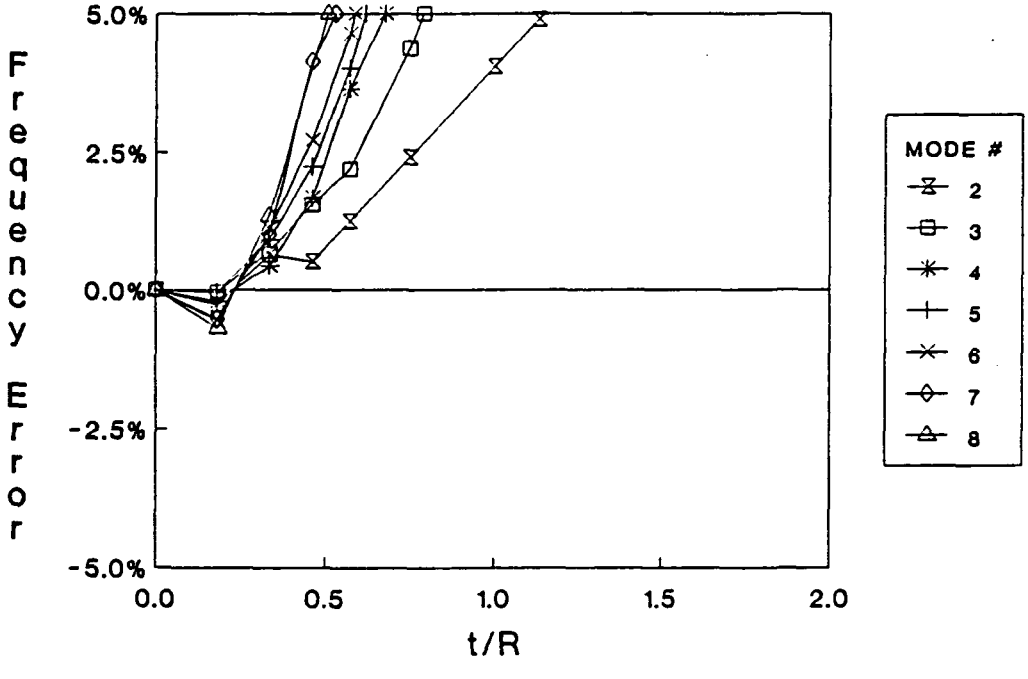

Figure 9.30 TI:EX ring out-of-plane bending frequency errors.

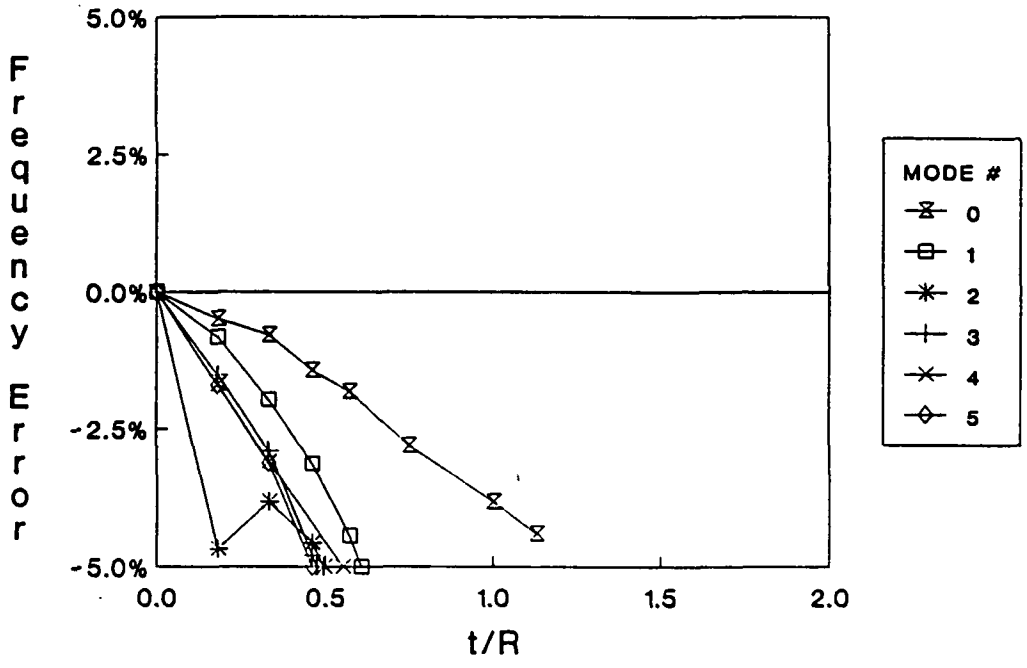

Figure 9.31 TI:TR ring torsional frequency errors.

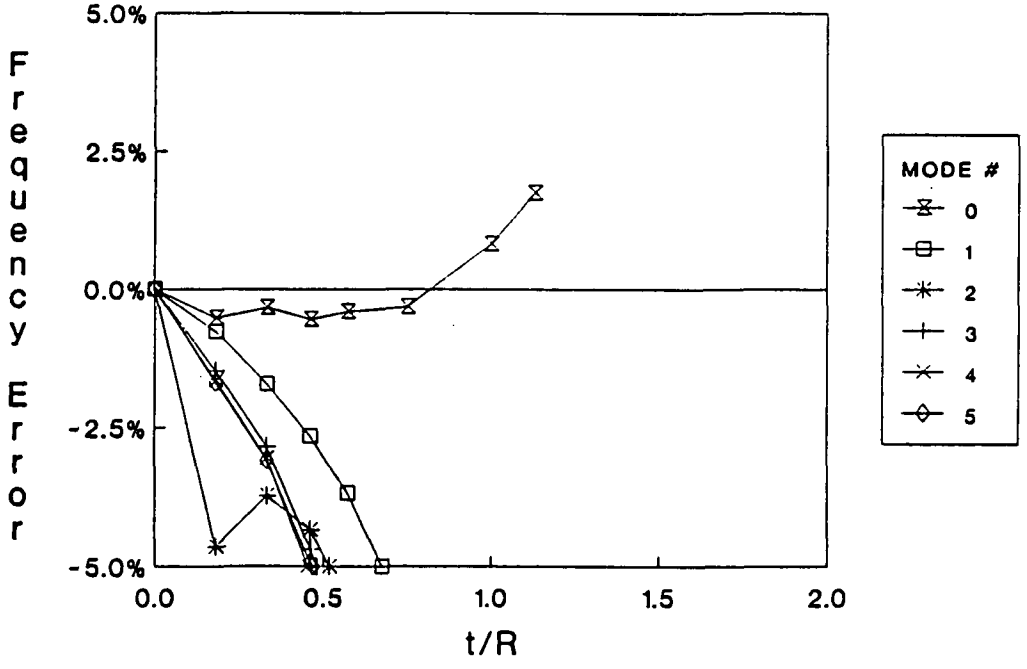

Figure 9.32 TI:EX ring torsional frequency errors.

beams provide comparable accuracy while eliminating the difficult determination of exact I_{ij}'s. The fact that the TR curvature approximation is based on conventional beam cross-sectional properties makes this option most appealing.

Figures 9.25-32 illustrate that 25 of the lowest ring frequencies may be predicted to an accuracy, $|e|$, of five percent or less for $t/R \leq 0.45$. This number does not include the six rigid body modes for combined in-plane and out-of-plane responses, nor does it include the shear modes which are least important in the low range of t/R. The number of modes accurately predicted at even higher t/R's clearly demonstrates the versatility of the engineering beam formulation.

The in-plane frequencies are seen to be more accurate than their out-of-plane counterparts. Also, the torsional frequencies are almost always underpredicted; this differs from the typical pattern for all other modes, especially for high t/R. One might be led to believe that the ST-approximated torsional constant is responsible, since increasing I_0 would reduce the errors for the torsional frequencies. However, note from (9.36) that a larger I_0 would also produce higher out-of-plane bending frequencies, thus *increasing* their frequency errors for $t/R \geq 0.25$ (see Figures 9.29-30). This contradiction suggests that the reduced accuracy of the out-of-plane frequencies is primarily due to the diminished suitability of the underlying beam assumptions.

One other observation deserves mention. The PVAEB results were obtained from two sets of models to characterize the in-plane and out-of-plane responses for various t/R's. The maximum number of degrees-of-freedom ($p = 9$) used in the four-element models is:

$$n_{BE/RA} = 68, \text{ and} \tag{9.40a}$$

$$n_{TI} = 104, \tag{9.40b}$$

for the in-plane analyses and:

$$n_{BE/RA} = 64, \text{ and} \tag{9.41a}$$

$$n_{TI} = 100, \tag{9.41b}$$

for the out-of-plane models. For the modes investigated by Kuhl, the discretization error for the PVAEB frequencies is, at most, 0.25 percent and has been included in the frequency error computations in this section. The benefit of developing p-version finite elements for circular engineering beams is thus confirmed.

10. PROBLEMS INVOLVING GEOMETRIC NONLINEARITIES

The inclusion of geometric nonlinearities in PVAEB provides for the evaluation of structural stability from a primarily dynamic perspective. The problems evaluated in this chapter illustrate the key features in the PVAEB implementation. All problems in this chapter address a one-inch square steel bar with a length, L, of 100 inches. The slenderness of the bar allows for the application of Bernoulli-Euler beam theory and comparison with known solutions. Again, refer to Appendix 14.1 for interpretation of the PVAEB model inputs.

10.1 CANTILEVER BEAM WITH A DISTRIBUTED AXIAL LOAD

Figure 10.1 illustrates the cantilever beam subjected to a distributed axial load, Q. The corresponding single-element PVAEB model is displayed in Table 10.1. Note the beam properties as they are defined in the table, namely:

$$A = 1 \text{ in}^2, \tag{10.1a}$$

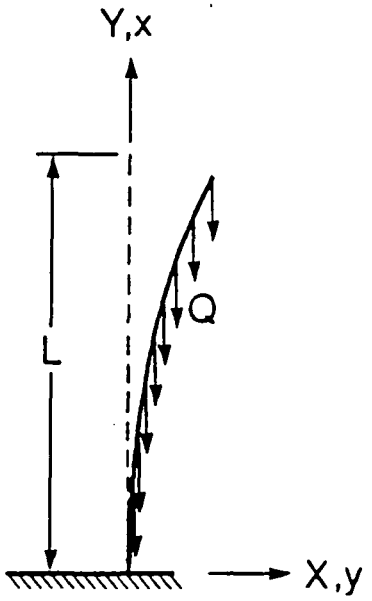

Figure 10.1 Cantilever beam with a distributed axial load sample problem.

Table 10.1 PVAEB sample input for the loaded cantilever problem.

```
TITLE = CANTILEVER BEAM WITH A DISTRIBUTED AXIAL LOAD
SUBTITLE = Q/Qc = 0.50
$
LOAD = 100
BEAM = BE
ANALYSIS = RE
JACOBI
SEQ
NUMEIG = 1
NONLIN = 1
$
ECHO = AL
ERREST
$
SUBCASE
 BRP = 2,3,3,1
$
SUBCASE
 BRP = 2,5,3,1
$
SUBCASE
 BRP = 2,7,3,1
$
SUBCASE
 BRP = 2,9,3,1
 SEGLODISP = HL
 SEFORCE = HL
 DEGLODISP
 DEFORCE
$
BEGINBULK
$
GRID, 1, 0., 0., 0., 123456
GRID, 2, 0., 100., 0., 345
$
CBAR, 1, 1, 1, 2, 1., 0., 0.
CBARI, 1, 1, 2
$
PBAR, 1, 2, 1., .0833333333333333333, .0833333333333333333, .140625
$
MAT, 2, 30000000., , .25, 7.35E-4
$
LOAD, 100, 1., 0.50, 1
PLOAD, 1, 1, FY, -19.593368597358709504, -19.593368597358709504
$
ENDDATA
```

$$I_{yy} = I_{zz} \equiv I = 1/12 \text{ in}^4, \tag{10.1b}$$

$$I_0 = 0.140625 \text{ in}^4, \tag{10.1c}$$

$$E = 30 \times 10^6 \text{ lb}_f/\text{in}^2, \tag{10.1d}$$

$$\nu = 0.25, \text{ and} \tag{10.1e}$$

$$\rho = 7.35 \times 10^{-4} \text{ (lb}_f \text{ sec}^2/\text{in})/\text{in}^3. \tag{10.1f}$$

Note that $G \equiv E/[2(1+\nu)] = 12 \times 10^6$ $\text{lb}_\text{f}/\text{in}^2$ is computed internally by PVAEB. Permanent single point constraints are applied to the grid points to enforce the clamped condition and, in conjunction with fixing $p_3 = 3$ and $p_4 = 1$, to make the problem planar.

The distributed axial load, Q, has units of $(\text{lb}_\text{f}/\text{in})$ and is defined as positive for compressive loading in the beam. The PLOAD card defines the distributed load in the model input (though a GRAV card could produce the same result). The resulting axial load on the beam is simply:

$$F_x = EAu_0' = -Q(L-x). \tag{10.2}$$

Thus, the *exact* axial force distribution may be extracted from the single-element model by specifying $p_1 = 2$. Typical h-version elements using $p_1 = 1$ produce an exact characterization of the axial load only in the limit as $h \to 0$.

The no-load fundamental natural frequency for the cantilever Bernoulli-Euler beam is [51]:

$$\omega_1|_{Q=0} = (\beta_1 L)^2 \sqrt{\frac{EI}{\rho A L^2}}, \text{ where} \tag{10.3a}$$

$$(\beta_1 L) = 1.875104, \tag{10.3b}$$

or:

$$\omega_1|_{Q=0} = 20.50582 \text{ rad/sec}, \tag{10.4}$$

for the given problem parameters. The critical distributed axial force is known to be [16]:

$$Q_C = \left(\frac{3z}{2}\right)^2 \frac{EI}{L^3}, \text{ where} \tag{10.5a}$$

$$z = \min_{z>0}\left(J_{-1/3}(z) \equiv 0\right). \tag{10.5b}$$

That is, z is the smallest positive (real) zero for the Bessel function of the first kind of order $-\frac{1}{3}$. Therefore (see [103], Equations 9.1.10 and 6.1.13):

$$z = 1.866351, \tag{10.6}$$

and:

$$Q_C = 19.59337 \text{ lb}_f/\text{in}, \tag{10.7}$$

for this particular problem. Note that the no-load fundamental eigenvector associated with (10.3-4) is different from the bifurcation vector corresponding to (10.5-7).

As discussed in Chapter 1, stability may be inferred from a dynamic eigenproblem of the form:

$$[[K] - \Lambda [K_G] - \omega^2 [M]] \{U\} = \{0\}, \tag{10.8}$$

where, for the cantilever problem:

$$\Lambda \equiv \frac{Q}{Q_C}. \tag{10.9}$$

Since the axial load in (10.2) does not change with structural deformation, $[K_G]$ may be computed from the linear static solution without iteration (specified in the PVAEB input by NONLIN=1). Defining:

$$\overline{\omega} \equiv \frac{\omega_1|_Q}{\omega_1|_{Q=0}}, \tag{10.10}$$

allows for the comparison of the finite element eigensolution with the known values, namely:

$$\overline{\omega} \equiv 1 \text{ when } \Lambda = 0, \text{ and} \tag{10.11a}$$

$$\overline{\omega} \equiv 0 \text{ when } \Lambda = 1. \tag{10.11b}$$

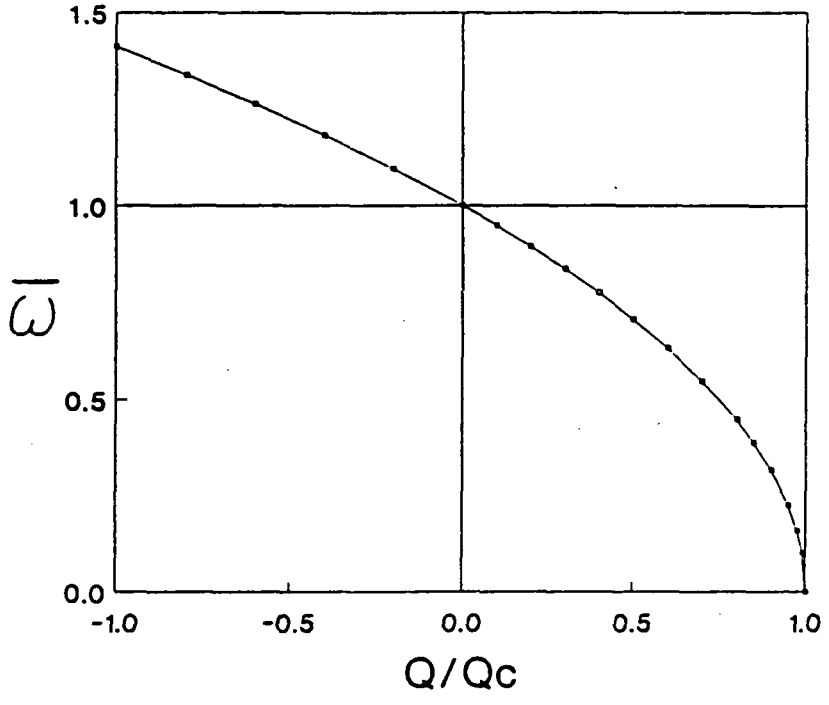

Figure 10.2 Cantilever frequency dependence on distributed axial load.

Figure 10.2 illustrates $\overline{\omega}$ versus Λ obtained from the $p_2 = 9$ finite element solutions. Not only are the two known values in (10.11) predicted, but the dependence of $\overline{\omega}$ to arbitrary Λ may be characterized. Note that $\Lambda < 0$ implies tensile axial forces in the beam which stiffen the fundamental frequency. Table 10.2 displays typical results produced by the PVAEB program. Note the following observations:

1) with $n_G = 2$, $n_P = 0$, $n_E = 1$, $n_D = 4$, $p_1 = 2$, $p_3 = 3$, $p_4 = 1$, and $n_C = 9$, then (see (7.49) and (7.76)):

$$n = p_2 + 1; \tag{10.12}$$

2) the linear and nonlinear static results are identical since the geometric nonlinearities are independent of deformation;

3) the static strain energy is independent of p_2 and is exact for $p_1 = 2$ (note the error estimate);

Table 10.2 PVAEB sample results for the loaded cantilever problem.

CANTILEVER BEAM WITH A DISTRIBUTED AXIAL LOAD — SUBCASE # 4, BE P-LEVELS = 2, 9, 3, 1
Q/Qc = 0.50 — NONLIN = 1, LOAD = 100

LINEAR AND NONLINEAR STATIC ELEMENT GLOBAL DISPLACEMENTS

ELEM #	GRID #	XI	XG	YG	ZG	XG-DISP	YG-DISP	ZG-DISP	XG-ROT	YG-ROT	ZG-ROT
1	1	-1.000	0.00000E+00	0.00000E+00	0.00000E+00	0.00000E+00	0.00000E+00	0.00000E+00	0.00000E+00	0.00000E+00	0.00000E+00
		0.000	0.00000E+00	0.50000E+02	0.00000E+00	0.00000E+00	-.12246E-02	0.00000E+00	0.00000E+00	0.00000E+00	0.00000E+00
	2	1.000	0.00000E+00	0.10000E+03	0.00000E+00	0.00000E+00	-.16328E-02	0.00000E+00	0.00000E+00	0.00000E+00	0.00000E+00

LINEAR AND NONLINEAR STATIC ELEMENT FORCES

ELEM #	GRID #	XI	AXIAL-FORCE	YL-MOMENT	ZL-MOMENT	YL-SHEAR	ZL-SHEAR	TORQUE
1	1	-1.000	-.97966842987E+03	0.00000000000E+00	0.00000000000E+00	0.00000000000E+00	0.00000000000E+00	0.00000000000E+00
		0.000	-.48983421493E+03	0.00000000000E+00	0.00000000000E+00	0.00000000000E+00	0.00000000000E+00	0.00000000000E+00
	2	1.000	-.73183646643E-13	0.00000000000E+00	0.00000000000E+00	0.00000000000E+00	0.00000000000E+00	0.00000000000E+00

EIGENVALUE # 1, OMEGA = 0.14515393617283E+02 RAD/SEC, FREQ = 0.23101966451151E+01 HZ.

DYNAMIC ELEMENT GLOBAL DISPLACEMENTS

ELEM #	GRID #	XI	XG	YG	ZG	XG-DISP	YG-DISP	ZG-DISP	XG-ROT	YG-ROT	ZG-ROT
1	1	-1.000	0.00000E+00	0.00000E+00	0.00000E+00	0.00000E+00	0.00000E+00	0.00000E+00	0.00000E+00	0.00000E+00	0.00000E+00
		0.000	0.00000E+00	0.50000E+02	0.00000E+00	0.24860E+01	0.00000E+00	0.00000E+00	0.00000E+00	0.00000E+00	-.86348E-01
	2	1.000	0.00000E+00	0.10000E+03	0.00000E+00	0.73974E+01	0.00000E+00	0.00000E+00	0.00000E+00	0.00000E+00	-.10234E+00

DYNAMIC ELEMENT FORCES

ELEM #	GRID #	XI	AXIAL-FORCE	YL-MOMENT	ZL-MOMENT	YL-SHEAR	ZL-SHEAR	TORQUE
1	1	-1.000	0.00000000000E+00	0.00000000000E+00	0.60693091808E+04	0.44620341830E+02	0.00000000000E+00	0.00000000000E+00
		0.000	0.00000000000E+00	0.00000000000E+00	0.22775910517E+04	0.80089045953E+02	0.00000000000E+00	0.00000000000E+00
	2	1.000	0.00000000000E+00	0.00000000000E+00	0.49745798397E-02	-.32199403398E-02	0.00000000000E+00	0.00000000000E+00

CANTILEVER BEAM WITH A DISTRIBUTED AXIAL LOAD — # SUBCASES = 4, BEAM = BE, ANALYSIS = RE
Q/Qc = 0.50 — NONLIN = 1, LOAD = 100

ERROR ESTIMATES

CASE	#DOF	(NON)LINEAR STRAIN ENERGY	EXTRAPOLATED ENERGY	DELTA ENERGY	CONVERGENCE EXPONENT RUNNING	CONVERGENCE EXPONENT CUMULATIVE	% EST. ERROR IN ||V|| RUNNING	% EST. ERROR IN ||V|| CUMULATIVE
1	4	0.53319457359995E+00	0.00000000000000E+00	0.00000000E+00	0.0000	0.0000	0.0000	0.0000
2	6	0.53319457359995E+00	0.53319457359995E+00	0.00000000E+00	0.0000	0.0000	0.0000	0.0000
3	8	0.53319457359995E+00	0.53319457359995E+00	0.00000000E+00	0.0000	0.0000	0.0000	0.0000
4	10	0.53319457359995E+00	0.53319457359995E+00	0.00000000E+00	0.0000	0.0000	0.0000	0.0000

CASE	#DOF	OMEGA # 1	EXTRAPOLATED OMEGA	DELTA OMEGA	CONVERGENCE EXPONENT RUNNING	CONVERGENCE EXPONENT CUMULATIVE	% EST. ERROR IN OMEGA RUNNING	% EST. ERROR IN OMEGA CUMULATIVE
1	4	0.14617632660406E+02	0.00000000000000E+00	0.00000000E+00	0.0000	0.0000	0.0000	0.7043
2	6	0.14515758161264E+02	0.14433740863605E+02	-0.10187450E+00	2.0000	13.9098	0.5682	0.0025
3	8	0.14515393919409E+02	0.14515387046679E+02	-0.36424186E-03	13.8659	24.6518	0.0000	0.0000
4	10	0.14515393617283E+02	0.14515393616164E+02	-0.30212600E-06	25.1042	25.1042	0.0000	0.0000

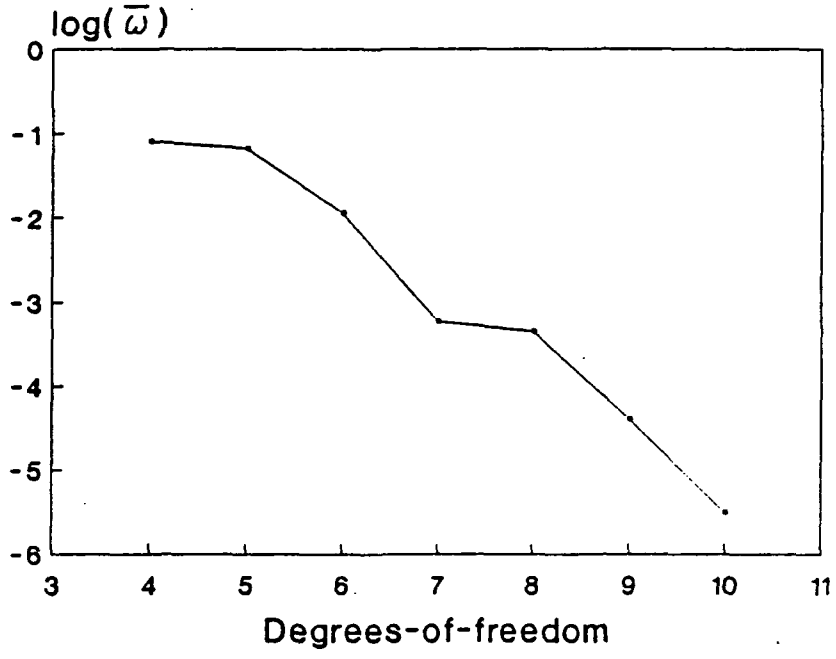

Figure 10.3 Convergence of $\bar{\omega}$ for the cantilever beam subjected to critical distributed axial loading.

4) the fundamental eigenvector for arbitrary Λ does not correspond to either the no-load fundamental eigenvector (except when $\Lambda = 0$) or the bifurcation vector (except when $\Lambda = 1$);
5) dynamic displacements and forces are extracted from the fundamental eigenvector and do not include the static contributions; and
6) the error estimate for the fundamental frequency suggests convergence to at least nine significant digits for $\Lambda = 0.5$ and $p_2 = 9$.

Accuracy of the fundamental natural frequency diminishes slightly with increasing Λ. Figure 10.3 illustrates the worst-case convergence for $\Lambda = 1$. As expected, $\log(\bar{\omega}) \to -\infty$ (i.e., $\bar{\omega} \to 0$) as $p_2 \to \infty$ for the case of critical loading. Exponential convergence (8.11) still exists for problems involving geometric nonlinearities.

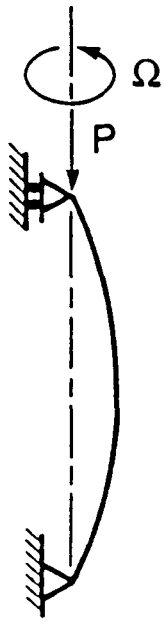

Figure 10.4 Axially loaded, axially rotating shaft sample problem.

10.2 AXIALLY LOADED, AXIALLY ROTATING SHAFT

A slightly different problem is used to illustrate the interaction between geometric nonlinearities and rotating coordinate system effects. The pinned-pinned straight beam subjected to an axial point load and axial rotation is illustrated in Figure 10.4. The analytical advantage of the pinned-pinned configuration is that the eigenvectors are sinusoid for all loading conditions. Thus, the interaction between the various loading parameters is known exactly.

For a nonrotating shaft, the exact natural frequencies for Bernoulli-Euler beam flexure are [27]:

$$\omega_n|_{P,\Omega=0} = \sqrt{\left(\frac{n^4\pi^4 EI}{\rho AL^4}\right)\left(1 - \frac{PL^2}{n^2\pi^2 EI}\right)}, \text{ or} \tag{10.13a}$$

$$\omega_n|_{P,\Omega=0} = (\omega_n|_{P=\Omega=0})\sqrt{1 - (P/n^2P_C)}, \tag{10.13b}$$

Table 10.3 PVAEB sample input for the shaft problem.

```
TITLE = AXIALLY LOADED, AXIALLY ROTATING SHAFT
SUBTITLE = P/Pc = 0.50, W/Wc = 0.00
$
LOAD = 100
BEAM = BE
ANALYSIS = RE  $ NOTE: USE 'IM' FOR PROBLEMS WITH CORIOLIS COUPLING.
SEQ            $ NOTE: ONLY AVAILABLE FOR 'RE' ANALYSES.
NUMEIG = 2
NONLIN = 1
ERREST
$
SUBCASE
 BRP = 1,3,3,1
$
SUBCASE
 BRP = 1,5,5,1
$
SUBCASE
 BRP = 1,7,7,1
$
SUBCASE
 BRP = 1,9,9,1
 SELOCDISP = HL
 SEFORCE = HL
 DELOCDISP
$
BEGINBULK
$
GRID,    1,    0.,    0.,    0.,    1235
GRID,    2,    0., 100.,    0.,    135
$
CBAR, 1, 1, 1, 2, 1., 0., 0.
CBARI, 1, 1, 4
$
PBAR, 1, 2, 1., .0833333333333333333, .0833333333333333333, .140625
$
MAT, 2, 30000000., , .25, 7.35E-4
$
LOAD, 100, 1., 0.50, 1, 0.00, 2
FORCE,  1, 2, 2467.40110027233959,  0., -1.,  0.
RFORCE, 2, 1, 57.5607017757049890,  0.,  1.,  0.
$
ENDDATA
```

where $\omega_n|_{P=\Omega=0}$ are the no-load natural frequencies and P_C is the critical Euler buckling load. For the particular problem parameters:

$$\omega_1|_{P=\Omega=0} = 57.56070 \text{ rad/sec, and} \tag{10.14a}$$

$$P_C = 2467.401 \text{ lb}_\text{f}. \tag{10.14b}$$

Note that positive P is taken to impart a compressive axial force in the beam. The corresponding in-plane and out-of-plane eigenvectors in terms of

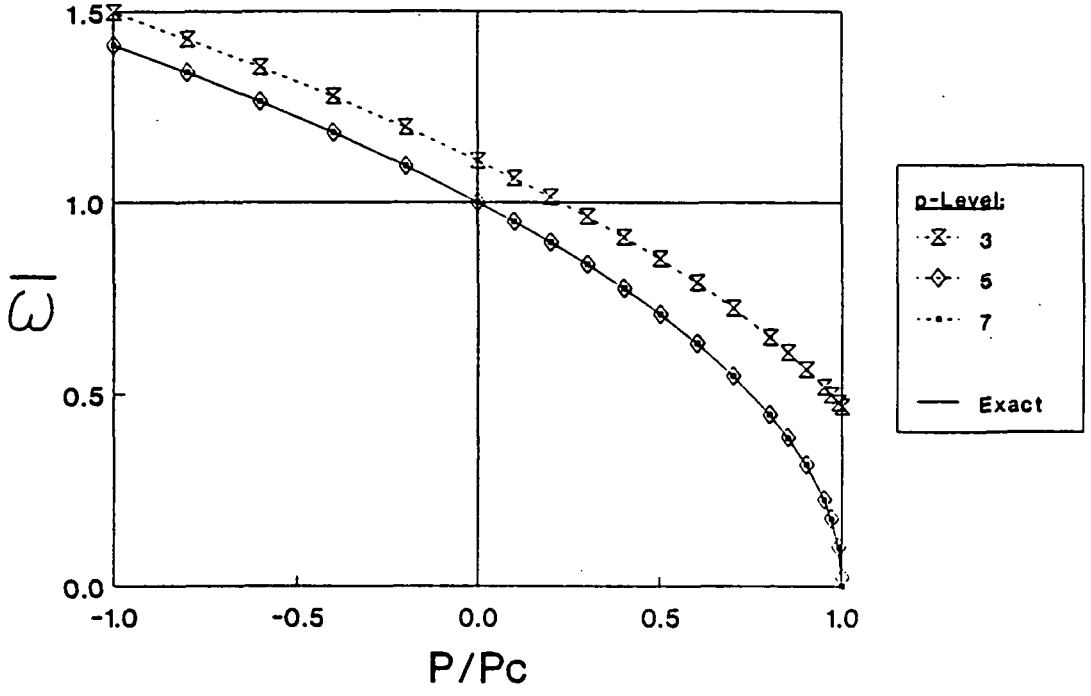

Figure 10.5 Frequency dependence on axial load for the nonrotating shaft.

local coordinates are:

$$\left\{ \begin{matrix} v_0(x,t) \\ w_0(x,t) \end{matrix} \right\}_{2n-1} = \sin\left(\frac{n\pi x}{L}\right) \left\{ \begin{matrix} \cos\left((\omega_n|_{P,\Omega=0})\, t\right) \\ 0 \end{matrix} \right\}, \text{ and} \tag{10.15a}$$

$$\left\{ \begin{matrix} v_0(x,t) \\ w_0(x,t) \end{matrix} \right\}_{2n} = \sin\left(\frac{n\pi x}{L}\right) \left\{ \begin{matrix} 0 \\ \cos\left((\omega_n|_{P,\Omega=0})\, t\right) \end{matrix} \right\}. \tag{10.15b}$$

The same natural frequencies correspond to both in-plane and out-of-plane responses since $I_{yy} = I_{zz} \equiv I$ for the sample problem.

The single-element PVAEB model for this problem is provided in Table 10.3. Note the change in the permanent single point constraints and the reporting of elemental displacements in the local frame. The effect of the axial point load is exactly characterized by $p_1 = 1$. Defining:

$$\overline{\omega}|_{P,\Omega=0} \equiv \frac{\omega_1|_{P,\Omega=0}}{\omega_1|_{P=\Omega=0}}, \tag{10.16}$$

provides for a dimensionless quantification of the effect of axial load on the fundamental frequency. Figure 10.5 compares the exact solution to the results obtained

from PVAEB at various p-levels (i.e., $p_2 = p_3 \equiv p = 3, 5, 7$). Accurate results may be obtained using $p = 5$ except near the critical loading. Table 10.4 presents typical results from the PVAEB analyses.

With the addition of shaft rotation, the exact (Bernoulli-Euler) natural frequencies relative to the rotating frame are [27]:

$$\omega_{n\mp}|_{P,\Omega} = \left| \omega_n|_{P,\Omega=0} \mp \Omega \right|. \tag{10.17}$$

Thus, the nonspinning natural frequencies split into two frequencies, one decreasing and one increasing with rotational velocity. Furthermore, the eigenvectors are now coupled, namely (for positive Ω):

$$\left\{ \begin{matrix} v_0(x,t) \\ w_0(x,t) \end{matrix} \right\}_{2n-1} = \sin\left(\frac{n\pi x}{L}\right) \left\{ \begin{matrix} \cos\left((\omega_{n-}|_{P,\Omega})\, t\right) \\ -\sin\left((\omega_{n-}|_{P,\Omega})\, t\right) \end{matrix} \right\}, \text{ and} \tag{10.18a}$$

$$\left\{ \begin{matrix} v_0(x,t) \\ w_0(x,t) \end{matrix} \right\}_{2n} = \sin\left(\frac{n\pi x}{L}\right) \left\{ \begin{matrix} -\sin\left((\omega_{n+}|_{P,\Omega})\, t\right) \\ \cos\left((\omega_{n+}|_{P,\Omega})\, t\right) \end{matrix} \right\}. \tag{10.18b}$$

The eigenvectors associated with the decreasing and increasing natural frequencies rotate against and in the direction of Ω, respectively. These results are accurately predicted by PVAEB, as seen in the sample output of Table 10.5.

The dimensionless fundamental frequency for the combined loading case may be defined as:

$$\overline{\omega}|_{P,\Omega} \equiv \frac{\omega_{1-}|_{P,\Omega}}{\omega_1|_{P=\Omega=0}} = \sqrt{1-\Lambda} - |\overline{\Omega}|, \text{ where} \tag{10.19a}$$

$$\Lambda \equiv \frac{P}{P_C}, \text{ and} \tag{10.19b}$$

$$\overline{\Omega} \equiv \frac{\Omega}{\omega_1|_{P=\Omega=0}}. \tag{10.19c}$$

Figure 10.6 displays the relationship between Λ and $\overline{\Omega}$ for the first critical shaft speed ($\overline{\omega} \equiv 0$). Note that this curve is identical in shape to the exact curve in Figure 10.5. Generalizing in words, the critical shaft speeds are equal to the

Table 10.4 PVAEB sample results for the axially loaded, nonrotating shaft.

```
AXIALLY LOADED, AXIALLY ROTATING SHAFT                          SUBCASE #  4, BE P-LEVELS =  1, 9, 9, 1
P/Pc = 0.50, W/Wc = 0.00                                        LOAD =  100

LINEAR AND NONLINEAR STATIC ELEMENT LOCAL DISPLACEMENTS
ELEM #  GRID #    XI          U0                V0                W0                PHI1              V0'               W0'
    1       1   -1.000  0.00000000000E+00 0.00000000000E+00 0.00000000000E+00 0.00000000000E+00 0.00000000000E+00 0.00000000000E+00
               -0.500  -.10280837918E-02 0.00000000000E+00 0.00000000000E+00 0.00000000000E+00 0.00000000000E+00 0.00000000000E+00
                0.000  -.20561675836E-02 0.00000000000E+00 0.00000000000E+00 0.00000000000E+00 0.00000000000E+00 0.00000000000E+00
                0.500  -.30842513753E-02 0.00000000000E+00 0.00000000000E+00 0.00000000000E+00 0.00000000000E+00 0.00000000000E+00
            2   1.000  -.41123351671E-02 0.00000000000E+00 0.00000000000E+00 0.00000000000E+00 0.00000000000E+00 0.00000000000E+00
LINEAR AND NONLINEAR STATIC ELEMENT FORCES
ELEM #  GRID #    XI       AXIAL-FORCE        YL-MOMENT         ZL-MOMENT         YL-SHEAR          ZL-SHEAR          TORQUE
    1       1   -1.000  -.12337005501E+04 0.00000000000E+00 0.00000000000E+00 0.00000000000E+00 0.00000000000E+00 0.00000000000E+00
               -0.500  -.12337005501E+04 0.00000000000E+00 0.00000000000E+00 0.00000000000E+00 0.00000000000E+00 0.00000000000E+00
                0.000  -.12337005501E+04 0.00000000000E+00 0.00000000000E+00 0.00000000000E+00 0.00000000000E+00 0.00000000000E+00
                0.500  -.12337005501E+04 0.00000000000E+00 0.00000000000E+00 0.00000000000E+00 0.00000000000E+00 0.00000000000E+00
            2   1.000  -.12337005501E+04 0.00000000000E+00 0.00000000000E+00 0.00000000000E+00 0.00000000000E+00 0.00000000000E+00
EIGENVALUE #   1,    OMEGA =  0.40701562556850E+02 RAD/SEC,    FREQ =  0.64778548724868E+01 HZ.
DYNAMIC ELEMENT LOCAL DISPLACEMENTS
ELEM #  GRID #    XI          U0                V0                W0                PHI1              V0'               W0'
    1       1   -1.000  0.00000000000E+00 0.00000000000E+00 0.00000000000E+00 0.00000000000E+00 -.16387820600E+00 0.62935543325E-12
               -0.500  0.00000000000E+00 0.36885558385E+01 0.14165475169E-10 0.00000000000E+00 -.11587951887E+00 0.44502198665E-12
                0.000  0.00000000000E+00 0.52164044352E+01 0.20033002273E-10 0.00000000000E+00 0.36994795831E-19 -.15148340101E-25
                0.500  0.00000000000E+00 0.36885558385E+01 0.14165475169E-10 0.00000000000E+00 0.11587951887E+00 -.44502198665E-12
            2   1.000  0.00000000000E+00 0.00000000000E+00 0.00000000000E+00 0.00000000000E+00 0.16387820600E+00 -.62935543325E-12
EIGENVALUE #   2,    OMEGA =  0.40701562556850E+02 RAD/SEC,    FREQ =  0.64778548724868E+01 HZ.
DYNAMIC ELEMENT LOCAL DISPLACEMENTS
ELEM #  GRID #    XI          U0                V0                W0                PHI1              V0'               W0'
    1       1   -1.000  0.00000000000E+00 0.00000000000E+00 0.00000000000E+00 0.00000000000E+00 0.62935543325E-12 0.16387820600E+00
               -0.500  0.00000000000E+00 0.14165475169E-10 0.36885558385E+01 0.00000000000E+00 0.44502198665E-12 0.11587951887E+00
                0.000  0.00000000000E+00 0.20033002273E-10 0.52164044352E+01 0.00000000000E+00 0.65740028999E-27 -.36996245459E-19
                0.500  0.00000000000E+00 0.14165475169E-10 0.36885558385E+01 0.00000000000E+00 -.44502198665E-12 -.11587951887E+00
            2   1.000  0.00000000000E+00 0.00000000000E+00 0.00000000000E+00 0.00000000000E+00 -.62935543325E-12 -.16387820600E+00

AXIALLY LOADED, AXIALLY ROTATING SHAFT                          # SUBCASES =  4, BEAM = BE, ANALYSIS = RE
P/Pc = 0.50, W/Wc = 0.00                                        NONLIN =  1, LOAD =  100

ERROR ESTIMATES

                                                                          CONVERGENCE EXPONENT  % EST. ERROR IN OMEGA
CASE #DOF     OMEGA #   1 & 2      EXTRAPOLATED OMEGA     DELTA OMEGA     RUNNING CUMULATIVE    RUNNING CUMULATIVE
  1     5  0.49021714609100E+02 0.00000000000000E+00 0.00000000E+00   0.0000     0.0000      0.0000   20.4418
  2     9  0.40724949191486E+02 0.36415760873109E+02 -0.82967654E+01   2.0000    10.1590     11.8333    0.0575
  3    13  0.40701573464219E+02 0.40700993150833E+02 -0.23375727E-01  10.1182    20.8499      0.0014    0.0000
  4    17  0.40701562556850E+02 0.40701562516093E+02 -0.10907369E-04  20.8499    20.8499      0.0000    0.0000
```

Table 10.5 PVAEB sample results for the axially loaded, axially rotating shaft.

```
AXIALLY LOADED, AXIALLY ROTATING SHAFT                          BE P-LEVELS =  1, 9, 9, 1
P/Pc = 0.50, W/Wc = 0.50                                        NONLIN =  1, ANALYSIS = IM, LOAD =  100

EIGENVALUE #   1,    OMEGA =  0.11921211668998E+02 RAD/SEC,    FREQ =  0.18973197647658E+01 HZ.
DYNAMIC ELEMENT LOCAL DISPLACEMENTS:  REAL COMPONENT
ELEM #  GRID #    XI          U0                 V0                 W0                 PHI1               V0'                W0'
    1       1   -1.000  0.00000000000E+00 0.00000000000E+00 0.00000000000E+00 0.00000000000E+00 -.16387820600E+00 -.13056997412E-13
               -0.500  0.16008621939E-15 0.36885558385E+01 -.15509646256E-12 0.00000000000E+00 -.11587951887E+00 -.41081199727E-14
                0.000  0.32017243879E-15 0.52164044352E+01 -.18986945582E-12 0.00000000000E+00 0.21575173297E-15 0.23190912115E-15
                0.500  0.48025865818E-15 0.36885558385E+01 -.15568949423E-12 0.00000000000E+00 0.11587951887E+00 0.30064553813E-14
            2   1.000  0.64034487757E-15 0.00000000000E+00 0.00000000000E+00 0.00000000000E+00 0.16387820600E+00 0.27165349962E-14
DYNAMIC ELEMENT LOCAL DISPLACEMENTS:  IMAGINARY COMPONENT
ELEM #  GRID #    XI          U0                 V0                 W0                 PHI1               V0'                W0'
    1       1   -1.000  0.00000000000E+00 0.00000000000E+00 0.00000000000E+00 0.00000000000E+00 0.00000000000E+00 0.16387820600E+00
               -0.500  -.15554452349E-15 -.13489361169E-12 -.36885558385E+01 0.00000000000E+00 -.49823077748E-14 0.11587951887E+00
                0.000  -.31108904697E-15 -.21937493388E-12 -.52164044352E+01 0.00000000000E+00 -.22136685096E-15 -.20984011559E-15
                0.500  -.46663357046E-15 -.13424973524E-12 -.36885558385E+01 0.00000000000E+00 0.60489997203E-14 -.11587951887E+00
            2   1.000  -.62217809395E-15 0.00000000000E+00 0.00000000000E+00 0.00000000000E+00 0.10045570121E-13 -.16387820600E+00
EIGENVALUE #   2,    OMEGA =  0.69481913444940E+02 RAD/SEC,    FREQ =  0.11058389980245E+02 HZ.
DYNAMIC ELEMENT LOCAL DISPLACEMENTS:  REAL COMPONENT
ELEM #  GRID #    XI          U0                 V0                 W0                 PHI1               V0'                W0'
    1       1   -1.000  0.00000000000E+00 0.00000000000E+00 0.00000000000E+00 0.00000000000E+00 -.12992099538E-05 0.16387588580E+00
               -0.500  0.57136166245E-07 0.21309759054E-04 0.36885522975E+01 0.00000000000E+00 0.99501189183E-06 0.11587963757E+00
                0.000  0.11427233249E-06 0.41208386591E-04 0.52164096344E+01 0.00000000000E+00 0.57127289477E-07 0.11152095641E-06
                0.500  0.17140849873E-06 0.21003571674E-04 0.36885519993E+01 0.00000000000E+00 -.13358493212E-05 -.11588009149E+00
            2   1.000  0.22854466498E-06 0.00000000000E+00 0.00000000000E+00 0.00000000000E+00 -.24379089686E-05 -.16387951199E+00
DYNAMIC ELEMENT LOCAL DISPLACEMENTS:  IMAGINARY COMPONENT
ELEM #  GRID #    XI          U0                 V0                 W0                 PHI1               V0'                W0'
    1       1   -1.000  0.00000000000E+00 0.00000000000E+00 0.00000000000E+00 0.00000000000E+00 -.16387625964E+00 0.31754654029E-05
               -0.500  -.48292275796E-07 -.36885528919E+01 0.28454962460E-04 0.00000000000E+00 -.11587960612E+00 0.60383499839E-06
                0.000  -.96584551593E-07 -.52164087636E+01 0.30742029503E-04 0.00000000000E+00 -.10252568046E-06 -.40043688836E-07
                0.500  -.14487682739E-06 -.36885526410E+01 0.28715038064E-04 0.00000000000E+00 0.11588000697E+00 -.33289304996E-06
            2   1.000  -.19316910319E-06 0.00000000000E+00 0.00000000000E+00 0.00000000000E+00 0.16387930765E+00 0.13276998680E-17
```

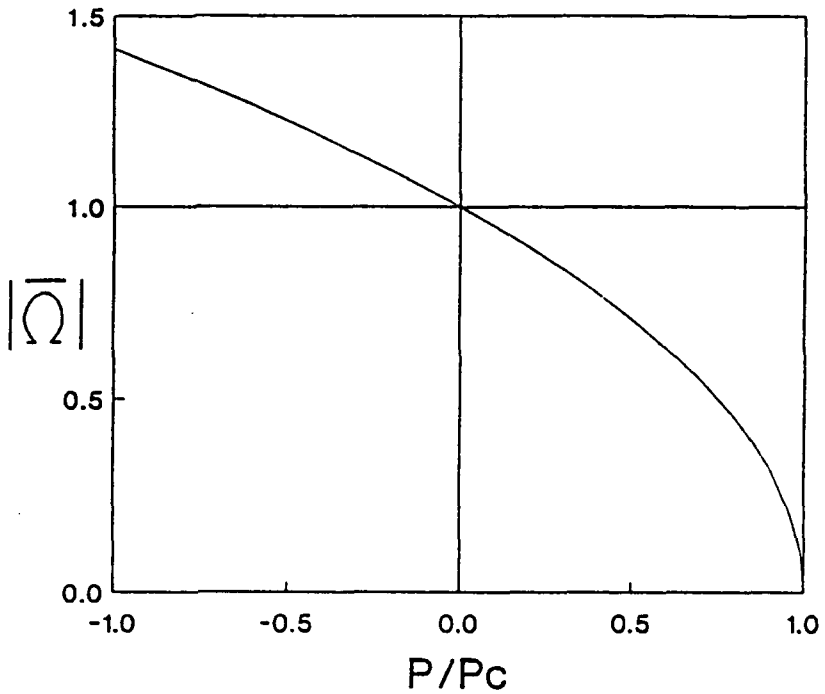

Figure 10.6 First critical shaft speed for the axially loaded shaft.

nonrotating shaft natural frequencies regardless of the magnitude of the applied axial load. This relationship is readily apparent from (10.19).

Equations 10.17 and 10.18 for the spinning shaft include the effects of both centrifugal softening and Coriolis coupling. It is interesting to note that ignoring Coriolis coupling produces nonsplitting fundamental frequencies of the form:

$$\overline{\omega}|_{P,\Omega,No[C]} = \sqrt{1 - \Lambda - \overline{\Omega}^2}, \tag{10.20}$$

with uncoupled eigenvectors similar to (10.15). While (10.20) generally overestimates the true $\overline{\omega}$, it *will* accurately predict the critical speeds of an axially loaded shaft. On the other hand, ignoring centrifugal softening produces splitting frequencies with:

$$\overline{\omega}|_{P,\Omega,No[K_s]} = \sqrt{1 - \Lambda + 2\overline{\Omega}^2 - 2|\overline{\Omega}|\sqrt{1 - \Lambda + \overline{\Omega}^2}}, \tag{10.21}$$

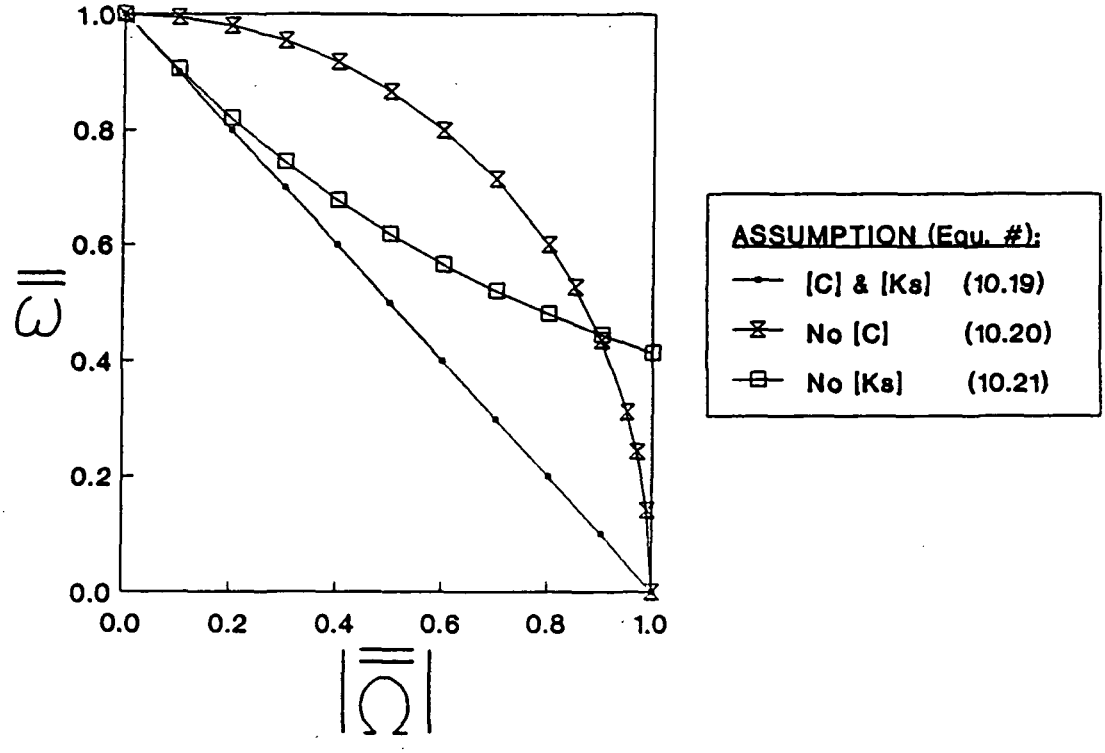

Figure 10.7 Rotating coordinate system effects on shaft frequency.

and coupled eigenvectors as in (10.18). While this relation does produce rotation-induced reductions of the fundamental frequency, $\overline{\omega} = 0$ only when $\Lambda = 1$ or $\overline{\Omega} = \infty$. Defining:

$$\overline{\overline{\omega}} \equiv \frac{\overline{\omega}}{\sqrt{1-\Lambda}}, \text{ and} \tag{10.22a}$$

$$\overline{\overline{\Omega}} \equiv \frac{\overline{\Omega}}{\sqrt{1-\Lambda}}, \tag{10.22b}$$

allows (10.19-21) to be reduced to the single curves in Figure 10.7. Note that Coriolis coupling is primarily responsible for the reduction of the fundamental frequency for small $|\overline{\overline{\Omega}}|$, while the centrifugal softening dominates for near-critical $|\overline{\overline{\Omega}}|$. PVAEB may be used to verify these relations by including NOCOR or NOSOFT cards in the case control.

It is important to note that longitudinal and torsional vibrations for straight beams are unaffected by axial loading or axial rotation. This observation is

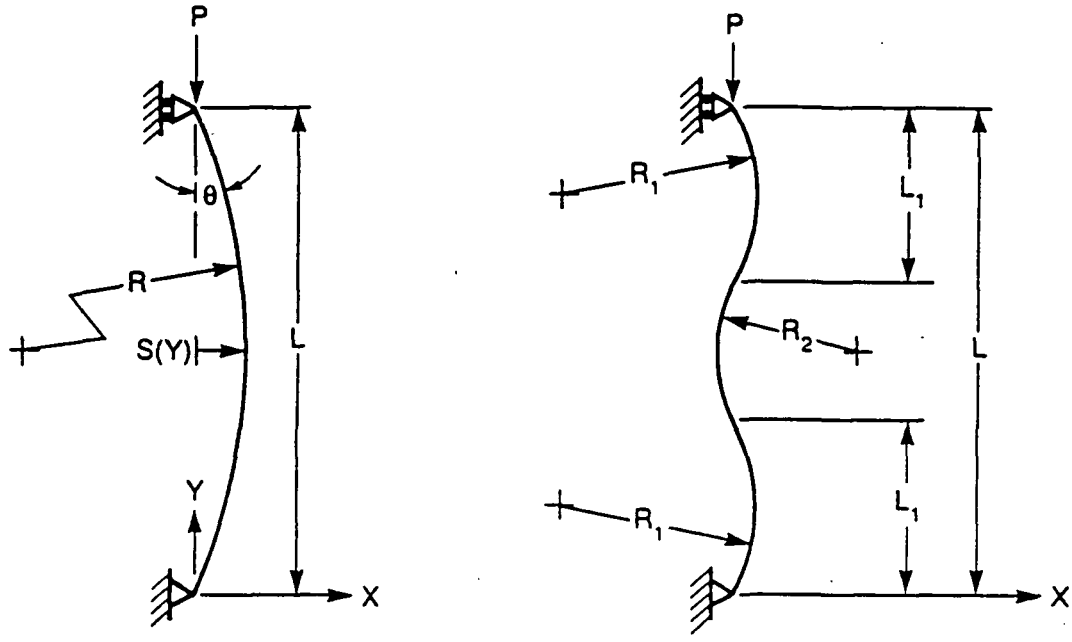

Circular Bow Dominant Third Harmonic

Figure 10.8 Beams with initial imperfections.

particularly useful in verifying the proper formulation of rotating coordinate effects. Though not presented here, PVAEB accurately predicts this behavior.

10.3 BEAMS WITH INITIAL IMPERFECTIONS

The preceding examples in this chapter involve geometric nonlinearities which are unaffected by the structural deformations. Therefore, the basic nonlinear iteration scheme outlined in Chapter 1 has not been utilized. This section addresses two problems which require iteration in order to converge to the nonlinear static solution. Both problems involve pinned-ended beams with small initial imperfections subjected to axial loading, as illustrated in Figure 10.8. The initial bows are defined using shallow circular arcs to allow for the use of circular beam elements.

The classical formulation for initially bowed beams is presented in [71] and contains some simplifying assumptions in comparison with the ensuing finite

element model. The overall beam length is taken to be the span between the pinned ends (as opposed to the slightly larger sum of the circular arc lengths), and the beam cross-sectional properties are defined in the planes normal to the centerline (as if the beam is actually straight). The unloaded and loaded shapes of the beam are represented by the Fourier series:

$$S_0(Y) = \sum_{n=1}^{\infty} s_n \sin\left(\frac{n\pi Y}{L}\right), \text{ and} \tag{10.23a}$$

$$S(Y) = \sum_{n=1}^{\infty} \bar{s}_n \sin\left(\frac{n\pi Y}{L}\right), \tag{10.23b}$$

respectively. Solving the governing differential equation results in:

$$\bar{s}_n = \frac{s_n}{1-(P/n^2P_C)}, \tag{10.24}$$

where P_C is again the critical Euler buckling load (see (10.13-14)). It follows that if $s_1 \neq 0$ and as $P \rightarrow P_C$, the amplitude of the first mode becomes large in comparison with the others, namely:

$$S(Y) \rightarrow \frac{s_1}{1-(P/P_C)} \sin\left(\frac{\pi Y}{L}\right). \tag{10.25}$$

Table 10.6 displays the PVAEB input for a beam with a one-percent initial circular bow, that is:

$$S_0\left(\frac{L}{2}\right) = 0.01L = 1.0 \text{ in}, \tag{10.26}$$

such that (see Figure 10.8):

$$R = 1250.5 \text{ in, and} \tag{10.27a}$$

$$\theta_0 = 0.0399947 \text{ radians}, \tag{10.27b}$$

where θ_0 is the unloaded angle between the beam and the centerline at $Y = L$. Provisions are made for the evaluation of this problem using all beam types

Table 10.6 PVAEB sample input for the beam with an initial circular bow.

```
TITLE = BEAM WITH AN INITIAL CIRCULAR BOW
SUBTITLE = So(L/2) = 0.01L, P/Pc = 0.5
$
BEAM = BE    $ NOTE: PROVISIONS FOR 'TI' BEAM ARE INCLUDED.
CIRC = ST    $ NOTE: PROVISIONS FOR 'TR' OR 'EX' APPROXIMATIONS ARE INCLUDED.
ANALYSIS = ST
NONLIN = -12
LOAD = 100
$
ECHO=AL
SEGLODISP = AL
SEFORCE = AL
ERREST
$
SUBCASE
 BRP = 3,3,3,1
 TIP = 3,3,1,1,2,1
$
SUBCASE
 BRP = 5,5,3,1
 TIP = 5,5,1,1,4,1
$
SUBCASE
 BRP = 7,7,3,1
 TIP = 7,7,1,1,6,1
$
SUBCASE
 BRP = 9,9,3,1
 TIP = 9,9,1,1,8,1
$
BEGINBULK
$
GRID, 1, 0., 0., 0., 12345
GRID, 2, 0., 100., 0., 1345
$
CBARC, 1, 1, 1, 2, 1., 0., 0., 1250.5
CBARI,  1,   2,   4
$
PBARC 1 2 1. .08333333333333 .08333333333333 .140625 .8333333333333 .8333333333333 +P1
+P1, 0., 0., 0., 1250.5, 1.000000053291, .08333334132694, , , +P2
+P2, .08333333777422, -6.664001705473D-05, 0., 0.
$
MAT, 2, 30000000, , .25, 1.
$
LOAD, 100, 1., 0.5, 1
FORCE, 1, 2, 2467.40110027233959, 0., -1., 0.
$
ENDDATA
```

($k_y = k_z \equiv \frac{5}{6}$) and curvature approximations. Recall that PVAEB defines the beam properties and displacement variable relative to the beam axis. As the beam deforms, the integrated forces and moments used to compute the geometric nonlinearities will change. Therefore, NONLIN=−12 is specified so that nonlinear iterations will continue until the error in nonlinear strain energy is at most 10^{-12} for each subcase (see (1.34)). Also, comparisons with the classical

solutions will be made at $Y = L/2$ since that is the only place where the local beam axes are parallel to the global axes.

Two solutions from the classical formulation are used for comparison with the PVEAB results. The first solution assumes a sinusoidal bow, namely:

$$(S_0(Y))_{\text{sinusoid}} \equiv \sin\left(\tfrac{\pi Y}{L}\right) \text{ in;} \tag{10.28}$$

thus:

$$(S(Y))_{\text{sinusoid}} = \frac{1.0}{1-(P/P_C)} \sin\left(\tfrac{\pi Y}{L}\right) \text{ in.} \tag{10.29}$$

One might be led to believe that the shape of the small initial bow is insignificant. However, the Fourier series for the circular bow is:

$$\begin{aligned}(S_0(Y))_{\text{arc}} = \Big(&1.0321 \sin\left(\tfrac{\pi Y}{L}\right) \\ &+0.0383 \sin\left(\tfrac{3\pi Y}{L}\right) \\ &+0.0083 \sin\left(\tfrac{5\pi Y}{L}\right) \\ &+0.0030 \sin\left(\tfrac{7\pi Y}{L}\right) \\ &+\ldots\Big) \text{in.}\end{aligned} \tag{10.30}$$

Based on (10.25), the circular imperfection will produce slightly larger deformations than the sinusoid.

Figure 10.9 displays the loaded midspan position as a function of the applied load normalized using the classical sinusoid solution. The PVAEB results are for a BE beam with ST curvature approximation and $p_1 = p_2 \equiv p = 9$. As can be seen, the nonlinear PVAEB and classical arc solutions compare quite well, with the minor formulation differences having minimal effect. The difference caused by the shape of the initial bow is more significant than one might expect. The substantial effect of nonlinearities is better illustrated in Figure 10.10.

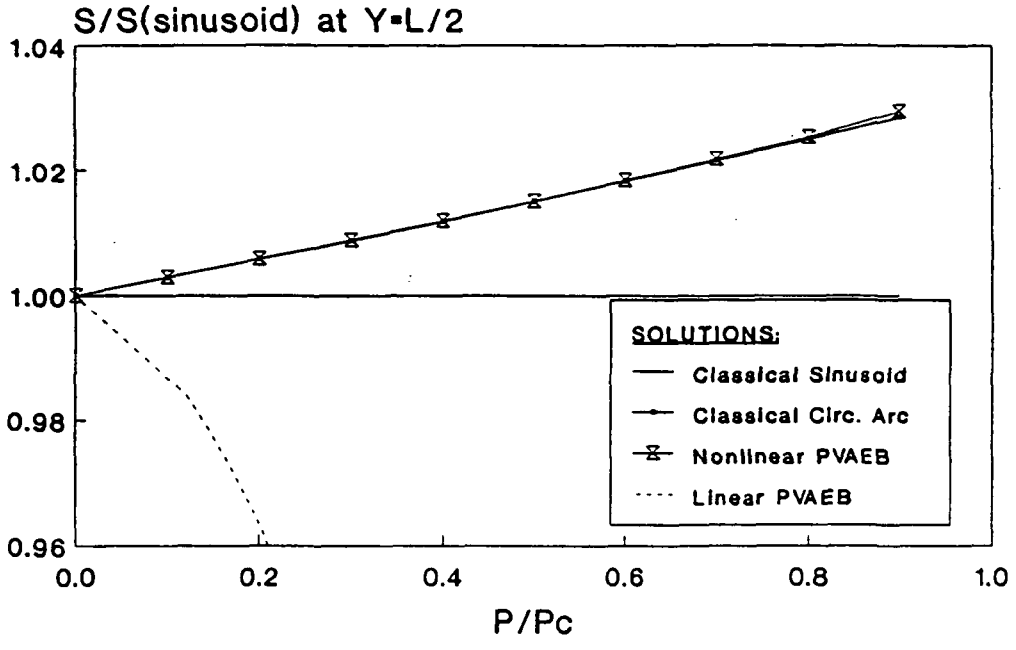

Figure 10.9 Midspan deflection versus axial load for the circular-bowed beam.

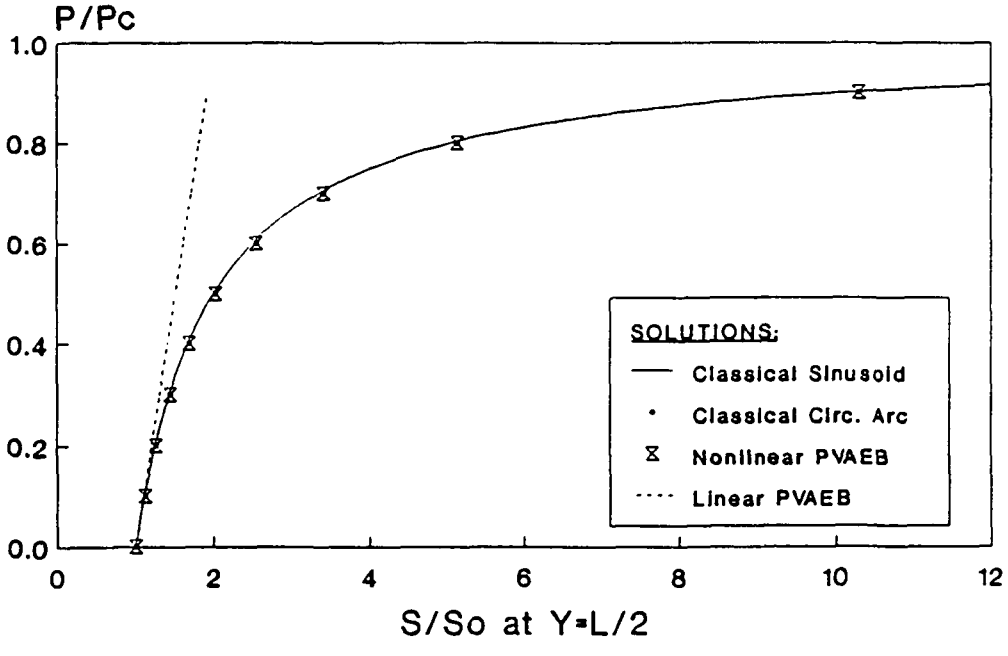

Figure 10.10 Axial load versus midspan deflection for the circular-bowed beam.

A collection of PVAEB results is provided in Table 10.7. F_x, F_y, and M_z are the *local* axial force, shear force, and bending moment, respectively, for the planar problem. The displacements ($\Delta_{X_M} \equiv S(L/2) - S_0(L/2)$ and Δ_{Y_T}) and rotation ($\theta_{Z_T} \equiv \theta - \theta_0$) listed are specified in the global frame. For the linear analyses, the axial and shear forces at the top of the beam are seen to converge via extension to:

$$(F_{x_T})_{LINEAR} = -P\cos\theta_0, \text{ and} \tag{10.31a}$$

$$(F_{y_T})_{LINEAR} = -P\sin\theta_0. \tag{10.31b}$$

The linear bending moment (with ST curvature approximation) at the midspan converges to:

$$(M_{z_M})_{LINEAR} = -PS_0\left(\tfrac{L}{2}\right). \tag{10.32}$$

$M_{z_T} \to 0$ for all cases since the beam is pinned, and $F_{x_M} \to -P$ for all cases since the local beam axes are parallel to the global axes at the midspan. Note that these values are independent of beam type.

The nonlinear results may only be confirmed once the small rotation (Section 2.2) and small axial strain (Section 6.2) assumptions are invoked. For example:

$$\begin{aligned}(F_{x_T})_{NONLINEAR} &= -P\cos\theta \\ &= -P\cos(\theta_0 + \theta_Z) \\ &= -P\left(\cos\theta_0\cos\theta_Z - \sin\theta_0\sin\theta_Z\right).\end{aligned} \tag{10.33}$$

The small rotation assumption implies:

$$(F_{x_T})_{NONLINEAR} \cong -P\left(\cos\theta_0 - \theta_Z\sin\theta_0\right), \tag{10.34}$$

while the small axial strain assumption further simplifies this to:

$$\begin{aligned}(F_{x_T})_{NONLINEAR} &\cong -P\cos\theta_0 \\ &\cong (F_{x_T})_{LINEAR}.\end{aligned} \tag{10.35}$$

Table 10.7 PVAEB results for the circular-bowed beam.

p[1]	Beam Type	CA[2]	NL#[3]	P/P_C[4]	Strain Energy (in-lb$_f$)	Top					Mid-Span		
						F_{x_T} (lb$_f$)	F_{y_T} (lb$_f$)	M_{z_T} (in-lb$_f$)	Δ_{Y_T} (in)	$\theta^{(5)}_{Z_T}$ (rad)	F_{x_M} (lb$_f$)	M_{z_M} (in-lb$_f$)	$\Delta^{(6)}_{X_M}$ (in)
3	BE	ST	0	0.5	16.0651	-1233.37	0.02632	-8.23E+2	-.026044	.016452	-1233.37	-822.138	.41114
5	BE	ST	0	0.5	18.7746	-1232.71	-49.3433	7.52E−2	-.030436	.016453	-1233.70	-1233.67	.51407
7	BE	ST	0	0.5	18.7746	-1232.71	-49.3283	-1.82E−6	-.030436	.016453	-1233.70	-1233.70	.51407
9	BE	ST	0	0.5	18.7746	-1232.71	-49.3283	2.0E−10	-.030436	.016453	-1233.70	-1233.70	.51407
∞	BE	ST	0	0.5	18.7746	-1232.71	-49.3283	0	-.030436	.016453	-1233.70	-1233.70	.51407
3	BE	ST	1	0.5	25.5155	-1233.83	0.04470	-1.40E+3	-.041364	.027943	-1233.14	-1396.43	.69836
3	BE	ST	2	0.5	25.5179	-1233.83	0.04470	-1.40E+3	-.041368	.027946	-1233.14	-1396.57	.69843
3	BE	ST	5*	0.5	25.5179	-1233.83	0.04470	-1.40E+3	-.041368	.027946	-1233.14	-1396.57	.69843
5	BE	ST	4*	0.5	34.9862	-1232.67	-101.593	5.99E+1	-.056717	.032680	-1233.68	-2480.24	1.0286
7	BE	ST	3*	0.5	34.9943	-1232.71	-89.2899	-7.82E+0	-.056731	.032684	-1233.70	-2504.41	1.0302
9	BE	ST	2*	0.5	34.9943	-1232.71	-89.6220	5.16E−3	-.056731	.032684	-1233.70	-2504.66	1.0302
∞	BE	ST	∞ *	0.5	34.9943	-1232.71	-89.6183	0	-.056731	.032684	-1233.70	-2504.66	1.0302
9	BE	ST	0	0.9	60.8296	-2218.89	-88.7909	3.7E−10	-.054785	.029616	-2220.66	-2220.66	.92533
9	BE	ST	3*	0.9	534.163	-2218.88	-738.273	2.84E−1	-0.48108	0.29261	-2220.66	-22860.7	9.2945
9	BE	TR	3*	0.9	534.076	-2218.88	-738.219	2.84E−1	-0.48101	0.29259	-2220.66	-22859.0	9.2938
9	BE	EX	3*	0.9	534.076	-2218.88	-738.218	2.84E−1	-0.48101	0.29259	-2220.66	-22859.0	9.2938
9	TI	ST	3*	0.9	535.464	-2218.89	-739.674	2.85E−1	-0.48226	0.29326	-2220.66	-22911.8	9.3175
9	TI	TR	3*	0.9	535.377	-2218.89	-739.619	2.85E−1	-0.48218	0.29324	-2220.66	-22910.1	9.3168
9	TI	EX	3*	0.9	535.377	-2218.89	-739.619	2.85E−1	-0.48218	0.29324	-2220.66	-22910.1	9.3167

(1) Refers to the polynomial order (p) for u_0 and v_0. For TI beams, the polynomial order for u_y is $p-1$.

(2) CA ≡ curvature approximation. Recall that all nonlinear terms are derived using the ST curvature approximation.

(3) NL# ≡ nonlinear iteration number. Zero denotes linear analysis; * denotes nonlinear error $\leq 10^{-12}$ (see (1.34)).

(4) $P = 1233.70$ lb$_f$ for $P/P_C = 0.5$; $P = 2220.66$ lb$_f$ for $P/P_C = 0.9$.

(5) $\theta_{Z_T} \equiv \theta - \theta_0$. See Figure 10.8.

(6) $\Delta_{X_M} \equiv S(\frac{L}{2}) - S_0(\frac{L}{2})$. See (10.23).

Similarly:

$$
\begin{aligned}
(F_{y_T})_{NONLINEAR} &= -P \sin\theta \\
&= -P \sin(\theta_0 + \theta_Z) \\
&= -P(\sin\theta_0 \cos\theta_Z + \cos\theta_0 \sin\theta_Z) \\
&\cong -P(\sin\theta_0 + \theta_Z \cos\theta_0) \\
&\cong (F_{y_T})_{LINEAR} + \theta_Z \, (F_{z_T})_{LINEAR} \, . \qquad (10.36)
\end{aligned}
$$

The nonlinear midspan bending moment (with ST curvature approximation) is simply:

$$
\begin{aligned}
(M_{z_M})_{NONLINEAR} &= -PS\left(\tfrac{L}{2}\right) \\
&= -P\left(S_0\left(\tfrac{L}{2}\right) + \Delta_{X_M}\right) . \qquad (10.37)
\end{aligned}
$$

The discretization error for the nonlinear forces and moments is more than that for comparable linear results at the same p-level, but still quite acceptable for the single element model with $p = 9$. Errors of idealization will dominate as $P \rightarrow P_C$ but cannot be discerned by p-extension.

Table 10.7 also displays results obtained by utilizing the various beam types and curvature approximations. All listed values are identical to at least three significant digits. The minute changes in the displacements and rotations are also reflected in the nonlinear forces and moments. The TI strain energies are slightly larger than their BE counterparts due to the inclusion of the shear strain energy. The TR and EX curvature approximations produce virtually identical results. All of these results are to be expected for the long, shallow geometry of the problem, but they help confirm the proper formulation and execution within PVAEB.

The nonlinear iteration error (1.34) versus nonlinear iteration number is plotted in Figure 10.11 for various p-levels and load amplitudes. As expected, more

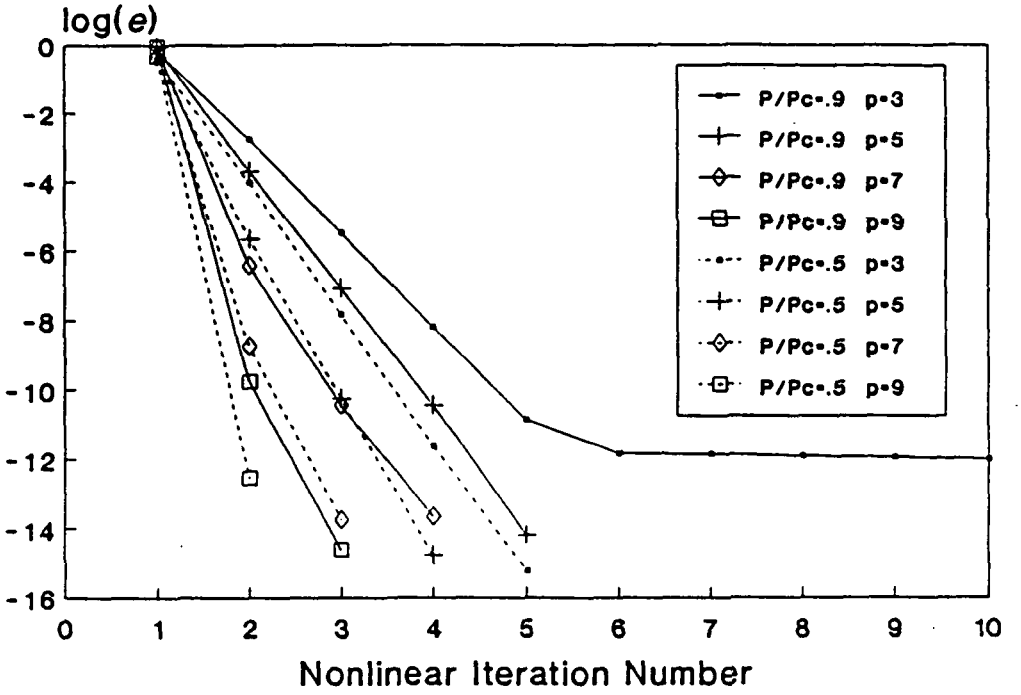

Figure 10.11 Convergence of nonlinear strain energy for the circular-bowed beam.

iterations are required to achieve the 10^{-12} threshold tolerance as the load increases. However, the figure also shows faster convergence for increasing p-levels. This trend has been seen in a variety of PVAEB analyses. Computational efficiency for nonlinear problems is typically enhanced by p-extensions in comparison with h-version models having the same number of degrees-of-freedom.

The PVAEB model for the circular bowed beam in Table 10.6 increases the polynomial order ($p_1 = p_2 \equiv p$) by two for each extension. At times there is strong justification for this approach. Table 10.8 displays the error estimates generated from two separate analyses of the same problem, one using only the odd polynomial orders while the other uses all polynomial orders. Note that the nonlinear strain energy for the all p-level analysis is not monotonic, thus invoking the less

Table 10.8 Effect of skipping polynomial orders on error estimates.

BEAM WITH AN INITIAL CIRCULAR BOW
So(L/2) = 0.01L, P/Pc = 0.5

BEAM = BE, ANALYSIS = ST
NONLIN = -12, LOAD = 100, CIRC = ST

ERROR ESTIMATES: ODD p-LEVELS ONLY

		LINEAR			CONVERGENCE EXPONENT		% EST. ERROR IN ||V||	
p	#DOF	STRAIN ENERGY	EXTRAPOLATED ENERGY	DELTA ENERGY	RUNNING	CUMULATIVE	RUNNING	CUMULATIVE
3	5	0.16065056543127E+02	0.00000000000000E+00	0.00000000E+00	0.0000	0.0000	0.0000	37.9893
5	9	0.18774577950246E+02	0.19984185721281E+02	0.27095214E+01	2.0000	32.6455	24.6025	0.0026
7	13	0.18774577962818E+02	0.18774577962818E+02	0.12572000E-07	0.0000	0.0000	0.0000	0.0000
9	17	0.18774577962818E+02	0.18774577962818E+02	0.00000000E+00	0.0000	0.0000	0.0000	0.0000

		NONLINEAR			CONVERGENCE EXPONENT		% EST. ERROR IN ||V||		
p	#DOF	STRAIN ENERGY	EXTRAPOLATED ENERGY	DELTA ENERGY	RUNNING	CUMULATIVE	RUNNING	CUMULATIVE	NL#
3	5	0.25517880060715E+02	0.00000000000000E+00	0.00000000E+00	0.0000	0.0000	0.0000	52.0384	5*
5	9	0.34986151939639E+02	0.39213059028444E+02	0.94682719E+01	2.0000	12.0029	32.8319	1.5287	4*
7	13	0.34994328737323E+02	0.34994429742107E+02	0.81767977E-02	11.9822	24.8036	0.1699	0.0160	3*
9	17	0.34994329630458E+02	0.34994329631609E+02	0.89313500E-06	24.8095	24.8095	0.0006	0.0006	2*

ERROR ESTIMATES: ALL p-LEVELS

		LINEAR			CONVERGENCE EXPONENT		% EST. ERROR IN ||V||	
p	#DOF	STRAIN ENERGY	EXTRAPOLATED ENERGY	DELTA ENERGY	RUNNING	CUMULATIVE	RUNNING	CUMULATIVE
3	5	0.16065056543127E+02	0.00000000000000E+00	0.00000000E+00	0.0000	0.0000	0.0000	37.9893
4	7	0.18716819500190E+02	0.21479072580464E+02	0.26517630E+01	2.0000	11.4371	35.8611	5.5465
5	9	0.18774577950246E+02	0.18778200733918E+02	0.57758450E-01	11.2602	61.0403	1.3890	0.0026
6	11	0.18774577962775E+02	0.18774577962775E+02	0.12529000E-07	0.0000	28.2953	0.0000	0.0002
7	13	0.18774577962818E+02	0.18774577962818E+02	0.42999826E-10	0.0000	0.0000	0.0000	0.0000
8	15	0.18774577962818E+02	0.18774577962818E+02	0.00000000E+00	0.0000	0.0000	0.0000	0.0000
9	17	0.18774577962818E+02	0.18774577962818E+02	0.00000000E+00	0.0000	0.0000	0.0000	0.0000

		NONLINEAR			CONVERGENCE EXPONENT		% EST. ERROR IN ||V||		
p	#DOF	STRAIN ENERGY	EXTRAPOLATED ENERGY	DELTA ENERGY	RUNNING	CUMULATIVE	RUNNING	CUMULATIVE	NL#
3	5	0.25517880060715E+02	0.00000000000000E+00	0.00000000E+00	0.0000	0.0000	0.0000	52.0384	5*
4	7	0.37043127578933E+02	0.49048593743743E+02	0.11525248E+02	2.0000	4.5518	49.4739	24.1964	15*
5	9	0.34986151939639E+02	0.31836407991970E+02	-0.20569756E+01	2.0000	21.9792	31.4540	1.5286	4*
6	11	0.34995849497413E+02	0.35015487051905E+02	0.96975578E-02	2.0000	8.3827	2.3682	0.6592	7*
7	13	0.34994328737323E+02	0.34990495154596E+02	-0.15207601E-02	2.0000	58.6470	1.0467	0.0049	3*
8	15	0.34994329860453E+02	0.34994333249899E+02	0.11231300E-05	2.0000	-17.5272	0.0311	0.0172	4*
9	17	0.34994329630458E+02	0.34994328821882E+02	-0.22999500E-06	2.0000	2.0000	0.0152	0.0152	2*

NOTE: NL# = NONLINEAR ITERATION NUMBER; * DENOTES NONLINEAR ERROR <= 10**12 (SEE (1.34)).

accurate quadratic error estimator. Also note that the number of nonlinear iterations required for convergence is larger for the even polynomial subcases (though the number still decreases as p increases). Therefore, skipping polynomial orders is beneficial for some nonlinear problems even when symmetric/antisymmetric biasing is not present.

The second problem illustrated in Figure 10.8 possesses an initial shape that is predominantly third-harmonic with:

$$L_1 = 34.0 \text{ in}, \tag{10.38a}$$

$$R_1 = 145.00 \text{ in, and} \tag{10.38b}$$

$$R_2 = 134.47 \text{ in.} \tag{10.38c}$$

The geometry is specified such that the adjoining circular arcs are tangent, although this is not required. The Fourier series for the initial shape is:

$$\begin{aligned} S_0(Y) = \Big(& 0.0570 \sin\left(\tfrac{\pi Y}{L}\right) \\ & +1.0118 \sin\left(\tfrac{3\pi Y}{L}\right) \\ & -0.0152 \sin\left(\tfrac{5\pi Y}{L}\right) \\ & +0.0063 \sin\left(\tfrac{7\pi Y}{L}\right) \\ & +\ldots\Big) \text{ in.} \end{aligned} \tag{10.39}$$

Thus, the midspan deflection ($\Delta_{X_M} \equiv S\left(\frac{L}{2}\right) - S_0\left(\frac{L}{2}\right)$) will start out negative as the load is applied. However, amplification of the first harmonic as $P \to P_C$ will cause the midspan deflection to go positive. The classical solution is illustrated in Figure 10.12 along with PVAEB results using BE beams with the ST curvature approximation. Again, the classical and nonlinear PVAEB solutions are in excellent agreement while the linear PVAEB results are completely erroneous.

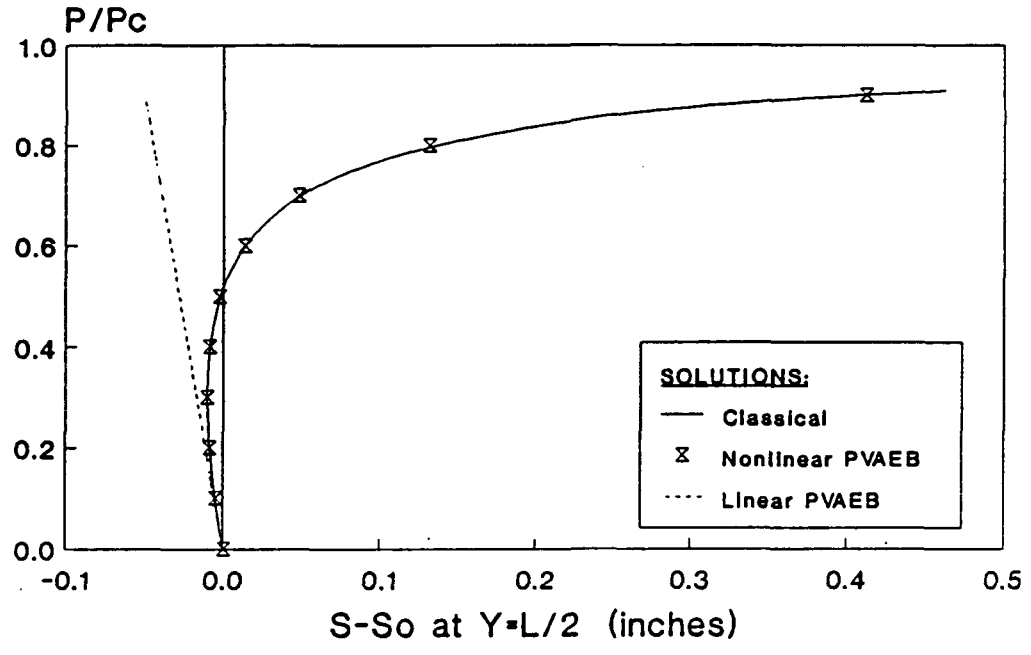

Figure 10.12 Load/displacement relationship for the beam with a predominantly third-harmonic imperfection.

11. THE DARRIEUS VERTICAL-AXIS WIND TURBINE

The Darrieus vertical-axis wind turbine (VAWT) is the primary motivation behind this research. All of the capabilities incorporated into the PVAEB formulations have a direct and significant effect on this class of structure. Furthermore, the history of the development of VAWT structural analysis provides enlightening examples of errors in idealization and discretization.

The vertical-axis wind turbine addressed in this study is named for the French mathematician, G. J. M. Darrieus. United States Patent Number 1,835,018 was issued to him in 1931 for a "turbine having its rotating shaft transverse to the flow of current" [104].* Figure 11.1 illustrates the typical configuration for a modern Darrieus VAWT. This particular machine is over 100 feet tall with a 63-foot (19-meter) equatorial diameter. The rotor is supported by two bearing assemblies, one located in the base structure and the other mounted on top of the rotor and anchored to the ground via guy cables. The airfoil-shaped blades on this particular VAWT are extruded aluminum, although wood, steel, and composite blades have been used on other machines. The mast is fabricated from thin-walled steel pipe and must provide lateral and vertical support for the blades, transfer torque from the blades to the drivetrain, and resist the axial thrust load induced by the guy cables. Horizontal struts are attached between the blades and mast to improve the lateral support and torque transfer.

VAWT's are as technically different from conventional horizontal-axis wind turbines (HAWT's) as they are visually. The vertical spin axis allows extraction of wind power from any direction without yawing. Peak power is aerodynamically regulated without the use of pitch controls. The ground-based drivetrain

* The *first* windmills, believed to have been used by the Persians over 2000 years ago to grind grain, utilized a vertical spin axis.

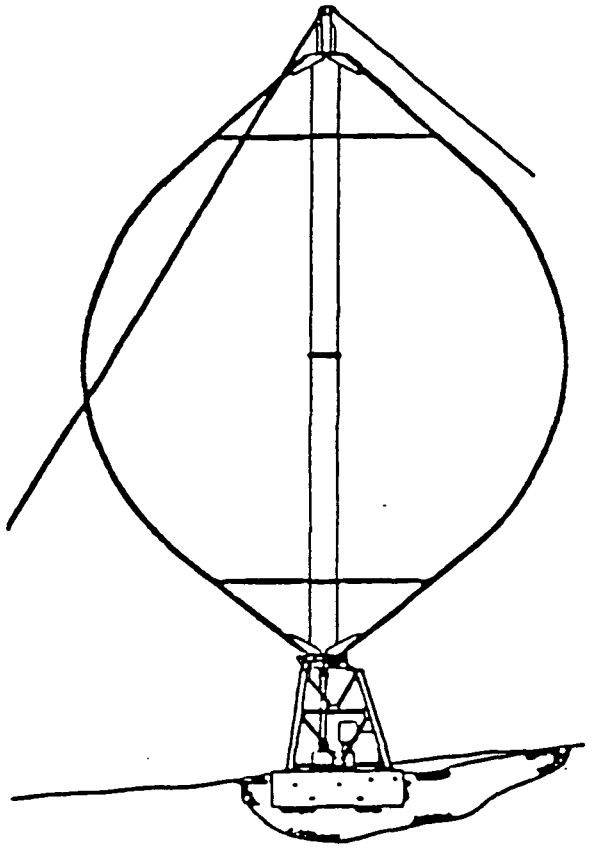

Figure 11.1 The FloWind-19 vertical-axis wind turbine.

components significantly reduce design and installation costs and simplify maintenance. Also, vertical-axis wind turbines are *theoretically* more efficient than their horizontal-axis counterparts since the blades pass through the wind twice (upwind and downwind relative to the mast) for each revolution of the rotor. All of these attributes make VAWT's cost competitive with horizontal-axis machines in spite of the relatively small investment in research.

Wind energy in the United States was primarily used for pumping water and generating direct-current, battery-stored electricity in rural environments prior to the proliferation of utility grids. The notion of generating electricity for utility applications via the wind progressed slowly during the era of cheap fossil

fuels. The oil crisis of the 1970's produced renewed interest in alternative energy sources. The United States federal wind energy program commenced in 1973 under the direction of the National Science Foundation. This program was later transferred to the Energy Research and Development Agency and eventually to the Department of Energy (DOE). The program's goal was to accelerate all aspects of wind energy technology leading to cost-effective production of electric power.

VAWT development was initiated in 1974 at Sandia National Laboratories, Albuquerque, New Mexico and still continues. Canada instituted VAWT research in 1972 through their National Research Council. Early research focused on proof-of-concept issues since the Darrieus configuration remained relatively undeveloped after issuance of the initial patent. Several wind tunnel and small full-scale turbines were built, culminating in 1977 with the construction of a 17-meter (equatorial diameter) test machine in Albuquerque. This was the first VAWT to undergo major structural testing.

A troposkien (turning rope) blade geometry produces purely tensile stresses in a rotating blade [105]. This ideal shape is often approximated by a series of straight and/or circular segments for manufacturing ease. Geometric nonlinearities were recognized early in the development as having a significant effect on the bending stresses in nontroposkien blades as well as on the in-plane (flatwise) blade bending frequencies [106]. Both MARC [107] and NASTRAN [108] finite element analyses proved quite effective in predicting the nonlinear static blade stresses. A single-blade model was used in these two analyses, with appropriate rigid constraints imposed to represent the mast and strut connections. Centrifugal softening was recognized but not incorporated into the formulations.

Test data from the DOE/Sandia 17-meter VAWT also identified rotation-induced changes in the natural frequencies and mode shapes. Coriolis coupling of in-plane and out-of-plane modes was readily apparent. Without the inclusion of rotating coordinate system effects, the errors in idealization would render eigensolutions for rotating VAWT's completely erroneous. Recall that extensions of finite element models provide no insight into this type of error.

The first attempt at VAWT dynamic analysis with rotation was VAWTDYN [109]. The VAWTDYN model consisted of a limited degree-of-freedom, rigid-linked, spring-connected representation with provisions for Coriolis coupling and centrifugal softening. The spring and link variables were adjusted to match frequencies from a real finite element eigenanalysis with geometric nonlinearities. Uncertainties were not quantifiable, but they proved to be unacceptable in the evaluation of the DOE 100-kW VAWT [110]. Numerous structural modifications were necessary to correct a severe resonance condition in the original configuration of this machine.

The FEVD (Finite Element VAWT Dynamics) analytical capability and the experimental verification outlined in [27] was borne out of the VAWTDYN experience. FEVD demonstrated that the VAWTDYN formulation was theoretically correct but that the number of degrees-of-freedom was insufficient to accurately predict the interaction of geometric nonlinearities, centrifugal softening, and Coriolis coupling. That is, errors in discretization caused VAWTDYN to fail.

FEVD is a modified NASTRAN-based capability specifically tailored for VAWT analyses. In comparison with PVAED, FEVD is limited by the following attributes:

1) the FEVD spin axis is assumed to coincide with the global Z-axis;

2) FEVD elements are straight, h-version, Bernoulli-Euler beams;
3) centrifugal softening is not included during the iterative solution of the nonlinear static problem (1.36) but only incorporated into the dynamic eigenproblem (1.37);
4) the number of nonlinear iterations in FEVD must be explicitly specified by the user without knowledge of strain energy convergence (1.34);
5) the number of degrees-of-freedom must be statically condensed to sixty or less for complex eigensolutions within FEVD with no measure of the condensation error (which may be easily performed using a variation of (8.28)); and
6) no provision for discretization error estimation is provided in FEVD.

Thus, PVAEB eliminates numerous uncertainties associated with the FEVD capability. These shortcomings will be addressed via analyses of the turbine illustrated in Figure 11.1

The finite element model for the FloWind-19 VAWT is displayed in Figure 11.2. All of the physical properties are extracted from a comparable FEVD analysis for direct comparison. Note that only the rotor is modeled: the guy cables are replaced by a set of equal, orthogonal, linear springs in the horizontal plane coupled with an axial thrust load, while the base structure is assumed infinitely rigid. Insufficient information is available to quantify the idealization error associated with the rigid-base assumption. The drivetrain flexibility is modeled with a torsional spring attached to the bottom of the mast. Note that the stationary constraints are symmetric such that the rotor natural frequencies are independent of position regardless of the rotational speed.

Each blade of the FloWind-19 is fabricated from three lengths of raw, straight, extruded aluminum blade material. The circular segments are produced by an incremental bending operation which introduces plastic deformations and

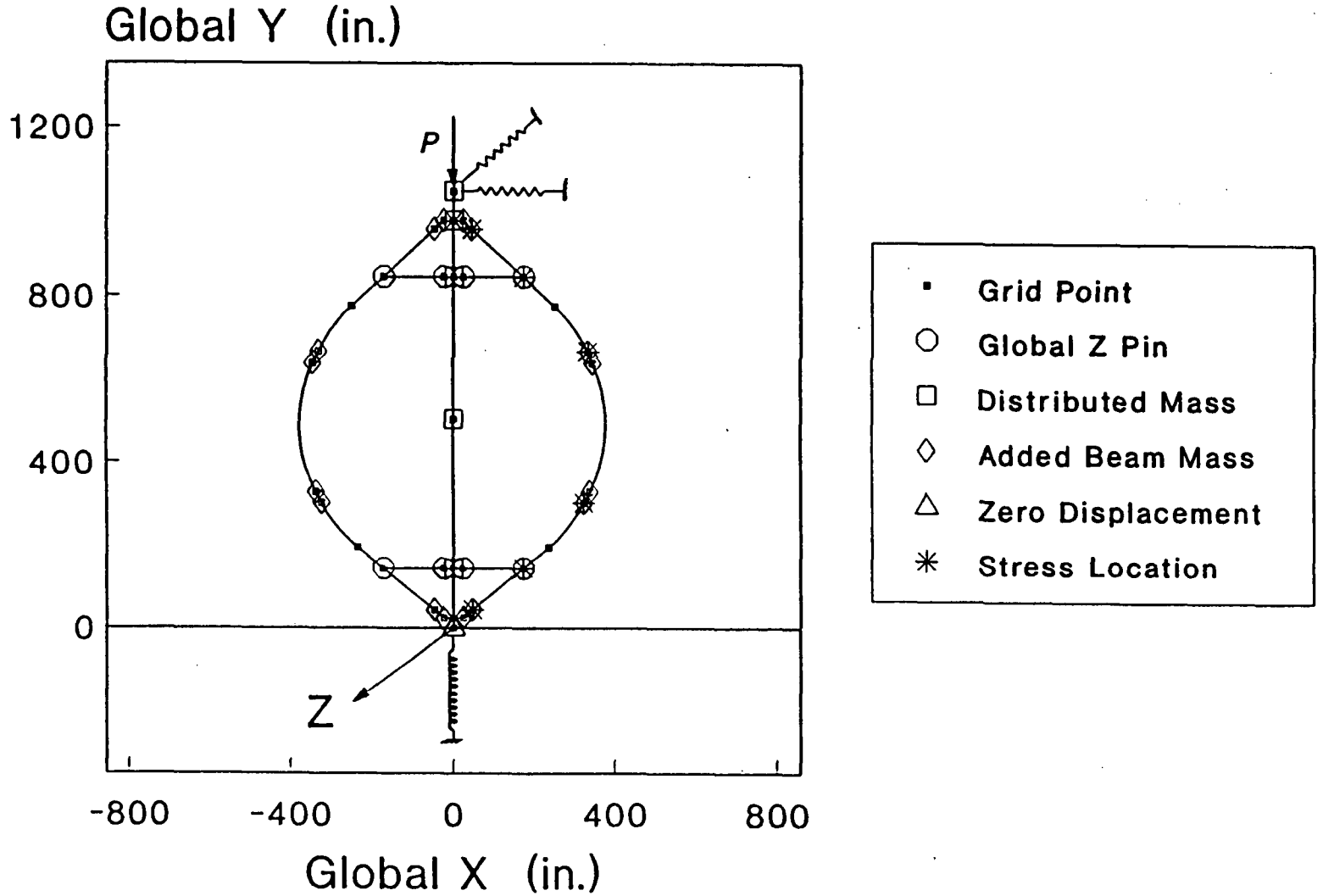

Figure 11.2 PVAEB model for the FloWind-19 VAWT.

residual stresses into the blade. The center blade section is completely circular except for short straight segments at each end for the blade-to-blade joints. The upper and lower segments are straight except for segments adjacent to the blade-to-blade joints. Thus, connection-induced stress concentrations never interact with the residual stresses in the circular segments. The blade-to-blade joints are flagged in Figure 11.2 by the added beam mass (and stiffness) used in their idealization. The connections between the blades and mast, termed blade roots, include the added mass and stiffness of mounting hardware.

The mast is modeled in PVAEB using six elements, with distributed masses used to characterize the flanges and bearings. Note that eight pseudo-rigid outrigger elements are used at the blade-to-mast and strut-to-mast interfaces to accurately model the mast diameter. If implemented into PVAEB, rigid links could accurately represent these outrigger elements and reduce the number of degrees-of-freedom (because they would be independent of p-extension). The struts are connected to the mast and blade with global Z pins to model the flexible steel plates used in their attachment.

The resulting PVAEB model requires 35 grid points and 40 elements (34 straight and 6 circular) to exactly capture the model geometry. With $n_P = 8$, $n_C = 3$, and specifying $p \equiv p_1 = p_2 = p_3 = p_4 + 1 = p_5 + 1 = p_6 + 1 \geq 2$, the resulting number of degrees-of-freedom is (7.49,76):

$$\begin{aligned} n_{BE/RA} &= (35 \times 6) + 8 + (40 \times (4p - 9)) - 3 \\ &= 160p - 145, \end{aligned} \tag{11.1}$$

or:

$$\begin{aligned} n_{TI} &= (35 \times 6) + 8 + (40 \times (6p - 9)) - 3 \\ &= 240p - 145, \end{aligned} \tag{11.2}$$

where the subscripts denote the type of beam idealization. In comparison, the FEVD model contains 115 grid points and 120 straight BE elements ($p_1 = p_4 \equiv 1$, $p_2 = p_3 \equiv 3$) such that:

$$n_{FEVD} = (115 \times 6) + 8 - 3$$

$$= 695. \tag{11.3}$$

Therefore, the number of degrees-of-freedom is smaller for the PVAEB model in comparison with the FEVD model only when $p = 5$ for BE/RA idealizations and $p = 3$ for TI idealizations. Still, the significant decrease in the number of grid points and elements for the PVAEB model greatly simplifies the mesh generation procedure. Separate specification of the polynomial orders for straight and circular elements would be beneficial in this instance.

One of the first concerns in the analysis of VAWT's is the rotation-induced static blade stresses. Since the spin axis lies in the plane of the blades, these stresses are generated entirely from tension and in-plane bending. Figure 11.3 plots the linear and nonlinear PVAEB flatwise stresses at operating speed for the innermost and outermost fibers of the blade. The stresses are plotted as a function of blade span from top to bottom. The effects of gravity and centrifugal softening are included in the BE:ST beam idealization with $p = 9$. The added stiffness of the blade roots and blade-to-blade joints induce the discontinuities seen in the stresses. The locations of the blade-to-strut connections are identified by the darkened symbols. These results are obtained from a full-rotor model such that the minor effects of mast and strut deformation are included.

The most apparent observation from this figure is the significant reduction of bending stresses due to tensile stiffening. Peak stresses are analytically reduced by nearly 18 percent with the inclusion of geometric nonlinearities. The peak

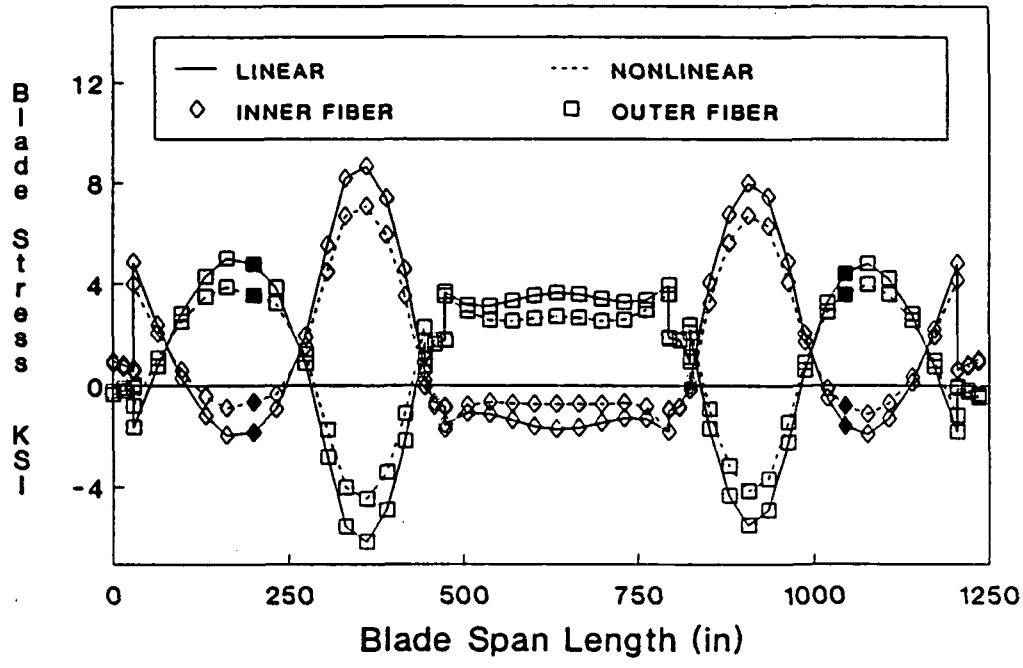

Figure 11.3 FloWind-19 static blade stresses at 52 rpm.

stresses occur in regions devoid of stress concentration; connections at the roots, struts, and joints all experience the same approximate stress levels. This is not mere coincidence. Numerous iterations of the blade geometry were performed to achieve this desired state. Though not apparent, the blade geometry is not symmetric about the equator. A slight droop is incorporated to account for the effects of gravity and to balance the stresses experienced in the upper and lower blade sections. Note that the maximum blade rotation from the undeformed to the deformed position is only 0.021 radians, thus validating the use of small-rotation theory.

Table 11.1 compares the blade stresses at strategic joint locations along the blade (flagged in Figure 11.2) for a variety of analytical assumptions. As expected, beam type and curvature approximation are seen to have little effect on these long, gently curving blades. In fact, the ST curvature approximation

Table 11.1 Comparison of FloWind-19 static blade stresses at 52 rpm.

Beam Type	CA[1]	Linear/ Nonlinear	Centrifugal Softening?	Loc.[2]	Stress (ksi)					
					Upper Root	Upper Strut	Upper Joint	Lower Joint	Lower Strut	Lower Root
TI	TR	Nonlinear	Yes	O	-817	3586	2283	2396	3604	-1190
				C	1588	1475	1140	1124	1396	1482
				I	3992	-636	-1576	-163	-811	4155
BE	TR	Nonlinear	Yes	O	-829	3595	2284	2398	3613	-1204
				C	1588	1475	1142	1126	1396	1483
				I	4004	-644	-14	-162	-820	4169
BE	ST	Nonlinear	Yes	O	-829	3595	2294	2409	3614	-1204
				C	1588	1475	1139	1123	1397	1483
				I	4004	-644	-16	-163	-821	4170
BE	ST	Linear	Yes	O	-1702	4907	1655	2061	4468	-1848
				C	1609	1488	1144	1128	1408	1502
				I	4920	-1931	634	195	-1651	4852
BE	ST	Linear	No	O	-1657	4805	1728	2078	4432	-1835
				C	1605	1485	1142	1125	1405	1498
				I	4867	-1834	556	172	-1621	4831
BE	ST	Nonlinear	No	O	-811	3545	2324	2422	3586	-1196
				C	1585	1474	1137	1121	1394	1480
				I	3981	-596	-50	-180	-798	4156
NASTRAN (BE/ST/Nonlinear/No Soft)				O	-648	3604	2248	2349	3664	-1111
				C	1594	1479	1168	1150	1399	1476
				I	3835	-646	87	-50	-866	4064

[1] CA ≡ curvature approximation. [2] Locations: O ≡ outer fiber, C ≡ centroid, I ≡ inner fiber.

might indeed be considered the more accurate assumption in light of the method used to fabricate the circular segments. The effect of geometric nonlinearities produces the most significant differences. Ignoring centrifugal softening causes only minor changes in the blade stresses for *this* turbine due to its relatively stiff design. This is the first known time that the effect of centrifugal softening on blade stresses has been quantified.

Comparison of equivalent PVAEB and NASTRAN analyses deserves further scrutiny. The PVAEB model uses 11 elements per blade, excluding outriggers and struts, to capture the exact geometry. By (at most) $p = 9$, all stresses have converged to the values listed in the table. Six nonlinear iterations are required at $p = 9$ for automatic convergence of the strain energy to one part in 10^{12} (i.e., NONLIN=−12 is specified in the PVAEB input). The FEVD/NASTRAN analysis uses rule-of-thumb assumptions developed from previous sensitivity studies: 40 (straight) elements per blade and four nonlinear iterations. Granted, $n_{BE}|_{p=9} = 1295$ is nearly double n_{FEVD} and the accuracy of the FEVD stresses may be viewed as acceptable now that accurate PVAEB results are available for comparison. However, the quantification of error via p-extension without the arduous, user-intensive process of mesh refinement easily justifies the additional computational costs.

Figure 11.4 illustrates the front, top, and side views of the mode shapes for the six lowest natural frequencies of the nonrotating FloWind-19. The modal nomenclature, defined in terms of these nonrotating shapes, diminishes in physical significance as the modes become rotationally coupled. The natural frequencies listed are for the TI:TR beam idealization with the inclusion of the nonlinear effects from gravity and guy cable thrust. The first propeller mode, P 1, involves pseudo-rigid rotation of the rotor inertia on the drivetrain spring. The butterfly

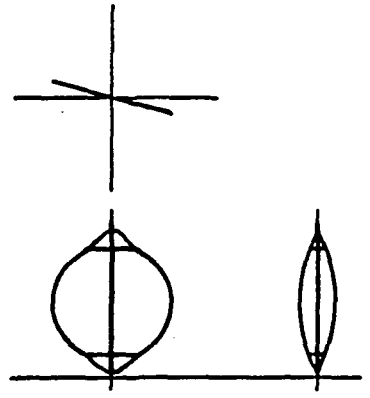

First Propeller
(P 1) f = 0.694 Hz

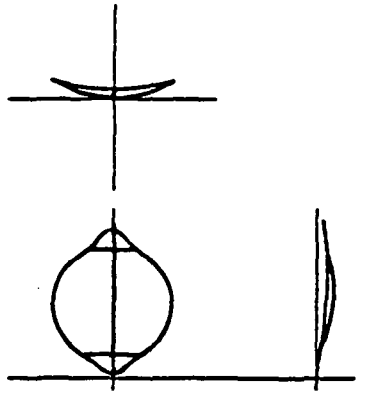

First Butterfly
(B 1) f = 2.443 Hz

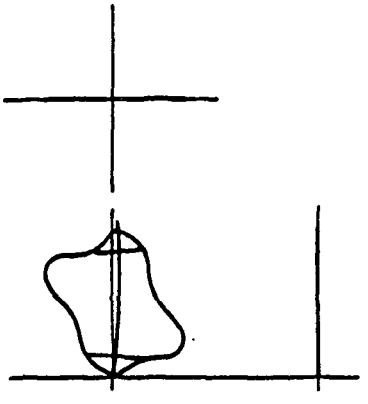

First Antisymmetric Flatwise
(FA 1) f = 2.477 Hz

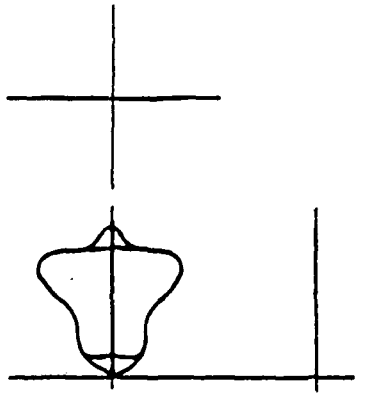

First Symmetric Flatwise
(FS 1) f = 2.499 Hz

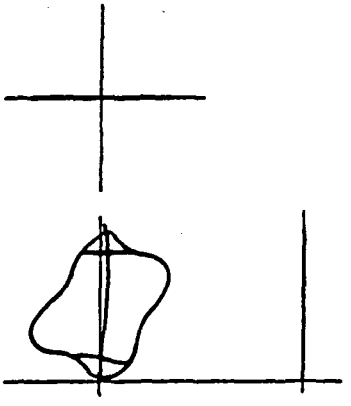

First Tower
(T 1) f = 3.070 Hz

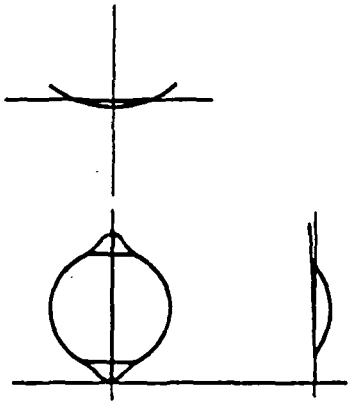

Second Butterfly
(B 2) f = 4.296 Hz

Figure 11.4 FloWind-19 mode shapes and natural frequencies at zero rpm.

modes, B 1 and B 2, are out-of-plane motions dominated by the tower height and stiffness/mass and the guy cable stiffness; they are also affected by the out-of-plane (lead-lag) blade stiffness/mass and the strut stiffness and location. The first tower mode, T 1, is the in-plane equivalent to the first butterfly mode, with similar rotor features governing the natural frequency. The first pair of flatwise blade modes, FA 1 and FS 1, are dominated by the in-plane (flatwise) blade stiffness/mass and the strut location.

Figure 11.5 displays the same six modes for the FloWind-19 at its nominal operating speed. Three-views of both the real and imaginary (90° phase) components of the complex eigenvector are displayed, as seen in the global frame. Recall that the global frame rotates with the rotor relative to the stationary inertial frame. However, the 90° phase is defined in terms of the natural frequency for each mode and *not* the rotational speed. The 90° phase for the nonrotating modes in Figure 11.4 is merely the undeformed shape since the eigenvectors are entirely real and the static deformations are not included in the dynamic eigenvectors. The most noticable change from the nonrotating to rotating mode shapes is the coupling of the "butterfly" and "tower" motions.

The rotation-induced changes in natural frequencies are best viewed via the Campbell diagram, or "fan plot," in Figure 11.6. The first propeller frequency changes very little with rotational speed. The first butterfly and tower frequencies split in a manner similar to the axially rotating shaft of Section 10.2; this concurs with the mode shape observations. The flatwise modes exhibit higher natural frequencies as the rotational speed increases; this is primarily the result of tension stiffening.

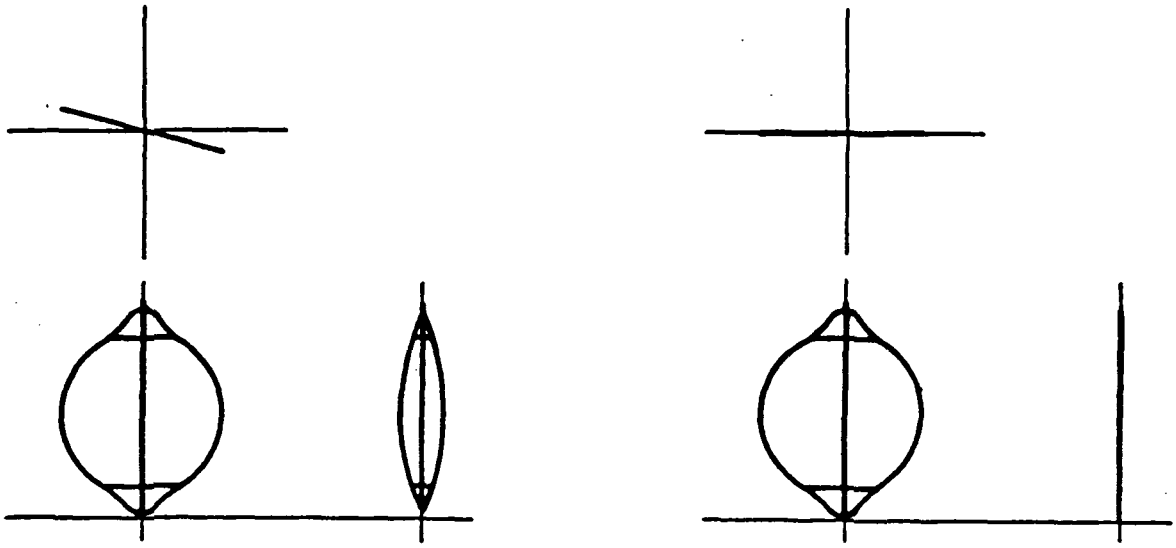

Real Component

Imaginary Component

First Propeller
(F 1) f = 0.696 Hz

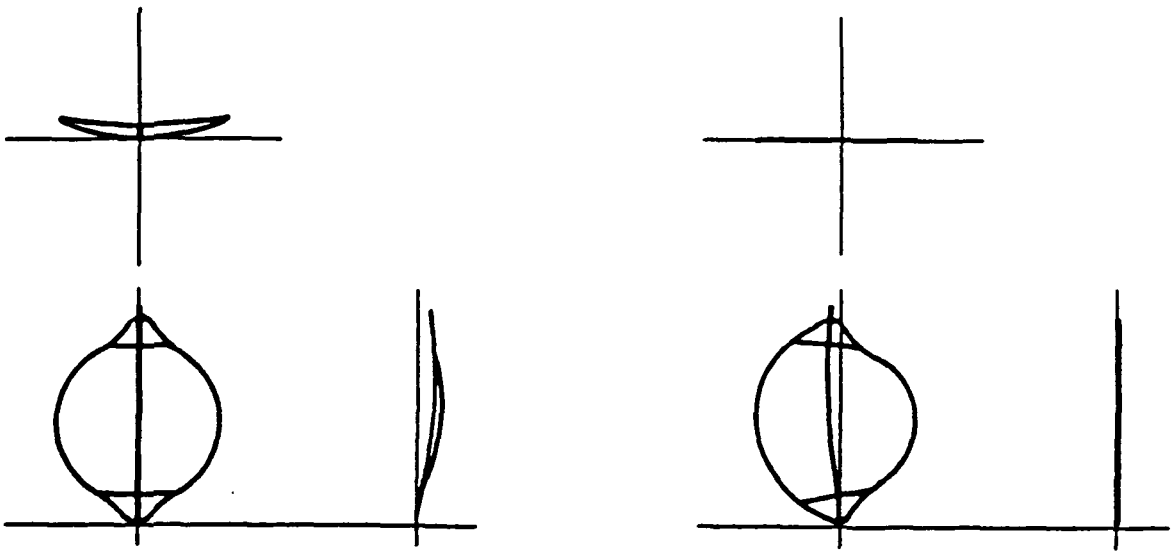

Real Component

Imaginary Component

First Butterfly
(B 1) f = 2.026 Hz

Figure 11.5 FloWind-19 mode shapes and natural frequencies at 52 rpm.

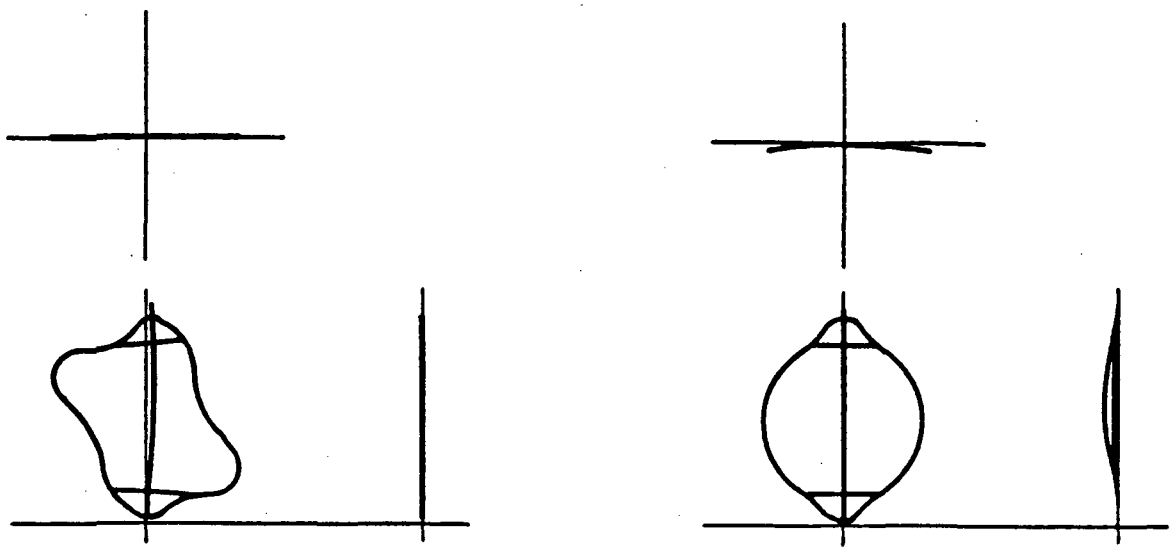

Real Component Imaginary Component

First Antisymmetric Flatwise
(FA 1) f = 3.034 Hz

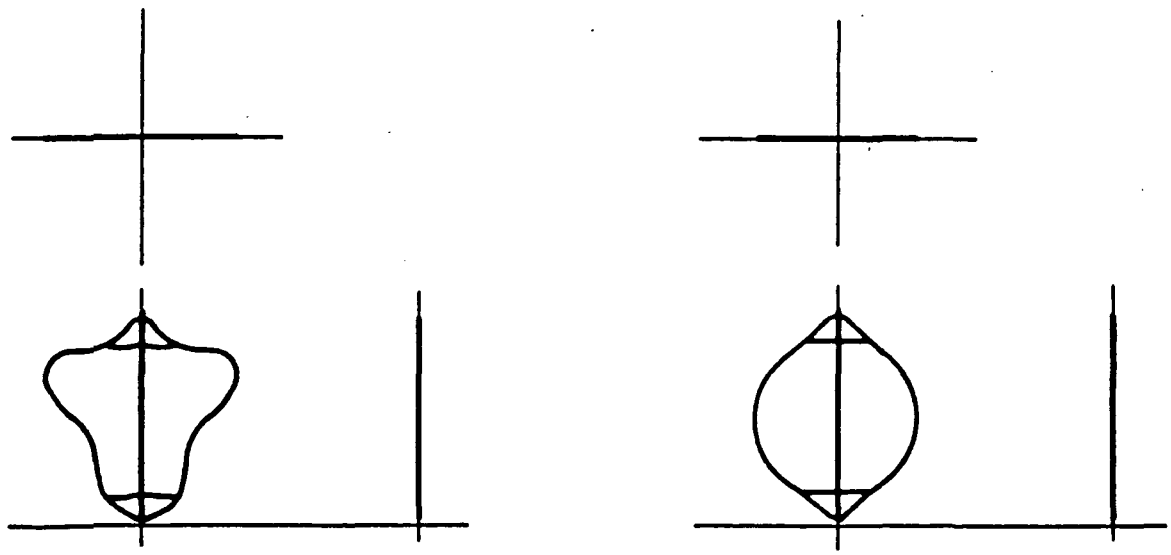

Real Component Imaginary Component

First Symmetric Flatwise
(FS 1) f = 3.059 Hz

Figure 11.5 FloWind-19 mode shapes and natural frequencies at 52 rpm (continued).

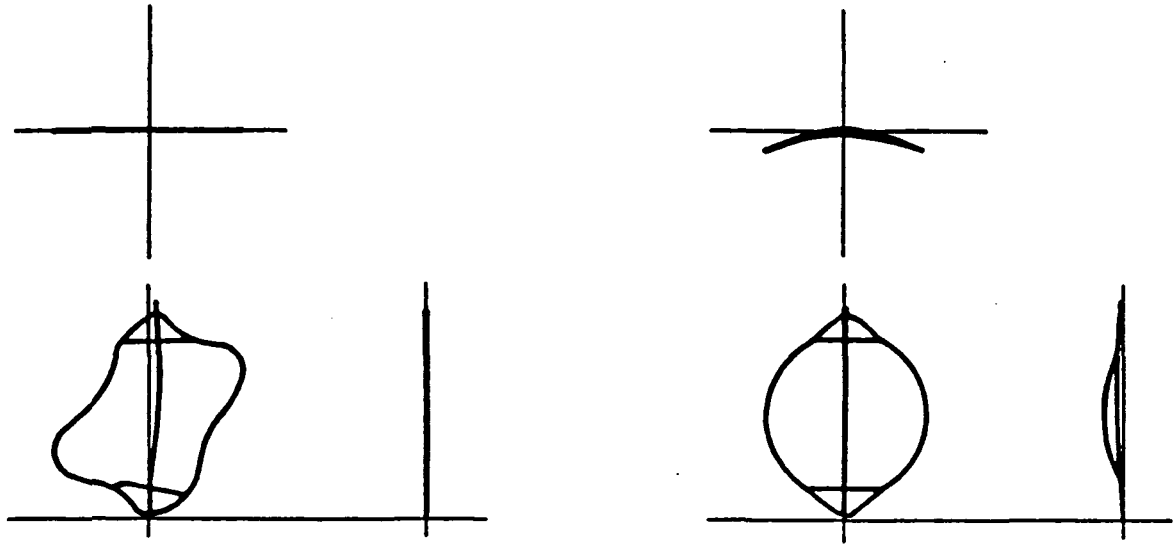

Real Component Imaginary Component

First Tower
(T 1) f = 3.276 Hz

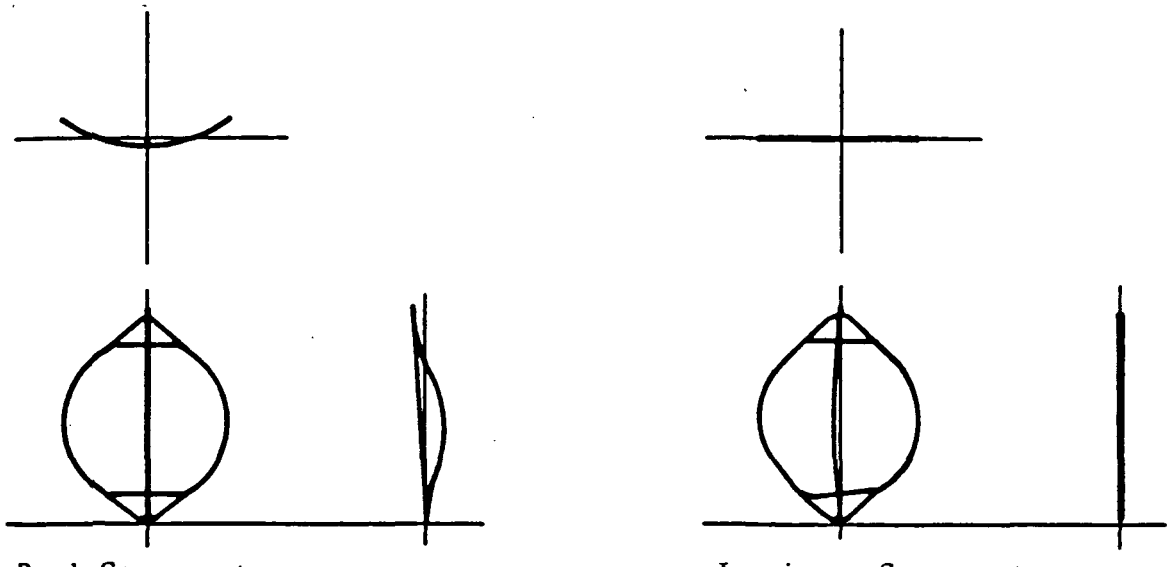

Real Component Imaginary Component

Second Butterfly
(B 2) f = 4.617 Hz

Figure 11.5 FloWind-19 mode shapes and natural frequencies at 52 rpm (continued).

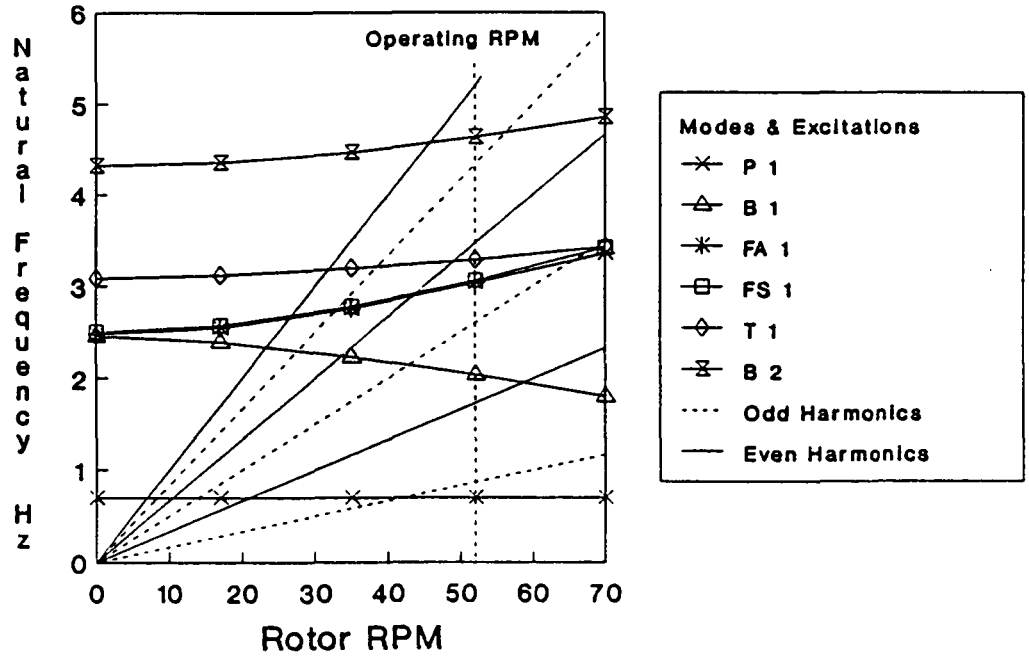

Figure 11.6 Natural frequency versus rotor rpm for the FloWind-19 VAWT.

Figure 11.6 also contains dashed and solid lines emanating from the origin. These lines represent odd and even harmonics, respectively, of the rotor rotational speed. For steady-state conditions (i.e., constant rotor rpm and constant windspeed *and* wind direction), these lines also represent the aerodynamic excitation frequencies. In general, resonance problems are likely to occur where symmetric modes (P 1, FS 1, etc.) cross even excitation frequencies and where antisymmetric modes (B 1, FA 1, T 1, B 2, etc.) cross odd excitation frequencies. The three-per-rev crossing of the first tower mode produced the serious resonance problem experienced by the DOE 100-kW VAWT. Note that the natural frequencies and excitation frequencies are well separated at the nominal operating speed for this turbine. Again, this is the product of numerous design iterations, where various rotor parameters are adjusted to "tune" the rotor to this dynamically inert state.

Table 11.2 Effect of idealization parameters on strain energy and natural frequencies.[1]

Case	Linear/ Nonlinear	Centrifugal Softening?	Coriolis Coupling?	Strain Energy (in-lb$_f$)	Natural Frequency (Hz)					
					P 1	B 1	FA 1	FS 1	T 1	B 2
1	Nonlinear	Yes	Yes	7020	0.695	2.223	2.749	2.772	3.186	4.448
2	Nonlinear	No	Yes	7001	0.904	2.284	2.775	2.799	3.237	4.484
3	Nonlinear	Yes	No	7020	0.695	2.411	2.763	2.793	3.046	4.315
4	Linear	Yes	Yes	7443	0.382	2.222	2.434	2.450	3.166	4.414
5	Linear	No	No	7443	0.694	2.468	2.476	2.499	3.108	4.306

[1] FloWind-19: 35 rpm, TI beam, TR curvature approximation. Underlined values denote errors of more than two percent relative to Case 1.

Table 11.3 Effect of beam type and curvature approximation on strain energy and natural frequencies.[1]

Beam Type	CA[2]	Strain Energy (in-lb$_f$)	Natural Frequency (Hz)					
			P 1	B 1	FA 1	FS 1	T 1	B 2
TI	TR	17398	0.696	2.026	3.034	3.059	3.276	4.617
TI	ST	17406	0.696	2.026	3.034	3.059	3.276	4.617
RA	TR	17361	0.696	2.035	3.039	3.062	3.289	4.635
RA	ST	17369	0.696	2.035	3.039	3.062	3.289	4.635
BE	TR	17361	0.697	2.036	3.040	3.062	3.291	4.638
BE	ST	17369	0.697	2.036	3.040	3.062	3.291	4.638
NASTRAN[3]		-	0.71	2.01	3.06	3.09	3.26	4.58

[1] FloWind-19: 52 rpm, nonlinear, centrifugal softening, Coriolis coupling.

[2] CA ≡ curvature approximation.

[3] Centrifugal softening not included during generation of geometric nonlinearity terms. Model statically condensed to sixty dof's prior to eigensolution.

The effects of various idealization parameters are detailed for the first known time in Table 11.2. The TI:TR beam idealization is used for all cases. Case 1 represents the most accurate results with the inclusion of geometric nonlinearities, centrifugal softening, and Coriolis coupling. Cases 2-4 each exclude a different one of these three factors, while all three parameters are removed for Case 5. Again, strain energy and flatwise frequencies are seen to be most significantly affected by geometric nonlinearities. Butterfly and tower frequencies are affected by all three factors: Coriolis coupling, centrifugal softening, and geometric nonlinearities, in that order of significance.

The most interesting effects are exhibited by the first propeller mode. Its frequency is the only one accurately predicted when all three factors are ignored. Coriolis coupling is insignificant for this mode, but the effects of geometric nonlinearities and centrifugal softening cancel each other almost exactly, as discussed in [19]. In fact, the results are listed for a rotor speed of 35 rpm because the Case 4 assumptions are unstable at the nominal 52 rpm operating speed.

Table 11.3 provides a sensitivity assessment for the VAWT results to beam type and curvature approximation. All values are within one-half percent of each other. Again, this is as expected but helps to confirm the proper formulation and execution of PVAEB. FEVD/NASTRAN results are also included in this table. No doubt these results should be viewed as acceptable now that comparisons with accurate solutions can be made. The error induced by static condensation has obviously been minimized by a judicious selection of the condensed degrees-of-freedom, though it is never quantified or isolated from the discretization error in FEVD. Modern eigensolvers eliminate the condensation error; error estimates as presented in Table 11.4 confirm the elimination of discretization error. The

Table 11.4 Error estimates for the FloWind-19 at 52 rpm.

FLOWIND-19 VAWT MODEL
52 RPM, GRAVITY, GUY CABLE LOAD

# SUBCASES = 7, BEAM = BE, ANALYSIS = IM
NONLIN = -12, LOAD = 100, CIRC = ST

ERROR ESTIMATES

CASE	#DOF	LINEAR STRAIN ENERGY	EXTRAPOLATED ENERGY	DELTA ENERGY	CONVERGENCE EXPONENT RUNNING	CONVERGENCE EXPONENT CUMULATIVE	% EST. ERROR IN ||V|| RUNNING	% EST. ERROR IN ||V|| CUMULATIVE
1	335	0.19030212928115E+05	0.00000000000000E+00	0.00000000E+00	0.0000	0.0000	0.0000	19.7592
2	495	0.19764375755339E+05	0.20384793099354E+05	0.73416283E+03	2.0000	7.6494	17.4457	4.4387
3	655	0.19796455559582E+05	0.19800473387895E+05	0.32079804E+02	7.8389	6.1669	1.4245	1.8715
4	815	0.19802167070019E+05	0.19804430560189E+05	0.57115104E+01	5.7625	7.9341	1.0691	0.7864
5	975	0.19803391044750E+05	0.19803930388688E+05	0.12239747E+01	6.6087	41.1467	0.5219	0.0197
6	1135	0.19803391764828E+05	0.19803391765673E+05	0.72007800E-03	44.4189	18.3639	0.0007	0.0049
7	1295	0.19803391808352E+05	0.19803391811930E+05	0.43524000E-04	19.5447	19.5447	0.0013	0.0013

CASE	#DOF	NONLINEAR STRAIN ENERGY	EXTRAPOLATED ENERGY	DELTA ENERGY	CONVERGENCE EXPONENT RUNNING	CONVERGENCE EXPONENT CUMULATIVE	% EST. ERROR IN ||V|| RUNNING	% EST. ERROR IN ||V|| CUMULATIVE	NL#
1	335	0.16762757824155E+05	0.00000000000000E+00	0.00000000E+00	0.0000	0.0000	0.0000	18.6786	8*
2	495	0.17331066705560E+05	0.17811326225256E+05	0.56830888E+03	2.0000	7.1152	16.4206	4.6571	9*
3	655	0.17361022918599E+05	0.17365424263333E+05	0.29956213E+02	7.3369	5.6618	1.5920	2.1076	6*
4	815	0.17367815184433E+05	0.17371428073306E+05	0.67922658E+01	4.8400	9.7170	1.4421	0.7288	7*
5	975	0.17368737807302E+05	0.17368978003322E+05	0.92262287E+00	8.7986	60.8994	0.3719	0.0031	6*
6	1135	0.17368737827675E+05	0.17368737885042E+05	0.20373000E-04	2.0000	10.0918	0.0057	0.0014	6*
7	1295	0.17368737824059E+05	0.17368737824059E+05	-0.36160000E-05	0.0000	0.0000	0.0000	0.0000	6*

CASE	#DOF	OMEGA # 1	EXTRAPOLATED OMEGA	DELTA OMEGA	CONVERGENCE EXPONENT RUNNING	CONVERGENCE EXPONENT CUMULATIVE	% EST. ERROR IN OMEGA RUNNING	% EST. ERROR IN OMEGA CUMULATIVE
1	335	0.43977459320986E+01	0.00000000000000E+00	0.00000000E+00	0.0000	0.0000	0.0000	0.4664
2	495	0.43879172367805E+01	0.43795941269985E+01	-0.98286953E-02	2.0000	1.6850	0.1900	0.2418
3	655	0.43809504386747E+01	0.37357755941564E+01	-0.69667981E-02	0.0414	3.8355	17.2702	0.0827
4	815	0.43778829454909E+01	0.43731125500302E+01	-0.30674932E-02	2.2735	8.6140	0.1091	0.0126
5	975	0.43773357170391E+01	0.43771424594926E+01	-0.54722845E-03	7.4943	27.9819	0.0044	0.0001
6	1135	0.43773321599509E+01	0.43773321091299E+01	-0.35570882E-05	28.0524	23.8835	0.0000	0.0000
7	1295	0.43773320670914E+01	0.43773320629726E+01	-0.92859500E-07	23.9534	23.9534	0.0000	0.0000

CASE	#DOF	OMEGA # 2	EXTRAPOLATED OMEGA	DELTA OMEGA	CONVERGENCE EXPONENT RUNNING	CONVERGENCE EXPONENT CUMULATIVE	% EST. ERROR IN OMEGA RUNNING	% EST. ERROR IN OMEGA CUMULATIVE
1	335	0.12830631908359E+02	0.00000000000000E+00	0.00000000E+00	0.0000	0.0000	0.0000	0.3211
2	495	0.12791228935769E+02	0.12757835878237E+02	-0.39402973E-01	2.0000	8.2242	0.2617	0.0130
3	655	0.12790049848812E+02	0.12789941915977E+02	-0.11790870E-02	8.8498	4.4337	0.0008	0.0037
4	815	0.12789638409087E+02	0.12789227949218E+02	-0.41143973E-03	3.1771	8.9628	0.0032	0.0005
5	975	0.12789571238608E+02	0.12789549808677E+02	-0.67170479E-04	7.9183	28.9173	0.0002	0.0000
6	1135	0.12789570881922E+02	0.12789570877654E+02	-0.35668600E-06	29.2050	18.6736	0.0000	0.0000
7	1295	0.12789570860854E+02	0.12789570859730E+02	-0.21068000E-07	22.6151	22.6151	0.0000	0.0000

Table 11.4 Error estimates for the FloWind-19 at 52 rpm (continued).

FLOWIND-19 VAWT MODEL
52 RPM, GRAVITY, GUY CABLE LOAD

# SUBCASES = 7, BEAM = BE, ANALYSIS = IM
NONLIN = -12, LOAD = 100, CIRC = ST

ERROR ESTIMATES

CASE	#DOF	OMEGA # 3	EXTRAPOLATED OMEGA	DELTA OMEGA	CONVERGENCE EXPONENT RUNNING	CONVERGENCE EXPONENT CUMULATIVE	% EST. ERROR IN OMEGA RUNNING	% EST. ERROR IN OMEGA CUMULATIVE
1	335	0.20781086238017E+02	0.00000000000000E+00	0.00000000E+00	0.0000	0.0000	0.0000	8.8096
2	495	0.19111277087756E+02	0.17576937229513E+02	-0.16698092E+01	2.0000	12.6257	8.7293	0.0665
3	655	0.19103668967354E+02	0.19103509587169E+02	-0.76081204E-02	13.8769	3.2649	0.0008	0.0266
4	815	0.19099111165676E+02	0.19081540482446E+02	-0.45578017E-02	1.0558	10.3363	0.0921	0.0028
5	975	0.19098581376078E+02	0.19098464461914E+02	-0.52978960E-03	9.5424	31.5069	0.0006	0.0000
6	1135	0.19098579497641E+02	0.19098579481736E+02	-0.18784370E-05	31.4577	40.8592	0.0000	0.0000
7	1295	0.19098579501413E+02	0.19098579501413E+02	0.37720000E-08	0.0000	0.0000	0.0000	0.0000

CASE	#DOF	OMEGA # 4	EXTRAPOLATED OMEGA	DELTA OMEGA	CONVERGENCE EXPONENT RUNNING	CONVERGENCE EXPONENT CUMULATIVE	% EST. ERROR IN OMEGA RUNNING	% EST. ERROR IN OMEGA CUMULATIVE
1	335	0.21900723621495E+02	0.00000000000000E+00	0.00000000E+00	0.0000	0.0000	0.0000	13.8340
2	495	0.19253971972045E+02	0.16693273084203E+02	-0.26467516E+01	2.0000	13.4705	15.3397	0.0769
3	655	0.19244533057906E+02	0.19244370899514E+02	-0.94389141E-02	14.5720	3.6311	0.0008	0.0278
4	815	0.19239734340981E+02	0.19229103989862E+02	-0.47987169E-02	1.7051	10.3964	0.0553	0.0029
5	975	0.19239184713280E+02	0.19239065268508E+02	-0.54962770E-03	9.6126	31.3398	0.0006	0.0000
6	1135	0.19239182701903E+02	0.19239182684411E+02	-0.20113770E-05	31.2833	37.0987	0.0000	0.0000
7	1295	0.19239182709044E+02	0.19239182709044E+02	0.71409998E-08	0.0000	0.0000	0.0000	0.0000

CASE	#DOF	OMEGA # 5	EXTRAPOLATED OMEGA	DELTA OMEGA	CONVERGENCE EXPONENT RUNNING	CONVERGENCE EXPONENT CUMULATIVE	% EST. ERROR IN OMEGA RUNNING	% EST. ERROR IN OMEGA CUMULATIVE
1	335	0.22031718949286E+02	0.00000000000000E+00	0.00000000E+00	0.0000	0.0000	0.0000	6.5492
2	495	0.20694899802091E+02	0.19493857954767E+02	-0.13368191E+01	2.0000	11.2352	6.1611	0.0841
3	655	0.20679127742512E+02	0.20678447566393E+02	-0.15772060E-01	11.3763	8.4685	0.0033	0.0079
4	815	0.20677649595528E+02	0.20677352637463E+02	-0.14781470E-02	8.1814	11.0328	0.0014	0.0007
5	975	0.20677505048615E+02	0.20677478323058E+02	-0.14454691E-03	10.3634	27.1568	0.0001	0.0000
6	1135	0.20677503991327E+02	0.20677503974634E+02	-0.10572880E-05	27.4047	18.9517	0.0000	0.0000
7	1295	0.20677503933216E+02	0.20677503928428E+02	-0.58111000E-07	19.5284	19.5284	0.0000	0.0000

CASE	#DOF	OMEGA # 6	EXTRAPOLATED OMEGA	DELTA OMEGA	CONVERGENCE EXPONENT RUNNING	CONVERGENCE EXPONENT CUMULATIVE	% EST. ERROR IN OMEGA RUNNING	% EST. ERROR IN OMEGA CUMULATIVE
1	335	0.29442610782245E+02	0.00000000000000E+00	0.00000000E+00	0.0000	0.0000	0.0000	1.0264
2	495	0.29150707767558E+02	0.28901731620744E+02	-0.29190301E+00	2.0000	9.5490	0.8615	0.0248
3	655	0.29145280724662E+02	0.29144941355115E+02	-0.54270429E-02	10.1144	4.9651	0.0012	0.0062
4	815	0.29143658430116E+02	0.29142393886626E+02	-0.16222945E-02	3.7770	10.6210	0.0043	0.0006
5	975	0.29143482992367E+02	0.29143447059045E+02	-0.17543775E-03	9.8854	28.1967	0.0001	0.0000
6	1135	0.29143481927680E+02	0.29143481913344E+02	-0.10646870E-05	28.4373	19.0651	0.0000	0.0000
7	1295	0.29143481869252E+02	0.29143481865486E+02	-0.58428000E-07	21.2638	21.2638	0.0000	0.0000

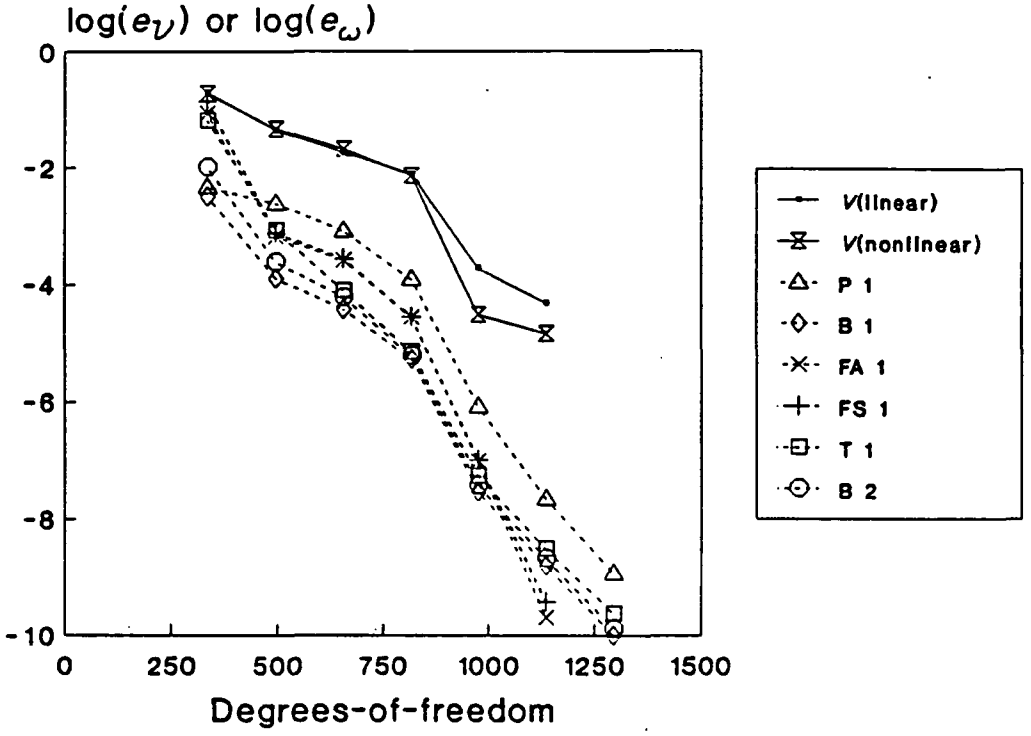

Figure 11.7 Convergence of relative errors for the FloWind-19 at 52 rpm.

engineer must still resolve errors in idealization, but may now do so without the distraction of other analytical uncertainties.

Figure 11.7 displays the estimated errors in energy norm (8.45) and natural frequency (8.46) *relative* to the extrapolated values at $p = 9$ for the BE:ST idealization of the FloWind-19 at 52 rpm (i.e., the "cumulative" error estimates in Table 11.4). All of the listed natural frequencies are seen to converge faster than the (linear and nonlinear) strain energies. The different vibrational modes exhibit slightly different rates of convergence, and the order of increasing error does not coincide with the order of increasing natural frequency. Note that exponential convergence is indicated even with the inclusion of centrifugal softening, Coriolis coupling, and geometric nonlinearities.

Table 11.5 presents some comparative information on eigensolvers and extensions. Skyline efficiency reflects the success in reducing storage requirements

Table 11.5 Eigensolver comparison for the VAWT problem.[1]

p-Level[2]	Number of DOF's	Skyline Efficiency[3] (%)	Error in Energy Norm (%)	Sequential Subspace Iteration		Nonsequential Subspace Iteration		Nonsequential Lanczos Method	
				# SI's[4]	CPU Sec.[5]	# SI's[4]	CPU Sec.[5]	# LS's[4]	CPU Sec.[5]
3	335	45.4	28.933	-	-	30	436	49	148
4	495	37.1	2.4746	18	630	15[6•]	529	49	350
5	655	42.7	1.3088	12	757	15[6•]	859	51	645
6	815	44.9	0.0169	7	680	15[6°]	1247	51	998
7	975	46.0	0.0051	6	824	15[6°]	1730	51	1427
8	1135	54.0	0.0001	4	687	15[6°]	2036	51	2254
9	1295	60.0	0.0000	3	621	15[6°]	2268	51	2563

[1] FloWind-19: BE beam; ST curvature approximation; linear analysis with 0 rpm, gravity, and guy cable thrust loading; ten eigenvalues computed to 10^{-12} accuracy.

[2] Refers to polynomial order (p) for u_0, v_0, and w_0. Polynomial order for ϕ_1 is p-1.

[3] Skyline efficiency (%) $\equiv \left(1 - \frac{\text{Skyline vector dimension}}{(\#\text{DOF})(\#\text{DOF}+1)/2}\right) \times 100$, for constrained eigenproblem.

[4] # SI's ≡ number of subspace iterations; # LS's ≡ number of Lanczos steps.

[5] For Digital VAXstation 3100: roughly 0.4 Mflops (double precision).

[6] Failed Sturm sequence check: • ≡ 2 of first 10 and 0 of first 6 eigenvalues missing;
° ≡ 2 of first 10 and 1 of first 6 eigenvalues missing; and
◦ ≡ 3 of first 10 and 1 of first 6 eigenvalues missing.

and computational costs. PVAEB does not contain a skyline optimizer, yet p-extension generally improves the skyline efficiency. The benefits of sequential eigensolutions as discussed in Section 8.2 are demonstrated for the subspace iteration method. Not only are the number of subspace iterations reduced as the solution becomes more exact, but the sequential solution algorithm aids in tracking the lowest modes to prevent Sturm sequence failure.

The complex Lanczos solver compares favorably with nonsequential subspace iteration even though the analyzed problem is entirely real. Sturm sequence failure is avoided and solution time is significantly less than that for subspace iteration at the low p-levels. Solution time becomes relatively greater at the high p-levels, but this is primarily due to the added complexities of assuming a gyroscopic eigensystem and utilizing a state variable formulation (8.31). This comparison is merely intended to be enlightening rather than definitive.

12. SUMMARY AND CONCLUSIONS

The subject of this research has been the application of the p-version of the finite element method to static and dynamic analyses of the class of problems which can be accurately modeled by (a hierarchy of) engineering beam formulations. The objectives of this investigation included identifying the underlying assumptions of classical beam theory, rigorously deriving the strain and kinetic beam energies, and constructing hierarchic finite element spaces based on p-extensions. These formulations are capable of accounting for rotating coordinate system effects and geometric nonlinearities. They have been implemented into a computer program named PVAEB (p-Version Analysis of Elastic Beams) for evaluation of a diverse set of demonstrative problems.

Beam elements possessing either a straight or circular beam axis have been developed. The circular beam elements assist in minimizing the number of elements necessary to capture the problem geometry. However, curvature of the beam axis affects the definition of the cross-sectional properties. These curvature-dependent properties may be related to conventional cross-sectional properties through a hierarchy of curvature approximations, whose applicability depends on the relative magnitude between the radius of the beam axis and the characteristic cross-sectional dimension.

Quality control and error estimation procedures based on p-extensions were implemented and their numerical performance was studied. These procedures address the quantification of the error of discretization and consist of:

1) the estimation of the error in energy norm and/or natural frequencies,
2) the performance of equilibrium checks for the entire model and for individual elements, and

3) the observation of convergence for all quantities of interest.

Errors of idealization may be quantified to a lesser extent through the hierarchies of beam formulations and curvature approximations and by inclusion of rotating coordinate system effects and geometric nonlinearities, as applicable. The suitability of the underlying beam assumptions, and of the other limitations imposed in the formulations, may only be assessed by comparison with results from less restrictive theories and/or experimentation.

The implementation of hierarchic finite element spaces allows for algorithmic enhancements of established eigensolution techniques. This study documents the procedure by which the computational effort for an eigensolution may be reduced by utilizing the results of a previous eigensolution in a hierarchic sequence. This procedure was implemented for real (nonrotating) eigensolvers using threshold Jacobian and subspace iteration techniques. Application to block Lanczos and/or complex eigensolvers merits further investigation, as does refinement of the intrinsic eigensolver logic to fully capitalize on the hierarchic solution sequence.

The principal conclusions of this work are as follows:

1) A hierarchy of straight and circular beam element formulations can be successfully implemented in the p-version of the finite element method for static and dynamic analyses.
2) Rigorous derivation of the circular beam formulations and implementation of extendable polynomial-based approximations for the displacement variables eliminate all locking-type phenomena and characterize all (strain-free) rigid body motions as $p \rightarrow \infty$.
3) A distinct relationship exists between beam type and curvature approximation for circular beam elements. The straight (ST) approximation is most appropriate for Bernoulli-Euler and Rayleigh beam idealizations. Timoshenko

beams, coupled with the truncated-series (TR) approximation, significantly extend the range of applicability. The exact (EX) characterization of curvature is most difficult to quantify and is rarely beneficial; the engineering beam assumptions become invalid before significant differences between the TR and EX idealizations occur.

4) Exponential convergence for p-extensions has been realized for both strain energy and natural frequencies for the class of problems investigated. Inclusion of circular beam elements, rotating coordinate system effects, and/or geometric nonlinearities may affect the solution accuracy and rate of convergence, but not the exponential nature of the convergence.
5) Significant improvement in computational effort has been demonstrated for sequential eigensolutions of problems utilizing hierarchic extensions. Although the sequential set of eigensolutions does require more effort than the nonsequential eigensolution of the highest-order approximation, quantification of the error of discretization easily justifies the additional cost.
6) The versatility of the formulations has been exhibited by the diversity of the sample problems investigated, from moderately thick rings less than four inches in diameter to a vertical-axis wind turbine over one hundred feet tall.
7) Inclusion of centrifugal softening, Coriolis coupling, and geometric nonlinearities have a profound effect on the predicted response of vertical-axis wind turbines. The interaction of these effects has been documented for the first time in this report.

13. ACKNOWLEDGEMENTS

I wish to express my sincerest appreciation to my advisor, Dr. Barna A. Szabó, for his guidance and encouragement during this research.

Support for this work through the National Aeronautics and Space Administration, Graduate Student Researchers Program, Lewis Research Center, under Training Grant NGT-50138, is gratefully acknowledged. Special gratitude is extended to my NASA technical advisor, Dr. Christos C. Chamis, and to Dr. Francis J. Montegani, Chief, Office of University Affairs, NASA-LeRC. Additional support through the Department of Mechanical Engineering, Washington University, is appreciatively recognized, with special thanks to Dr. Salvatore P. Sutera, Chairman, and Prof. Wallace B. Diboll, Jr., Assistant Chairman.

The assistance of Ann Lacy in preparing this manuscript is deeply appreciated. I also wish to thank the members of my faculty committee, particularly Dr. David A. Peters at Georgia Institute of Technology. Dr. O. A. Bauchau at Rensselaer Polytechnic Institute is acknowledged for graciously providing the Lanczos gyroscopic eigensolver used in PVAEB.

Finally, I am forever grateful for the love, understanding, and assistance of my parents, Joel and Marjorie Watson, and of my wonderful wife, Vickie White.

14. APPENDICES

APPENDIX 14.1

Input Cards for PVAEB Models

General comments regarding model input:

1) NASTRAN similarity:
   - Program is designed to interpret an input deck of cards.
   - Many of PVAEB's bulk data cards are modeled after similar cards in NASTRAN. NASTRAN documentation may be used to enhance the descriptions below.

2) Free format:
   - Active columns may be separated by spaces, commas, or equal signs.
   - Commas or equal signs must be used to separate blank columns.
   - All information on an individual card must be contained within the first 120 characters of a single line.

3) Identification numbers (ID's):
   - $0 < \text{ID} < 10000$ (integer).
   - No two ID's may be the same for a given type of card.

4) Continuation flags ($+C_i$'s):
   - Defined using up to eight characters beginning with a "+".
   - Continuation cards are considered individual cards for the purpose of reading in the free format.
   - Continuation cards must follow the card it is continuing immediately, and the continuation flags must be identical.

5) Packed six-digit format:
   - Up to six contiguous digits with values between one and six.

- Represents any or all of the six global degrees-of-freedom at the point of interest.

Table 14.1.1 Abridged list of allowable case control cards.

Card	Input/Comment	Location		Required ?
		Main	Subcase	
$	Comment line (also flags comments appended to the ends of cards).	X	X	N
TITLE =	Title ($\leq$ 60 characters).	X		N
SUBTITLE =	Subtitle ($\leq$ 60 characters).	X		N
ANALYSIS =	ST = static, RE = real eigenvalue, or IM = complex eigenvalue. Note: Static analysis will be be performed before RE/IM analyses if load is specified.	X		Y
NUMEIG =	# of eigenvalue/vector's desired (required for RE/IM analyses).	X		Y/N
NOSOFT	No centrifugal softening flag: exclude $[K_S]$ matrix in ST/RE/IM analyses.	X		N
NOCOR	No Coriolis coupling flag: exclude $[C]$ matrix from IM analysis.	X		N
SEQ	Sequential solution flag: use previous RE eigensolution to start next eigensolution.	X		N
NOSTURM	No Sturm sequence check flag: do not check if lowest eigenvalues were found by non-Jacobi eigensolver.	X		N
JACOBI	Jacobi solution flag: use RE Jacobi solver exclusively.	X		N
JACOPTION	Optional Jacobi solution flag: use RE Jacobi solver if RE subspace iteration fails.	X		N

Table 14.1.1 Abridged list of allowable case control cards (continued).

Card	Input/Comment	Location		Required ?
		Main	Subcase	
LOAD =	LOAD Card ID # for analysis.	X		N
SPC =	SPCADD Card ID # for analysis.	X		N
BEAM =	Analysis beam type: BE = Bernoulli-Euler, RA = Rayleigh, or TI = Timoshenko.	X		Y
CIRC =	Circular beam approximation (required for circular elements): EX = exact, TR = truncated series, or ST = straight approximation.	X		Y/N
NONLIN =	Nonlinear analysis value: 0 = linear (default), +# = number of iterations, or −# = exponent for automatic convergence check of strain energy ($e \leq 10^{-\#}$).	X		N
RBM =	Shift value (α) for rigid body analysis: $[\hat{K}] = [K] + \alpha[M]$.	X		N
NOSTOP	Don't stop for input data error.	X		N
SUBCASE	Subcase flag.	X	X	Y
LABEL =	Subcase label ($\leq$ 60 characters).		X	N
BRP =	BE/RA subcase p-levels: p_1, p_2, p_3, p_4.		X	Y/N°
TIP =	TI subcase p-levels: p_1, p_2, p_3, p_4, p_5, p_6.		X	Y/N°
ENDCASE	End of subcase flag (SUBCASE or BEGINBULK cards also end subcase input).	X		N
BEGINBULK	Bulk data flag: signals the end of case control cards and the start of bulk data cards.	X	X	Y

° One or the other is required for each subcase depending on the analysis beam type.

Table 14.1.1 Abridged list of allowable case control cards (continued).

Card	Input/Comment	Location		Required ?
		Main	Subcase	
	Static report requests:			
SGDISP =	SP†: Global grid displacements.	X°	X	N
SELOCDISP =	SP†: Local element displacements.	X°	X	N
SEGLODISP =	SP†: Global element displacements.	X°	X	N
SEFORCE =	SP†: Element forces & moments.	X°	X	N
SVFORCE =	SP†: Virtual work forces & moments.	X°	X	N‡
SCFORCE =	SP†: Constraint forces & moments.	X°	X	N
SESTRESS =	SP†: Element stresses.	X°	X	N
	Dynamic report requests*:			
DGDISP	Global grid displacements.	X°	X	N
DELOCDISP	Local element displacements.	X°	X	N
DEGLODISP	Global element displacements.	X°	X	N
DEFORCE	Element forces & moments.	X°	X	N
DVFORCE	Virtual work forces & moments.	X°	X	N‡
DCFORCE	Constraint forces & moments.	X°	X	N
DESTRESS	Element stresses.	X°	X	N
ERREST	Error estimation flag: perform error estimates for linear & nonlinear static and dynamic solutions as needed.	X		N
ECHO =	Echo input model data into results file: CC = case control only, or AL = case control & bulk data.	X		N
REPORT	Activities report echo flag: write activities report into results file.	X		N

° Triggers report for every subcase.

† SP ≡ Specification: LO = linear case only, HI = highest nonlinear case only, HL = linear and highest nonlinear cases, or AL = all cases.

‡ Limited to linear analyses.

* Prints report for each of the desired eigenvalue/vector's.

Table 14.1.2 Complete list of allowable bulk data cards.

Card (Col. 1)	Column 2	3	4	5	6	7	8	9	10
GRID	GID	X	Y	Z	$PC^{*\dagger}$				
CBAR	EID	PID	GID_A	GID_B	V_1	V_2	V_3		$+C_1^*$
$+C_1^*$	$PF_A^{*\dagger}$	$PF_B^{*\dagger}$							
CBARC	EID	PID	GID_A	GID_B	V_1	V_2	V_3	R	$+C_1^*$
$+C_1^*$	$PF_A^{*\dagger}$	$PF_B^{*\dagger}$							
CBARI	EID_{LO}	EID_{HI}	N_{DIV}						
PBAR	PID	MID	A	I_{yy}	I_{zz}	I_0	$k_y^{*\triangleright}$	$k_z^{*\triangleright}$	$+C_1^*$
$+C_1^*$	C_y^*	C_z^*	D_y^*	D_z^*	E_y^*	E_z^*	F_y^*	F_z^*	
PBARC	PID	MID	A	I_{yy}	I_{zz}	$-I_0$	$k_y^{*\triangleright}$	$k_z^{*\triangleright}$	$+C_1$
$+C_1$	I_{yyy}	I_{yyz}	I_{yzz}	R	I_{00}	I_{20}			$+C_2$
$+C_2$	I_{02}	I_{10}	I_{01}	I_{11}					$+C_3^*$
$+C_3^*$	C_y^*	C_z^*	D_y^*	D_z^*	E_y^*	E_z^*	F_y^*	F_z^*	
MAT	MID	$E^{\diamond}$	$G^{\diamond}$	$\nu^{\diamond}$	ρ				
CSPR	SPID	K	GID_{AP}	DOF					
CONM	CMID	GID_{AP}	M						$+C_1^*$
$+C_1^*$	J_{XX}^*	J_{YY}^*	J_{ZZ}^*	J_{XY}^*	J_{YZ}^*	J_{ZX}^*			

* = Optional. † = Packed six-digit format. $^\triangleright$ = Required for TI analyses. $^\diamond$ = Only two values required.

Table 14.1.2 Complete list of allowable bulk data cards (continued).

Card (Col. 1)	Column 2	3	4	5	6	7	8	9	10
SPC $+C_1^*$	SID GID_7^*	$DOF^\dagger$ etc.	GID_1	GID_2^*	GID_3^*	GID_4^*	GID_5^*	GID_6^*	$+C_1^*$
SPC	SID	$DOF^\dagger$	GID_{LO}	THRU	GID_{HI}				
SPCADD $+C_1^*$	SAID SID_8^*	SID_1 etc.	SID_2^*	SID_3^*	SID_4^*	SID_5^*	SID_6^*	SID_7^*	$+C_1^*$
FORCE	LID	GID_{AP}	A	V_1	V_2	V_3			
MOMENT	LID	GID_{AP}	A	V_1	V_2	V_3			
GRAV	LID		A	V_1	V_2	V_3			
RFORCE	LID	GID_{AP}	A	V_1	V_2	V_3			
PLOAD	LID	EID_{AP}	Type	A_A	A_B				
LOAD $+C_1^*$	LCID S_4^*	S LID_4^*	S_1 etc.	LID_1	S_2^*	LID_2^*	S_3^*	LID_3^*	$+C_1^*$
ENDDATA°									

* = Optional. † = Packed six-digit format. ° = Signals the end of the bulk data cards.

Grid point specification (GRID):

- GID ≡ Grid identification number.
- X, Y, and Z ≡ Position in global frame.
- PC ≡ Permanent single point constraints.

Beam element specification (CBAR, CBARC, and CBARI):

- EID ≡ Element identification number.
- PID ≡ Property ID for particular element.
- GID_A and GID_B ≡ Grid points located at ends A and B, respectively, of the beam element. The local x-axis for straight beams is in the direction of $\{^G x_S\} = \{^G B\} - \{^G A\}$.
- V_1, V_2, and V_3 ≡ Components of the vector, $\{^G V\}$, used to define the orientation of the local frame. The local z-axis is oriented in the direction of $\{^G x_S\} \times \{^G V\}$ for *both* straight and circular elements. The local y-axis for straight elements is oriented in the direction of $\{^G z\} \times \{^G x_S\}$. $\{^G V\}$ also defines the direction of rotation from $\{^G x_S\}$ at end A of the local x- and y-axes for circular elements. The angle of rotation, $\frac{\theta}{2} \leq 90°$ (see Figure 2.3), is determined using $\{^G B\}$, $\{^G A\}$, and R.
- R ≡ radius of circular element.
- PF_A and PF_B ≡ Pin flags at ends A and B, respectively.
- EID_{LO} and EID_{HI} ≡ Low and high element identification numbers for the computation of element report information at points other than the beam ends. Elements whose identification number satisfies $EID_{LO} \leq EID \leq EID_{HI}$ will be affected by the particular CBARI card.
- N_{DIV} ≡ Number of divisions defining the internal points for element report information, where $\xi_i = 2 \times (i-1)/N_{DIV} - 1,\ i = 1, 2, \ldots, (N_{DIV} + 1)$.

Beam properties specification (PBAR and PBARC):

- PID ≡ Property identification number.
- MID ≡ Material ID for particular set of properties.
- A, I_{yy}, I_{zz}, I_0, k_y, k_z, I_{yyy}, I_{yyz}, I_{yzz}, R, I_{00}, I_{20}, I_{02}, I_{10}, I_{01}, and I_{11} ≡ Cross-sectional properties. PBAR may be used for circular beams using the TR or ST curvature approximation.
- C_y, C_z, D_y, D_z, E_y, E_z, F_y, and F_z ≡ Stress recovery coefficients (four points in the local yz-plane for the computation of element stresses).

Material specification (MAT):

- MID ≡ Material identification number.
- E, G, and ν ≡ Young's modulus, shear modulus, and Poisson's ratio, respectively. Only two of these three properties need to be specified, the missing property being computed from $G = E/[2(1+\nu)]$.
- ρ ≡ Material density.

Global spring specification (CSPR):

- SPID ≡ Spring identification number.
- K ≡ Spring constant.
- GID_{AP} ≡ Grid ID where spring is applied.
- DOF ≡ Number of the global degree-of-freedom affected by spring.

Distributed mass specification (CONM):

- CMID ≡ Distributed mass identification number.
- GID_{AP} ≡ Grid ID where mass is applied.
- M ≡ Mass.
- J_{XX}, J_{YY}, J_{ZZ}, J_{XY}, J_{YZ}, and J_{ZX} ≡ Mass moments of inertia. These terms are ignored in problems using Bernoulli-Euler beams.

Single point constraint specification (SPC and SPCADD):

- SID ≡ Single point constraint identification number.
- DOF ≡ Global degrees-of-freedom to be constrained.
- GID_i ≡ ID's of constrained grids.
- GID_{LO} and GID_{HI} ≡ Low and high grid point identification numbers used in conjunction with the THRU option.
- THRU ≡ Special capability such that grid points whose identification number satisfies $GID_{LO} \leq GID \leq GID_{HI}$ are constrained.
- SAID ≡ SPC combination identification number.
- SID_i ≡ ID's of single point constraints to be combined.

Load specification (FORCE, MOMENT, GRAV, RFORCE, PLOAD, and LOAD):

- LID ≡ Load identification number.
- GID_{AP} ≡ Grid ID where load is applied.
- A ≡ Amplitude of point force (FORCE), point moment (MOMENT), gravitational acceleration (GRAV), or rotational velocity (RFORCE). The rotational velocity is specified in radians per unit time.
- V_1, V_2, and V_3 ≡ Components of the vector, $\{^G V\}$, used to define the orientation of the load terms in the global frame.
- EID_{AP} ≡ Element ID where distributed load is applied.
- Type ≡ Load type. The type specifies the direction and reference frame for the distributed load. Distributed loads may be defined in the global frame (Type = FX, FY, or FZ for loads in the direction of the global axes, X, Y, or Z, respectively) or the local element frame (Type = FXE, FYE, or FZE for loads in the direction of the local axes, x, y, or z, respectively).

- A_A and A_B ≡ Amplitudes of distributed force per unit length at ends A and B, respectively.
- LCID ≡ Load combination identification number.
- S ≡ Combined load scale factor.
- S_i ≡ Scale factor for individual loads to be combined.
- LID_i ≡ ID's of loads to be combined.

APPENDIX 14.2

Curvature Approximations for Rectangular and Toroidal Beams

Objective:

Compare the approximations used to compute the curvature-dependent moments of area defined by:

$$I_{ij} = \iint \left(\frac{R}{R+y}\right) y^i z^j dy dz, \quad i,j = 0,1,2,$$

for beams of rectangular and circular cross sections.

Definition of Approximations:

- Exact Integration (EX):
  - Direct integration of I_{ij}'s.
  - Additional mass moments (J_{yyy}, J_{yyz}, and J_{yzz}) included in kinetic energy formulations.
- Truncated Series Approximation (TR):
  - Substitute: $\frac{R}{R+y} = 1 - \frac{y}{R} + \left(\frac{y}{R}\right)^2 - \cdots$.
  - Ignore all series terms involving $y^k z^l$, $(k+l) \geq 3$, within integrals.
  - No additional beam properties must be defined beyond those required for straight beams.
- "Straight" Approximation (ST):
  - Substitute: $\frac{R}{R+y} \cong 1$.
  - Ignores curvature effects in defining beam properties but maintains coupling of displacement terms.
  - Identical results for circular beam modeled with ST elements or an infinite number of straight elements.

Resulting Approximations for Moments of Area:

Curvature Approximation	I_{00}	I_{20}	I_{02}	I_{10}	I_{01}	I_{11}
EX	I_{00}	I_{20}	I_{02}	I_{10}	I_{01}	I_{11}
TR	$A+\frac{I_{yy}}{R^2}$	I_{yy}	I_{zz}	$-\frac{I_{yy}}{R}$	0	0
ST	A	I_{yy}	I_{zz}	0	0	0

Guide to Ensuing Tables:

- Results are nondimensionalized in terms of:

$$\eta \equiv \frac{t}{R},$$

where t is the thickness of the rectangular beam ($-t/2 \le y \le t/2$, independent of z-depth) or the cross-sectional diameter of the toroid ($\sqrt{y^2+z^2} \le t/2$).

- Curvature-dependent moments are nondimensionalized as follows:

$$C_{00} \equiv \frac{I_{00}}{A} = 1+Z,$$

$$C_{20} \equiv \frac{I_{20}}{I_{yy}},$$

$$C_{02} \equiv \frac{I_{02}}{I_{zz}}, \text{ and}$$

$$C_{10} \equiv \frac{I_{10}t}{I_{yy}},$$

where Z is the Winkler-Bach constant. Note that $I_{01} = I_{11} = J_{yyy} = J_{yyz} = J_{yzz} \equiv 0$ for both rectangular and toroidal beams due to dual-symmetry about the local y- and z-axes; no comparisons are required for these terms.

- The curvature approximation error is defined as:

$$(e\%) \equiv \frac{\left|(C_{ij})_{EX} - (C_{ij})_{CA}\right|}{(C_{ij})_{EX}} \times 100, \quad CA = TR, ST.$$

Table 14.2.1 Comparisons of C_{00}.

η	RECTANGULAR BEAM			TOROID		
	$(C_{00})_{EX}$	$(C_{00})_{TR}$ (e%)	$(C_{00})_{ST}$ (e%)	$(C_{00})_{EX}$	$(C_{00})_{TR}$ (e%)	$(C_{00})_{ST}$ (e%)
0.0	1.0	1.0 (0.0)	1.0 (0.0)	1.0	1.0 (0.0)	1.0 (0.0)
0.01	1.000008	1.000008 (0.0000)	1.0 (0.0008)	1.000006	1.000006 (0.0000)	1.0 (0.0006)
0.02	1.000033	1.000033 (0.0000)	1.0 (0.0033)	1.000025	1.000025 (0.0000)	1.0 (0.0025)
0.05	1.000208	1.000208 (0.0000)	1.0 (0.0208)	1.000156	1.000156 (0.0000)	1.0 (0.0156)
0.1	1.000835	1.000833 (0.0001)	1.0 (0.0834)	1.000626	1.000625 (0.0001)	1.0 (0.0625)
0.2	1.00335	1.00333 (0.0020)	1.0 (0.334)	1.00251	1.00250 (0.0013)	1.0 (0.251)
0.5	1.02165	1.02083 (0.0803)	1.0 (2.12)	1.01613	1.01563 (0.0492)	1.0 (1.59)
1.0	1.09861	1.08333 (1.39)	1.0 (8.98)	1.07180	1.06250 (0.868)	1.0 (6.70)
1.5	1.2973	1.1875 (8.46)	1.0 (22.9)	1.2038	1.1406 (5.25)	1.0 (16.9)
1.9	1.9282	1.3008 (32.5)	1.0 (48.1)	1.5241	1.2256 (19.6)	1.0 (34.4)

Table 14.2.2 Comparisons of C_{20}.

η	RECTANGULAR BEAM		TOROID	
	$(C_{20})_{EX}$	$(C_{20})_{TR/ST}$ (ϵ%)	$(C_{20})_{EX}$	$(C_{20})_{TR/ST}$ (ϵ%)
0.0	1.0	1.0 (0.0)	1.0	1.0 (0.0)
0.01	1.000013	1.0 (0.0013)	1.000013	1.0 (0.0013)
0.02	1.000060	1.0 (0.0060)	1.000050	1.0 (0.0050)
0.05	1.000375	1.0 (0.0375)	1.000313	1.0 (0.0313)
0.1	1.00150	1.0 (0.150)	1.00125	1.0 (0.125)
0.2	1.00604	1.0 (0.600)	1.00503	1.0 (0.501)
0.5	1.03926	1.0 (3.78)	1.03253	1.0 (3.15)
1.0	1.1833	1.0 (15.5)	1.1487	1.0 (12.9)
1.5	1.5855	1.0 (36.9)	1.4491	1.0 (31.0)
1.9	3.0854	1.0 (67.6)	2.3229	1.0 (57.0)

Table 14.2.3 Comparisons of C_{02}.

η	RECTANGULAR BEAM		TOROID	
	$(C_{02})_{EX}$	$(C_{02})_{TR/ST}$ (e%)	$(C_{02})_{EX}$	$(C_{02})_{TR/ST}$ (e%)
0.0	1.0	1.0 (0.0)	1.0	1.0 (0.0)
0.01	1.000008	1.0 (0.0008)	1.000004	1.0 (0.0004)
0.02	1.000033	1.0 (0.0033)	1.000017	1.0 (0.0017)
0.05	1.000208	1.0 (0.0208)	1.000104	1.0 (0.0104)
0.1	1.000835	1.0 (0.0834)	1.000417	1.0 (0.0417)
0.2	1.00335	1.0 (0.334)	1.00167	1.0 (0.167)
0.5	1.02165	1.0 (2.12)	1.01067	1.0 (1.06)
1.0	1.09861	1.0 (8.98)	1.04615	1.0 7 (4.41)
1.5	1.2973	1.0 (22.9)	1.1220	1.0 (10.9)
1.9	1.9282	1.0 (48.1)	1.2578	1.0 (20.5)

Table 14.2.4 Comparisons of C_{10}.

η	RECTANGULAR BEAM			TOROID		
	$(C_{10})_{EX}$	$(C_{10})_{TR}$ (e%)	$(C_{10})_{ST}$ (e%)	$(C_{10})_{EX}$	$(C_{10})_{TR}$ (e%)	$(C_{10})_{ST}$ (e%)
0.0	0.0	0.0 (0.0)	0.0 (0.0)	0.0	0.0 (0.0)	0.0 (0.0)
0.01	-0.010000	-0.01 (0.0000)	0.0 (100.)	-0.010000	-0.01 (0.0000)	0.0 (100.)
0.02	-0.020001	-0.02 (0.0050)	0.0 (100.)	-0.020001	-0.02 (0.0050)	0.0 (100.)
0.05	-0.050017	-0.05 (0.0350)	0.0 (100.)	-0.050016	-0.05 (0.0313)	0.0 (100.)
0.1	-0.10015	-0.1 (0.150)	0.0 (100.)	-0.10013	-0.1 (0.125)	0.0 (100.)
0.2	-0.20121	-0.2 (0.601)	0.0 (100.)	-0.20101	-0.2 (0.501)	0.0 (100.)
0.5	-0.51963	-0.5 (3.78)	0.0 (100.)	-.51626	-0.5 (3.15)	0.0 (100.)
1.0	-1.1833	-1.0 (15.5)	0.0 (100.)	-1.1487	1.0 (12.9)	0.0 (100.)
1.5	-2.3782	-1.5 (36.9)	0.0 (100.)	-2.1736	-1.5 (31.0)	0.0 (100.)
1.9	-5.8623	-1.9 (67.6)	0.0 (100.)	-4.4135	-1.9 (57.0)	0.0 (100.)

APPENDIX 14.3

Elemental Matrices for Bernoulli-Euler and Rayleigh Beams

Displacement Assumptions:

Displacement assumptions with respect to the elemental coordinate system:

$$u(x,y,z,t) = u_0(x,t) - y\left(\frac{dv_0(x,t)}{dx} - \frac{u_0(x,t)}{R}\right) - z\left(\frac{dw_0(x,t)}{dx}\right),$$

$$v(x,z,t) = v_0(x,t) - z\phi_1(x,t),$$

$$w(x,y,t) = w_0(x,t) + y\phi_1(x,t),$$

where $R = \infty$ for straight elements.

Mapping with respect to beam axis:

$$x = Q(\xi) = \left(\frac{1-\xi}{2}\right)x_A + \left(\frac{1+\xi}{2}\right)x_B,$$

$$h = x_B - x_A,$$

where A and B subscripts refer to the end nodes of the element and h is the elemental length.

Displacement variables in terms of elemental shape functions:

$$u_0\left(Q(\xi),t\right) \cong \sum_{j=1}^{p_1+1} u_{0,j}N_j(\xi)e^{i\omega t},$$

$$v_0\left(Q(\xi),t\right) \cong \sum_{j=1}^{p_2+1} v_{0,j}L_j(\xi)e^{i\omega t},$$

$$w_0\left(Q(\xi),t\right) \cong \sum_{j=1}^{p_3+1} w_{0,j}L_j(\xi)e^{i\omega t}, \text{ and}$$

$$\phi_1\left(Q(\xi),t\right) \cong \sum_{j=1}^{p_4+1} \phi_{i,j}N_j(\xi)e^{i\omega t},$$

where $i = \sqrt{-1}$.

Stiffness Matrix:

1) General Form: $[K] = [[k_{ij}]]$; $i,j = 1,2,3,4$; $[k_{ji}] = [k_{ij}]^T$.
2) Stiffness matrices for BE and RA beams are identical.

3) Differences in circular-beam approximations are dictated by the definitions of the I_{ij}'s:

Elem. Type	Approx.	I_{00}	I_{20}	I_{02}	I_{10}	I_{01}	I_{11}
Straight	(St)	A	I_{yy}	I_{zz}	0	0	0
Circular	ST	A	I_{yy}	I_{zz}	0	0	0
Circular	TR	$A+\frac{I_{yy}}{R^2}$	I_{yy}	I_{zz}	$-\frac{I_{yy}}{R}$	0	0
Circular	EX	I_{00}	I_{20}	I_{02}	I_{10}	I_{01}	I_{11}

4) Individual Stiffness Submatrix Terms and Applicability:

Submatrix	Term	BE/RA Applicability
$[k_{11}]$	$\int_{-1}^{+1} \frac{2}{h} E I_{00} \{N^*\} \{N^*\}^T d\xi$	$St/ST/TR/EX$
	$\int_{-1}^{+1} \frac{2}{h} E \left(\frac{I_{20}}{R^2} + 2\frac{I_{10}}{R}\right) \{N^*\} \{N^*\}^T d\xi$	$ST/TR/EX$
$[k_{12}]$	$\int_{-1}^{+1} E \left(\frac{I_{00}}{R} + \frac{I_{10}}{R^2}\right) \{N^*\} \{L\}^T d\xi$	$ST/TR/EX$
	$\int_{-1}^{+1} -\frac{4}{h^2} E \left(\frac{I_{20}}{R} + I_{10}\right) \{N^*\} \{L^{**}\}^T d\xi$	$ST/TR/EX$
$[k_{13}]$	$\int_{-1}^{+1} -\frac{4}{h^2} E \left(I_{01} + \frac{I_{11}}{R}\right) \{N^*\} \{L^{**}\}^T d\xi$	EX
$[k_{14}]$	$\int_{-1}^{+1} -E \left(\frac{I_{01}}{R} + \frac{I_{11}}{R^2}\right) \{N^*\} \{N\}^T d\xi$	EX
$[k_{22}]$	$\int_{-1}^{+1} \frac{8}{h^3} E I_{20} \{L^{**}\} \{L^{**}\}^T d\xi$	$St/ST/TR/EX$
	$\int_{-1}^{+1} \frac{h}{2} E \frac{I_{00}}{R^2} \{L\} \{L\}^T d\xi$	$ST/TR/EX$
	$\int_{-1}^{+1} -\frac{2}{h} E \frac{I_{10}}{R} \left[\{L\} \{L^{**}\}^T + \{L^{**}\} \{L\}^T\right] d\xi$	TR/EX
$[k_{23}]$	$\int_{-1}^{+1} -\frac{2}{h} E \frac{I_{01}}{R} \{L\} \{L^{**}\}^T d\xi$	EX
	$\int_{-1}^{+1} \frac{8}{h^3} E I_{11} \{L^{**}\} \{L^{**}\}^T d\xi$	EX
$[k_{24}]$	$\int_{-1}^{+1} -\frac{h}{2} E \frac{I_{01}}{R^2} \{L\} \{N\}^T d\xi$	EX
	$\int_{-1}^{+1} \frac{2}{h} E \frac{I_{11}}{R} \{L^{**}\} \{N\}^T d\xi$	EX
$[k_{33}]$	$\int_{-1}^{+1} \frac{8}{h^3} E I_{02} \{L^{**}\} \{L^{**}\}^T d\xi$	$St/ST/TR/EX$
	$\int_{-1}^{+1} \frac{2}{h} G \frac{I_0}{R^2} \{L^*\} \{L^*\}^T d\xi$	$ST/TR/EX$

4) Individual Stiffness Submatrix Terms and Applicability (continued):

Submatrix	Term	BE/RA Applicability
$[k_{34}]$	$\int_{-1}^{+1} \frac{2}{h} E \frac{I_{02}}{R} \{L^{**}\} \{N\}^T d\xi$	*ST/TR/EX*
	$\int_{-1}^{+1} -\frac{2}{h} G \frac{I_0}{R} \{L^*\} \{N^*\}^T d\xi$	*ST/TR/EX*
$[k_{44}]$	$\int_{-1}^{+1} \frac{2}{h} G I_0 \{N^*\} \{N^*\}^T d\xi$	*St/ST/TR/EX*
	$\int_{-1}^{+1} \frac{h}{2} E \frac{I_{02}}{R^2} \{N\} \{N\}^T d\xi$	*ST/TR/EX*

Centrifugal Softening Matrix:

1) General Form: $[K_S] = [[k_{ij}]_S]$; $i,j = 1,2,3,4$; $[k_{ji}]_S = [k_{ij}]_S^T$.

2) The centrifugal softening matrix exists only for problems with rotation.

3) Individual Centrifugal Softening Submatrix Terms and Applicability:

Submatrix	Term	Applicability
$[k_{11}]_S$	$\int_{-1}^{+1} -\frac{h}{2} m \left(\Omega_y^2 + \Omega_z^2\right) \{N\} \{N\}^T d\xi$	BE/RA: *St/ST/TR/EX*
	$\int_{-1}^{+1} -h \frac{J_{yy}}{R^2} \left(\Omega_y^2 + \Omega_z^2\right) \{N\} \{N\}^T d\xi$	BE/RA: *TR/EX*
	$\int_{-1}^{+1} -\frac{h}{2} \frac{J_{yy}}{R^2} \frac{I_{yy}}{AR^2} \left(\Omega_y^2 + \Omega_z^2\right) \{N\} \{N\}^T d\xi$	BE: *TR/EX*
	$\int_{-1}^{+1} -\frac{h}{2} \left[\frac{J_0}{R^2} \Omega_y^2 + \frac{J_{xx}}{R^2} \Omega_z^2\right] \{N\} \{N\}^T d\xi$	RA: *ST/TR/EX*
	$\int_{-1}^{+1} -\frac{h}{2} \left[\left(\frac{J_{yyy}}{R^3} + \frac{J_{yzz}}{R^3}\right) \Omega_y^2 + \frac{J_{yzz}}{R^3} \Omega_z^2\right] \{N\} \{N\}^T d\xi$	RA: *EX*
$[k_{12}]_S$	$\int_{-1}^{+1} \frac{h}{2} m \Omega_x \Omega_y \{N\} \{L\}^T d\xi$	BE/RA: *St/ST/TR/EX*
	$\int_{-1}^{+1} \frac{h}{2} \frac{J_{yy}}{R^2} \Omega_x \Omega_y \{N\} \{L\}^T d\xi$	BE/RA: *TR/EX*
	$\int_{-1}^{+1} \frac{J_{yy}}{R} \left(\Omega_y^2 + \Omega_z^2\right) \{N\} \{L^*\}^T d\xi$	BE/RA: *TR/EX*
	$\int_{-1}^{+1} \frac{J_{yy}}{R} \frac{I_{yy}}{AR^2} \left(\Omega_y^2 + \Omega_z^2\right) \{N\} \{L^*\}^T d\xi$	BE: *TR/EX*
	$\int_{-1}^{+1} \left(\frac{J_0}{R} \Omega_y^2 + \frac{J_{xx}}{R} \Omega_z^2\right) \{N\} \{L^*\}^T d\xi$	RA: *ST/TR/EX*
	$\int_{-1}^{+1} \left[\left(\frac{J_{yyy}}{R^3} + \frac{J_{yzz}}{R^3}\right) \Omega_y^2 + \frac{J_{yzz}}{R^3} \Omega_z^2\right] \{N\} \{L^*\}^T d\xi$	RA: *EX*

3) Individual Centrifugal Softening Submatrix Terms and Applicability (continued):

Submatrix	Term	Applicability
$[k_{13}]_S$	$\int_{-1}^{+1} \frac{h}{2} m\Omega_x\Omega_x \{N\}\{L\}^T d\xi$	BE/RA: *St/ST/TR/EX*
	$\int_{-1}^{+1} \frac{h}{2} \frac{J_{yy}}{R^2}\Omega_x\Omega_x \{N\}\{L\}^T d\xi$	BE/RA: *TR/EX*
	$\int_{-1}^{+1} \frac{J_0}{R}\Omega_y\Omega_x \{N\}\{L^*\}^T d\xi$	RA: *ST/TR/EX*
	$\int_{-1}^{+1} \left[\left(\frac{J_{yyy}}{R^2} + \frac{J_{yzz}}{R^2}\right)\Omega_y\Omega_z - \frac{J_{yyz}}{R^2}\Omega_z^2\right]$ $\{N\}\{L^*\}^T d\xi$	RA: *EX*
$[k_{14}]_S$	$\int_{-1}^{+1} \frac{h}{2} \frac{J_{yy}}{R}\Omega_x\Omega_x \{N\}\{N\}^T d\xi$	BE/RA: *TR/EX*
	$\int_{-1}^{+1} \frac{h}{2} \frac{J_{yy}}{R} \frac{I_{yy}}{AR^2}\Omega_x\Omega_x \{N\}\{N\}^T d\xi$	BE: *TR/EX*
	$\int_{-1}^{+1} -\frac{h}{2} \frac{J_{zz}}{R}\Omega_x\Omega_x \{N\}\{N\}^T d\xi$	RA: *ST/TR/EX*
	$\int_{-1}^{+1} -\frac{h}{2} \left(\frac{J_{yzz}}{R^2}\Omega_x + \frac{J_{yyz}}{R^2}\Omega_y\right)\Omega_x$ $\{N\}\{N\}^T d\xi$	RA: *EX*
$[k_{22}]_S$	$\int_{-1}^{+1} -\frac{h}{2} m\left(\Omega_x^2 + \Omega_z^2\right)\{L\}\{L\}^T d\xi$	BE/RA: *St/ST/TR/EX*
	$\int_{-1}^{+1} -\frac{J_{yy}}{R}\Omega_x\Omega_y\Big[\{L\}\{L^*\}^T +$ $\{L^*\}\{L\}^T\Big] d\xi$	BE/RA: *TR/EX*
	$\int_{-1}^{+1} -\frac{2}{h} J_{yy} \frac{I_{yy}}{AR^2}\left(\Omega_y^2 + \Omega_z^2\right)\{L^*\}\{L^*\}^T d\xi$	BE: *TR/EX*
	$\int_{-1}^{+1} -\frac{2}{h}\left(J_0\Omega_y^2 + J_{zz}\Omega_z^2\right)\{L^*\}\{L^*\}^T d\xi$	RA: *St/ST/TR/EX*
	$\int_{-1}^{+1} -\frac{2}{h}\left[\left(\frac{J_{yyy}}{R} + \frac{J_{yzz}}{R}\right)\Omega_y^2 + \frac{J_{yzz}}{R}\Omega_z^2\right]$ $\{L^*\}\{L^*\}^T d\xi$	RA: *EX*
$[k_{23}]_S$	$\int_{-1}^{+1} \frac{h}{2} m\Omega_y\Omega_z \{L\}\{L\}^T d\xi$	BE/RA: *St/ST/TR/EX*
	$\int_{-1}^{+1} -\frac{J_{yy}}{R}\Omega_z\Omega_z \{L^*\}\{L\}^T d\xi$	BE/RA: *TR/EX*
	$\int_{-1}^{+1} -\frac{2}{h} J_0\Omega_y\Omega_z \{L^*\}\{L^*\}^T d\xi$	RA: *St/ST/TR/EX*
	$\int_{-1}^{+1} -\frac{2}{h}\left[\left(\frac{J_{yyy}}{R} + \frac{J_{yzz}}{R}\right)\Omega_y\Omega_z - \frac{J_{yyz}}{R}\Omega_z^2\right]$ $\{L^*\}\{L^*\}^T d\xi$	RA: *EX*

3) Individual Centrifugal Softening Submatrix Terms and Applicability (continued):

Submatrix	Term	Applicability
$[k_{24}]_S$	$\int_{-1}^{+1} \frac{h}{2} \frac{J_{yx}}{R} \Omega_y \Omega_z \{L\} \{N\}^T d\xi$	BE/RA: TR/EX
	$\int_{-1}^{+1} -J_{yy} \frac{I_{yy}}{AR^2} \Omega_z \Omega_z \{L^*\} \{N\}^T d\xi$	BE: TR/EX
	$\int_{-1}^{+1} J_{zz} \Omega_z \Omega_z \{L^*\} \{N\}^T d\xi$	RA: $St/ST/TR/EX$
	$\int_{-1}^{+1} \left(\frac{J_{yzz}}{R} \Omega_z + \frac{J_{yyz}}{R} \Omega_y \right) \Omega_z \{L^*\} \{N\}^T d\xi$	RA: EX
$[k_{33}]_S$	$\int_{-1}^{+1} -\frac{h}{2} m \left(\Omega_x^2 + \Omega_y^2 \right) \{L\} \{L\}^T d\xi$	BE/RA: $St/ST/TR/EX$
	$\int_{-1}^{+1} -\frac{2}{h} \left(J_0 \Omega_z^2 + J_{yy} \Omega_z^2 \right) \{L^*\} \{L^*\}^T d\xi$	RA: $St/ST/TR/EX$
	$\int_{-1}^{+1} -\frac{2}{h} \left[\left(\frac{J_{yyy}}{R} + \frac{J_{yzz}}{R} \right) \Omega_z^2 + \frac{J_{yyy}}{R} \Omega_x^2 \right] \{L^*\} \{L^*\}^T d\xi$	RA: EX
$[k_{34}]_S$	$\int_{-1}^{+1} -\frac{h}{2} \frac{J_{yy}}{R} \left(\Omega_x^2 + \Omega_y^2 \right) \{L\} \{N\}^T d\xi$	BE/RA: TR/EX
	$\int_{-1}^{+1} -J_{yy} \Omega_x \Omega_y \{L^*\} \{N\}^T d\xi$	RA: $St/ST/TR/EX$
	$\int_{-1}^{+1} -\left(\frac{J_{yyy}}{R} \Omega_y + \frac{J_{yyz}}{R} \Omega_z \right) \Omega_z \{L^*\} \{N\}^T d\xi$	RA: EX
$[k_{44}]_S$	$\int_{-1}^{+1} -\frac{h}{2} J_{yy} \frac{I_{yy}}{AR^2} \left(\Omega_x^2 + \Omega_y^2 \right) \{N\} \{N\}^T d\xi$	BE: TR/EX
	$\int_{-1}^{+1} -\frac{h}{2} \left(J_{yy} \Omega_y^2 + J_{zz} \Omega_z^2 \right) \{N\} \{N\}^T d\xi$	RA: $St/ST/TR/EX$
	$\int_{-1}^{+1} -\frac{h}{2} \left(\frac{J_{yyy}}{R} \Omega_y^2 + \frac{J_{yzz}}{R} \Omega_z^2 + 2 \frac{J_{yyz}}{R} \Omega_y \Omega_z \right) \{N\} \{N\}^T d\xi$	RA: EX

Geometric Nonlinearity Matrix:

1) General Form: $[K_G] = [[k_{ij}]_G]$; $i,j = 1,2,3,4$; $[k_{ji}]_G = [k_{ij}]_G^T$.
2) Geometric nonlinearity matrices for BE and RA beams are identical.
3) The ST circular-beam approximation is used in deriving the nonlinear terms for all circular beams.
4) The geometric nonlinearity matrix exists only for problems with a nonzero load vector.
5) Individual Geometric Nonlinearity Submatrix Terms and Applicability:

Submatrix	Term	BE/RA Applicability
$[k_{11}]_G$	$\int_{-1}^{+1} \frac{h}{2}\frac{F_x}{R^2}\{N\}\{N\}^T d\xi$	*ST/TR/EX*
$[k_{12}]_G$	$\int_{-1}^{+1} -\frac{F_x}{R}\{N\}\{L^*\}^T d\xi$	*ST/TR/EX*
$[k_{13}]_G$	$\int_{-1}^{+1} -\frac{M_y}{R^2}\{N\}\{L^*\}^T d\xi$	*ST/TR/EX*
$[k_{14}]_G$	$\int_{-1}^{+1} \frac{M_y}{R}\{N\}\{N^*\}^T d\xi$	*ST/TR/EX*
	$\int_{-1}^{+1} \frac{h}{2}\frac{F_x}{R}\{N\}\{N\}^T d\xi$	*ST/TR/EX*
$[k_{22}]_G$	$\int_{-1}^{+1} \frac{2}{h}F_x\{L^*\}\{L^*\}^T d\xi$	*St/ST/TR/EX*
$[k_{23}]_G$	$\int_{-1}^{+1} \frac{2}{h}\frac{M_y}{R}\{L^*\}\{L^*\}^T d\xi$	*ST/TR/EX*
$[k_{24}]_G$	$\int_{-1}^{+1} -\frac{2}{h}M_y\{L^*\}\{N^*\}^T d\xi$	*St/ST/TR/EX*
	$\int_{-1}^{+1} -F_x\{L^*\}\{N\}^T d\xi$	*St/ST/TR/EX*
$[k_{33}]_G$	$\int_{-1}^{+1} \frac{2}{h}F_x\{L^*\}\{L^*\}^T d\xi$	*St/ST/TR/EX*
	$\int_{-1}^{+1} \frac{2}{h}\frac{F_x I_{xx}}{AR^2}\{L^*\}\{L^*\}^T d\xi$	*ST/TR/EX*
$[k_{34}]_G$	$\int_{-1}^{+1} -\frac{2}{h}M_x\{L^*\}\{N^*\}^T d\xi$	*St/ST/TR/EX*
	$\int_{-1}^{+1} F_y\{L^*\}\{N\}^T d\xi$	*St/ST/TR/EX*
	$\int_{-1}^{+1} -\frac{2}{h}\frac{F_x I_{xx}}{AR}\{L^*\}\{N^*\}^T d\xi$	*ST/TR/EX*
$[k_{44}]_G$	$\int_{-1}^{+1} \frac{2}{h}\frac{F_x(I_{yy}+I_{xx})}{A}\{N^*\}\{N^*\}^T d\xi$	*St/ST/TR/EX*

Coriolis Matrix:

1) General Form: $[C] = [[c_{ij}]]$; $i,j = 1,2,3,4$; $[c_{ji}] = -[c_{ij}]^T$.

2) The Coriolis matrix exists only for problems with rotation.

3) Individual Coriolis Submatrix Terms and Applicability:

Submatrix	Term	Applicability
$[c_{12}]$	$\int_{-1}^{+1} -hm\Omega_z \{N\}\{L\}^T d\xi$	BE/RA: $St/ST/TR/EX$
	$\int_{-1}^{+1} -h\frac{J_{yy}}{R^2}\Omega_z \{N\}\{L\}^T d\xi$	BE/RA: TR/EX
$[c_{13}]$	$\int_{-1}^{+1} hm\Omega_y \{N\}\{L\}^T d\xi$	BE/RA: $St/ST/TR/EX$
	$\int_{-1}^{+1} h\frac{J_{yy}}{R^2}\Omega_y \{N\}\{L\}^T d\xi$	BE/RA: TR/EX
	$\int_{-1}^{+1} -\frac{J_{yy}}{R^2}(\Omega_x y_C - \Omega_y x_C)\{N\}\{L^*\}^T d\xi$	BE/RA: TR/EX
	$\int_{-1}^{+1} -\frac{J_{yy}}{R}\frac{I_{yy}}{AR^2}\Omega_x \{N\}\{L^*\}^T d\xi$	BE: TR/EX
	$\int_{-1}^{+1} -\frac{J_0}{R}\Omega_x \{N\}\{L^*\}^T d\xi$	RA: $ST/TR/EX$
	$\int_{-1}^{+1} -\left(\frac{J_{yyy}}{R^2} + \frac{J_{yzz}}{R^2}\right)\Omega_x \{N\}\{L^*\}^T d\xi$	RA: EX
$[c_{14}]$	$\int_{-1}^{+1} h\frac{J_{yy}}{R}\Omega_y \{N\}\{N\}^T d\xi$	BE/RA: TR/EX
	$\int_{-1}^{+1} h\frac{J_{yy}}{R}\frac{I_{yy}}{AR^2}\Omega_y \{N\}\{N\}^T d\xi$	BE: TR/EX
	$\int_{-1}^{+1} \frac{h}{2}\left(2\frac{J_{yy}}{R} - \frac{J_{xx}}{R}\right)\Omega_y \{N\}\{N\}^T d\xi$	RA: $ST/TR/EX$
	$\int_{-1}^{+1} \frac{h}{2}\left[\left(2\frac{J_{yyy}}{R^2} - \frac{J_{yzz}}{R^2}\right)\Omega_y + 3\frac{J_{yyz}}{R^2}\Omega_z\right]$ $\{N\}\{N\}^T d\xi$	RA: EX
$[c_{22}]$	$\int_{-1}^{+1} 2\frac{J_{yy}}{R}\Omega_z \left[\{L^*\}\{L\}^T - \{L\}\{L^*\}^T\right] d\xi$	BE/RA: TR/EX
$[c_{23}]$	$\int_{-1}^{+1} -hm\Omega_z \{L\}\{L\}^T d\xi$	BE/RA: $St/ST/TR/EX$
	$\int_{-1}^{+1} \frac{2}{h}\frac{J_{yy}}{R}(\Omega_x y_C - \Omega_y x_C)\{L^*\}\{L^*\}^T d\xi$	BE/RA: TR/EX
	$\int_{-1}^{+1} -2\frac{J_{yy}}{R}\Omega_y \{L^*\}\{L\}^T d\xi$	BE/RA: TR/EX
	$\int_{-1}^{+1} \frac{2}{h}J_{yy}\frac{I_{yy}}{AR^2}\Omega_x \{L^*\}\{L^*\}^T d\xi$	BE: TR/EX
	$\int_{-1}^{+1} \frac{2}{h}J_0\Omega_x \{L^*\}\{L^*\}^T d\xi$	RA: $St/ST/TR/EX$
	$\int_{-1}^{+1} \frac{2}{h}\left(\frac{J_{yyy}}{R} + \frac{J_{yzz}}{R}\right)\Omega_x \{L^*\}\{L^*\}^T d\xi$	RA: EX

3) Individual Coriolis Submatrix Terms and Applicability (continued):

Submatrix	Term	Applicability
$[c_{24}]$	$\int_{-1}^{+1} -h\frac{J_{yy}}{R}\Omega_x \{L\}\{N\}^T d\xi$	BE/RA: TR/EX
	$\int_{-1}^{+1} -2J_{yy}\frac{J_{yy}}{AR^2}\Omega_y \{L^*\}\{N\}^T d\xi$	BE: TR/EX
	$\int_{-1}^{+1} -(2J_{yy}-J_{zz})\Omega_y \{L^*\}\{N\}^T d\xi$	RA: $St/ST/TR/EX$
	$\int_{-1}^{+1} -\left[\left(2\frac{J_{yyx}}{R}-\frac{J_{yzz}}{R}\right)\Omega_y + 3\frac{J_{yyz}}{R}\Omega_z\right]$ $\{L^*\}\{N\}^T d\xi$	RA: EX
$[c_{34}]$	$\int_{-1}^{+1} \frac{J_{yy}}{R}(\Omega_z y_C - \Omega_y z_C)\{L^*\}\{N\}^T d\xi$	BE/RA: TR/EX
	$\int_{-1}^{+1} J_{yy}\frac{J_{yy}}{AR^2}\Omega_z \{L^*\}\{N\}^T d\xi$	BE: TR/EX
	$\int_{-1}^{+1} -(2J_{zz}-J_{yy})\Omega_z \{L^*\}\{N\}^T d\xi$	RA: $St/ST/TR/EX$
	$\int_{-1}^{+1} -\left[\left(2\frac{J_{yzz}}{R}-\frac{J_{yyx}}{R}\right)\Omega_z + 3\frac{J_{yyz}}{R}\Omega_y\right]$ $\{L^*\}\{N\}^T d\xi$	RA: EX

Mass Matrix:

1) General Form: $[M] = [[m_{ij}]]$; $i,j = 1,2,3,4$; $[m_{ji}] = [m_{ij}]^T$.

2) Individual Mass Submatrix Terms and Applicability:

Submatrix	Term	Applicability
$[m_{11}]$	$\int_{-1}^{+1} \frac{h}{2} m \{N\}\{N\}^T d\xi$	BE/RA: $St/ST/TR/EX$
	$\int_{-1}^{+1} h\frac{J_{yy}}{R^2}\{N\}\{N\}^T d\xi$	BE/RA: TR/EX
	$\int_{-1}^{+1} \frac{h}{2}\frac{J_{yy}}{R^2}\frac{J_{yy}}{AR^2}\{N\}\{N\}^T d\xi$	BE: TR/EX
	$\int_{-1}^{+1} \frac{h}{2}\frac{J_{yy}}{R^2}\{N\}\{N\}^T d\xi$	RA: $ST/TR/EX$
	$\int_{-1}^{+1} \frac{h}{2}\frac{J_{yyx}}{R^3}\{N\}\{N\}^T d\xi$	RA: EX

2) Individual Mass Submatrix Terms and Applicability (continued):

Submatrix	Term	Applicability
$[m_{12}]$	$\int_{-1}^{+1} -\frac{J_{yy}}{R}\{N\}\{L^*\}^T d\xi$	BE/RA: TR/EX
	$\int_{-1}^{+1} -\frac{J_{yy}}{R}\frac{I_{yy}}{AR^2}\{N\}\{L^*\}^T d\xi$	BE: TR/EX
	$\int_{-1}^{+1} -\frac{J_{yy}}{R}\{N\}\{L^*\}^T d\xi$	RA: $ST/TR/EX$
	$\int_{-1}^{+1} -\frac{J_{yyy}}{R^2}\{N\}\{L^*\}^T d\xi$	RA: EX
$[m_{13}]$	$\int_{-1}^{+1} -\frac{J_{yyz}}{R^2}\{N\}\{L^*\}^T d\xi$	RA: EX
$[m_{22}]$	$\int_{-1}^{+1} \frac{h}{2}m\{L\}\{L\}^T d\xi$	BE/RA: $St/ST/TR/EX$
	$\int_{-1}^{+1} \frac{2}{h}J_{yy}\frac{I_{yy}}{AR^2}\{L^*\}\{L^*\}^T d\xi$	BE: TR/EX
	$\int_{-1}^{+1} \frac{2}{h}J_{yy}\{L^*\}\{L^*\}^T d\xi$	RA: $St/ST/TR/EX$
	$\int_{-1}^{+1} \frac{2}{h}\frac{J_{yyy}}{R}\{L^*\}\{L^*\}^T d\xi$	RA: EX
$[m_{23}]$	$\int_{-1}^{+1} \frac{2}{h}\frac{J_{yyz}}{R}\{L^*\}\{L^*\}^T d\xi$	RA: EX
$[m_{33}]$	$\int_{-1}^{+1} \frac{h}{2}m\{L\}\{L\}^T d\xi$	BE/RA: $St/ST/TR/EX$
	$\int_{-1}^{+1} \frac{2}{h}J_{zz}\{L^*\}\{L^*\}^T d\xi$	RA: $St/ST/TR/EX$
	$\int_{-1}^{+1} \frac{2}{h}\frac{J_{yzz}}{R}\{L^*\}\{L^*\}^T d\xi$	RA: EX
$[m_{34}]$	$\int_{-1}^{+1} \frac{h}{2}\frac{J_{yy}}{R}\{L\}\{N\}^T d\xi$	BE/RA: TR/EX
$[m_{44}]$	$\int_{-1}^{+1} \frac{h}{2}J_0\{N\}\{N\}^T d\xi$	BE/RA: $St/ST/TR/EX$
	$\int_{-1}^{+1} \frac{h}{2}\left(\frac{J_{yyy}}{R}+\frac{J_{yzz}}{R}\right)\{N\}\{N\}^T d\xi$	BE/RA: EX

Load Vector:

1) General Form: $\{R\} = \{\{r_i\}\}$; $i = 1,2,3,4$.

2) Contributions to the elemental load vectors are from:

   a) distributed loads (f's),

   b) gravitational acceleration (g's), and

   c) centrifugal acceleration (Ω's).

3) Individual Load Subvector Terms and Applicability:

Subvector	Term	Applicability
$\{r_1\}$	$\int_{-1}^{+1} \frac{h}{2}\Big[m\Big(g_x + (\Omega_y^2+\Omega_z^2)\,x_C - (\Omega_y y_C + \Omega_z z_C)\,\Omega_x\Big) + f_x\Big]\{N\}\,d\xi$	BE/RA: $St/ST/TR/EX$
	$\int_{-1}^{+1} \frac{h}{2}\frac{J_{yy}}{R^2}\Big(g_x + (\Omega_y^2+\Omega_z^2)\,x_C - (\Omega_y y_C + \Omega_z z_C)\,\Omega_x\Big)\{N\}\,d\xi$	BE/RA: TR/EX
	$\int_{-1}^{+1} -\frac{h}{2}\frac{J_{yy}}{R}\Omega_x\Omega_y\{N\}\,d\xi$	BE/RA: TR/EX
	$\int_{-1}^{+1} -\frac{h}{2}\frac{J_{yy}}{R}\frac{J_{yy}}{AR^2}\Omega_x\Omega_y\{N\}\,d\xi$	BE: TR/EX
	$\int_{-1}^{+1} -\frac{h}{2}\frac{J_{yy}}{R}\Omega_x\Omega_y\{N\}\,d\xi$	RA: $ST/TR/EX$
	$\int_{-1}^{+1} -\frac{h}{2}\Big(\frac{J_{yyy}}{R^2}\Omega_y + \frac{J_{yyz}}{R^2}\Omega_z\Big)\Omega_x\{N\}\,d\xi$	RA: EX
$\{r_2\}$	$\int_{-1}^{+1} \frac{h}{2}\Big[m\Big(g_y + (\Omega_z^2+\Omega_x^2)\,y_C - (\Omega_z z_C + \Omega_x x_C)\,\Omega_y\Big) + f_y\Big]\{L\}\,d\xi$	BE/RA: $St/ST/TR/EX$
	$\int_{-1}^{+1} -\frac{J_{yy}}{R}\Big(g_x + (\Omega_y^2+\Omega_z^2)\,x_C - (\Omega_y y_C + \Omega_z z_C)\,\Omega_x\Big)\{L^*\}\,d\xi$	BE/RA: TR/EX
	$\int_{-1}^{+1} \frac{h}{2}\frac{J_{yy}}{R}(\Omega_z^2+\Omega_x^2)\{L\}\,d\xi$	BE/RA: TR/EX
	$\int_{-1}^{+1} J_{yy}\frac{J_{yy}}{AR^2}\Omega_x\Omega_y\{L^*\}\,d\xi$	BE: TR/EX
	$\int_{-1}^{+1} J_{yy}\Omega_x\Omega_y\{L^*\}\,d\xi$	RA: $St/ST/TR/EX$
	$\int_{-1}^{+1} \Big(\frac{J_{yyy}}{R}\Omega_y + \frac{J_{yyz}}{R}\Omega_z\Big)\Omega_x\{L^*\}\,d\xi$	RA: EX

3) Individual Load Subvector Terms and Applicability (continued):

Subvector	Term	Applicability
$\{r_3\}$	$\int_{-1}^{+1} \frac{h}{2}\Big[m\Big(g_z + (\Omega_x^2+\Omega_y^2)\, z_C - (\Omega_x x_C + \Omega_y y_C)\,\Omega_z\Big) + f_z\Big]\{L\}\, d\xi$	BE/RA: $St/ST/TR/EX$
	$\int_{-1}^{+1} -\frac{h}{2}\frac{J_{yz}}{R}\Omega_y\Omega_z\{L\}\, d\xi$	BE/RA: TR/EX
	$\int_{-1}^{+1} J_{zz}\Omega_z\Omega_z\{L^*\}\, d\xi$	RA: $St/ST/TR/EX$
	$\int_{-1}^{+1} \Big(\frac{J_{yzz}}{R}\Omega_z + \frac{J_{yyz}}{R}\Omega_y\Big)\Omega_z\{L^*\}\, d\xi$	RA: EX
$\{r_4\}$	$\int_{-1}^{+1} \frac{h}{2}\frac{J_{yy}}{R}\Big(g_z + (\Omega_x^2+\Omega_y^2)\, z_C - (\Omega_x x_C + \Omega_y y_C)\,\Omega_z\Big)\{N\}\, d\xi$	BE/RA: TR/EX
	$\int_{-1}^{+1} -\frac{h}{2} J_{yy}\frac{I_{yy}}{AR^2}\Omega_y\Omega_z\{N\}\, d\xi$	BE: TR/EX
	$\int_{-1}^{+1} \frac{h}{2}(J_{zz} - J_{yy})\Omega_y\Omega_z\{N\}\, d\xi$	RA: $St/ST/TR/EX$
	$\int_{-1}^{+1} \frac{h}{2}\Big[\Big(\frac{J_{yzz}}{R} - \frac{J_{yyy}}{R}\Big)\Omega_y\Omega_z + \frac{J_{yyz}}{R}(\Omega_y^2 - \Omega_z^2)\Big]\{N\}\, d\xi$	RA: EX

APPENDIX 14.4

Elemental Matrices for Timoshenko Beams

Displacement Assumptions:

Displacement assumptions with respect to the elemental coordinate system:

$$u(x,y,z,t) = u_0(x,t) + yu_y(x,t) + zu_z(x,t),$$

$$v(x,z,t) = v_0(x,t) - z\phi_1(x,t),$$

$$w(x,y,t) = w_0(x,t) + y\phi_1(x,t).$$

Mapping with respect to beam axis:

$$x = Q(\xi) = \left(\frac{1-\xi}{2}\right) x_A + \left(\frac{1+\xi}{2}\right) x_B,$$

$$h = x_B - x_A,$$

where A and B subscripts refer to the end nodes of the element and h is the elemental length.

Displacement variables in terms of elemental shape functions:

$$u_0\,(Q(\xi),t) \cong \sum_{j=1}^{p_1+1} u_{0,j} N_j(\xi) e^{i\omega t},$$

$$v_0\,(Q(\xi),t) \cong \sum_{j=1}^{p_2+1} v_{0,j} N_j(\xi) e^{i\omega t},$$

$$w_0\,(Q(\xi),t) \cong \sum_{j=1}^{p_3+1} w_{0,j} N_j(\xi) e^{i\omega t},$$

$$\phi_1\,(Q(\xi),t) \cong \sum_{j=1}^{p_4+1} \phi_{1,j} N_j(\xi) e^{i\omega t},$$

$$u_y\,(Q(\xi),t) \cong \sum_{j=1}^{p_5+1} u_{y,j} N_j(\xi) e^{i\omega t}, \text{ and}$$

$$u_z\,(Q(\xi),t) \cong \sum_{j=1}^{p_6+1} u_{z,j} N_j(\xi) e^{i\omega t},$$

where $i = \sqrt{-1}$.

Stiffness Matrix:

1) General Form: $[K] = [[k_{ij}]]$; $i,j = 1,2,3,4,5,6$; $[k_{ji}] = [k_{ij}]^T$

2) Differences in circular-beam approximations are dictated by the definitions of the I_{ij}'s:

Elem. Type	Approx.	I_{00}	I_{20}	I_{02}	I_{10}	I_{01}	I_{11}
Straight	(St)	A	I_{yy}	I_{zz}	0	0	0
Circular	ST	A	I_{yy}	I_{zz}	0	0	0
Circular	TR	$A+\frac{I_{yy}}{R^2}$	I_{yy}	I_{zz}	$-\frac{I_{yy}}{R}$	0	0
Circular	EX	I_{00}	I_{20}	I_{02}	I_{10}	I_{01}	I_{11}

3) Individual Stiffness Submatrix Terms and Applicability:

Submatrix	Term	TI Applicability
$[k_{11}]$	$\int_{-1}^{+1} \frac{2}{h} EI_{00} \{N^*\} \{N^*\}^T d\xi$	$St/ST/TR/EX$
	$\int_{-1}^{+1} \frac{h}{2} Gk_y \frac{I_{00}}{R^2} \{N\} \{N\}^T d\xi$	$ST/TR/EX$
$[k_{12}]$	$\int_{-1}^{+1} E\frac{I_{00}}{R} \{N^*\} \{N\}^T d\xi$	$ST/TR/EX$
	$\int_{-1}^{+1} -Gk_y \frac{I_{00}}{R} \{N\} \{N^*\}^T d\xi$	$ST/TR/EX$
$[k_{14}]$	$\int_{-1}^{+1} -E\frac{I_{01}}{R} \{N^*\} \{N\}^T d\xi$	EX
$[k_{15}]$	$\int_{-1}^{+1} -\frac{h}{2} Gk_y \frac{I_{00}}{R} \{N\} \{N\}^T d\xi$	$ST/TR/EX$
	$\int_{-1}^{+1} \frac{2}{h} EI_{10} \{N^*\} \{N^*\}^T d\xi$	TR/EX
$[k_{16}]$	$\int_{-1}^{+1} \frac{2}{h} EI_{01} \{N^*\} \{N^*\}^T d\xi$	EX
$[k_{22}]$	$\int_{-1}^{+1} \frac{2}{h} Gk_y I_{00} \{N^*\} \{N^*\}^T d\xi$	$St/ST/TR/EX$
	$\int_{-1}^{+1} \frac{h}{2} E\frac{I_{00}}{R^2} \{N\} \{N\}^T d\xi$	$ST/TR/EX$
$[k_{24}]$	$\int_{-1}^{+1} -\frac{h}{2} E\frac{I_{01}}{R^2} \{N\} \{N\}^T d\xi$	EX
$[k_{25}]$	$\int_{-1}^{+1} Gk_y I_{00} \{N^*\} \{N\}^T d\xi$	$St/ST/TR/EX$
	$\int_{-1}^{+1} E\frac{I_{10}}{R} \{N\} \{N^*\}^T d\xi$	TR/EX
$[k_{26}]$	$\int_{-1}^{+1} E\frac{I_{01}}{R} \{N\} \{N^*\}^T d\xi$	EX
$[k_{33}]$	$\int_{-1}^{+1} \frac{2}{h} Gk_z I_{00} \{N^*\} \{N^*\}^T d\xi$	$St/ST/TR/EX$
$[k_{36}]$	$\int_{-1}^{+1} Gk_z I_{00} \{N^*\} \{N\}^T d\xi$	$St/ST/TR/EX$

3) Individual Stiffness Submatrix Terms and Applicability (continued):

Submatrix	Term	TI Applicability
$[k_{44}]$	$\int_{-1}^{+1} \frac{2}{h} GI_0 \{N^*\}\{N^*\}^T d\xi$	$St/ST/TR/EX$
	$\int_{-1}^{+1} \frac{h}{2} E\frac{I_{02}}{R^2} \{N\}\{N\}^T d\xi$	$ST/TR/EX$
$[k_{45}]$	$\int_{-1}^{+1} -E\frac{I_{11}}{R} \{N\}\{N^*\}^T d\xi$	EX
$[k_{46}]$	$\int_{-1}^{+1} -E\frac{I_{02}}{R} \{N\}\{N^*\}^T d\xi$	$ST/TR/EX$
	$\int_{-1}^{+1} G\frac{I_0}{R} \{N^*\}\{N\}^T d\xi$	$ST/TR/EX$
$[k_{55}]$	$\int_{-1}^{+1} \frac{2}{h} EI_{20} \{N^*\}\{N^*\}^T d\xi$	$St/ST/TR/EX$
	$\int_{-1}^{+1} \frac{h}{2} Gk_y I_{00} \{N\}\{N\}^T d\xi$	$St/ST/TR/EX$
$[k_{56}]$	$\int_{-1}^{+1} \frac{2}{h} EI_{11} \{N^*\}\{N^*\}^T d\xi$	EX
$[k_{66}]$	$\int_{-1}^{+1} \frac{2}{h} EI_{02} \{N^*\}\{N^*\}^T d\xi$	$St/ST/TR/EX$
	$\int_{-1}^{+1} \frac{h}{2} Gk_x I_{00} \{N\}\{N\}^T d\xi$	$St/ST/TR/EX$
	$\int_{-1}^{+1} \frac{h}{2} G\frac{I_0}{R^2} \{N\}\{N\}^T d\xi$	$ST/TR/EX$

Centrifugal Softening Matrix:

1) General Form: $[K_S] = [[k_{ij}]_S]$; $i,j = 1,2,3,4,5,6$; $[k_{ji}]_S = [k_{ij}]_S^T$.

2) The centrifugal softening matrix exists only for problems with rotation.

3) Individual Centrifugal Softening Submatrix Terms and Applicability:

Submatrix	Term	TI Applicability
$[k_{11}]_S$	$\int_{-1}^{+1} -\frac{h}{2} m\left(\Omega_y^2 + \Omega_z^2\right)\{N\}\{N\}^T d\xi$	$St/ST/TR/EX$
$[k_{12}]_S$	$\int_{-1}^{+1} \frac{h}{2} m\Omega_x\Omega_y \{N\}\{N\}^T d\xi$	$St/ST/TR/EX$
$[k_{13}]_S$	$\int_{-1}^{+1} \frac{h}{2} m\Omega_z\Omega_x \{N\}\{N\}^T d\xi$	$St/ST/TR/EX$
$[k_{14}]_S$	$\int_{-1}^{+1} \frac{h}{2} \frac{J_{yy}}{R}\Omega_z\Omega_x \{N\}\{N\}^T d\xi$	TR/EX
$[k_{15}]_S$	$\int_{-1}^{+1} -\frac{h}{2} \frac{J_{yy}}{R}\left(\Omega_y^2 + \Omega_z^2\right)\{N\}\{N\}^T d\xi$	TR/EX
$[k_{22}]_S$	$\int_{-1}^{+1} -\frac{h}{2} m\left(\Omega_z^2 + \Omega_x^2\right)\{N\}\{N\}^T d\xi$	$St/ST/TR/EX$

3) Individual Centrifugal Softening Submatrix Terms and Applicability (continued):

Submatrix	Term	TI Applicability
$[k_{23}]_S$	$\int_{-1}^{+1} \frac{h}{2} m\Omega_y\Omega_z \{N\}\{N\}^T d\xi$	*St/ST/TR/EX*
$[k_{24}]_S$	$\int_{-1}^{+1} \frac{h}{2} \frac{J_{yy}}{R}\Omega_y\Omega_z \{N\}\{N\}^T d\xi$	*TR/EX*
$[k_{25}]_S$	$\int_{-1}^{+1} \frac{h}{2} \frac{J_{yy}}{R}\Omega_z\Omega_y \{N\}\{N\}^T d\xi$	*TR/EX*
$[k_{33}]_S$	$\int_{-1}^{+1} -\frac{h}{2} m\left(\Omega_z^2+\Omega_y^2\right)\{N\}\{N\}^T d\xi$	*St/ST/TR/EX*
$[k_{34}]_S$	$\int_{-1}^{+1} -\frac{h}{2} \frac{J_{yy}}{R}\left(\Omega_z^2+\Omega_y^2\right)\{N\}\{N\}^T d\xi$	*TR/EX*
$[k_{35}]_S$	$\int_{-1}^{+1} \frac{h}{2} \frac{J_{yy}}{R}\Omega_z\Omega_z \{N\}\{N\}^T d\xi$	*TR/EX*
$[k_{44}]_S$	$\int_{-1}^{+1} -\frac{h}{2}\left(J_{yy}\Omega_y^2+J_{zz}\Omega_z^2\right)\{N\}\{N\}^T d\xi$	*St/ST/TR/EX*
	$\int_{-1}^{+1} -\frac{h}{2}\left(\frac{J_{yyy}}{R}\Omega_y^2+\frac{J_{yzz}}{R}\Omega_z^2+ 2\frac{J_{yyz}}{R}\Omega_y\Omega_z\right)\{N\}\{N\}^T d\xi$	*EX*
$[k_{45}]_S$	$\int_{-1}^{+1} -\frac{h}{2} J_{zz}\Omega_z\Omega_z \{N\}\{N\}^T d\xi$	*St/ST/TR/EX*
	$\int_{-1}^{+1} -\frac{h}{2}\left(\frac{J_{yzz}}{R}\Omega_z+\frac{J_{yyz}}{R}\Omega_y\right)\Omega_z \{N\}\{N\}^T d\xi$	*EX*
$[k_{46}]_S$	$\int_{-1}^{+1} \frac{h}{2} J_{yy}\Omega_z\Omega_y \{N\}\{N\}^T d\xi$	*St/ST/TR/EX*
	$\int_{-1}^{+1} \frac{h}{2}\left(\frac{J_{yyy}}{R}\Omega_y+\frac{J_{yyz}}{R}\Omega_z\right)\Omega_z \{N\}\{N\}^T d\xi$	*EX*
$[k_{55}]_S$	$\int_{-1}^{+1} -\frac{h}{2}\left(J_0\Omega_y^2+J_{zz}\Omega_z^2\right)\{N\}\{N\}^T d\xi$	*St/ST/TR/EX*
	$\int_{-1}^{+1} -\frac{h}{2}\left[\left(\frac{J_{yyy}}{R}+\frac{J_{yzz}}{R}\right)\Omega_y^2+\frac{J_{yzz}}{R}\Omega_z^2\right] \{N\}\{N\}^T d\xi$	*EX*
$[k_{56}]_S$	$\int_{-1}^{+1} -\frac{h}{2} J_0\Omega_y\Omega_z \{N\}\{N\}^T d\xi$	*St/ST/TR/EX*
	$\int_{-1}^{+1} -\frac{h}{2}\left[\left(\frac{J_{yyy}}{R}+\frac{J_{yzz}}{R}\right)\Omega_y\Omega_z-\frac{J_{yyz}}{R}\Omega_z^2\right] \{N\}\{N\}^T d\xi$	*EX*

3) Individual Centrifugal Softening Submatrix Terms and Applicability (continued):

Submatrix	Term	TI Applicability
$[k_{66}]_S$	$\int_{-1}^{+1} -\frac{h}{2}\left[J_0\Omega_z^2 + J_{yy}\Omega_x^2\right]\{N\}\{N\}^T d\xi$	$St/ST/TR/EX$
	$\int_{-1}^{+1} -\frac{h}{2}\left[\left(\frac{J_{yyx}}{R} + \frac{J_{yzz}}{R}\right)\Omega_z^2 + \frac{J_{yyx}}{R}\Omega_x^2\right]$	EX
	$\{N\}\{N\}^T d\xi$	

Geometric Nonlinearity Matrix:

1) General Form: $[K_G] = [[k_{ij}]_G]$; $i,j = 1,2,3,4,5,6$; $[k_{ji}]_G = [k_{ij}]_G^T$.
2) The ST circular-beam approximation is used in deriving the nonlinear terms for all circular beams.
3) The geometric nonlinearity matrix exists only for problems with a nonzero load vector.
4) Individual Geometric Nonlinearity Submatrix Terms and Applicability:

Submatrix	Term	TI Applicability
$[k_{11}]_G$	$\int_{-1}^{+1} \frac{h}{2}\frac{F_z}{R^2}\{N\}\{N\}^T d\xi$	$ST/TR/EX$
$[k_{12}]_G$	$\int_{-1}^{+1} -\frac{F_z}{R}\{N\}\{N^*\}^T d\xi$	$ST/TR/EX$
$[k_{14}]_G$	$\int_{-1}^{+1} \frac{M_y}{R}\{N\}\{N^*\}^T d\xi$	$ST/TR/EX$
	$\int_{-1}^{+1} \frac{h}{2}\frac{F_x}{R}\{N\}\{N\}^T d\xi$	$ST/TR/EX$
$[k_{16}]_G$	$\int_{-1}^{+1} \frac{h}{2}\frac{M_y}{R^2}\{N\}\{N\}^T d\xi$	$ST/TR/EX$
$[k_{22}]_G$	$\int_{-1}^{+1} \frac{2}{h}F_z\{N^*\}\{N^*\}^T d\xi$	$St/ST/TR/EX$
$[k_{24}]_G$	$\int_{-1}^{+1} -\frac{2}{h}M_y\{N^*\}\{N^*\}^T d\xi$	$St/ST/TR/EX$
	$\int_{-1}^{+1} -F_z\{N^*\}\{N\}^T d\xi$	$St/ST/TR/EX$
$[k_{26}]_G$	$\int_{-1}^{+1} -\frac{M_y}{R}\{N^*\}\{N\}^T d\xi$	$ST/TR/EX$
$[k_{33}]_G$	$\int_{-1}^{+1} \frac{2}{h}F_z\{N^*\}\{N^*\}^T d\xi$	$St/ST/TR/EX$
$[k_{34}]_G$	$\int_{-1}^{+1} -\frac{2}{h}M_z\{N^*\}\{N^*\}^T d\xi$	$St/ST/TR/EX$
	$\int_{-1}^{+1} F_y\{N^*\}\{N\}^T d\xi$	$St/ST/TR/EX$

4) Individual Geometric Nonlinearity Submatrix Terms and Applicability: (continued):

Submatrix	Term	TI Applicability
$[k_{44}]_G$	$\int_{-1}^{+1} \frac{2}{h} \frac{F_x(I_{yy}+I_{zz})}{A} \{N^*\}\{N^*\}^T d\xi$	*St/ST/TR/EX*
$[k_{46}]_G$	$\int_{-1}^{+1} \frac{F_x I_{xx}}{AR} \{N^*\}\{N\}^T d\xi$	*ST/TR/EX*
$[k_{66}]_G$	$\int_{-1}^{+1} \frac{h}{2} \frac{F_x I_{xx}}{AR^2} \{N\}\{N\}^T d\xi$	*ST/TR/EX*

Coriolis Matrix:

1) General Form: $[C] = [[c_{ij}]]$; $i,j = 1,2,3,4,5,6$; $[c_{ji}] = -[c_{ij}]^T$.

3) The Coriolis matrix exists only for problems with rotation.

3) Individual Coriolis Submatrix Terms and Applicability:

Submatrix	Term	TI Applicability
$[c_{12}]$	$\int_{-1}^{+1} -hm\Omega_z \{N\}\{N\}^T d\xi$	*St/ST/TR/EX*
$[c_{13}]$	$\int_{-1}^{+1} hm\Omega_y \{N\}\{N\}^T d\xi$	*St/ST/TR/EX*
$[c_{14}]$	$\int_{-1}^{+1} h\frac{J_{yy}}{R}\Omega_y \{N\}\{N\}^T d\xi$	*TR/EX*
$[c_{23}]$	$\int_{-1}^{+1} -hm\Omega_x \{N\}\{N\}^T d\xi$	*St/ST/TR/EX*
$[c_{24}]$	$\int_{-1}^{+1} -h\frac{J_{yy}}{R}\Omega_x \{N\}\{N\}^T d\xi$	*TR/EX*
$[c_{25}]$	$\int_{-1}^{+1} h\frac{J_{yy}}{R}\Omega_z \{N\}\{N\}^T d\xi$	*TR/EX*
$[c_{35}]$	$\int_{-1}^{+1} -h\frac{J_{yy}}{R}\Omega_y \{N\}\{N\}^T d\xi$	*TR/EX*
$[c_{45}]$	$\int_{-1}^{+1} -\frac{h}{2}(2J_{yy} - J_{zz})\Omega_y \{N\}\{N\}^T d\xi$	*St/ST/TR/EX*
	$\int_{-1}^{+1} -\frac{h}{2}\left[\left(2\frac{J_{yyy}}{R} - \frac{J_{yzz}}{R}\right)\Omega_y + 3\frac{J_{yyz}}{R}\Omega_z\right] \{N\}\{N\}^T d\xi$	*EX*
$[c_{46}]$	$\int_{-1}^{+1} -\frac{h}{2}(2J_{zz} - J_{yy})\Omega_z \{N\}\{N\}^T d\xi$	*St/ST/TR/EX*
	$\int_{-1}^{+1} \frac{h}{2}\frac{J_{yy}}{R}(\Omega_z y_C - \Omega_y z_C)\{N\}\{N\}^T d\xi$	*TR/EX*
	$\int_{-1}^{+1} -\frac{h}{2}\left[\left(2\frac{J_{yzz}}{R} - \frac{J_{yyy}}{R}\right)\Omega_z + 3\frac{J_{yyz}}{R}\Omega_y\right] \{N\}\{N\}^T d\xi$	*EX*

3) Individual Coriolis Submatrix Terms and Applicability:
(continued):

Submatrix	Term	TI Applicability
$[c_{56}]$	$\int_{-1}^{+1} \frac{h}{2} J_0 \Omega_x \{N\}\{N\}^T d\xi$	$St/ST/TR/EX$
	$\int_{-1}^{+1} \frac{h}{2} \frac{J_{yy}}{R} (\Omega_x y_C - \Omega_y x_C) \{N\}\{N\}^T d\xi$	TR/EX
	$\int_{-1}^{+1} \frac{h}{2} \left(\frac{J_{yyy}}{R} + \frac{J_{yzz}}{R} \right) \Omega_x \{N\}\{N\}^T d\xi$	EX

Mass Matrix:

1) General Form: $[M] = [[m_{ij}]]; \quad i,j = 1,2,3,4,5,6; \quad [m_{ji}] = [m_{ij}]^T.$

2) Individual Mass Submatrix Terms and Applicability:

Submatrix	Term	TI Applicability
$[m_{11}]$	$\int_{-1}^{+1} \frac{h}{2} m \{N\}\{N\}^T d\xi$	$St/ST/TR/EX$
$[m_{15}]$	$\int_{-1}^{+1} \frac{h}{2} \frac{J_{yy}}{R} \{N\}\{N\}^T d\xi$	TR/EX
$[m_{22}]$	$\int_{-1}^{+1} \frac{h}{2} m \{N\}\{N\}^T d\xi$	$St/ST/TR/EX$
$[m_{33}]$	$\int_{-1}^{+1} \frac{h}{2} m \{N\}\{N\}^T d\xi$	$St/ST/TR/EX$
$[m_{34}]$	$\int_{-1}^{+1} \frac{h}{2} \frac{J_{yy}}{R} \{N\}\{N\}^T d\xi$	TR/EX
$[m_{44}]$	$\int_{-1}^{+1} \frac{h}{2} J_0 \{N\}\{N\}^T d\xi$	$St/ST/TR/EX$
	$\int_{-1}^{+1} \frac{h}{2} \left(\frac{J_{yyy}}{R} + \frac{J_{yzz}}{R} \right) \{N\}\{N\}^T d\xi$	EX
$[m_{55}]$	$\int_{-1}^{+1} \frac{h}{2} J_{yy} \{N\}\{N\}^T d\xi$	$St/ST/TR/EX$
	$\int_{-1}^{+1} \frac{h}{2} \frac{J_{yyy}}{R} \{N\}\{N\}^T d\xi$	EX
$[m_{56}]$	$\int_{-1}^{+1} \frac{h}{2} \frac{J_{yyz}}{R} \{N\}\{N\}^T d\xi$	EX
$[m_{66}]$	$\int_{-1}^{+1} \frac{h}{2} J_{zz} \{N\}\{N\}^T d\xi$	$St/ST/TR/EX$
	$\int_{-1}^{+1} \frac{h}{2} \frac{J_{yzz}}{R} \{N\}\{N\}^T d\xi$	EX

Load Vector:

1) General Form: $\{R\} = \{\{r_i\}\}; \quad i = 1,2,3,4,5,6.$

2) Contributions to the elemental load vectors are from:
   a) distributed loads (f's),
   b) gravitational acceleration (g's), and
   c) centrifugal acceleration (Ω's).
3) Individual Load Subvector Terms and Applicability:

Subvector	Term	TI Applicability
$\{r_1\}$	$\int_{-1}^{+1} \frac{h}{2}\Big[m\Big(g_x + (\Omega_y^2+\Omega_z^2)\,x_C - (\Omega_y y_C + \Omega_z z_C)\,\Omega_x\Big) + f_x\Big]\,\{N\}\,d\xi$	*St/ST/TR/EX*
	$\int_{-1}^{+1} -\frac{h}{2}\frac{J_{yz}}{R}\Omega_x\Omega_y\,\{N\}\,d\xi$	*TR/EX*
$\{r_2\}$	$\int_{-1}^{+1} \frac{h}{2}\Big[m\Big(g_y + (\Omega_z^2+\Omega_x^2)\,y_C - (\Omega_z z_C + \Omega_x x_C)\,\Omega_y\Big) + f_y\Big]\,\{N\}\,d\xi$	*St/ST/TR/EX*
	$\int_{-1}^{+1} \frac{h}{2}\frac{J_{yz}}{R}\,(\Omega_z^2+\Omega_x^2)\,\{N\}\,d\xi$	*TR/EX*
$\{r_3\}$	$\int_{-1}^{+1} \frac{h}{2}\Big[m\Big(g_z + (\Omega_x^2+\Omega_y^2)\,z_C - (\Omega_x x_C + \Omega_y y_C)\,\Omega_z\Big) + f_z\Big]\,\{N\}\,d\xi$	*St/ST/TR/EX*
	$\int_{-1}^{+1} -\frac{h}{2}\frac{J_{yz}}{R}\Omega_y\Omega_z\,\{N\}\,d\xi$	*TR/EX*
$\{r_4\}$	$\int_{-1}^{+1} \frac{h}{2}\,(J_{zz}-J_{yy})\,\Omega_y\Omega_z\,\{N\}\,d\xi$	*St/ST/TR/EX*
	$\int_{-1}^{+1} \frac{h}{2}\frac{J_{yz}}{R}\Big(g_z + (\Omega_x^2+\Omega_y^2)\,z_C - (\Omega_x x_C + \Omega_y y_C)\,\Omega_z\Big)\,\{N\}\,d\xi$	*TR/EX*
	$\int_{-1}^{+1} \frac{h}{2}\Big[\Big(\frac{J_{yzz}}{R}-\frac{J_{yyy}}{R}\Big)\,\Omega_y\Omega_z + \frac{J_{yyz}}{R}\,(\Omega_y^2-\Omega_z^2)\Big]\,\{N\}\,d\xi$	*EX*
$\{r_5\}$	$\int_{-1}^{+1} -\frac{h}{2}J_{yy}\Omega_x\Omega_y\,\{N\}\,d\xi$	*St/ST/TR/EX*
	$\int_{-1}^{+1} \frac{h}{2}\frac{J_{yy}}{R}\Big(g_x + (\Omega_y^2+\Omega_z^2)\,x_C - (\Omega_y y_C + \Omega_z z_C)\,\Omega_x\Big)\,\{N\}\,d\xi$	*TR/EX*
	$\int_{-1}^{+1} -\frac{h}{2}\Big(\frac{J_{yyy}}{R}\Omega_y + \frac{J_{yyz}}{R}\Omega_z\Big)\,\Omega_z\,\{N\}\,d\xi$	*EX*

3) Individual Load Subvector Terms and Applicability (continued):

Subvector	Term	TI Applicability
$\{r_6\}$	$\int_{-1}^{+1} -\frac{h}{2} J_{xx} \Omega_x \Omega_z \{N\} d\xi$	*St/ST/TR/EX*
	$\int_{-1}^{+1} -\frac{h}{2} \left(\frac{J_{yxz}}{R} \Omega_x + \frac{J_{yyz}}{R} \Omega_y \right) \Omega_z \{N\} d\xi$	*EX*

APPENDIX 14.5

Global Matrix Terms for Distributed Masses

Formulation:

1) The degrees-of-freedom are the three displacements, U_1, U_2, and U_3, and the three rotations, U_4, U_5, and U_6, about the global axes, X, Y, and Z, respectively, for the grid point coinciding with the center of mass. The row and column numbers of the matrices and vector below relate to these numbered degrees-of-freedom.
2) Individual terms flagged by a † are ignored in problems using Bernoulli-Euler beams.

Centrifugal Softening Matrix: $[K_S] = k_{ijS}; \quad i,j = 1,2,3,4,5,6; \quad k_{ijS} = k_{jiS}.$

$$k_{11S} = -M\left(\Omega_Y^2 + \Omega_Z^2\right)$$

$$k_{22S} = -M\left(\Omega_Z^2 + \Omega_X^2\right)$$

$$k_{33S} = -M\left(\Omega_X^2 + \Omega_Y^2\right)$$

$$k_{12S} = M\Omega_X\Omega_Y$$

$$k_{23S} = M\Omega_Y\Omega_Z$$

$$k_{13S} = M\Omega_Z\Omega_X$$

$$\dagger k_{44S} = -\left(J_{XX} + J_{YY}\right)\Omega_Y^2 - \left(J_{ZZ} + J_{XX}\right)\Omega_Z^2 - 2J_{YZ}\Omega_Y\Omega_Z$$

$$\dagger k_{55S} = -\left(J_{YY} + J_{ZZ}\right)\Omega_Z^2 - \left(J_{XX} + J_{YY}\right)\Omega_X^2 - 2J_{ZX}\Omega_Z\Omega_X$$

$$\dagger k_{66S} = -\left(J_{ZZ} + J_{XX}\right)\Omega_X^2 - \left(J_{YY} + J_{ZZ}\right)\Omega_Y^2 - 2J_{XY}\Omega_X\Omega_Y$$

$$\dagger k_{45S} = \left(J_{XX} + J_{YY}\right)\Omega_X\Omega_Y - J_{XY}\Omega_Z^2 + J_{YZ}\Omega_Z\Omega_X + J_{ZX}\Omega_Y\Omega_Z$$

$$\dagger k_{56S} = \left(J_{YY} + J_{ZZ}\right)\Omega_Y\Omega_Z - J_{YZ}\Omega_X^2 + J_{ZX}\Omega_X\Omega_Y + J_{XY}\Omega_Z\Omega_X$$

$$\dagger k_{46S} = \left(J_{ZZ} + J_{XX}\right)\Omega_Z\Omega_X - J_{ZX}\Omega_Y^2 + J_{XY}\Omega_Y\Omega_Z + J_{YZ}\Omega_X\Omega_Y$$

Coriolis Damping Matrix: $[C] = c_{ij}; \quad i,j = 1,2,3,4,5,6; \quad c_{ij} = -c_{ji}.$

$$c_{12} = -2M\Omega_Z$$

$$c_{23} = -2M\Omega_X$$

$$c_{13} = +2M\Omega_Y$$

$$\dagger c_{45} = +\left(J_{XX} + J_{YY} - 2J_{ZZ}\right)\Omega_Z - 3J_{YZ}\Omega_Y - 3J_{ZX}\Omega_X$$

$$\dagger c_{56} = +\left(J_{YY} + J_{ZZ} - 2J_{XX}\right)\Omega_X - 3J_{ZX}\Omega_Z - 3J_{XY}\Omega_Y$$

$$\dagger c_{46} = -\left(J_{ZZ} + J_{XX} - 2J_{YY}\right)\Omega_Y + 3J_{XY}\Omega_X + 3J_{YZ}\Omega_Z$$

Mass Matrix: $[M] = m_{ij}; \quad i,j = 1,2,3,4,5,6; \quad m_{ij} = m_{ji}.$

$m_{11} = M$

$m_{22} = M$

$m_{33} = M$

$\dagger m_{44} = (J_{YY} + J_{ZZ})$

$\dagger m_{55} = (J_{ZZ} + J_{XX})$

$\dagger m_{66} = (J_{XX} + J_{YY})$

$\dagger m_{45} = -J_{XY}$

$\dagger m_{56} = -J_{YZ}$

$\dagger m_{46} = -J_{ZX}$

Load Vector: $\{R\} = r_i; \quad i = 1,2,3,4,5,6.$

$$r_1 = M\left[g_X + \left(\Omega_Y^2 + \Omega_Z^2\right)(X_C - X_\Omega) - \Omega_X\Omega_Y\,(Y_C - Y_\Omega) - \Omega_Z\Omega_X\,(Z_C - Z_\Omega)\right]$$

$$r_2 = M\left[g_Y + \left(\Omega_Z^2 + \Omega_X^2\right)(Y_C - Y_\Omega) - \Omega_Y\Omega_Z\,(Z_C - Z_\Omega) - \Omega_X\Omega_Y\,(X_C - X_\Omega)\right]$$

$$r_3 = M\left[g_Z + \left(\Omega_X^2 + \Omega_Y^2\right)(Z_C - Z_\Omega) - \Omega_Z\Omega_X\,(X_C - X_\Omega) - \Omega_Y\Omega_Z\,(Y_C - Y_\Omega)\right]$$

$$\dagger r_4 = (J_{ZZ} - J_{YY})\,\Omega_Y\Omega_Z + J_{YZ}\left(\Omega_Y^2 - \Omega_Z^2\right) + J_{ZX}\Omega_X\Omega_Y - J_{XY}\Omega_Z\Omega_X$$

$$\dagger r_5 = (J_{XX} - J_{ZZ})\,\Omega_Z\Omega_X + J_{ZX}\left(\Omega_Z^2 - \Omega_X^2\right) + J_{XY}\Omega_Y\Omega_Z - J_{YZ}\Omega_X\Omega_Y$$

$$\dagger r_6 = (J_{YY} - J_{XX})\,\Omega_X\Omega_Y + J_{XY}\left(\Omega_X^2 - \Omega_Y^2\right) + J_{YZ}\Omega_Z\Omega_X - J_{ZX}\Omega_Y\Omega_Z$$

15. BIBLIOGRAPHY

[1] Babuška, I., Szabó, B., and Katz, I. N., "The p-Version of the Finite Element Method," *SIAM Journal of Numerical Analysis*, **18**, pp. 515-545 (1981).

[2] Szabó, B., and Babuška, I., "Comments on Error Estimation," presented at: CSM Contract/Grant Review, Langley Research Center, National Aeronautics and Space Administration, August 28-30, 1989.

[3] Szabó, B., "Estimation and Control of Error Based on p-Convergence," in: I. Babuška, J. Gago, E. R. de A. Oliveira, and O. C. Zienkiewicz, editors, *Accuracy Estimates and Adaptive Refinements in Finite Element Computations*, John Wiley and Sons, New York, pp. 61-78 (1986).

[4] Segerlind, L. J., *Applied Finite Element Analysis*, John Wiley and Sons, New York (1976).

[5] Gordon, W. J., "Blending-Function Methods of Bivariate and Multivariate Interpolation and Approximation," *SIAM Journal of Numerical Analysis*, **8**, pp. 158-177 (1971).

[6] Szabó, B., and Sahrmann, G. J., "Hierarchic Plate and Shell Models Based on p-Extension," *International Journal for Numerical Methods in Engineering*, **26**, pp. 1855-1881 (1988).

[7] Szabó, B., "On Geometric Idealizations in Finite Element Computations," *Washington University Technical Note*, WU/CCM-87/4 (1987).

[8] Brussat, T. R., and Malone, R. L., "Stress Analysis of Lugs Using PROBE," *Lockheed Corporation Technical Report*, LR 31229 (1987).

[9] Holzer, H., *Die Berechnung der Drehschwingungen*, Springer-Verlag, Berlin (1921).

[10] Myklestad, N. O., "A New Method of Calculating Natural Modes of Uncoupled Bending Vibration of Airplane Wings and Other Types of Beams," *Journal of Aeronautical Science*, **11**, pp. 153-162 (1944).

[11] Meirovitch, L., *Analytical Methods in Vibrations*, Macmillan, New York (1967).

[12] Lord Rayleigh, *Theory of Sound*, Dover, New York, Second Edition (1945 reissue).

[13] Ritz, W., "Über eine neue Methode zur Lösung gewisser Variationsprobleme der Mathematischen Physik," *Journal für Reine und Angewandte Mathematik*, **135**, pp. 1-61 (1909).

[14] Bathe, K. J., and Wilson, E. L., *Numerical Methods in Finite Element Analysis*, Prentice-Hall, Englewood Cliffs, NJ (1976).

[15] Meirovitch, L., "A New Method of Solution of the Eigenvalue Problem for Gyroscopic Systems," *American Institute of Aeronautics and Astronautics Journal*, **12**, pp. 1337-1342 (1974).

[16] Timoshenko, S. P., and Gere, J. M., *Theory of Elastic Stability*, McGraw-Hill, New York, Second Edition (1961).

[17] Przemieniecki, J. S., *Theory of Matrix Structural Analysis*, Dover, New York (1968 reissue).

[18] Bokaian, A., "Natural Frequencies of Beams Under Compressive Axial Loads," *Journal of Sound and Vibration*, **126**, pp. 49-65 (1988).

[19] Peters, D. A., "The Effect of Rotation on Structural Stiffness," *Proceedings of the Fifth World Congress on Theory of Machines and Mechanisms*, ASME, pp. 280-283 (1979).

[20] Hodges, D. H., and Rutkowski, M. J., "Free-Vibration Analysis of Rotating Beams by a Variable-Order Finite-Element Method," *American Institute of Aeronautics and Astronautics Journal*, **19**, pp. 1459-1466 (1981).

[21] Meirovitch, L., and Baruh, H., "On the Inclusion Principle for the Hierarchical Finite Element Method," *International Journal for Numerical Methods in Engineering*, **19**, pp. 281-291 (1983).

[22] Hinnant, H. E., "Derivation of a Tapered p-Version Beam Finite Element," *National Aeronautics and Space Administration Technical Paper*, NASA TP-2931 (1989).

[23] Tessler, A., and Dong, S. B., "On a Hierarchy of Conforming Timoshenko Beam Elements," *Computers and Structures*, **14**, pp. 335-344 (1981).

[24] Dawe, D. J., "Numerical Studies Using Circular Arch Finite Elements," *Computers and Structures*, **4**, pp. 729-740 (1974).

[25] Yang, T. Y., *Finite Element Structural Analysis*, Prentice-Hall, Englewood Cliffs, NJ (1986).

[26] Petyt, M., and Fleischer, C. C., "Free Vibration of a Curved Beam," *Journal of Sound and Vibration*, **18**, pp. 17-30 (1971).

[27] Carne, T. G., Lobitz, D. W., Nord, A. R., and Watson, R. A., "Finite Element Analysis and Modal Testing of a Rotating Wind Turbine," *Sandia National Laboratories Report*, SAND82-0345 (1982).

[28] Leung, A. Y. T., and Fung, T. C., "Spinning Finite Elements," *Journal of Sound and Vibration*, **125**, pp. 523-537 (1988).

[29] Szabó, B., and Babuška, I., *Introduction to Finite Element Analysis*, John Wiley and Sons, New York (1990 – to be published).

[30] Bathe, K. J., and Wilson, E. L., "Solution Methods for Eigenvalue Problems in Structural Mechanics," *International Journal for Numerical Methods in Engineering*, **6**, pp. 213-226 (1973).

[31] Timoshenko, S. P., *History of Strength of Materials*, Dover, New York (1953 reissue).

[32] Hodges, D. H., Ormiston, R. A., and Peters, D. A., "On the Nonlinear Deformation Geometry of Euler-Bernoulli Beams," *National Aeronautics and Space Administration Technical Paper*, NASA TP-1566 (1980).

[33] Danielson, D. A., and Hodges, D. H., "A Beam Theory for Large Global Rotation, Moderate Local Rotation, and Small Strain," *Journal of Applied Mechanics*, ASME, **55**, pp. 179-184 (1988).

[34] Krishna Murty, A. V., "Vibrations of Short Beams," *American Institute of Aeronautics and Astronautics Journal*, **8**, pp. 34-38 (1970).

[35] Levinson, M., "A New Rectangular Beam Theory," *Journal of Sound and Vibration*, **74**, pp. 81-87 (1981).

[36] Gardner, T. G., and Bert, C. W., "Vibration of Shear Deformable Rings: Theory and Experiment," *Journal of Sound and Vibration*, **103**, pp. 549-565 (1985).

[37] Lincoln, J. W., and Volterra, E., "Experimental and Theoretical Determination of Frequencies of Elastic Toroids," *Experimental Mechanics*, **24**, pp. 211-217 (1967).

[38] Timoshenko, S. P., and Goodier, J. N., *Theory of Elasticity*, McGraw-Hill, New York, Third Edition (1970).

[39] Bickford, W. B., and Maganty, S. P., "On the Out-of-Plane Vibrations of Thick Rotating Rings," *Journal of Sound and Vibration*, **110**, pp. 121-127 (1986).

[40] Pipes, L. A., *Matrix Methods for Engineering*, Prentice-Hall, Englewood Cliffs, NJ (1963).

[41] Crandall, S. H., Karnopp, D. C., Kurtz, E. F., and Pridmore-Brown, D. C., *Dynamics of Mechanical and Electromechanical Systems*, McGraw-Hill, New York (1968).

[42] Craig, J. J., *Introduction to Robotics: Mechanics and Control*, Addison-Wesley, Reading, MA (1986).

[43] Sokolnikoff, I. S., *Mathematical Theory of Elasticity*, McGraw-Hill, New York, Second Edition (1956).

[44] Timoshenko, S. P., "On the Correction for Shear of the Differential Equation for Transverse Vibrations of Prismatic Bars," *Philosophical Magazine*, **41**, pp. 744-746 (1921).

[45] Mindlin, R. D., and Deresiewicz, H., "Timoshenko's Shear Coefficient for Flexural Vibrations of Beams," *Proceedings of the Second U. S. National Congress of Applied Mechanics*, ASME, pp. 175-178 (1955).

[46] Timoshenko, S. P., "On the Transverse Vibrations of Bars of Uniform Cross-Section," *Philosophical Magazine*, **43**, pp. 125-131 (1922).

[47] Cowper, G. R., "The Shear Coefficient in Timoshenko's Beam Theory," *Journal of Applied Mechanics*, ASME, **33**, pp. 335-340 (1966).

[48] Hutchinson, J. R., "Transverse Vibrations of Beams, Exact Versus Approximate Solutions," *Journal of Applied Mechanics*, ASME, **48**, pp. 923-928 (1981).

[49] Volterra, E., and Gaines, J. H., *Advanced Strength of Materials*, Prentice-Hall, Englewood Cliffs, NJ (1971).

[50] Thomas, D. L., Wilson, J. M., and Wilson, R. R., "Timoshenko Beam Finite Elements," *Journal of Sound and Vibration*, **31**, pp. 315-330 (1973).

[51] Rao, S. S., *Mechanical Vibrations*, Addison-Wesley, Reading, MA (1986).

[52] Saada, A. S., *Elasticity: Theory and Applications*, Pergamon Press, New York (1974).

[53] Dawe, D. J., "Curved Finite Elements for the Analysis of Shallow and Deep Arches," *Computers and Structures*, **4**, pp. 559-580 (1974).

[54] Volterra, E., and Morell, J. D., "A Note on the Lowest Natural Frequency of Elastic Arcs," *Journal of Applied Mechanics*, ASME, **27**, pp. 744-746 (1960).

[55] Popov, E. P., *Introduction to Mechanics of Solids*, Prentice-Hall, Englewood Cliffs, NJ (1968).

[56] Beer, F. P., and Johnston, E. R., *Vector Mechanics for Engineers: Dynamics*, McGraw-Hill, New York, Second Edition (1972).

[57] Langhaar, H. L., *Energy Methods in Applied Mechanics*, John Wiley and Sons, New York (1962).

[58] Filipich, C. P., and Laura, P. A. A., "First and Second Natural Frequencies of Hinged and Clamped Circular Arcs: A Discussion of a Classical Paper," *Journal of Sound and Vibration*, **125**, pp. 393-396 (1988).

[59] Wang, T. M., and Moore, J. A., "Lowest Natural Extensional Frequency of Clamped Elliptic Arcs," *Journal of Sound and Vibration*, **30**, pp. 1-7 (1973).

[60] Hoppe, R., "The Bending Vibration of a Circular Ring," *Crelle Journal of Mathematics*, **73**, pp. 158-170 (1871).

[61] Den Hartog, J. P., "The Lowest Natural Frequency of Circular Arcs," *Philosophical Magazine*, **5**, pp. 400-408 (1928).

[62] Seidel, B. S., and Erdelyi, E. A., "On the Vibration of a Thick Ring in Its Own Plane," *Journal of Engineering for Industry*, ASME, **86**, pp. 240-244 (1964).

[63] Kirkhope, J., "Simple Frequency Expression of In-Plane Vibration of Thick Circular Rings," *Journal of the Acoustical Society of America*, **59**, pp. 86-89 (1976).

[64] Kirkhope, J., "In-Plane Vibration of a Thick Circular Ring," *Journal of Sound and Vibration*, **50**, pp. 219-227 (1977).

[65] Kuhl, W., "Messungen zu den Theorien der Eigenschwingungen von Kreisringen beliebiger Wandstärke," *Akustische Zeitschrift*, **7**, pp. 10-152 (1942).

[66] Kirkhope, J., "Out-of-Plane Vibration of a Thick Circular Ring," *Journal of the Engineering Mechanics Division*, ASCE, **102**, pp. 239-247 (1976).

[67] Martin, H. C., "Finite Elements and the Analysis of Geometrically Nonlinear Problems," in: Gallagher, R. H., Yamada, Y., and Oden, J. T., editors, *Recent Advances in Matrix Methods of Structural Analysis and Design*, The University of Alabama Press, University, AL (1971).

[68] Elias, Z. M., *Theory and Methods of Structural Analysis*, John Wiley and Sons, New York (1986).

[69] Argyris, J. H., Hilpert, O., Malejannakis, G. A., and Scharpf, D. W., "On the Geometrical Stiffness of a Beam in Space – A Consistent V. W. Approach," *Computer Methods in Applied Mechanics and Engineering*, **20**, pp. 105-131 (1979).

[70] Love, A. E. H., *A Treatise on the Mathematical Theory of Elasticity*, Dover, New York, Fourth Edition (1927 reissue).

[71] Allen, H. G., and Bulson, P. S., *Background to Buckling*, McGraw-Hill (UK), London (1980).

[72] MacNeal, R. H., editor, *MSC/NASTRAN Theoretical Manual (Level 15.5)*, MacNeal-Schwendler Corporation, Los Angeles (1972).

[73] Column Research Committee of Japan, Tsuyoshi, H., chairman, *Handbook of Structural Stability*, Corona Publishing, Tokyo (1971).

[74] Langhaar, H. L., Boresi, A. P., and Carver, D. R., "Energy Theory of Buckling of Circular Elastic Rings and Arches," *Proceedings of the Second U. S. National Congress of Applied Mechanics*, ASME, pp. 437-443 (1955).

[75] Bickford, W. B., and Reddy, E. S., "On the In-Plane Vibrations of Rotating Rings," *Journal of Sound and Vibration*, **101**, pp. 13-22 (1985).

[76] Dym, C. L., *Stability Theory and its Application to Structural Mechanics*, Noordhoff, Leyden (1974).

[77] Boresi, A. P., "A Refinement of the Theory of Buckling of Rings Under Uniform Pressure," *Journal of Applied Mechanics*, ASME, **22**, pp. 95-102 (1955).

[78] Wempner, G. A., and Kesti, N. E., "On the Buckling of Circular Arches and Rings." *Proceedings of the Fourth U. S. National Congress of Applied Mechanics*, ASME, pp. 843-849 (1962).

[79] Hodges, D. H., "Orthogonal Polynomials as Variable-Order Finite Element Shape Functions," *American Institute of Aeronautics and Astronautics Journal*, **21**, pp. 796-797 (1983).

[80] Schaeffer, H. G., *MSC/NASTRAN Primer*, Schaeffer Analysis, Mont Vernon, NH (1979).

[81] Babu, C. R., and Prathap, G., "A Linear Thick Curved Beam Element," *International Journal for Numerical Methods in Engineering*, **23**, pp. 1313-1328 (1986).

[82] Hughes, T. J. R., Taylor, R. L., and Kanoknukulchai, W., "A Simple and Efficient Element for Plate Bending," *International Journal for Numerical Methods in Engineering*, **11**, pp. 1529-1543 (1977).

[83] Lee, S. W., and Pian, T. H. H., "Improvements of Plate and Shell Finite Elements by Mixed Formulation," *American Institute of Aeronautics and Astronautics Journal*, **16**, pp. 29-34 (1978).

[84] Noor, A. K., and Peters, J. M., "Mixed Models and Reduced/Selective Integration Displacement Models for Nonlinear Analysis of Curved Beams," *International Journal for Numerical Methods in Engineering*, **17**, pp. 615-631 (1981).

[85] Tessler, A., and Spiridigliozzi, L., "Curved Beam Elements with Penalty Relaxation," *International Journal for Numerical Methods in Engineering*, **23**, pp. 2245-2262 (1986).

[86] Prathap, G., and Babu, C. R., "Field-Consistent Strain Interpolations for the Quadratic Shear Flexible Beam Element," *International Journal for Numerical Methods in Engineering*, **23**, pp. 1973-1984 (1986).

[87] Szabó, B. A., "Superconvergent Procedures for the Computation of Engineering Data from Finite Element Solutions," presented at: Symposium on Frontiers in Computational Mechanics, Massachusetts Institute of Technology, March 17-18, 1989.

[88] Jennings, A., "A Compact Storage Scheme for the Solution of Symmetric Linear Simultaneous Equations," *Computer Journal*, **9**, pp. 281-285 (1966).

[89] Bathe, K. J., and Ramaswamy, S., "An Accelerated Subspace Iteration Method," *Computer Methods in Applied Mechanics and Engineering*, **23**, pp. 313-331 (1980).

[90] Cullum, J. K., and Willoughby, R. A., *Lanczos Algorithms for Large Symmetric Matrices*, Birkhäuser, Boston (1984).

[91] Parlett, B. N., *State-of-the-Art in Extracting Eigenvalues and Eigenvectors in Structural Mechanics*, Department of Mathematics, University of California, Berkeley (1985).

[92] Nour-Omid, B., Parlett, B. N., and Taylor, R. L., "Lanczos Versus Subspace Iteration for Solution of Eigenvalue Problems," *International Journal for Numerical Methods in Engineering*, **19**, pp. 859-871 (1983).

[93] Bauchau, O. A., "A Solution of the Eigenproblem for Undamped Gyroscopic Systems with the Lanczos Algorithm," *International Journal for Numerical Methods in Engineering*, **23**, pp. 1705-1713 (1980).

[94] Rodrigues, J. F. D., and Gmuer, T. E. C., "A Subspace Iteration Method for the Eigensolution of Large Undamped Gyroscopic Systems," *International Journal for Numerical Methods in Engineering*, **28**, pp. 511-522 (1989).

[95] Guyan, R. J., "Reduction of Stiffness and Mass Matrices," *American Institute of Aeronautics and Astronautics Journal*, **3**, p. 380 (1965).

[96] Miller, C. A., "Dynamic Reduction of Structural Models," *Proceedings of the American Society of Civil Engineers, Structural Division*, **106**, No. ST10 (1980).

[97] Paz, M., *Structural Dynamics: Theory and Computation*, Van Nostrand Reinhold, New York (1980).

[98] Roark, R. J., and Young, W. C., *Formulas for Stress and Strain*, McGraw-Hill, New York, Fifth Edition (1975).

[99] Meck, H. R., "An Accurate Polynomial Displacement Function for Finite Ring Elements," *Computers and Structures*, **11**, pp. 265-269 (1980).

[100] Blevins, R. D., *Formulas for Natural Frequency and Mode Shape*, Van Nostrand Reinhold, New York (1979).

[101] Ambati, G., Bell, J. F. W., and Sharp, J. C. K., "In-Plane Vibrations of Annular Rings," *Journal of Sound and Vibration*, **47**, pp. 415-432 (1976).

[102] Rao, S. S., and Sundararajan, V., "In-Plane Flexural Vibrations of Circular Rings," *Journal of Applied Mechanics*, ASME, **36**, pp. 620-625 (1969).

[103] Abramowitz, M., and Stegun, I. A., *Handbook of Mathematical Functions*, Dover, New York (1972).

[104] Blackwell, B. F., "The Vertical-Axis Wind Turbine - 'How It Works'," *Sandia Laboratories Report*, SLA-74-0160 (1974).

[105] Blackwell, B. F., and Reis, G. E., "Blade Shape for a Troposkien Type of Vertical-Axis Wind Turbine," *Sandia Laboratories Report*, SLA-74-0154 (1974).

[106] Weingarten, L. I., and Nickell, R. E., "Nonlinear Stress Analysis of Vertical-Axis Wind Turbine Blades," *Sandia Laboratories Report*, SAND74-0378 (1974).

[107] Watson, R. A., "Comparison with Strain Gage Data of Centrifugal Stresses Predicted by Finite Element Analysis on the DOE/Sandia 17-m Darrieus Turbine," *Sandia Laboratories Report*, SAND79-1990 (1980).

[108] Watson, R. A., "Comparison of MARC and NASTRAN Predictions of the Nonlinear Centrifugal Blade Stresses for the DOE/Sandia 17-Meter Darrieus Turbine," *Stanford University Graduate Independent Study* (1980).

[109] Lobitz, D. W., and Sullivan, W. N., "VAWTDYN - A Numerical Package for the Dynamic Analysis of Vertical Axis Wind Turbines," *Sandia National Laboratories Report*, SAND80-0085 (1980).

[110] Nellums, R. O., "Field Test Report of the Department of Energy's 100-kW Vertical Axis Wind Turbine," *Sandia National Laboratories Report*, SAND84-0941 (1985).

[111] Watson, R. A., "FloWind-19 Performance and Structural Review," *FloWind Engineering Technical Report*, ETR-60002 (1985).

16. VITA

Biographical items on the author of the dissertation, Mr. Robert A. Watson.

1) Born [redacted].

2) Attended Washington University, St. Louis, Missouri, from August, 1975 to May, 1979. Awarded a Dean's Scholarship (1975–1979), the Joseph P. Razek Prize: Outstanding Junior Mechanical Engineer (1978), the Erwin C. Hoelscher Memorial Award: Outstanding Senior Mechanical Engineer (1979), and the St. Louis ASHRAE Student Award (1979). Member of Tau Beta Pi and Pi Tau Sigma honor societies. Received the degree of Bachelor of Science in Mechanical Engineering summa cum laude in May, 1979.

3) Attended Stanford University, Stanford, California, from September, 1979 to June, 1980. Awarded a National Science Foundation Graduate Fellowship (1979), a Stanford Engineering Graduate Fellowship (1979), and the Institute for Energy Studies Fellowship (1979). Received the degree of Master of Science in Mechanical Engineering in June, 1980.

4) Employed as Member of Technical Staff for the Wind Energy Research and Reactor Safety Studies Divisions at Sandia National Laboratories, Albuquerque, New Mexico, from July, 1980 to September, 1983.

5) Employed as Lead Engineer at FloWind Corporation and Senior Structural Engineer at Flow Industries, Inc., Kent, Washington, from October, 1983 to July, 1986.

6) Attended Washington University, St. Louis, Missouri, from August, 1986 to present date. Awarded a National Aeronautics and Space Administration Graduate Student Researchers Program Fellowship (1987–1989). Instructor for senior and graduate courses in mechanical vibrations (1986–1987).

7) To be employed as Senior Member of Technical Staff for the Containment Technology Division at Sandia National Laboratories, Albuquerque, New Mexico, upon completion of degree requirements.

May, 1990.

Short Title: p-Version Beam Finite Elements Watson, D.Sc. 1990

REPORT DOCUMENTATION PAGE

Form Approved
OMB No. 0704-0188

1. AGENCY USE ONLY (*Leave blank*)	2. REPORT DATE	3. REPORT TYPE AND DATES COVERED
	September 1991	Final Contractor Report May 90

4. TITLE AND SUBTITLE

Hierarchic Extensions in the Static and Dynamic Analysis of Elastic Beams

5. FUNDING NUMBERS

WU-505-63-5B
G-NGT-50138

6. AUTHOR(S)

Robert A. Watson

7. PERFORMING ORGANIZATION NAME(S) AND ADDRESS(ES)

Washington University
Sever Institute of Technology
Saint Louis, Missouri 63130

8. PERFORMING ORGANIZATION REPORT NUMBER

None

9. SPONSORING/MONITORING AGENCY NAMES(S) AND ADDRESS(ES)

National Aeronautics and Space Administration
Lewis Research Center
Cleveland, Ohio 44135-3191

10. SPONSORING/MONITORING AGENCY REPORT NUMBER

NASA CR-187210

11. SUPPLEMENTARY NOTES

Project Manager, C.C. Chamis, Structures Division, NASA Lewis Research Center, (216) 433-3252. This report was submitted as a dissertation in partial fulfillment of the requirements for the degree Doctor of Science to the Sever Institute of Washington University, Saint Louis, Missouri in 1990. Research was performed under the NASA Lewis Graduate Student Research Program.

12a. DISTRIBUTION/AVAILABILITY STATEMENT

Unclassified - Unlimited
Subject Category 39

12b. DISTRIBUTION CODE

13. ABSTRACT (*Maximum 200 words*)

Approximate solutions of static and dynamic beam problems by the p-version of the finite element method are investigated. Within a hierarchy of engineering beam idealizations, rigorous formulations of the strain and kinetic energies for straight and circular beam elements are presented. These formulations include rotating coordinate system effects and geometric nonlinearities to allow for the evaluation of vertical-axis wind turbines, the motivating problem for this research. Hierarchic finite element spaces, based on extensions of the polynomial orders used to approximate the displacement variables, are constructed. The developed models are implemented into a general-purpose computer program for evaluation. Quality control procedures are examined for a diverse set of sample problems. These procedures include: 1) estimating discretization errors in energy norm and natural frequencies, 2) performing static and dynamic equilibrium checks, 3) observing convergence for quantities of interest, and 4) comparing with more exacting theories and experimental data. It is demonstrated that p-extensions produce exponential rates of convergence in the approximation of strain energy and natural frequencies for the class of problems investigated.

14. SUBJECT TERMS

Finite elements; p-version; Curved beams; Error estimate; Convergence criteria; Centrifugal softening; Geometric nonlinearities; Vertical-axis; Wind turbines

15. NUMBER OF PAGES

316

16. PRICE CODE

A14

17. SECURITY CLASSIFICATION OF REPORT	18. SECURITY CLASSIFICATION OF THIS PAGE	19. SECURITY CLASSIFICATION OF ABSTRACT	20. LIMITATION OF ABSTRACT
Unclassified	Unclassified	Unclassified	